Università degli Studi di Milano
Facoltà di Scienze Matematiche, Fisiche e Naturali
Dottorato di Ricerca in
Fisica, Astrofisica e Fisica Applicata

3D Quantum Theory of Free Electron Lasers

Coordinatore Prof. Gianpaolo Bellini

Tutore Prof. Nicola Piovella
Cotutore Prof. Roberto Pozzoli

Tesi di Dottorato di
Luca Volpe
Ciclo XX

Anno Accademico 2006-2007

To my family, in the hope of the birth of a new life.

Acknowledgments

First of all I wish to thank my tutor Nicola Piovella. During these years he followed me patiently giving me the possibility to approach the interesting physics of the quantum free electron laser and of the collective phenomena.
Then I should sincerely thank Rodolfo Bonifacio for the helpful discussion about the physics of the free electron laser and M. Mary Cola, for her support during these years and for the stimulating discussions about the collective phenomena.
Thanks to Stefano Olivares, Andrea R. Rossi and Alberto Bacci. They keep cheerful the atmosphere of our group.
Thank to my friend Jennifer for aid in the correction of text.
A special thought to my friends: Silvia, Elena, Miriam, Andrea A, Matteo B, Alfredo, Matteo P, Massimo M, Massimo B, Gabriele, Andrea C, Guido, Fabio, Luigi, Giuliana e Alessandro for sharing the everyday difficulties.
Finally a wish to thank the members of commission: Prof. D. Jaroszynski, Prof. R. Fedele and Dr. B. Vacchini for their willingness.

Contents

Prologue

The realization of a Free Electron Laser (FEL) operating in the quantum regime could provide a compact and monochromatic X-ray source. In this thesis we developed a three dimensional (3D) quantum theory for a FEL with a laser wiggler, based on a discrete Wigner function formalism taking into account the longitudinal momentum quantization. Starting from the exact quantum treatment, a motion equation for the Wigner function coupled with self-consistent radiation field is derived in the realistic limit in which the normalized electron beam emittance is much larger than the Compton wavelength quantum limit. The model describes the 3D spatial and temporal evolution of the electron and radiation beams, including diffraction, propagation, laser wiggler, emittance and quantum recoil effects. It can be solved numerically and reduces to the 3D Maxwell-Vlasov model in the classical limit. We discuss the experimental requirements for a Quantum X-ray FEL with a laser wiggler, presenting preliminary numerical results and parameters for a possible future experiment. Moreover we present a systematic statistical analysis of the 1D SASE which confirm the "Quantum purification" phenomenon.

Introduction

Physical, chemical and biological processes are intrinsically dynamic in nature since they are related to electronic and atomic structures that evolve with time. The characteristic time scale spans from few femtoseconds, in the case of electronic processes, to a few tens or hundreds femtoseconds, as in the case of atomic and molecular processes. The nascent capability to measure these phenomena at the relevant time scales will open completely new prospectives and analyses. However, current available, fully coherent (atomic or molecular laser) light sources emit radiation only in a limited range of wavelengths. Their use is limited to optical and spectroscopic techniques in the infrared, visible and near-ultraviolet range, excluding all the measurement needing photons with energy higher than few eV. There is therefore a strong scientific need for a tunable, coherent light source with an energy range from the vacuum ultraviolet (VUV) to the X-ray region, with a stable and well-characterized temporal structure in the femtosecond and picosecond time domain.

The "Free Electron Laser" (FEL) can produce radiation pulsed with high peak brilliance and with photons' energies ranging from the VUV to the hard X-ray, *i.e.* from 10 eV (120 nm) to 10 keV (0.12 nm). These special proprieties of the FEL come from its basic design which is different from that of common atomic and molecular lasers (AML). In fact, while for AML the radiation wavelength is defined and fixed by the quantum state of the optical medium, in the FEL process radiation arises from the bremsstrahlung of ultra-relativistic electrons in a periodic magnetic field (wiggler); therefore its wavelength depend only on e-beam energy γ and on the magnetic field period λ_w, through the following resonant relation $\lambda_r \propto \lambda_w/2\gamma^2$. Therefore the emitted radiation wavelength can, in principle, range from microwaves ($\lambda \simeq 1$ cm) to X-rays ($\lambda \simeq 1$ Å). The analogy between FEL device and AML is improved inasmuch as the FEL process involves collective behaviour. In fact, if the

wiggler is long enough and the electron current is high enough, then the electron beam will start to bunch under the action of the periodic wiggler potential (*i.e.* electrons faster than γ_r will decelerate, slower electrons will accelerate) and give rise to exponential grow of radiation until saturation set a limit on the conversion of kinetic electron into radiation energy; this is the *High-Gain Steady state regime* described by R. Bonifacio, C.Pellegrini and L.M.Narducci [14]. In this regime the radiated power is proportional to $N_e^{4/3}$ (N_e is the number of electrons). In 1988 it was shown [15] [16] that when the propagation effects are taken into account the FEL can operate in a completely different regime, the *superradiant regime*, in which the peak of the radiation power scales as N_e^2. In general, FEL radiation can be of two different kinds: basic *self-emission* comes from the direct interaction of the e-beam with the wiggler magnetic field, while *stimulated- emission* occurs when a seed radiation field co-propagates with the electron beam [23]. The self emission occur starting from random noise in the particle phases: the electrons enter the wiggler in an unprepared state, so that the initial emission is proportional to N_e (incoherent radiation), then the electrons begin to bunch on interacting with the self-radiation and wiggler field, involving to emit radiation with intensity proportional to $N_e^{4/3}$ (steady state regime) or with intensity proportional to N_e^2 (superradiant regime) *i.e.*when the propagation effects become relevant. The FEL self-emission in which the propagation effects are considerate is a particular mode operation called **S***elf* **A***mplified* **S***pontaneous* **E***mission* (**SASE**) [15, 16, 17]. The SASE-FEL mode operation is important at wavelength not accessible to coherent radiation source, such as the XUV region or the far infra-red spectrum. The realization of a single pass FEL in the SASE mode is presently the goal of several projects (such as LCLS [53] at Stanford, USA, XFEL [54] in Hamburg, Germany and [55] in Japan), to obtain a high-brightness X-ray source. These projects [53, 54, 55] are all based on the classical theory of SASE [17, 18, 19, 21]. However, such sources will radiate a pulse with a broad spectrum composed of many random superradiant spikes [17, 18]. Recently it has been shown that a FEL can operate in a quantum regime [35], in which the spiking behaviour observed in the SASE mode disappears and the spectrum reduces to a single narrow line [30, 31], providing an enormous improvement in the coherence of SASE-FEL X-ray sources. The quantum regime in an FEL occurs when the electron momentum spread $\Delta(p_z) = mc\Delta(\gamma)$ is less than the momentum $\hbar k_r$ of

the emitted photon (m is the electron mass, c is the speed of light, $\hbar$ is the Plank constant and $k_r = 2\pi/\lambda_r$ where λ_r is the radiation wavelength). In this limit [27, 35] the photon emission probability is much larger than that of absorption, and each electron coherently emits a single photon, recoiling by $\hbar k_r$. The particle ensemble behaves like a two-state system with only two possible average momenta, $p = mc\gamma_0$ and $p = mc\gamma_0 - \hbar k_r$. In this sense, a FEL in the quantum regime is more similar to a laser where, instead of the electronic transitions between internal energy levels, as normally occurs in a laser, the electrons back-scatter the photons of the pump field (i.e. the static or laser wiggler) into the forward radiation mode, making recoil transitions between discrete momentum levels, separated by $\hbar k_r$. On the contrary, in a classical FEL the electron has comparable probabilities to emit or absorb a photon, so that the net gain is given by the difference between the emission and absorption probabilities. The transition between classical and quantum regimes is controlled by the Quantum FEL (QFEL) parameter $\bar{\rho} = \rho(mc\gamma_0)/(\hbar k_r)$ (where ρ is the classical FEL parameter). It has been shown [27, 47] that in the classical regime ($\bar{\rho} \gg 1$) many momentum states become occupied and the multiple transitions between the different momentum states lead to a multi-frequency spectrum with equally spaced lines and an envelope width $\Delta\omega/\omega \sim 2\rho$. The many sequential transitions occur randomly under the gain curve, leading to the multiple-line chaotic spectrum observed in the classical SASE. Conversely, in the quantum regime $\bar{\rho} < 1$, the momentum spread $\Delta(p)$ cannot be smaller than the photon recoil $\hbar k$ and only a single frequency, corresponding to a single momentum transition, occurs with line width equal to the ratio between the emitted radiation and the bunch length in unit of cooperation length $\Delta\omega/\omega \simeq \lambda/l_b$. Therefore in the quantum regime the classical random spiking behaviour almost disappears and a strong narrowing of the spectrum occurs; this phenomenon is called "quantum purification".

The one-dimensional analysis of the quantum FEL suggests that an experiment in the X-ray region, confirming the existence of the "quantum purification" phenomenon (see chapter (3) and (4) and [30, 31, 47]), could be envisaged in the near future. Therefore, the extension of the 1D quantum model to a "more realistic" 3D scheme is more than ever necessary. However, in order to realize a QFEL experiment, a laser wiggler must be used instead of the magneto static wiggler [39, 48, 49]. Such a choice sets some stringent conditions on the electron and laser beam parameters

which should be verified by numerical simulations.

In a classical framework, the extension from 1D to 3D is rather straightforward, as shown by the different classical models in the literature [56, 57, 51, 52]. Several SASE-FEL experiments based on these theories are actually in progress [54, 53, 55] and some numerical, experimental friendly codes have been developed for 3D simulations, for instance `GENESIS` [50]. Conversely, the extension from 1D to 3D theory in a quantum framework is not so straightforward as in the classical case. This fact is principally linked to the different nature of electron-radiation interaction along the longitudinal and transverse directions. In fact, whereas along the longitudinal axis the photon recoil effect is dominant and needs a quantum description, in transverse dynamics the quantum effects appear less relevant. For these reasons, a model describing either the quantum behaviour along the longitudinal axis *and* the approximately classical behaviour along the transverse coordinates, is necessary.

As shown in chapter 3 (see ref. [24, 29]), in the 1D quantum model the electrons are treated as bosons which interact with each other only via the radiation field. In particular the e-beam is described by a Schrödinger wave-field obeying the bosonic equal-time commutation relation. The extension of the Schrödinger model into 3D geometry does not lead to a correct model, because the 3D Schrödinger equation describes a pure state (*i.e.* $\Delta x \Delta p_x \sim \hbar$) with a transverse normalized emittance $\epsilon_n = \gamma \epsilon_r$ equal to the Compton wavelength $\epsilon_n \simeq \lambda\!\!\!^{-}_c$ and a transverse momentum distribution with a width near Heisenberg's Uncertainty Principle (HUP) limit *i.e.* $\Delta x' \sim \lambda\!\!\!^{-}_c/(\sigma\gamma_r)$. We are interested to describing only electron beams in which the transverse momentum distribution is thermal, *i.e.* with a width $\Delta x' \sim \epsilon_n/(\sigma\gamma_r)$ much larger than the quantum limit. Therefore a mixed state with $\Delta x \Delta p_x \gg \hbar$ will be necessary and can be conveniently represented with a Wigner distribution function.

The aim of this thesis is to develop a three dimensional, time dependent quantum model based on a discrete Wigner function formalism which describes the three dimensional spatial and temporal evolution of electron and radiation beams, including diffraction, propagation, laser wiggler, emittance and quantum recoil effects. Following the previous considerations, this model should admit three fundamental limits: 1) transverse classical limit *i.e.* there should exist a parameter ruling the transition from quantum to classical behaviour for the transverse motion only. We

will show that this parameter can be defined as the ratio between the Compton wavelength (*i.e.* the longitudinal emittance) and the transverse normalized emittance *i.e.* $\alpha = \lambda\!\!\!^{-}_c/\epsilon_n$; when $\alpha \sim 1$ the transverse emittance is of the order of the Compton wavelength *i.e.* we are describing a 3D ultracold e-beam. On the contrary when $\alpha \ll 1$ the transverse emittance ϵ_n is much larger than the Compton wavelength *i.e.* we have a thermal transverse momentum distribution
2) 1D limit *i.e.* the 3D equations should reduce to 1D equations when transverse effects are neglected;
3) full classical limit *i.e.* the 3D Maxwell-Wigner equations should reduce to the 3D classical Maxwell-Vlasov equations when $\bar{\rho} \gg 1$ (for the longitudinal motion) and $\alpha \ll 1$ (for the transverse motion).

Summarizing, our 3D quantum model should admit the classical limit, in agreement with the Correspondence Principle which a quantum theory should satisfy.

The Wigner function is usually defined in the first quantization formalism, however we shall see that it can be defined also starting from the second quantization formalism following the quantum statistical approach used in ref. [45]. This new point of view permits us to formulate our 3D theory in a more complete and rigorous way. In Particular: 1) The theory treats, from the dynamic point of view, fermions and bosons in the same way; the difference between fermions and bosons statistic appears only when we consider the quantum commutation rules of the creation and annihilation operators and in the choice of the initial state (*i.e.* boundary condition). 2) The energy spread effects can be included in the initial condition in a natural way and do not appear explicitly in the evolution equation, while in the 1D Schrödinger model it must be added as a weight distribution of the initial momentum in the driving term (bunching factor) of the field evolution equation (see section 3.2.4). Nevertheless in this model we neglect some important aspect such the quantization of the self radiation e.m. field that would allows us to investigate the 3D photons statistic and the space charge effects. The quantization of the e.m. field is necessary for the complete knowledge of the FEL process and we think that our model can be extended to include it in a natural way. The space charge effects are also demanded; these are included in this model only in the Paraxial approximation *i.e.* assuming that the transverse repulsion between neighbour electrons is smaller than longitudinal one. in this way we obtain only an indication of the tendency of

the phenomenon. Although

This work can be divided in three parts: the first part (cap.1, cap.2) contains a review of classical FEL theory, the second part (cap.3, cap.4) introduces the quantum FEL theory as it was recently developed by R.Bonifacio et al, and presents a 1D numerical analysis of the statistical propriety of SASE radiation in the quantum regime. This analysis proves the existence of the phenomenon of "quantum purification" predicted earlier but never investigated in details. The third and final part (cap.5, cap.6), which contains the main result of this thesis, presents the extension of 1D quantum theory in a more realistic 3D model based on a discrete Wigner function, in which all important longitudinal and transverse effects are included. A complete discussion of the requirement for a future QFEL experiment and some numerical simulations complete this work.

In chapter 1 we introduce the basic physics of the FEL process, such as *self* and *stimulated* emission. Moreover we show the existence of the instability solution which leads to collective phenomena *i.e.* the high-gain steady-state and superradiance regime in which the intensity of the emitted radiation is proportional respectively to $N_e^{4/3}$ and N_e^2, where N_e is the number of electrons. In chapter 2 we obtain the classical 3D Hamiltonian (sec. 2.1.1) describing N_e electrons interacting with a laser wiggler (or magneto static wiggler) and with a self-emitted e.m. field. The 3D Maxwell evolution equation for the self-emitted field are also obtained (sec. 2.1.2). In order to explain more clearly the basic physics and the different regimes of the FEL, a complete overview of the classical theory is presented in section 2.2 assuming 1D approximation (Paraxial approximation). The 1D theory is based on set of $2N_e+1$ equations describing the evolution of the dynamical variables: electron phase with respect to wiggler potential θ and electron energy γ, for each electron of the e-beam, and complex radiation field amplitude. In sections 2.2.1 and 2.2.2 the 1D system is solved analytically (linear approximation) and numerically in the steady state regime (no propagation effects), showing exponential growth and collective behaviour, which leads to a radiation power proportional to $N_e^{4/3}$. Subsequently, in section 2.2.4, the propagation effects (*i.e.* the difference between electrons and photons velocities "slippage") are included, describing the superradiant regime in which the radiation power is proportional to N_e^2. Finally we introduce (sec. 2.2.3) the SASE mode operation which is based on two ingredients: starting from noise,

and superradiance effects. In section 2.3 we move to a fluid dynamics description of the FEL system, obtaining 3D Maxwell-Vlasov coupled equations. Finally, in section 2.3.3 we discuss why a laser wiggler is necessary in the quantum regime. Chapters 3 and 4 are dedicated to the 1D quantum theory. In particular, in sections 3.1 and 3.2 we present the 1D steady state model as it was developed in [28, 29, 30] and [24]. Propagation effects (slippage) are taken into account in section 3.2.1 using the multiple scaling method [4, 35] and a linear analysis is performed; in section 3.2.4, following [32], the energy spread effect is considered; finally, in section 3.3, the discrete Wigner function [41] is introduced and following Ref.[44], the 1D model is reformulated in terms of them. For a pure state the Wigner model is equivalent to the Schrödinger model and in addition, it admits a classical limit. Chapter 4 is dedicated to numerical integration of the 1D quantum model. In particular a numerical analysis of the quantum SASE radiation proprieties is performed similarly to the study by Saldin [18] for the classical SASE. The difference between classical and quantum regimes are investigated and the existence of "quantum purification" [30] phenomenon is numerically proved.

Up to this point the quantum theory is presented in the 1D approximation; the third and final part of the thesis (chapters 5 and 6) is devoted to developing a 3D quantum theory for a FEL. In particular in chapter 5 we introduce, following [45], the second quantized Wigner formalism in which the multi particle nature of the FEL is treated in a natural way. In section 5.2 we obtain the 3D Quantum Hamiltonian in second quantized formalism, while in sections 5.3 and 5.4 the evolution equations of the e-beam Wigner function and the self-radiation e.m. field are obtained. The Wigner evolution equation obtained in section 5.3 describes an electron beam with a transverse normalized emittance till to the 'ultracold' limit of the Compton wavelength, then we expand its evolution equation in terms of a characteristic parameter which permits to perform a classical transverse approximation, keeping intact the longitudinal quantum recoil effects. In chapter 6 we discuss the beam and the wiggler field requirements in order to operate a FEL in a high-gain quantum regime; in particular the section 6.1 is dedicated to the emittance criteria for the e-beam. A numerical parallel code `QFEL3D` has been developed [49] for solving our working equation; in section 6.2 we present preliminary numerical simulation neglecting the propagation and energy spread effects, while in section **??**

a more accurate numerical study is performed in the particular two-level approximation. The inhomogeneous broadening due to the emittance and the transverse laser profile effects are numerically investigate and particular Flattened laser beam profile are proposed and tested instead of the usual Gaussian profile. Finally a set of possible experimental parameters for a future QFEL experiment is presented.

Chapter 1

The Free Electron Laser

The Free Electron Laser is essentially a device that transform the kinetic energy of an electron beam (e-beam) into e.m. radiation. The relativistic e-beam passing through a periodic magnetic field oscillates in the transverse direction and emits radiation (synchrotron radiation) confined in a narrow cone along the propagation direction. The periodic magnetic field is provided by the so-called wiggler, an insertion device usually realized with two arrays of permanent magnets with alternating polarities or with two helical coils with current circulating in opposite directions. The wavelength of the emitted radiation depends on the wiggler period, on the strength of the magnetic field and on the electron energy. This means that the FEL can be continuously tuned in frequency, ranging from microwaves ($\lambda \simeq 1$ cm) to X-rays ($\lambda \simeq 1$ Å); this is one of the main advantages of FELs with respect atomic and molecular lasers, where the wavelength of the radiation field is fixed by the quantum transition between two atomic or molecular states, and it has, in general, a small tunability, since the energy levels of the active media are fixed; moreover another advantage of the FEL with respect atomic and molecular lasers is that its main processes happen in vacuum, with no thermal dispersion o breakdown effects in the active medium. For this reason the FEL can provide a powerful source of tunable, coherent e.m radiation.

In general, the FEL radiation can be of two different kinds: basic *spontaneous emission* comes from the direct interaction of the e-beam with the wiggler magnetic field with no injected field, while *stimulated emission* occurs when also a seed radiation field co-propagates with the electron beam. In this chapter we introduce

the basic physical description of these two processes, then we introduces a quantum regime comparing the different behaviour between classical and quantum regimes.

1.1 FEL Spontaneous Emission

It is well known that a free charge cannot radiate because of the energy-momentum conservation; the word "free" in FEL describes the state of the electrons used as active medium: the electrons are not bound as in atomic or molecular lasers. In the FEL the electrons are not really "free" because of the interaction with the periodic magnetic field that generates a radiation which is particularly intense and confined around the instantaneous velocity vector. The FEL radiation is really a synchrotron radiation, i.e. the radiation emitted by an electric charge moving at relativistic speed when a transverse force is applied to it. This radiation is greater than that due to a parallel force by a factor γ^2, where

$$\gamma = \sqrt{\frac{1}{1-\beta^2}} \tag{1.1}$$

is the electron energy, γmc^2 in the rest mass unit, with $\vec{\beta} = \vec{v}/c$.

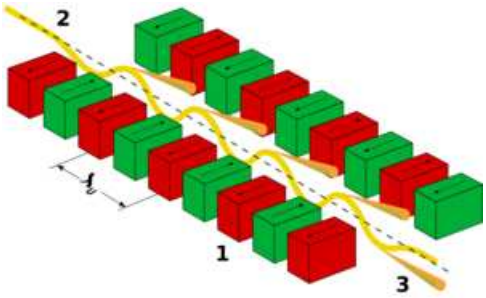

Figure 1.1: Planar wiggler

The magnetic field is generated by the "wiggler", whose simplest realization can be made in different ways; we assume, for the moment, an helical wiggler made of two helical coils with current circulating in opposite directions. In the following we will substitute the helical wiggler with an helical polarized conterpropagating laser. In both cases, the electrons inside the wiggler are periodically deflected by

the Lorenz force

$$\vec{F} = -e\vec{\beta} \times \vec{B}_w \tag{1.2}$$

generated by the wiggler magnetic field $\vec{B}_w$ on electrons with charge $-e$, which are traveling at speed $\vec{v}$ along the wiggler. Since the magnetic field of the wiggler have a periodic alternated polarization, the electrons will "wiggle", i.e. oscillate transversally along the same longitudinal trajectory. Its main features are the following:

i) The intensity is proportional to the electrons current *i.e.* the radiation is incoherent ($I \propto N_e$ where N_e is the number of electrons).

ii) the emitted radiation is confined in a narrow cone along the direction of electrons motion (that will be identify with the z-axis) within an angle of order of $\simeq 1/\gamma\sqrt{N_w}$ where N_w is the number of wiggler period.

iii) it is narrow-band radiation, with on axis spectral distribution

$$\frac{d^2I}{d\Omega d\omega} \propto \mathrm{sinc}^2\left(\pi N_w \frac{\omega - \omega_s}{\omega_s}\right) \tag{1.3}$$

where sinc(x)=sin(x)/x. Hence the spectrum is peaked around a spontaneous frequency $\omega_s = 2\pi c/\lambda_s$ where, for on axis radiation,

$$\lambda_s = \frac{1-\beta_\parallel}{\beta_\parallel}\lambda_w \tag{1.4}$$

with $\beta_\parallel = \langle v_\parallel \rangle / c$ and λ_w the ondulator period, and its full line-width at half height is

$$\frac{\Delta\omega}{\omega} \simeq \frac{1}{N_w} \tag{1.5}$$

The above equation show that the spontaneous emission line-width can be reduced simply by increasing the number of wiggler periods.

The above result are most easily explained in the (average) longitudinal electron rest frame, here each electron "sees" N_w-periods wiggler as N_w-periods conterpropagating pseudo-radiation field [1], with Lorentz contracted wavelength $\lambda'_w = \lambda_w/\gamma_\parallel$. Hence, it oscillates N_w times, emitting a wave packet of length $N_w\lambda'_w$ peaked at $\lambda'_s \simeq \lambda'_w$. In other terms, it acts as a "relativistic mirror" where the radiation is reflected by a Compton back-scattering. In this process we neglect the Compton shift, in agreement with the assumption of a purely classical description. From this

picture we obtain the same result of eq. (1.3,1.5). In fact it well known that the Fourier transform of a plane-wave truncated after N_w oscillations is a sinc-function with line-width $\Delta\omega/\omega_r = N_w^{-1}$. The resonant condition (1.4) can be also derived using the laboratory frame, requiring that during the time necessary for an electron to travel a wiggler period λ_w the electromagnetic wave will slip over it by a radiation wavelength λ_r,

$$\frac{\lambda_w}{v_\parallel} = \frac{\lambda_w + \lambda_r}{c}. \tag{1.6}$$

From eq.(1.6) we can write $(k_w + k_r)dz/dt - \omega_r = 0$, $(v_\parallel = dz/dt)$ or equivallently $d\left[(k_w + k_r)z - \omega_r t\right]/dt = 0$, showing that the resonant relation can be obtained also by imposing the relative phase θ of the electron in the wiggler and e.m. field to be constant.

$$\frac{d\theta}{dt} = 0, \qquad \theta = (k_w + k_r)z - \omega_r t. \tag{1.7}$$

In the next section we will show that the module of electron transverse velocity $\mathbf{v} = c\vec{\beta}$ is approximately:

$$|\vec{\beta}_\perp| \simeq \frac{a_w}{\gamma} \tag{1.8}$$

where

$$a_w = \frac{e\lambda_w B_w}{2\pi mc^2} \tag{1.9}$$

is the wiggler parameter. Thus, from $1/\gamma^2 = 1 - \beta_\parallel^2 - \beta_\perp^2$ it follows

$$\frac{1}{\gamma_\parallel^2} = \frac{1 + a_w^2}{\gamma^2}. \tag{1.10}$$

where $\gamma_\parallel^2 = 1/(1 - \beta_\parallel^2)$. Finally using the resonant condition (1.4) in the ultrarelativistic limit $\gamma_\parallel \gg 1$ we obtain:

$$\lambda_s = \frac{1 - \beta_\parallel}{\beta_\parallel}\lambda_w \simeq \frac{\lambda_w}{2\gamma_\parallel^2} \simeq \lambda_w \frac{1 + a_w^2}{2\gamma^2}. \tag{1.11}$$

This relation shows the high tunability of the FEL; in fact, the wavelength λ_s can be changed by varying either electron energy γ, wiggler magnetic field B_w or its period λ_w.

1.2 FEL Stimulated Emission

Stimulated emission takes place when a radiation field with wavelength $\lambda \simeq \lambda_s$, co-propagates with the electron beam inside the wiggler. From the resonant relation (1.11) one can define the resonant electron energy

$$\gamma_r = \sqrt{\frac{\lambda_w(1+a_w^2)}{2\lambda}} \tag{1.12}$$

We shall see in the next section that if the electron energy and the radiation wavelength preserve the relation (1.12), then the relative phase (1.7) between the transverse oscillations of the electrons and the radiation remain constant. Depending on the value of this relative phase, one of these processes occurs for each electron:

- the electron gives energy to the field and decelerates, *i.e. stimulated emission* which provides "gain",
- the electron takes energy from the field and accelerates, *i.e. absorption*,

If the first of these two processes dominates, then the injected radiation field is amplified as in the first amplified experiment [65] ; moreover if the wiggler is long enough or if the process happens in an optical cavity, then the spontaneous emission is amplified, as in the first FEL oscillator experiment [66].

This oversimplified picture of the FEL gain process is at the single-particle level and leads to the Madey's small signal regime: let consider a "long" electron pulse so that the slippage of the radiation over the electrons can be neglected (*steady state regime*). Then we realize that the initial electron phase θ are randomly distributed over each radiation wavelength. Hence for a nearly mono energetic and resonant electron beam, on average half electrons will decelerate and half electrons will accelerate with the result that no net gain will occurs. The Madey's small signal regime occurs when we inject, in a short wiggler, a low current electron beam with average energy slightly above resonance $\langle\gamma\rangle_0 > \gamma_r$, such that gain (slightly) prevails over absorption.

Electron Bunching and High-gain regime

However, electron can communicate each other via the common radiation field, or even directly for high enough current density, In fact, if the wiggler is long enough

and the electron current is high enough, then the electron beam will start to bunch: electrons faster than γ_r will decelerate, slower electrons will accelerate, so that the electron energy will be driven toward resonance. This energy modulation becomes space modulation, i.e. the electrons start to bunch in packets on the scale of the radiation wavelength (*microbunching*), around a phase that produces gain. Since most of electrons have nearly the same phase, they emit coherent collective synchrotron radiation. The variable representing how strongly bunched the electrons are, is the *bunching parameter*:

$$B \equiv \frac{1}{N_e} \sum_{j=1}^{N_e} e^{-i\theta_j} \equiv \langle e^{-i\theta} \rangle. \tag{1.13}$$

Given the physical meaning and mathematical definition of the phase θ, it should be clear how B is the measure of the longitudinal modulation of the electron beam on the scale of the radiation wavelength. A bunching equal to zero represents a completely random distribution of phases, while an ideal bunching of $|B| = 1$ can only be possible with all electrons perfectly in phase. We shall see the existence of a collective instability for the system, which lead to electron *self-buncing* and to exponential grow of radiation until saturation, set a limit, on the conversion of kinetic electron into radiation energy; this is *High-Gain Steady state regime*. In this regime the radiated power is proportional to $N_e^{4/3}$, whereas in the incoherent radiation case, the power is proportional to N_e.

A completely new physics appears if the propagation effect, due to the different velocity of the electrons and the radiation beam, is taken into account. As a consequence of this effect (known as *slippage*) the radiation pulse moves ahead with respect to the electron pulse by a radiation wavelength λ_r each every wiggler period λ_w, *i.e.* by $l_s = N_w \lambda_r$ at the end of a N_w period wiggler. From analytical and numerical studies it has been shown [15] [16] that when the slippage length l_s is large the FEL can operate in completely different regime, the *superradiant regime*, in which the peak of the radiation power scales as N_e^2 (see chapter 2). Radiation intensities scaling as N_e^2 may also arise from coherent synchrotron radiation emitted by electron which have been pre-bunched by an external source. The radiation field emitted by these pre-bunched electrons sum up coherently to give N_e^2 scaling; this is the "superradiance" as defined by Dicke [12] *i.e.* spontaneous emission from a coherently prepared system. In a FEL the electrons enter the wiggler in unpre-

pared state, so that the initial emission is proportional to N_e (incoherent emission), then the electrons begin to bunch on interacting with the spontaneous radiation and wiggler field, involving to emit radiation with the intensity proportional to N_e^2. This behaviour is a self-organized phenomenon and is different from the Dicke's "superradiance" but more similar to the atomic "superfluorescence" [13].

The FEL can operate also in the absence of the input signal A_0 (*i.e.* self-emission), starting from the random noise in the particle phases; this mode operation is called **S***elf* **A***mplified* **S***pontaneous* **E***mission* (**SASE**). We shall see in next chapter that, when the SASE-FEL is dominated by the slippage, the emitted fields exhibit superradiant spikes [17]. The SASE-FEL mode operation is important at wavelength not accessible to coherent radiation source, such as the XUV region or in the far infra-red spectrum. The realization of a single pass FEL in the SASE mode is presently the goal of several projects (such as the LCLS [53] at Stanford, USA, XFEL [54] in Hamburg, Germany and [55] in Japan ...), to obtain a high-brightness X-ray source. This project are all based on the classical theory of SASE which will be shown in detail in the next chapter. However, such sources will radiate a pulse with a broad spectrum composed by many random superradiant spikes [17]. Recently it has been shown that an FEL can operate in a quantum regime [35], in which the spiking behaviour observed in SASE mode disappears and the spectrum reduces to a single narrow line [30, 31], providing a enormous improvement in the coherence of SASE-FEL based X-ray sources.

1.3 Quantum FEL

So far, most of the properties of FEL have been analysed and found remaining in a strictly classical framework; however, the classical theory is, after all, only an approximation. In attempt to extend the range of the FEL operation into the X-ray region, the quantum effects should be taken into account. In fact, at these wavelength, the electron recoil due to the emission of a photon becomes comparable to the emission line width, and a quantum mechanical treatment of the electron-photon interaction becomes compulsory. Let explain this fact more clearly: As we have anticipated above, the "classical theory" is only an approximation of the "reality", which seem to be quantum; the borde-line between the classical and quantum world is defined

by the Heisenberg Uncertainly Principle (HUP) which can be written in terms of the position and momentum uncertainty, $\Delta p \Delta x \geq \hbar$, or in terms of the energy and time uncertainty, $\Delta E \Delta t \geq \hbar$. When the Heisenberg inequality is strong (*i.e.* $\gg$) quantum effects can be neglected and the system behaves classically, conversely when the inequality tend to similarity (*i.e.* $\sim$) quantum effects become relevant so that quantum theory is necessary. Assuming that for a relativistic electron with energy $E_e = mc^2\gamma$, the interaction time is proportional to the inverse of the emitted photon frequency $\Delta t \propto \omega_r^{-1}$ the energy-time Uncertainly relation can be written as follows

$$\Delta\gamma\lambda_r \geq \lambda\!\!\!^{-}_c \tag{1.14}$$

where $\lambda_r = 2\pi c/\omega_r$ is the emitted photon wavelength, $\lambda\!\!\!^{-}_c = \lambda_c/2\pi$ and $\lambda_c = h/mc = 0.024$Å is the Compton wavelength.

This relation shows that reducing the emission wavelength the strong inequality is not anymore satisfied. Therefore, for a complete understanding of the basic FEL process we need a quantum theory which describes the interaction between the beam electrons and the emitted photons in terms of discrete momentum exchange. Such a theory should be tend to a classical description when the inequality in the HUP is strong (*i.e.* $\gg$), hence we should looking for a parameter which rules the transition between the classical and the quantum regime. This parameter can be found starting from Eq.(1.14) which can be written as follows

$$(mc\Delta\gamma)/(\hbar k_r) \geq 1 \tag{1.15}$$

where $k_r = 2\pi/\lambda_r$.

The dimensionless left side of Eq.(1.15)can be choose as our transition parameter, because it represent the ratio between the maximum classical electron momentum spread $mc\Delta\gamma$ and the photon recoil momentum $\hbar k_r$. The classical regime occurs when the electron momentum recoil is greater than the photons recoil *i.e.* $(mc\Delta\gamma)/(\hbar k_r) \gg 1$ then each electron emits many photons *i.e.*"multi-photons emission"; conversely the quantum effects become important when the electron momentum recoil is of the order of the photons recoil $(mc\Delta\gamma)/(\hbar k_r) \lesssim 1$ then each electron emits only one photon. The theoretical development of a complete 3D quantum theory for a FEL is the aim of this thesis. In chapters 3 and 4 we will obtained a complete 1D model which depend only by a single parameter, the "QFEL-Parameter"

(see Eq. (5.17)) which agree with the parameter defined in Eq.(1.15). Moreover we will shown that, ruling by the QFEL-Parameter, the 1D quantum model admit a classical limit. The complete 3D theory will developed in chapter 5.

Chapter 2

Classical FEL Theory

From the discussion of the previous chapter it results that a proper classical theory describing a high gain FEL amplifier must be a many-particle theory, moreover, the electron dynamics should be self-consistently related to the evolution of the e.m. field dynamics. One can set a self-consistent scheme for the FEL dynamics (similarly to that of the *Maxwell-Bloch* equations in laser physics [5]) which couple the Maxwell equations with the Newton-Lorentz equations for charged particles moving at relativistic speed in an e.m. field; alternatively one can use a Hamiltonian approach in analogy to ref. [10] [11] [57]. This approach allows to extend in a natural way the classical model to the quantum framework. We will obtain the electron dynamics equations starting from a full 3D relativistic Hamiltonian of a single electron interacting with a circular polarized e.m field and conterpropagating laser beam (e.m. wiggler) (instead of the usual static wiggler), the evolution equations of the e.m. field are derived from the Maxwell equations in the Slowly Varying Envelope Approximation (SVEA). The longitudinal electrostatic interaction between electrons (*i.e.* space-charge effects) will be also taken into account, but only in the 1D approximation. In the second part of this chapter we will overview the Classical 1D theory, its different regimes with their most relevant features.

2.1 3D FEL Model

The circularly polarized laser wiggler and the radiation fields are characterized by the transverse vector potential $\mathbf{A}$ which can be written in terms of the polarization

vector $\hat{e} = (\hat{x} + i\hat{y})/\sqrt{2}$ as:

$$\begin{aligned} \mathbf{a} &= \frac{e}{mc^2}\mathbf{A} = \mathbf{a}_l + \mathbf{a}_r. \\ \mathbf{a}_l &= \frac{\hat{e}}{\sqrt{2}} a_l e^{-ik_l(z+ct)} + c.c \qquad (2.1) \\ \mathbf{a}_r &= -i\frac{\hat{e}}{\sqrt{2}} a_r e^{ik_r(z-ct)} + c.c \qquad (2.2) \\ a_{r,l} &= \frac{e}{mc^2 k_{r,l}} E_{r,l}(\mathbf{x}_\perp, z) \qquad (2.3) \end{aligned}$$

where, E_l and $k_l = 2\pi/\lambda_l$ are respectively the electric field and the wave number of the laser wiggler, while E_r, k_r and ω_r are respectively the electric field amplitude, the wave number and the frequency of the radiation field. Note that we are assuming at the moment a single frequency only for the radiation field E_r.

2.1.1 3D Hamiltonian

The time dependent Hamiltonian equations can be derived from the modified Hamiltonian principle [2] [11]

$$\delta \int_{t_1}^{t_2} (p_x dx/dt + p_y dy/dt + p_z dz/dt - H)dt = 0. \qquad (2.4)$$

Since we are interested in the systems evolution along the z axis , we change the independent variable from t to z, and using $H = E$ (where E is the total energy) we obtain:

$$\delta \int_{z_1}^{z_2} (p_x dx/dz + p_y dy/dz - H dt/dz + p_z)dz = 0. \qquad (2.5)$$

In eq. (2.5) $(x, p_x), (y, p_y), (t, -E)$ appear as a new canonical variables with respect to a new Hamiltonian $H_1 = -p_z$. Hence, we can write

$$\frac{dx}{dz} = -\frac{\partial p_z}{\partial p_x}, \quad \frac{dy}{dz} = -\frac{\partial p_z}{\partial p_y}, \quad \frac{dp_x}{dz} = \frac{\partial p_z}{\partial x}, \quad \frac{dp_y}{dz} = \frac{\partial p_z}{\partial y}, \qquad (2.6)$$

$$\frac{dt}{dz} = \frac{\partial p_z}{\partial E}, \quad \frac{dE}{dz} = -\frac{\partial p_z}{\partial t}, \qquad (2.7)$$

Let H be the relativistic Hamiltonian for one electron interacting with e.m. field

$$H = c\sqrt{\left[\mathbf{p} - \frac{e}{c}\mathbf{A}\right]^2 + m^2c^2} + eV = mc^2\gamma + eV = E. \qquad (2.8)$$

where $E_z = -dV/dz$. Assuming all the variables in unit of mc, the second equation in (2.7) become:

$$\frac{d\gamma}{dz} = -\left(\frac{\partial p_z}{\partial t} - e_z\right), \tag{2.9}$$

$$e_z = \frac{e}{mc^2}E_z, \quad e_z = -\frac{d\Phi}{dz}, \quad \Phi = \frac{e}{mc^2}V \tag{2.10}$$

and the new Hamiltonian is

$$H(x, P_x, y, P_y, ct, -\gamma; z) = -\sqrt{\gamma^2 - 1 - P_x^2 - P_y^2 - |\mathbf{a}|^2 + 2\ (P_x a_x + P_y a_y)} + \Phi \tag{2.11}$$

where $\mathbf{P}_\perp = \gamma\eta_\perp + \mathbf{a}$ and $H = -P_z$ are respectivelly the transverse and longitudinal momenta and $\eta_\perp = \mathrm{d}\mathbf{x}_\perp/\mathrm{d}z$. Here, we shall adopt, the following notations for the transverse coordinates: $(P_x, P_y) = \mathbf{P}_\perp$ and $(x, y) = \mathbf{x}_\perp$.

The above Hamiltonian can be simplified with a general assumption:

1. the fast oscillating term 2 $(\mathbf{P}_\perp \cdot \mathbf{a}_\perp)$ can be neglected,
2. The ultra-relativistic limit, $\gamma \gg \sqrt{1 + P_\perp^2 + |\mathbf{a}|^2}$ is assumed,
3. the small term $|\mathbf{a}_r|^2 \ll |\mathbf{a}_l|^2$ can be neglected.

with 1)-3), the Hamiltonian (2.11) is approximated by

$$H(\mathbf{x}_\perp, \mathbf{P}_\perp, ct, -\gamma; z) = -\gamma + \frac{1}{2\gamma}\left[1 + \mathbf{P}_\perp^2 + |\mathbf{a}_l|^2 - i\left(\mathbf{a}_l^* \mathbf{a}_r e^{i\theta} - c.c.\right)\right] + \Phi \tag{2.12}$$

where $\theta = (k_r + k_w)\, z - c\,(k_r - k_w)\, t$ is electron phase in the wiggler and radiation potential. From the Hamiltonian (2.12), we obtain the equations of motion:

$$\frac{dx}{dz} = \frac{\partial H}{\partial P_x} = \frac{P_x}{\gamma} \tag{2.13}$$

$$\frac{dy}{dz} = \frac{\partial H}{\partial P_y} = \frac{P_y}{\gamma} \tag{2.14}$$

$$\frac{dP_x}{dz} = -\frac{\partial H}{\partial x} = -\frac{1}{2\gamma}\frac{\partial}{\partial x}\left[|a_l|^2 - i\left(a_l^* a_r e^{i\theta} - c.c.\right)\right] \tag{2.15}$$

$$\frac{dP_y}{dz} = -\frac{\partial H}{\partial y} = -\frac{1}{2\gamma}\frac{\partial}{\partial y}\left[|a_l|^2 - i\left(a_l^* a_r e^{i\theta} - c.c.\right)\right] \tag{2.16}$$

$$c\frac{dt}{dz} = -\frac{\partial H}{\partial \gamma} = 1 + \frac{1}{2\gamma^2}\left[1 + P_x^2 + P_y^2 + |a_l|^2 - i\left(a_l^* a_r e^{i\theta} - c.c.\right)\right] \tag{2.17}$$

$$\frac{d\gamma}{dz} = \frac{\partial H}{\partial (ct)} + e_z = -\frac{k_r}{2\gamma}\left[a_l^* a_r e^{i\theta} + c.c.\right] + e_z. \tag{2.18}$$

Note that using the definition of the total momenta of an electron in e.m potential as defined in Eq.(2.8) normalized to mc we obtain $P_{tot} \equiv \beta_\perp \gamma = \eta_\perp \gamma - \mathbf{a}$, since the transverse velocity of the electron in the total vector potential can be written as follows

$$\beta_\perp = -\frac{\mathbf{a}}{\gamma} + \eta_\perp \tag{2.19}$$

In the paraxial approximation $\eta_\perp \ll 1$ then Eq.(2.19) is reduced to the familiar expression found in literature $\beta_\perp = -\mathbf{a}/\gamma$ [6, 57].

2.1.2 Maxwell evolution equations

The evolution of the e.m. transverse potential $\mathbf{a}_r$ and of the longitudinal electrostatic field $e_z = -\partial\Phi/\partial z$ can be determined from the rescaled Maxwell equation, expressed in the Coulomb (or radiation) Gauge ($\nabla \cdot \mathbf{a}_r = 0$):

$$\left(\nabla_\perp^2 + \frac{\partial^2}{\partial z^2} - \frac{1}{c^2}\frac{\partial^2}{\partial t^2}\right)\mathbf{a}_r = -\frac{\mu_0 e}{mc^2}\mathbf{J}_\perp \tag{2.20}$$

$$\left(\nabla_\perp^2 + \frac{\partial^2}{\partial z^2} - \frac{1}{c^2}\frac{\partial^2}{\partial t^2}\right)\Phi = -\frac{e}{\epsilon_0 mc^2}\varrho \tag{2.21}$$

where $\mathbf{J}_\perp$ and ϱ are respectively the transverse component of the electron current and the electron density (for a beam of N_e electrons):

$$\mathbf{J}_\perp = ec\sum_{j=1}^{N}\beta_\perp\,\delta^3\Big(\mathbf{x} - \mathbf{x}_j(t)\Big), \qquad \varrho = e\sum_{j=1}^{N}\delta^3\Big(\mathbf{x} - \mathbf{x}_j(t)\Big) \tag{2.22}$$

vector potential

The evolution of the transverse e.m. field can be obtained in the following way: substituting the electron current (2.22) in (2.20) we get

$$\left[D^+D^- + \nabla_\perp^2\right]\mathbf{a}_r = -\frac{4\pi e^2}{\epsilon_0 mc^2}\sum_{j=1}^{N}\beta_\perp\,\delta^2\left(\mathbf{x}_\perp - \mathbf{x}_{\perp j}(t)\right)\delta\left(z - z_j(t)\right) \tag{2.23}$$

where we have defined $D^\pm = \partial/\partial_z \pm \partial/c\partial_t$. The radiation beam which propagates in the opposite direction with respect to the electron motion can be neglected because it does not interact resonantly with the electrons. The complex amplitudes

$a_{r,l}(\mathbf{x}_\perp, z)$ is assumed to be a slowly varying function of the longitudinal coordinate z; this means that the fast variation on the radiation wavelength scale does not affect significantly the field enveloped amplitude. This is known as Slowly Varying Envelope Approximation (SVEA):

$$\left|\frac{\partial a_r(\mathbf{x}_\perp, z, t)}{\partial z}\right| \ll k_r \ |a_r(\mathbf{x}_\perp, z, t)| \tag{2.24}$$

$$\left|\frac{\partial a_r(\mathbf{x}_\perp, z, t)}{\partial t}\right| \ll \omega_r \ |a_r(\mathbf{x}_\perp, z, t)| \tag{2.25}$$

or shortly $|D^- a_r(\mathbf{x}_\perp, z, t)| \ll k_r \ |a_r(\mathbf{x}_\perp, z, t)|$.

Note that this approximation is based on the presence, in the FELs dynamics, of two different scales; one of the order of the radiation wavelength, and the other on the scale of the interaction length, normally three or four order of magnitude larger then the radiation wavelength. More precisely (as we will shown in sec.(2.2.3) the second scale length coincides with the "cooperation" length l_c; moreover, the possibility to separate the two different scales can be done clearly by using a multiple scaling approach which will be introduced in chapter.3.

Because of (SVEA), the second order derivatives in longitudinal and temporal coordinate in eq. (2.23) can be neglected

$$\left[D^+ D^- + \nabla_\perp^2\right] \mathbf{a}_r \simeq \frac{\hat{e}}{\sqrt{2}} 2k_r \ e^{ik_r(z-ct)} \left[D^+ + \frac{\nabla_\perp^2}{i2k_r}\right] a_r + c.c. \tag{2.26}$$

Substituting Eq.(2.19) for the electron transverse velocity $\beta_\perp$, and projecting the equation (2.23) on the $\hat{e}$ direction we obtain

$$\begin{aligned}\left[D^+ + \frac{\nabla_\perp^2}{i2k_r}\right] a_r \ &= \ \frac{2\pi e^2}{\epsilon_0 m c^2 k_r} \sum_{j=1}^{N_e} \left\{ \frac{a_l(\mathbf{x}_\perp, z) e^{i\theta} - i a_r(\mathbf{x}_\perp, z)}{\gamma_j} - \eta_\perp e^{ik(z-ct)} \right\} \times \\ &\quad \times \delta\left(\mathbf{x}_\perp - \mathbf{x}_{\perp j}(t)\right) \delta\left(z - z_j(t)\right)\end{aligned} \tag{2.27}$$

We average Eq.(2.27) on the fast scale θ, over a longitudinal dimension l_b several λ's long $l_b = s\lambda_r$ (where s is an integer number). In particular we integrate both

side of Eq.(2.27) by $1/l_b \int_R \chi_{\left[-s\frac{\lambda_r}{2}, s\frac{\lambda_r}{2}\right]}$ or similarly by $1/(k_r l_b) \int_R \chi_{[-s\pi, s\pi]}$ where $\chi_{[a,b]}$ is equal to one within $[a, b]$ and zero otherwise; then the right side of Eq.(2.27) becomes:

$$\frac{1}{k_r l_b} \int_R \mathrm{d}z \chi_{[-s\pi,s\pi]} \delta(z - z_j(t)) e^{-i\theta} = \frac{1}{l_b} \int_R \mathrm{d}\theta \chi_{[-s\pi,s\pi]} \delta(\theta - \theta_j(t)) e^{-i\theta} = \frac{1}{l_b} \chi_{[-s\pi,s\pi]} e^{-i\theta_j(t)}. \tag{2.28}$$

Then, defining the average over N_e electrons of generic function as:

$$\langle f(\xi, \mathbf{x}_\perp) \rangle_\perp = \frac{1}{N_e} \sum_{j=1}^{N_e} f(\xi_j, \mathbf{x}_\perp) \delta(\mathbf{x}_\perp - \mathbf{x}_{\perp j}(t)) \tag{2.29}$$

and the total longitudinal electron density $n_e = \chi_{[-s\pi,s\pi]} N_e / l_b$ we obtain:

$$\left[D^+ + \frac{\nabla_\perp^2}{i2k_r} \right] a_r = \frac{k}{2} \left(\frac{\omega_p}{\omega_r} \right)^2 \left\{ \left\langle \frac{a_l e^{-i\theta}}{\gamma} \right\rangle_\perp - i \left\langle \frac{a_r}{\gamma} \right\rangle_\perp - \left\langle \eta_\perp e^{-ik(z-ct)} \right\rangle_\perp \right\} \tag{2.30}$$

where $\omega_p \equiv \sqrt{e^2 n_\parallel / \epsilon_0 m_e}$ is the longitudinal plasma frequency.

The first average in Eq.(2.30) shows that the e.m. field evolution is ruled by the sum of all electrons phases. As it has been suggested in chapter. 1, this average term is zero if the electron phase is homogeneously distributed. Furthermore, if most of electron have the same phase then the average is different from zero, and it may influence the radiation dynamics. The last two terms on the right side of Eq.(2.30) are usually neglected; the second term is proportional to a_r which is smaller compared to a_l, while the third, is a fast oscillating term; then the evolution equation for the self consistence radiation field can be written in a more simple way:

$$\left[D^+ + \frac{\nabla_\perp^2}{i2k_r} \right] a_r = \frac{k}{2} \left(\frac{\omega_p}{\omega_r} \right)^2 \left\langle \frac{a_l e^{-i\theta}}{\gamma} \right\rangle_\perp \tag{2.31}$$

Space charge effects

Here we investigate the longitudinal micro-bunch space charge effects *i.e.* the repulsion between neighbours electrons at the scale of the radiation wavelength. The macro space charge effects are not considerate because of its effects becomes important only for very low value of the e-beam energy. A full investigation of the space charge effect would be useful because of the local repulsion between electrons could be inhibit the establishment of the micro bunching in the FEL process. However a

complete solution of the Eq.(2.21) is out of the aim of this thesis; rather, here, we investigate the paraxial approximation of Eq.(2.21), in which only the longitudinal micro-bunching space charge effects are considerate *i.e.* $\nabla_\perp = 0$. Similarly to the evolution equation of the e.m. vector potential a_r we assume the SVEA approximation in Eq.(2.21), then the evolution of the longitudinal electrostatic field in the paraxial approximation can be written as follows:

$$\left[\frac{\partial}{\partial z} + \frac{1}{c}\frac{\partial}{\partial t}\right] e_z = \frac{4\pi e^2}{mc^2}\frac{n_e}{N_e}\sum_{j=1}^{N}\delta\left(\theta - \theta_j\right) \tag{2.32}$$

Neglecting the time dependence and Expanding the electron density in a Fourier series with respect to θ, we obtain

$$\frac{\partial e_z}{\partial z} = \frac{4\pi n_e e^2}{mc^2}\sum_{n=1}^{\infty} e^{in\theta}\langle e^{-in\theta}\rangle + c.c. \tag{2.33}$$

where $\langle f(\xi)\rangle = 1/N_e \sum_{j=1}^{N_e} f(\xi_j)$. Finally, the longitudinal electrostatic field is:

$$e_z(\theta, n) = k_r\left(\frac{\omega_p}{\omega}\right)^2 \sum_{n=1}^{\infty}\frac{e^{in\theta}\langle e^{-in\theta}\rangle}{in} + c.c. \tag{2.34}$$

Note that the first harmonic term (*i.e.* $n = 1$) is proportional to the bunching factor $B = \langle e^{-i\theta}\rangle$. Clearly, the longitudinal space-charge force is appreciable only if the electron density is large enough. Similarly to the transverse e.m. field, the e_z-field is proportional to the sum over the electron phases. This fact shows that the space-charge effects are negligible also if the electron phase is homogeneously distribute, such a way that the average is zero. Note also that if we sum the space-charge force over the electrons, the result is zero; this means that, it is an internal force with respect to the electron system and its macro effects can be negligible as above mentioned. As we have anticipate this treatment of the space charge effects is only a preliminary investigation, then for simplicity only the first harmonic term ($n = 1$) will be considerate.

$$e_z(\theta) = 2k_r\left(\frac{\omega_p}{\omega}\right)^2 \langle e^{-i\theta}\rangle \sin(\theta) \tag{2.35}$$

Eq. (2.31) and Eqs.(2.13-2.18) together with Eq.(2.35) form a self-consistent scheme for the 3D dynamics of N_e electrons interacting with radiation and laser wiggler fields.

The basic physics of FEL can be understood more clearly in the 1D scheme approximation. For this reason, before starting to analyze the full 3D model, i will review the one dimensional theory and its result.

2.2 1D FEL Equations

The 1D approach is exhaustive for almost everything of the FELs physics, moreover, at the same time it offers a very clear simple picture of the basic mechanism of the FEL process. In the previous section a set of closed 3D equations representing the evolution of the whole system has been obtained (2.13-2.18,2.31). The one-dimensional approximation consists in neglecting any dependence on transverse spatial coordinates (eq.2.13-2.16), so that our physical quantities depend on propagation direction (z) only, and time t. The dynamical variables are the electron phase θ, the electron energy γ and the dimensionless radiation field amplitude a_r. The electron dynamic equations (2.17,2.18) in the 1D approximation becomes:

$$c\frac{dt}{dz} = 1 + \frac{1}{2\gamma^2}\left[1 + |a_l|^2 - ia_l\left(a_r e^{i\theta} - c.c.\right)\right] \tag{2.36}$$

$$\frac{d\gamma}{dz} = -\frac{a_l k_r}{2\gamma}\left[a_r e^{i\theta} + c.c.\right] + e_z(\theta). \tag{2.37}$$

The 1D field evolution can be obtained neglecting the transverse dependence in the radiation field $a_r(z, \mathbf{x}_\perp) = a_r(z)$ and assuming magnetic wiggler $a_l(z, \mathbf{x}_\perp) = a_w$; then integrating both side of Eq.(2.31) by $1/\Sigma \int_{R^2} \mathrm{d}\mathbf{x}_\perp$, where Σ is the transverse section of the beam, we obtain

$$\left(\frac{\partial}{\partial z} + \frac{1}{c}\frac{\partial}{\partial t}\right) a_r = \frac{k}{2}\left(\frac{\omega_p}{\omega_r}\right)^2 a_w \left\langle \frac{e^{-i\theta}}{\gamma} \right\rangle \tag{2.38}$$

where the plasma frequency is $\omega_p \equiv \sqrt{e^2 n_e/\epsilon_0 m_e}$ with $n_e = n_\parallel/\Sigma$ ($n_\parallel = N_e/l_b$).

The evolution equation for each electron phase can be obtained from Eq (2.36)

$$\frac{d\theta}{dz} = (k_r + k_w) - k_r c\frac{dt}{dz} = k_w\left(\frac{\gamma^2 - \gamma_r^2}{\gamma^2}\right) \tag{2.39}$$

where $\gamma_r = k_r(1 + a_w^2)/2k_w$ is the resonant energy introduced in the previous section (1.12).

We assume that during the interaction with the e.m. field, the energy of each electron remains close to the resonant energy, $\gamma \simeq \gamma_r$, this assumption is known as the "Compton limit" *i.e.*

$$\frac{\gamma_j - \gamma_r}{\gamma_j} \simeq \frac{\gamma_j - \gamma_r}{\gamma_r} \ll 1 \tag{2.40}$$

With this assumption and taking into account the multi particle nature of the process, we define a new energy-variable $\eta_j = \dfrac{\gamma_j - \gamma_r}{\gamma_r}$. The phase (2.37), the energy (2.38) of each electron, the e.m. field (2.39) and the space charge terms (2.35) give rise to a close system of $2N_e + 1$ equations

$$\frac{d\theta_j}{dz} = 2k_w\eta_j \tag{2.41}$$

$$\frac{d\eta_j}{dz} = -\frac{a_w k}{2\gamma_r^2}\left[a_r e^{i\theta_j} + c.c.\right] + 2k_r\left(\frac{\omega_p}{\omega}\right)^2 \langle e^{-i\theta}\rangle \sin(\theta_j) \tag{2.42}$$

$$\left(\frac{\partial}{\partial z} + \frac{1}{c}\frac{\partial}{\partial t}\right) a_r = \frac{k a_w}{2\gamma_r}\left(\frac{\omega_p}{\omega_r}\right)^2 \langle e^{-i\theta}\rangle \tag{2.43}$$

Notice that we have still neglected in Eq.(2.43) the term proportional to a_r. Moreover, because of the Compton limit, γ can be carry out from the average in the field equation, so that $\langle e^{-i\theta}/\gamma\rangle \simeq \langle e^{-i\theta}\rangle/\gamma_r$.

Universal Scaling

One of the most profit features of the 1D FEL model is the possibility to introduce (2.41,2.42,2.43) a dimensionless scaling for all quantities so that no experimental parameters appeare explicitly in the equations. This allows a general analysis of the FEL interaction independently of the particular set of parameter and a simple interpretation of the basic physics of the process.

We start defining the fundamental FEL-parameter

$$\rho = \frac{1}{\gamma_r}\left(\frac{a_w\omega_p}{4k_w c}\right)^{2/3}. \tag{2.44}$$

In terms of ρ the system of coupled evolution equations (2.41,2.42,2.43) can be set in a dimensionless form by introducing the following variables and parameters.

$$\bar{p}_j = \frac{\eta_j}{\rho} \qquad A_r = \frac{\omega}{\omega_p\sqrt{\rho\gamma_r}} a_r \tag{2.45}$$

$$\bar{z} = z/l_g \quad \bar{t} = t/l_g \qquad l_g = 1/2k_w\rho \tag{2.46}$$

where l_g is the gain length. Note that in this universal scaling

$$\eta = \rho|\tilde{A}_r|^2 = \frac{\epsilon_0|E_0|^2}{mc^2\gamma_r n_e} = P_{rad}/P_{beam}, \qquad (\tilde{A}_r = (e/mc^2)A_r). \tag{2.47}$$

is the ratio between the e.m. field and the electron beam energy, *i.e.* the efficiency of the FEL.

Using this "Universal scaling" we obtain:

$$\frac{d}{dz}\theta_j = \bar{p}_j \tag{2.48}$$

$$\frac{d}{dz}\bar{p}_j = -\left[A_r e^{i\theta_j} + c.c.\right] + \varsigma\langle e^{-i\theta}\rangle \sin(\theta_j) \tag{2.49}$$

$$\left(\frac{\partial}{\partial\bar{z}} + \frac{1}{c}\frac{\partial}{\partial\bar{t}}\right) A_r = \langle e^{-i\theta}\rangle \tag{2.50}$$

where $\varsigma = 4\rho(1 + a_w^2)/a_w^2$ is the space-charge parameter. Note that the ς is proportional to ρ, which is much less than unit in the Compton limit (see Eq.(2.40) and Eq.(2.82)), so we will neglect it.

$$\frac{d}{dz}\theta_j = \bar{p}_j \tag{2.51}$$

$$\frac{d}{dz}\bar{p}_j = -\left[A_r e^{i\theta_j} + c.c.\right] \tag{2.52}$$

$$\left(\frac{\partial}{\partial\bar{z}} + \frac{1}{c}\frac{\partial}{\partial\bar{t}}\right) A_r = \langle e^{-i\theta}\rangle \tag{2.53}$$

As we have anticipate before the 1D FEL equations assume a dimensionless form, with the advantage of being solvable without having to specify the operating parameters. Once solved, the scaling can be reversed to find the real physical quantities needed for a particular experimental set-up.

The 1D FEL equations (2.51-2.53) form a Maxwell-pendulum model: in fact, writing explicitly the real and imaginary parts of the field $A_r = |A_r|\exp(i\phi)$ we get

$$\frac{d^2\theta_j}{d\bar{z}^2} = -2|A_r|\cos(\theta_j + \phi) \tag{2.54}$$

Of course, this equation greatly differs from an ordinary pendulum since, amplitude and phase off the field , are not constant, but their evolution is determined by Eq.(2.53).

2.2.1 Steady State regime

The set of equations (2.51-2.53) can be written in a simple way operating a standard transformation of coordinates

$$\bar{z} = \bar{z}, \quad \bar{z}_1 = \bar{z} - \langle v_\parallel \rangle \bar{t} \tag{2.55}$$

The differential operators of the FEL equations change as follows:

$$\frac{d}{d\bar{z}} \simeq \frac{\partial}{\partial \bar{z}} + \frac{1}{\langle v_\parallel \rangle} \frac{\partial}{\partial \bar{t}} \quad \Rightarrow \quad \frac{\partial}{\partial \bar{z}} \tag{2.56}$$

$$\frac{\partial}{\partial \bar{z}} + \frac{1}{c} \frac{\partial}{\partial \bar{t}} \quad \Rightarrow \quad \frac{\partial}{\partial \bar{z}} + \left(1 - \langle \beta_\parallel \rangle\right) \frac{\partial}{\partial \bar{z}_1} \tag{2.57}$$

where in the first step of the eq. (2.56) we assumed $\bar{z} \simeq \langle v_\parallel \rangle \bar{t}$ with ($\langle v_\parallel \rangle$ the longitudinal electron average velocity).

The relation (2.57) shows that the time derivative can be neglected if the difference between the electrons velocity and the speed of light is unimportant ($1 - \langle \beta_\parallel \rangle \simeq 0 \rightarrow \langle v_\parallel \rangle \simeq c$) or alternatively if the interaction time is small compared with the slippage time. This limit can be easily understood from equation (2.57) by normalizing $\bar{z}$ to the total length of the wiggler L_w and $\bar{t}$ to the electron pulse time $\tau_b = l_b / \langle v_\parallel \rangle$; the ratio between coefficients of the time derivative and the space derivative becomes:

$$\frac{L_w(1 - \langle \beta_\parallel \rangle)}{l_b \langle \beta_\parallel \rangle} = \frac{N_w \lambda_r}{l_b} = \frac{l_s}{l_b} = S \tag{2.58}$$

where we have used the resonant condition $\lambda_r = \lambda_w(1 - \langle \beta_\parallel \rangle)/\langle \beta_\parallel \rangle$.

If the slippage parameter S is much smaller than one, the time derivative can be neglected (*steady state regime*):

$$\frac{d\theta_j}{d\bar{z}} = \bar{p}_j \tag{2.59}$$

$$\frac{d\bar{p}_j}{d\bar{z}} = -\left[A_r e^{i\theta_j} + c.c.\right] \tag{2.60}$$

$$\frac{dA_r}{d\bar{z}} = \langle e^{-i\theta} \rangle. \tag{2.61}$$

Constant of motion

The set of equations (2.59-2.61) admits two constants of motion. The first can be obtained differentiating the average momentum

$$\frac{d}{d\bar{z}}\sum_{j=1}^{N_e}\bar{p}_j = -N_e\frac{d}{d\bar{z}}|A_r|^2 \quad \rightarrow \quad \langle\bar{p}\rangle + |A_r|^2 = \mathrm{C} \tag{2.62}$$

where C is a constant. The meaning of this conservation law becomes clear if we return to physical quantity, using the relation (2.45) and (2.47):

$$\langle\bar{p}\rangle + |A_r|^2 = \frac{1}{N_e}\sum_{j=1}^{N_e}\frac{\Delta\gamma_j}{\rho\gamma_r} + \frac{\epsilon_0|E_0|^2}{mc^2\gamma_r n_e\rho} \rightarrow \; mc^2\sum_{j=1}^{N_e}\Delta\gamma_j + \epsilon_0 V|E_0|^2 = \mathrm{C'} \tag{2.63}$$

where $n_e = N_e/V$.

The above relation agrees with the energy conservation low (the energy of the wiggler has been supposed constant) and shows that the energy of the emitted radiation field is extracted from the kinetic energy of the electron beam.

The second constant of motion is the total Hamiltonian of the system with $2N_e+1$ variables:

$$H(\theta_j, \bar{p}_j, \mathrm{Re}(A_r), \mathrm{Im}(A_r))_{j=1,N_e} = \sum_{j=1}^{N_e}\frac{\bar{p}_j^2}{2} - i\sum_{j=1}^{N_e}\left[A_r e^{i\theta_j} + c.c.\right] \tag{2.64}$$

This Hamiltonian can be written in a more compact form in which, the real and immaginary part of the radiation field are included as canonical variable $(\theta_0, \bar{p}_0)$. In fact defining $A_r = (\theta_0 + i\bar{p}_0)/\sqrt{2N_e}$, we obtain:

$$H(\theta_j, \bar{p}_j)_{j=0,N_e} = \sum_{j=1}^{N_e}\frac{\bar{p}^2}{2} - \sqrt{\frac{2}{N_e}}\sum_{j=1}^{N_e}\left[\theta_0\mathrm{sin}(\theta_j) + \bar{p}_0\mathrm{cos}(\theta_j)\right] \tag{2.65}$$

which gives the correct equations of motion (2.59),(2.60) and (2.61)

$$\frac{d\theta_j}{d\bar{z}} = \frac{\partial H}{\partial\bar{p}_j} \quad \frac{d\bar{p}_j}{d\bar{z}} = -\frac{\partial H}{\partial\theta_j} \qquad \text{for} \;\; j = 0, N_e \tag{2.66}$$

2.2.2 Linear analysis

It is well known that at the wiggler entrance ($\bar{z} = 0$) the electron beam exhibits a narrow longitudinal energy distribution. For simplicity, we assume here a Dirac

Delta distribution *i.e.* each electron has the same initial energy $\gamma_j(\bar{z}=0)=\gamma_0$, so that the dimensionless momentum $\bar{p}$ at time $\bar{z}=0$ is given by

$$\bar{p}(0)=\frac{\gamma_0-\gamma_r}{\rho\gamma_r}\equiv\delta \tag{2.67}$$

We define this value as the *detuning parameter* δ. It is particularly useful to redefine our variables so that the initial condition for $\bar{p}$ is zero:

$$\begin{aligned}\bar{p}'_j &= \bar{p}_j-\delta\\ \theta'_j &= \theta_j-\delta\bar{z}\\ A'_r &= A_r e^{i\delta\bar{z}}\end{aligned} \tag{2.68}$$

In this way the detuning parameter appears explicitly on the equations, which (dropping the primes) read:

$$\frac{d\theta_j}{d\bar{z}} = \bar{p}_j \tag{2.69}$$

$$\frac{d\bar{p}_j}{d\bar{z}} = -\left[A_r e^{i\theta_j}+c.c.\right] \tag{2.70}$$

$$\frac{dA_r}{d\bar{z}} = \langle e^{-i\theta}\rangle + i\delta A_r \tag{2.71}$$

This set of equations can be linearized in terms of three collective variables [14]

$$\mathcal{A} = A_r \quad \text{field amplitude} \tag{2.72}$$

$$\mathcal{B} = \langle e^{-i\theta}\rangle \quad \text{bunching} \tag{2.73}$$

$$\mathcal{P} = \langle \bar{p}e^{-i\theta}\rangle \quad \text{momentum bunching} \tag{2.74}$$

neglecting the second order terms $\langle e^{-i2\theta}\rangle$ and $\langle \bar{p}^2 e^{-i\theta}\rangle$ we obtain a close set of linear equations

$$\frac{d\mathcal{B}}{d\bar{z}} = -i\mathcal{P} \tag{2.75}$$

$$\frac{d\mathcal{P}}{d\bar{z}} = \mathcal{A} \tag{2.76}$$

$$\frac{d\mathcal{A}}{d\bar{z}} = \mathcal{B}+i\delta\mathcal{A} \tag{2.77}$$

which can be reduced to

$$\frac{d^3\mathcal{A}}{d\bar{z}^3} + i\delta\frac{d^2\mathcal{A}}{d\bar{z}^2} - i\mathcal{A} = 0 \tag{2.78}$$

Assuming a solution of the form $\mathcal{A} \propto e^{-i\lambda\bar{z}}$ one obtains the following dispersion relation which rules the stability of the system:

$$\lambda^3 - \delta\lambda^2 + 1 = 0 \tag{2.79}$$

when Eq.(2.79) has three real roots, then the system is stable, but if it has one real root and two complex-conjugate ones, then one of the latter will cause an exponential growth of the field until non-linear effects come into play.

If instead of choosing an ideal cold beam, we assume an initial energy distribution $f(p_0)$ with a finite width, then (2.79) is formalized by

$$\lambda - \delta + \int_{-\infty}^{+\infty} \frac{f(p_0)}{(\lambda + p_0)^2}\,\mathrm{d}p_0 = 0 \tag{2.80}$$

The above integral can analytically solved for instance in the case of a rectangular or Lorenz distribution [32]. for the rectangular case with half-width $\delta\gamma$, we obtain:

$$(\lambda - \delta)(\lambda^2 - \mu^2) + 1 = 0 \tag{2.81}$$

where $\mu \equiv \delta\gamma/\rho\gamma_r$ is the *energy spread parameter*. As the exponential behavior of $A_r(\bar{z})$ is determined by the imaginary part of the complex root of Eq.(2.81), it's relevant to plot it as a function of the detuning parameter δ for different values of the energy spread μ. Fig. 2.1 suggests some immediate considerations:

1. given a spread μ, the optimal gain occurs for the specific detuning shift
2. Energy spread ($\mu > 0$) lowers the growth rate, and shift the resonance to $\delta = \mu$
3. The width of the gain course shrink as $\sqrt{\mu}$.

Coming back to physical variables, this means that in order to preserve the exponential gain, the e-beam must satisfy:

$$\frac{\delta\gamma}{\gamma_r} \;\leq\; \rho \tag{2.82}$$

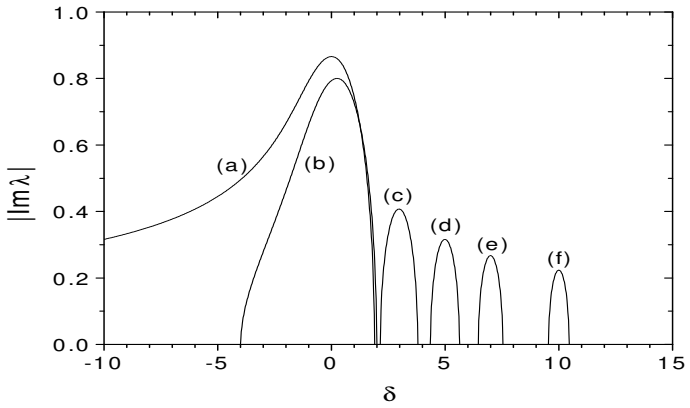

Figure 2.1: Immaginary part $|Im\lambda|$ vs. the detuning parameter for different values of μ: (a) $\mu = 0 \rightarrow$ (f) $\mu = 10$.

The solution for the cold beam case ($\mu = 0$) at resonance ($\delta = 0$) is:

$$\lambda^3 = -1 \quad \Rightarrow \quad \lambda_1 = 1 \ , \ \lambda_2 = \frac{-1 - \sqrt{3}i}{2}, \ \lambda_3 = \frac{-1 + \sqrt{3}i}{2} \tag{2.83}$$

and the form of the scaled field intensity is

$$\mathcal{A}(\bar{z}) = \frac{1}{3} \sum_{i=1}^{3} \left(\mathcal{A}(0) - i\frac{\mathcal{B}(0)}{\lambda_i} - i\mathcal{P}(0)\lambda_i \right) e^{-i\lambda_i \bar{z}} \tag{2.84}$$

For $\bar{z} \gg 1$ (exponential growth regime) the growing mode λ_3 dominates over the oscillatory λ_1 and decaying λ_2 modes, so that

$$\mathcal{A}(\bar{z}) \simeq \frac{1}{3} \left(\mathcal{A}(0) - i\frac{\mathcal{B}(0)}{\lambda_3} - i\mathcal{P}(0)\lambda_i \right) e^{-i\lambda_3 \bar{z}} \tag{2.85}$$

The first term in the bracket corresponds to the amplification of an external input signal, while the second and the third terms correspond initial coherent bunching.

As it result from linear analysis an exponential instability of the emitted radiation field takes place in the FEL, until non-linear effect moving to saturation this growth. The linear solution of the exponential growing mode fits well the numerical solution of the full non-linear system (2.59-2.61).

In fig. (2.2) is plotted the radiated power, as obtained from the numerical integration of the 1D non-linear equations. The figure shows that after an initial lethargy, the field power grows exponentially, reaching a saturation in few gain lengths. After

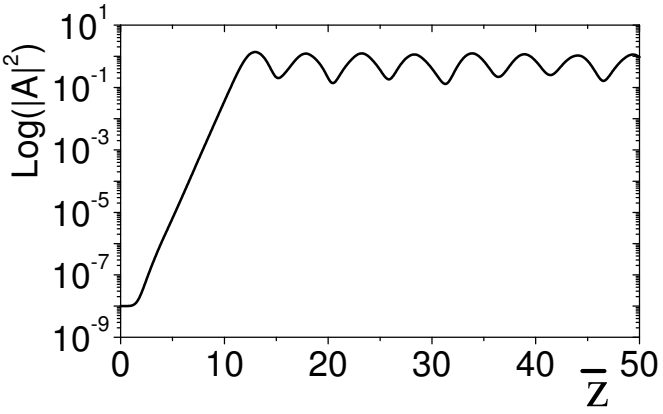

Figure 2.2: Radiation field intensity vs $\bar{z}$ (semi-log scale)

saturation, the amplification process is replaced by an oscillatory energy exchange between the electrons and the radiation field. In the case of a seed signal intensity $|A_0|^2$, the asymptotic linear solution is given by the (2.85)

$$|\mathcal{A}|^2 \simeq \frac{1}{9}|A_0|^2 \exp\left[\sqrt{3}\frac{z}{l_g}\right], \tag{2.86}$$

so that the l_g as defined in Eq(2.46) corresponds effectively to the FEL gain length. Since saturation occurs at $|\mathcal{A}|^2 \simeq 1$, from the eq. (2.86) we can estimate the saturation length as

$$z_{sat} \simeq \frac{l_g}{\sqrt{3}} \ln\left(\frac{9}{|A_0|^2}\right) \propto \frac{\lambda_w}{\rho} \tag{2.87}$$

Furthermore the result $|\mathcal{A}|^2 \simeq 1$ means that the saturation value is independent of the initial condition. Since we know that $|\mathcal{A}|^2$ is proportional to $|E|^2/\rho n_e$, and $\rho \propto n^{1/3}$ then

$$|\mathcal{A}|^2 \propto \frac{|E|^2}{n_e^{4/3}} \Rightarrow |E|^2 \propto n_e^{4/3} \tag{2.88}$$

i.e. the intensity is proportional to $n_e^{4/3}$ instead of n_e: this implies the existence of a collective behavior in the electron beam.

The independence of the saturated field amplitude on its initial value gives us another important information, related again to the importance of the ρ parameter. In the (2.47) we have defined the efficiency η of the FEL as $\eta = \rho|\mathcal{A}|^2$ then the measure of FEL efficiency will be given by ρ.

In this section we have shown that in the context of the 1D theory, ρ is the only parameter wich give the constraints on the FEL.

$$\begin{cases} \Delta\gamma/\gamma \simeq \rho & \text{Energy spread} \\ \eta = P_{rad}/P_{beam} \simeq \rho & \text{Efficiency} \\ l_g \propto 1/\rho & \text{Gain length} \end{cases} \tag{2.89}$$

2.2.3 Superadiant regime

The steady-state regime that we just described is based on the assumption that the slippage is negligible ($S \ll 1$ *i.e.* $l_s \ll l_b$): the wiggler is not long enough to appreciate the difference in velocity between the electrons and the radiation, so that all sections of the electron beam evolved almost identically and the peak power of radiation scale as $n_e^{4/3}$. When slippage is taken into account, the FEL can operate in a different regime of cooperative emission, the superradiant regime [15, 16, 17, 6, 7], where the peak power scale as n_e^2.

the slippage modifies substantially the interaction process between the radiation and the electron: in fact, the radiation propagates with respect to the electrons, interacting with different sections of the electron beam, so that there is a region, near the trailing edge of the electron pulse and of length l_s, where the electrons emit radiation without being affected by the radiation produced by the other electrons behind them.

Let us introduce a new characteristic length which will be useful for the analysis of the propagation effect, the cooperation length,

$$l_c = \frac{\lambda_r}{4\pi\rho} \tag{2.90}$$

its meaning can be better understood using the resonant relation (1.4), which allows to write it in terms of the relativistic parameter $\beta_\parallel$:

$$l_c = l_g \frac{1 - \langle\beta_\parallel\rangle}{\langle\beta_\parallel\rangle} = \begin{cases} 0 & \text{if } \langle\beta_\parallel\rangle \to 1 \\ \infty & \text{if } \langle\beta_\parallel\rangle \to 0 \end{cases} \tag{2.91}$$

if the velocity difference between the electrons and the radiation field is unimportant, then l_c tends to zero, otherwise the propagation effect becomes relevant, and l_c increases.

We define the electron pulse to be long or short with respect to the cooperation length. In general, if the electron pulse is long enough ($l_b \gg l_c$), the superradiant and the steady state instability will be present together: superradiance occurs in the region near the trailing edge of the electron pulse (slippage region) while the steady-state emission occurs in the remaining part of the beam, this is named "strong superradiance" because the peak power is greater with respect to the steady state regime. However in the short-bunch regime ($l_b \ll l_c$) the radiation emitted by electrons escapes from the electron pulse in a length shorter than the synchrotron period, so that the steady-state saturation can never occurs: this regime is called " weak superradiance" because the peak power il lower with respect to the steady state regime.

It's possible also to observe pure superradiance by tuning the system out of resonance: in fact, while the steady-state regime needs to resonance to produce exponential gain, Superradiance be close always on resonance with the electrons, since coherent spontaneous emission. So, when the system is detuned in such a way to prevent steady-state radiation, the superradiant instability travels forward unperturbed electrons, extracting energy from them with an even greater efficiency than in the steady-state resonance.

2.2.4 SASE regime

The **S***elf* **A***mplified* **S***pontaneous* **E***mission* (**SASE**) regime for a FEL is made up of three basic ingredient[17]:

1. high gain instability
2. propagation effect *i.e.* "slippage"
3. start-up from noise

The first experimental observation of the high-gain regime, also starting from noise, was carried out in the microwave range using a wave guide in the Livermore experiment [67]. Presently, short wavelength FEL, which amplify incoherent shot noise

via SASE are of greater interest worldwide as a potential source of ulra bright coherent X-ray radiation [68, 69]. Moreover the SASE FEL in the X-ray region is the goal of several project, such as the LCLS [53] at Standford, USA, and XFEL[54] in Hamburg, Germany. here we review the most important features of the SASE regime, which is characterize by the following characteristic length:

$$\begin{cases} l_b & \text{Bunch length} \\ l_c & \text{Cooperation length} \\ l_b & \text{Gain length} \end{cases} \tag{2.92}$$

An important parameter determining the evolution of the system is given by the ratio between l_b and l_c (the number of cooperation lengths in a bunch length), If the ratio l_b to l_c is greater than 2π (long bunch case) then the the radiation pulse contain many spikes each one having a maximum duration corresponding to about $2\pi l_c$ with width of order of $1/l_b$ and large intensity fluctuation. On the contrary if the ratio l_b to l_c is equal or less then 2π (short bunch case) only one single radiation pulse is present in this case, with no inner spike. In both cases the superradiant case occurs for sufficiently long ondulators. The final result is an almost chaotic temporal pulse structure with a broad spectral width and with a number of spikes of the order of the number of cooperation lengths in a electron bunch.

Finally we have been understood that in order to model correctly this spiking behavior, we must take into account not only the slippage between the radiation and electron pulse, but also the finite bunch length; the electron bunch behaves as a l_b/l_c statistical independent zone each of that give rise to a superradiant spike which growth and narrow extracting energy from electron within a cooperation length. In the chapter 4 we will shown that in the novel Quantum SASE regime [30] a completely different behavior occurs, the "classical" random spiking behavior almost disappears and a strong narrowing of the spectrum occours. This new phenomenon is called " Quantum purification ".

2.3 From 1D to 3D

The description of an N_e electron beam can be made introducing, in the transverse phase space $(\mathbf{x}_\perp, \eta_\perp)$ (where $\eta_\perp = \dfrac{\mathrm{d}\mathbf{x}_\perp}{\mathrm{d}z}$ and z is the longitudinal coordinat along

the beam direction), the second order moments; as for istance the rms beam size $\sigma_e^2 = \langle \mathbf{x}_\perp^2 \rangle$, the rms beam angular divergenze $\sigma'^2_e = \langle \eta_\perp^2 \rangle$ and the mixed terms $\langle \mathbf{x}_\perp \cdot \eta_\perp \rangle$. The rms beam size (for example in x direction) evolvs in the free space as:

$$\sigma_e(z) = \sqrt{\epsilon_x \left(\beta^* + \frac{z^2}{\beta^*} \right)} \tag{2.93}$$

where $\beta_x^* = \langle x^2 \rangle / \epsilon_x$ is one of the twiss parameters and $\epsilon_x = \sqrt{\langle x^2 \rangle \langle \eta_x^2 \rangle - \langle x \eta_x \rangle}$ is the rms emittance, that is conserved in the free space evolution and for a linear transport system. $z = 0$ correspond to the point where $\langle x \cdot \eta_x \rangle = 0$ and the beam size is minimum ("beam waist"). The radiation beam can be describes in a similar way, in fact, using the free space diffraction formula is possible to show that the radiation Gaussian beam size evolves as:

$$\sigma_r(z) = \sqrt{\frac{\lambda_r}{4\pi} \left(Z_r + \frac{z^2}{Z_r} \right)} \tag{2.94}$$

where $Z_r = 4\pi\sigma^2/\lambda_r$ is the Rayleigh range. The evolution equation of the electron beam size and of the radiation beam field are formally equivalent if we identify $\varepsilon_{rad} = \lambda_r / 4\pi$ as a rms emittance of the Gaussian radiation beam and β^* as the Rayleigh range of the electron beam. However the evolution in a free space of the conterpropagating laser beam size $\sigma_l(z)$ follow the same relation of eq.(2.94) where instead of Z_r we subsitute $Z_l = 4\pi\sigma_l^2/\lambda_l$ where λ_l is the laser beam wavelength.

2.3.1 Transverse effects

From this picture we can set some resonable condition that must be necessary satisfied in a 3D geometry:

1. The matching (*i.e.* the superposition) between electron and radiation beams requires that the beam waist and the Rayleigh range of each other must be comparable.

$$\sigma_e \simeq \sigma_r \tag{2.95}$$

$$\beta^* \simeq Z_r \quad \rightarrow \quad k_r \epsilon_r \simeq \frac{1}{2} \left(\frac{\sigma_e}{\sigma_r} \right)^2 \tag{2.96}$$

2. The electron beam should be contained in the laser beam and the electron beam should not diverge appreciably in a Rayleigh range Z_l

$$\sigma_e \leq \sigma_l \tag{2.97}$$

$$\beta^* \leq Z_l \quad \rightarrow \quad k_l \epsilon_r \leq \frac{1}{2}\left(\frac{\sigma_e}{\sigma_l}\right)^2 \tag{2.98}$$

The condition (2.96) is known as the "Pellegrini criterium" and it will be shown that it can be relaxed in particular condition depending on the ratio between the electron and the radiation beam size (2.95). Conditions (2.97) and (2.98) are more stringent and concern the matching between the e-beam and the laser wiggler profile. If conditions (2.97) and (2.98) are violated inhibition of the gain process occurs. If we use a magnetic wiggler instead of the laser wiggler then the homogeneous condition (2.98) can be written as $k_w \epsilon_r < 1$ that is usually satisfied. In fact, for a wiggler period of order $\lambda_w = 1$cm and emittance $\varepsilon_r \simeq 10^{-7}$m-rad, $k_w \epsilon_r \simeq 10^{-4}$. A FEL experiment with a laser wiggler does not require a focusing system for the electron beam , since the interaction between electrons and laser beam occurs in the free space near the beam waist zone *i.e.* the interaction length L_{int} is of the order of few laser Rayleigh range ($L_{int} \simeq Z_l$), Hence the gain process occurs if the condition (2.98) is satisfied. Furthermore if a magneto static wiggler instead of a laser wiggler is used, then the interaction length is usually more than one meter, and the electron beam must be conveniently focused to keep a nearly constant beam size. A linear magneto static wiggler provides a "natural" focusing effect in one transverse direction and needs external focusing (by quadrupole magnets) on the other transverse direction. This focusing force induces an oscillation of the electron motion with a frequency much smaller than the ondulator frequency λ_w. For a matched beam in two plane the beam size (averaged over the wiggler period λ_w) remains constant along the wiggler, while individual electron perform a periodic transverse motion, just called "betatron motion".

A potential deleterious effect for the FEL is the apparent energy spread induced by a betatron motion *i.e.* by the transverse velocities of the electron. The relation between the energy spread and the transverse velocity can be made taking into account the transverse dimension in the resonant condition; it straightforward demonstrate that an observer far away in the $\eta_\perp$ direction from the axis sees a

different period *i.e.*

$$\lambda_r^{\perp} = \frac{\lambda_w}{2\gamma_r^2}\left\{1 + a_w^2 + \eta_{\perp}^2\gamma^2\right\} \tag{2.99}$$

where λ_w is replaced by $\lambda_l/2$ for a laser wiggler. The above relation agrees with the resonance condition (1.11) when the angle of the observer tends to zero. From the transverse resonant relation (2.99) and using the relation $\Delta\gamma/\gamma \simeq \Delta\lambda/2\lambda$, we can argue that the energy spread normalized to the FEL parameter ρ has the following contributions:

1. The different longitudinal momentum distribution, (see Eq. 2.82)

$$\left(\frac{\Delta\gamma}{\rho\ \gamma_r}\right)_{1D} \simeq 1 \tag{2.100}$$

2. The off-axis variation of the wiggler parameter

$$\left(\frac{\Delta\gamma}{\rho\ \gamma_r}\right)_{a_w} \simeq \frac{1}{2\rho}\frac{\Delta a_w^2}{1 + a_w^2} \tag{2.101}$$

3. The angular divergence of the beam

$$\left(\frac{\Delta\gamma}{\rho\ \gamma_r}\right)_{\perp} \simeq \frac{1}{2\rho}\frac{\eta_{\perp}^2\gamma_r^2}{1 + a_w^2} \tag{2.102}$$

These effects are called "non homogeneous effects"and give rise to a broadening of the resonant condition.

2.3.2 Full 3D Model

A most useful scheme for modelling a beam of N_e electrons interacting with e.m. field is the Maxwell-Vlasov scheme. Following this scheme we introduce the transverse phase space variables $(\mathbf{x}_{\perp}, \eta_{\perp})$ ($\eta_{\perp} = \mathrm{d}\mathbf{x}_{\perp}/dz$) and the longitudinal phase space variables $(\theta, \bar{p})$. The electron distribution, for a given phase and longitudinal momentum, in the transverse phase-space, can be described by a distribution function $F(\mathbf{x}_{\perp}, \eta_{\perp})$ with a non negative value equal to the number of electrons per unit area at the transverse phase space point $(\mathbf{x}_{\perp}, \eta_{\perp})$. A Gaussian distribution function is normally adopted for its simplicity. Hence, the number of electrons within a $\mathrm{d}\mathbf{x}_{\perp}\mathrm{d}\eta_{\perp}$ at the beam waist is (such that $\langle \mathbf{x}_{\perp} \cdot \eta_{\perp} \rangle = 0$)

$$F(\mathbf{x}_{\perp}, \eta_{\perp})\ \mathrm{d}\mathbf{x}_{\perp}\mathrm{d}\eta_{\perp} = \frac{N_e}{2\pi\epsilon_r}\exp\left(-\frac{\mathbf{x}_{\perp}^2}{2\sigma_x^2} - \frac{\eta_{\perp}^2}{2\sigma_{x'}^2}\right)\ \mathrm{d}\mathbf{x}_{\perp}\mathrm{d}\eta_{\perp} \tag{2.103}$$

where the emittance is $\epsilon_r = \sigma_x \sigma_{x'}$.

The evolution equation of the electron beam distribution function can be obtain using the Liouville theorem $\partial f/\partial \bar{z} = \{H, f\}$ where $\{H, f\}$ i the Poisson bracket. [1] At the begining of this chapter we have obtained a three dimensional Hamiltonian with its associated equations of motion (2.13)-(2.17) and an evolution equation for the radiated e.m. field (2.31). Now we introduce the "3D Universal Scaling":

$$\begin{aligned}
&\theta = (k_r + k_l)\, z - c\,(k_r - k_l)\, t, \quad \bar{z} = \frac{z}{l_g}, \quad \bar{\mathbf{x}}_\perp = \frac{\mathbf{x}_\perp}{\sigma}, \\
&\bar{p} = \frac{\gamma - \gamma_r}{\rho \gamma_r}, \quad \bar{\mathbf{p}}_\perp = \frac{\sigma}{\epsilon_r}\eta_\perp, \quad \eta_\perp = \mathrm{d}\mathbf{x}_\perp/\mathrm{d}z, \quad a_l = a_0 g(\bar{z}, \mathbf{x}_\perp) \\
&A_r = \frac{a_0 a_r}{2\rho^2(1+a_0^2)}, \quad \mathcal{E} = \frac{\gamma_r}{\rho^2(1+a_0^2)} e_z = \frac{\gamma_r}{\rho^2(1+a_0^2)} \frac{e}{mc^2} E_z
\end{aligned} \tag{2.104}$$

where $a_0 = a_w$, $g(\bar{z}, \mathbf{x}_\perp)$ is the tranverse laser profile, σ is the rms electron 'radius' at the beam waist, ϵ_r is the rms beam emittance and ω_p is the plasma frequency. With this universal scaling the equations of motion (2.13)-(2.18) can be written:

$$\begin{cases}
\dfrac{\mathrm{d}\bar{\mathbf{x}}_\perp}{\mathrm{d}\bar{z}} = b\ (1 - \rho\bar{p})\bar{\mathbf{p}}_\perp \\[2ex]
\dfrac{\mathrm{d}\bar{\mathbf{p}}_\perp}{\mathrm{d}\bar{z}} = -\dfrac{2\rho}{X}(1 - \rho\bar{p})\nabla_{\mathbf{x}_\perp}\left[\dfrac{\xi}{2\rho^2}|g|^2 - i\left(g^* A e^{i\theta} - c.c.\right)\right] \\[2ex]
\dfrac{\mathrm{d}\theta}{\mathrm{d}\bar{z}} = \bar{p} + \left[\dfrac{\xi}{2\rho}(1 - |g|^2) - \dfrac{bX}{4}\bar{\mathbf{p}}_\perp^2\right] \\[2ex]
\dfrac{\mathrm{d}\bar{p}}{\mathrm{d}\bar{z}} = -(1 - \rho\bar{p})\left(g^* A e^{i\theta} + c.c.\right) + \mathcal{E}.
\end{cases} \tag{2.105}$$

Whereas the 1D theory is ruled only by the FEL parameter ρ, instead, in the 3D theory we must introduces new parameters which characterising the transversal dynamics.

[1] For a dynamical function $f(q(t), p(t), t)$ of conjugated Hamiltonian variables q and p the evolution in time is: $\frac{\mathrm{d}f}{\mathrm{d}t} = \frac{\partial f}{\partial t} + \left\{\frac{\partial q}{\partial t}\frac{\partial f}{\partial q} + \frac{\partial p}{\partial t}\frac{\partial f}{\partial p}\right\}$ where the second term in right side is the Poisson bracket. Assuming that the function does not depend explicitly on time (*i.e.* $\partial f/\partial t = 0$) and using the Hamiltonian equations $q = \frac{\partial H}{\partial p}$ and $p = -\frac{\partial H}{\partial q}$ we obtain: $\frac{\mathrm{d}f}{\mathrm{d}t} = \left\{\frac{\partial H}{\partial p}\frac{\partial f}{\partial q} - \frac{\partial H}{\partial q}\frac{\partial f}{\partial p}\right\} = \{H, f\}$

$$X = 2k_r\epsilon_r, \qquad b = \frac{l_g}{\beta^*} = \frac{l_g\epsilon_r}{\sigma^2} \qquad \xi = \frac{a_0^2}{1+a_0^2}. \tag{2.106}$$

In the Compton limit the term proportional to ρ (as for instance in $(1-\rho\bar{p}) \simeq 1$) can be neglected since the value of ρ ranges about from 10^{-5} to 10^{-3}, with this simplifications the Eqs. (2.107) becomes:

$$\begin{cases} \dfrac{d\bar{\mathbf{x}}_\perp}{d\bar{z}} = b\ \bar{\mathbf{p}}_\perp \\ \dfrac{d\bar{\mathbf{p}}_\perp}{d\bar{z}} = -\dfrac{\xi}{\rho X}\nabla_{\mathbf{x}_\perp}|g|^2 \\ \dfrac{d\theta}{d\bar{z}} = \bar{p} + \left[\dfrac{\xi}{2\rho}(1-|g|^2) - \dfrac{bX}{4}\bar{\mathbf{p}}_\perp^2\right] \\ \dfrac{d\bar{p}}{d\bar{z}} = -\left(g^* A_r e^{i\theta} + c.c.\right) + \mathcal{E}. \end{cases} \tag{2.107}$$

They can be obtained by the following Hamiltonian operator

$$\bar{H} = \frac{\bar{p}^2}{2} + \frac{b}{2}\bar{\mathbf{p}}_\perp^2 + \bar{p}\left[\frac{\xi}{2\rho}(1-|g|^2) - \frac{bX}{4}\bar{\mathbf{p}}_\perp^2\right] + \frac{\xi}{\rho X}|g|^2 - i\left(g^* A_r e^{i\theta} - c.c.\right) + \bar{\Phi}. \tag{2.108}$$

where $\bar{\Phi} = \gamma_r/(\rho^2(1+a_0^2))\Phi$ is such that $\mathcal{E} = -\partial\bar{\Phi}/\partial\theta$.

Now using the Liouville theorem, the Hamiltonian operator (2.108), the Maxwell evolution equation (2.31) and 3D Universal Scaling (2.104) we obtain the following Maxwell-Vlasov close system of equations for an e-beam interacting with a laser wiggler and radiation fields.

$$\begin{aligned} &\frac{\partial f}{\partial\bar{z}} + b\ \bar{\mathbf{p}}_\perp\nabla_{\mathbf{x}_\perp} f + \left\{\bar{p} + \frac{\xi}{2\rho}(1-|g|^2) - \frac{bX}{4}\bar{\mathbf{p}}_\perp^2\right\}\frac{\partial f}{\partial\theta} \\ &\qquad + \left\{\mathcal{E} - \left[g^* A e^{i\theta} + c.c.\right]\right\}\frac{\partial f}{\partial\bar{p}} - \frac{\xi}{\rho X}\nabla_{\mathbf{x}_\perp}|g|^2\nabla_{\mathbf{p}_\perp} f = 0 \\ &\left\{\frac{\partial}{\partial\bar{z}} + \frac{\partial}{\partial\bar{z}_1} - ia\nabla_\perp^2\right\} A_r = g\int_{-\pi}^{+\pi} d\theta \int_R d\bar{p}\int_{R^2} \mathrm{d}^2\bar{\mathbf{p}}_\perp\ e^{-i\theta} f + i\delta A_r \end{aligned} \tag{2.109}$$

where $b = l_g/\beta^*$ is the diffraction parameter of the electron beam, $a = l_g/Z_r = b/X$ and $Z_r = 4\pi\sigma^2/\lambda_r$ are respectively the diffraction parameter and the Rayleigh range of the emitted radiation with a transverse radius equal to the electron beam radius. The distribution function f and the radiation field A_r has the following dependence $f = f(\theta, \bar{p}, \bar{\mathbf{x}}_\perp, \bar{\mathbf{p}}_\perp, \bar{z}, \bar{z}_1)$, $A_r = A_r(\theta, \bar{\mathbf{x}}_\perp, \bar{z}, \bar{z}_1)$, and $g = g(\bar{\mathbf{x}}_\perp, \bar{z})$ is the laser wiggler profile.

The term $b\ \bar{\mathbf{p}}_\perp \nabla_{\mathbf{x}_\perp}$ corresponds, with the unscaled variables, to $\bar{\eta}_\perp \nabla_{\mathbf{x}_\perp}$ (where $\eta_\perp = \partial \mathbf{x}_\perp/\partial \bar{z}$) and describes the transverse drift of the beam, responsible for instance of the beam size increasing away from the beam waist; the comparison of two diffraction terms $a \simeq b$ that correspond to Eq. 2.96, will be investigate in detail in chap.6. It rule the matching between the electron and radiation beam. In fact, assuming the same initial spot size, if $b < a$ the electron beam is contained into the radiation beam that correspond to the "Pellegrini condition" $X < 1$ otherwise the radiation is confined into the electron beam size.

The phase term of Eq. (2.109) contains three terms which, with the unscaled variables, can be written as:

$$\begin{cases} \bar{p} = \dfrac{\gamma - \gamma_r}{\rho \gamma_r} = \left(\dfrac{\Delta\gamma}{\rho\ \gamma_r}\right)_{1D} \simeq 1 \\ \\ \dfrac{\xi}{2\rho}(1 - |g|^2) \simeq \dfrac{1}{2\rho}\dfrac{\Delta a_w^2}{1 + a_w^2} \simeq \left(\dfrac{\Delta\gamma}{\rho\ \gamma_r}\right)_{a_w} \\ \\ \dfrac{bX}{4}\bar{\mathbf{p}}_\perp^2 \simeq \dfrac{1}{2\rho}\dfrac{\vartheta^2\gamma_r^2}{1 + a_w^2} \simeq \left(\dfrac{\Delta\gamma}{\rho\ \gamma_r}\right)_{\perp} \end{cases}$$

and are responsible of the "non homogeneous effects" (2.100)-(2.102). The effects of the laser wiggler profile will be discussed later.

Finally, the last term $\mathrm{d}\mathbf{p}_\perp/dz = \xi/(2\rho X)\nabla_{\mathbf{x}_\perp}|g|^2$ corresponds with unscaled variables to a focusing force due to the laser wiggler profile $\dot{\bar{\eta}}_\perp = -a_w^2/(2\gamma_0)^2 \nabla_{\mathbf{x}_\perp}|g|^2$.

Note that $\bar{\mathbf{p}}_\perp \nabla_{\mathbf{x}_\perp} = \bar{p}_y \partial/\partial\bar{x} + \bar{p}_y \partial/\partial\bar{y}$ and the average in the field evolution equation is replaced by the average over an ensemble, $\langle \mathcal{O} \rangle = \int \mathcal{O} f(\xi) d\xi$ with $\int f(\xi) d\xi = 1$.

This closed set of equation can be solved numerically choosing a Gaussian initial

conditions at $f(\bar{z}=0)=f_0$:

$$f_0(\theta,\bar{p},\bar{\mathbf{x}}_\perp,\bar{\mathbf{p}}_\perp) \propto \exp\left\{-\frac{\left[\bar{\mathbf{x}}_\perp + b\bar{z}_0\bar{\mathbf{p}}_\perp\right]^2}{2} - \frac{\bar{\mathbf{p}}_\perp^2}{2}\right\} \tag{2.110}$$

where $\bar{z}_0$ is the waist position. Typically, a Gaussian phase-space profile correspond to a thermal distribution. In this treatment we have neglect the energy spread effects, which will be treated in section (3.2.4).

A complete numerical study will be developed afterwards when a fully three dimensional quantum theory of the FEL will be formulated. It will have the important property that it should tend to the classical limit, in agreement with the Correspondence Principle which every "respectable" quantum theory should admit.

2.3.3 Laser wiggler

Magnetic versus Laser wiggler

It has been proposed [58] [59] [60] that one can use, instead of a magneto static undulator, a high power laser pulse as the undulator, for a X-ray emission region. In fact since $\lambda_r \propto \lambda_w/2\gamma^2$, scaling down the wavelength of emitted radiation can be done or increasing the electron energy or, alternatively, reducing the undulator period. An infrared pulse, coming from high power Nd or CO_2 laser, whit a wavelength λ_l of 1 or 10 μm could yield X-ray FEL radiation with electrons energy about a hundred MeV

$$\lambda_r \propto \frac{\lambda_l}{4\gamma^2} \simeq 1A \tag{2.111}$$

Now with a simple argument we show why the laser wiggler is advisable for the X-ray FEL emission in the classical scheme while its is necessary in the Quantum regime.

We shall see in the third chapter that the FEL can operate also in a Quantum regime, the transition between Quantum and Classical regime is ruled by the Quantum FEL Parameter

$$\bar{\rho} = \rho\frac{mc\gamma}{\hbar k_r} = \rho\gamma\frac{\lambda_r}{\lambda_c} \tag{2.112}$$

where $\lambda_c = h/mc$ is the Compton wavelength and h is the Planck Constant

The QFEL-parameter is proportional to the ratio between the electron energy and the single photon energy, the quantum regime occurs when $\bar{\rho} \leq 1$.

Using the resonant relation and the definition of $\bar{\rho}$ in Eq.(2.112) the condition for the quantum regime can be written in terms of ρ:

$$\rho \leq \frac{\sqrt{2}\lambda_c}{\sqrt{\lambda_r \lambda_w (1 + a_w^2)}} \tag{2.113}$$

In the first chapter we have shown that to reach the high gain regime, a number of period of the order of $N_w \propto \frac{1}{\rho}$ is required, then the wiggler length is:

$$L_w = N_w \lambda_w \simeq \frac{\lambda_w}{\rho} \geq \frac{\sqrt{\lambda_r \lambda_w^3 (1 + a_w^2)}}{\lambda_c} \tag{2.114}$$

For an X-ray FEL experiment $\lambda_r \simeq 1A$ using a magnetic wiggler with a period $\lambda_w = 1$cm and $E = 3.5$ Gev, we obtain from the eq. (2.114) $L_w \geq 3$ Km that is possible but unpraticable. If we substitute the static wiggler with a Conterpropagating laser wiggler we must substitute in the resonant relation and otherwise $\lambda_w \rightarrow \lambda_l/2$, and for a tipical atomic laser the wavelength is about 1 μm that is three order of magnitude less then that of the magnetic wigller , then with this new parameter and assuming a most reasonable energy $E = 2.5$ Mev we obtain $L_w \geq 2$ mm.

Chapter 3

1D Quantum FEL Theory

As we have shown in the previous chapter most of the properties of a FEL can be analyzed and found remaining in a strictly classical framework. Even if the original proposal of an FEL by Madey was formulated in a quantum framework, the main bulk of the FEL theory has been later developed using classical physics. However, while for all existing FEL devices classical physics are a perfectly safe approximation, quantum effects could become relevant when operating in different regions for the range of the experimental parameters. In particular for very short wavelengths, the electron recoil from the emission of a photon can stop being negligible compared to the emission line width, making necessary a quantum mechanical treatment of the electron-photon interaction. The parameter which rules the transition between the classical and the quantum regime is the "Quantum FEL parameter" (QFEL-parameter) which can be defined as follows:

$$\bar{\rho} = \rho \frac{mc\gamma}{\hbar k_r} = \rho\gamma \frac{\lambda_r}{\lambda_c} \tag{3.1}$$

here $\lambda_c = h/mc = 0.024$Å is the Compton wavelength, $\omega = ck$ is the photon frequency and ρ is the classical FEL parameter (see Eq. (2.89)). The $\bar{\rho}$-parameter is approximatively equal to the ratio between the momentum of the electron and the momentum of the single photon, namely its represent the electron momemtum in unit of $\hbar k$. As we have anticipate in section (1.3), the QFEL-parameter is different representation of the Heisenberg's Uncertainly Principle (HUP) (see Eq. (1.15)). Note that from the eq. (2.82) the maximum induced energy spread in a FEL is

$\Delta(\gamma) \simeq \rho\gamma$ (see Eq.(2.100)), then from Eq. (5.17) we obtain:

$$\bar{\rho} \simeq \frac{mc\Delta(\gamma)}{\hbar k} \simeq \frac{\Delta(p_z)}{\hbar k} \tag{3.2}$$

which agrees with the definition given in section (1.3). This means that the classical momentum spread $\Delta(p_z)$ is proportional to the photon recoil through the $\bar{\rho}$ constant. From this picture we can summarize:

- $\bar{\rho} \gg 1 \rightarrow \Delta(p_z) \gg \hbar k$

  The momentum spread is much greater than the photon recoil, *i.e.* the number of photons emitted by each electron is large and the quantum effects are unimportant, so that the interaction can be interpreted in the classical framework; this is the most common situation especially at the low frequency emission.

- $\bar{\rho} \leq 1 \rightarrow \Delta(p_z) \leq \hbar k$

  The momentum spread is of order of the photon recoil, so that each electron emits only one photon via Compton backscattering and quantum effect become important. This regime occurs only in the high frequency emission range (*i.e.* X-ray)

Now, if each electron emits a single photon the peak energy of the resulting radiation field could be smaller than that in the classical case, where each electron emits many photons, however we argue that there is a net improving of its quality; we will show that in the quantum regime the spectral proprieties of the radiation field is better than in the classical case. This improving of the spectral proprieties becomes evident when propagation effects are taking in to account: in fact, as we have shown in the previous chapter, the radiation field in the classical SASE has an almost chaotic temporal pulse structure with a broad spectral width; on the contrary, in the quantum regime, we shall see that the random spiking behaviour almost disappears and a strong narrowing of the spectrum occurs, this is the phenomenon of "Quantum purification" [30] [31].

3.1 Hamiltonian model

We start from the classical steady state model (2.59-2.61) where we define a new scaled momentum and field variables in order to introduce the QFEL-parameter:

$$\bar{p}_j = \frac{p_j}{\bar{\rho}} = \frac{mc(\gamma_j - \gamma_r)}{\hbar k_r}, \qquad a = \sqrt{N_e \bar{\rho}} A_r \tag{3.3}$$

These new variables are still canonical and preserve the Poisson bracket

$$\{\theta_j, p_k\} = \delta_{i,j} \quad \{a, a^*\} = 1 \tag{3.4}$$

Note that as in the classical steady state theory we have supposed that the radiation field is monochromatic, i.e. a single mode.

In order to quantized the system the electrons dynamical variables become operators in the Hilbert space

$$\theta \to \hat{\theta}, \quad p \to \hat{p} = -i\partial/\partial\theta, \tag{3.5}$$

the field amplitude and its complex conjugate becomes respectively photon creation and annihilation operators

$$a, a^* \to \hat{a}, \hat{a}^\dagger. \tag{3.6}$$

Then the Poisson bracket (3.4) becomes Quantum Commutation Rules (QCR)

$$[\hat{\theta}_j, \hat{p}_k] = i\delta_{j,k}, \qquad [\hat{a}, \hat{a}^\dagger] = 1 \tag{3.7}$$

The Hamiltonian operator of N_e electrons interacting with a single mode of radiation (from eq. 2.64) is:

$$\hat{H} = \sum_{j=1}^{N_e} \left\{ \frac{\hat{p}_j^2}{2\bar{\rho}} - i\sqrt{\frac{\bar{\rho}}{N_e}} \left[\hat{a} e^{i\hat{\theta}_j} - \hat{a}^\dagger e^{-i\hat{\theta}_j} \right] \right\} \tag{3.8}$$

In the classical theory we have defined the detuning parameter $\delta = (\gamma_r - \gamma_0)\rho\gamma_r$ as the average initial momentum of all the electrons in the beam *i.e.* each electron come into wiggler device (or in the interaction region if we use a laser wiggler) with the same initial δ (see eq 2.67). In addition we have shown that it is also possible to introduce a more realistic thermal distribution (see eq. 2.80) for taking into account the initial energy of each electron. In the Quantum Mechanic framework this

approximation is forbidden by the Pauli Principle when we treat fermion particles, *i.e.* two or more fermion could not have the same quantum state. We will discuss this problem in the next section. 3.1.1 when the second quantized scheme will be introduced. For now we assume forward that under some specifical condition, (which in the FEL are usually satisfied), the electrons can be treated as "bosons" [37] [38]. This permit us to assume the same initial condition for all electrons.

Let us, as in eq. (2.68), define the operators such that the average momentum distribution is centered around γ_0

$$\hat{p}' = \hat{p} - \bar{\rho}\delta \qquad \hat{\theta}' = \hat{\theta} - \delta\bar{z} \qquad \hat{a} = \hat{a}e^{i\delta\bar{z}} \tag{3.9}$$

In fact, can be checked that:

$$\langle\hat{p}'_j\rangle = \frac{mc(\gamma_j - \gamma_r)}{\hbar k} - \bar{\rho}\frac{\gamma_r - \gamma_0}{\rho\gamma_r} = \frac{mc(\gamma_j - \gamma_0)}{\hbar k} \tag{3.10}$$

Then, dropping the prime, the Hamiltonian (3.8) can be written in the following way:

$$\hat{H} = \hat{H}_e + \hat{H}_{rad} + \hat{H}_{int} \tag{3.11}$$

with

$$\begin{cases} \hat{H}_e = \displaystyle\sum_{j=1}^{N_e} \frac{\hat{p}_j^2}{2\bar{\rho}} \\ \hat{H}_{rad} = -\delta\hat{a}^\dagger\hat{a} \\ \hat{H}_{int} = -i\displaystyle\sum_{j=1}^{N_e} \sqrt{\frac{\bar{\rho}}{N_e}}\left[\hat{a}e^{i\hat{\theta}_j} - \hat{a}^\dagger e^{-i\hat{\theta}_j}\right] \end{cases} \tag{3.12}$$

where H_e and H_{rad} are respectivelly the electrons and the emitted photons kinetic energy, while H_{int} is the interaction term. From this Hamiltonian and using the QCR (3.7) we obtain the equation of motion for the electron and photon operators:

$$\frac{d\hat{p}_j}{d\bar{z}} = -i[p_j, \hat{H}] = -i[p_j, \hat{H}_{int}] = -\sqrt{\frac{\bar{\rho}}{N_e}}\left[\hat{a}e^{i\hat{\theta}_j} + \hat{a}^\dagger e^{-i\hat{\theta}_j}\right] \tag{3.13}$$

$$\frac{d\hat{\theta}_j}{d\bar{z}} = -i[\theta_j, \hat{H}] = -i[\theta_j, \hat{H}_e] = \frac{\hat{p}_j}{\bar{\rho}} \tag{3.14}$$

$$\frac{d\hat{a}}{d\bar{z}} = -i[a, \hat{H}] = -i[a, \hat{H}] = i\delta\hat{a} + \sqrt{\frac{\bar{\rho}}{N_e}}\sum_j e^{-i\theta_j} \tag{3.15}$$

These equations imply the existence of the following integral of motion

$$\frac{d}{d\bar{z}}\left\{\sum_j \hat{p}_j + \hat{a}^\dagger \hat{a}\right\} = 0 \tag{3.16}$$

which represents, as in the classical case, the conservation of momentum.

3.1.1 Linear analysis and Collective operators

We perform a linear analysis of the Hamiltonian (following [31]) introducing, similary to the the classical case (eq.3.17), the quantum collective operator

$$\begin{cases} B = \sqrt{N_e}\langle e^{-i\hat{\theta}}\rangle & \text{Bunching operator} \\ \\ P = \sqrt{N_e}\left\{\dfrac{\langle p\ e^{-i\hat{\theta}}\rangle + \langle e^{-i\hat{\theta}}\ p\rangle}{2}\right\} & \text{Symmetric momentum operator} \end{cases} \tag{3.17}$$

where $\langle O\rangle = 1/N_e \sum_j^{N_e} O_j$. We consider $\hat{a}$, $\hat{p}_j$ and $\langle e^{-i\hat{\theta}}\rangle$ as fluctuation operators, *i.e.* we consider initial states for the electrons and the field such that

$$\langle a\rangle_0 = \langle p_j\rangle_0 = \sum_j e^{\langle -i\hat{\theta}_j\rangle_0} = 0 \tag{3.18}$$

Writing the Heisenberg equations of motion and neglecting the high order terms $\sqrt{N_e}\langle p\ e^{-i\hat{\theta}}\ p\rangle$ and $\hat{a}^\dagger\langle e^{-i2\hat{\theta}}\rangle$, we obtain the following equations in the linear regime:

$$\frac{dB}{d\bar{z}} = -\frac{i}{\bar{\rho}}P \tag{3.19}$$

$$\frac{dP}{d\bar{z}} = -\frac{i}{4\bar{\rho}}B - \sqrt{\bar{\rho}}a \tag{3.20}$$

$$\frac{da}{d\bar{z}} = \sqrt{\bar{\rho}}B + i\delta a \tag{3.21}$$

Comparing this set of linear equations with (2.76), follows that the quantum correction to the classical description is given by the term $-\dfrac{i}{4\bar{\rho}}B$. Looking for solution of the above linear system of the form $B(z) = B_0\exp(i\lambda\bar{z})$, we obtain the cubic characteristic equation

$$(\lambda - \delta)\left(\lambda^2 - \frac{1}{4\bar{\rho}^2}\right) + 1 = 0 \tag{3.22}$$

Notice that the above dispersion relation coincides with that of a classical FEL (2.81) whit an initial energy spread for a case of a squared distribution of width $1/2\bar{\rho}$ *i.e.* this extra term (with respect to the classical cold beam dispersion relation 2.79) represent the intrinsic "quantum momentum spread" which, in dimensional units, becomes $\hbar k/2$. The features of the solution of the cubic equation are shown in Fig (3.1)

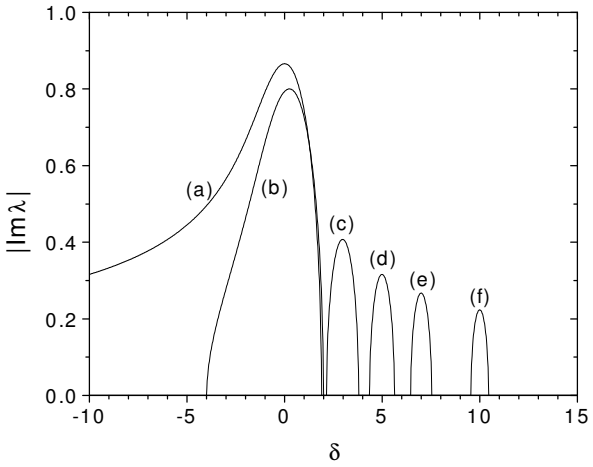

Figure 3.1: Immaginary part of cubic solution for different values of $\bar{\rho}$: (a)=∞, (b)=1, (c)=1/6, (d)=1/10, (e)=1/14, (f)=1/20.

When $\bar{\rho} \lesssim 1$ the resonance, *i.e.* the optimal gain, occurs for $\delta = 1/2\bar{\rho}$; the full width and the peak of the gain curve are respectively $4\sqrt{\bar{\rho}}$ and $|Im(\lambda)|_{max} \simeq \sqrt{\bar{\rho}}$, Hence the bandwidth narrows as square roots of $\bar{\rho}$ while as we have anticipate the peak decreases with the same scaling laws. Note also that the field and the bunching grow exponentially as $\exp(\sqrt{\bar{\rho}}\bar{z})$, so we introduce the quantum gain length

$$\tilde{l_g} = \frac{l_g}{\sqrt{\bar{\rho}}} = \frac{\lambda_w}{4\pi\rho\sqrt{\bar{\rho}}} \tag{3.23}$$

that, in the quantum regime is larger that the classical one.

A more accurate study of the behaviour of the cubic equation and of its physical meaning will be done when the propagation effects will be also treated.

3.1.2 Fermions or Bosons

First of all we should answer to the following question: *in a FEL should the electrons be treated as fermion ?* It is well known that the Pauli exclusion principle asserts that there can not be more than one electron per each momentum state *i.e.* the energy spread would be must larger then how is usually assumed. The Pauli Principle becomes relevant if we treat indistinguishable particles, *i.e.*, if the single particle wave packets overlap. This condition is satisfied if, and only if [37][36]

$$\varepsilon_{\parallel}\varepsilon_{\perp}^2 < N_e \lambda\!\!\!^{-3}_c \tag{3.24}$$

where $\lambda\!\!\!^{-}_c = \lambda_c/2\pi$, $\lambda_c = h/mc$ is the Compton wavelength, while $\varepsilon_{\parallel}$ and $\varepsilon_{\perp}$ are respectively the longitudinal and transverse normalized emittance. Let us discuss the (3.24) condition starting from the 1D theory. One must impose that the classical phase space area in unit of the minimum wave-packet quantum uncertainly area $\Delta z \Delta p/\hbar$ must be smaller than the number of electrons of the beam N_e. Since $p = \gamma mc$ and $\varepsilon = \Delta\gamma\Delta z$, one has $\varepsilon_{\parallel} < N_e \lambda\!\!\!^{-}_c$ and the 3D extension leads to Eq. (3.24). Note that since $\Delta z = l_b$ (where l_b is the bunch length), $N_e = I l_b/ec$ (where I is the beam current, e is the electron charge and c is the speed of light) and $\Delta\gamma = \gamma\rho$, Eq. (3.24) can be written as

$$\frac{\gamma\rho\varepsilon_{\perp}^2}{I}\frac{ec}{\lambda\!\!\!^{-3}_c} < 1 \qquad \text{or} \qquad I > \frac{ec}{\lambda\!\!\!^{-3}_c}\gamma\rho\varepsilon_{\perp}^2 \tag{3.25}$$

Checking this inequality for a reasonable value of parameter [39] $\gamma = 50$, $\varepsilon_{\perp} = 10^{-6}$ m-mrad, then we obtain $I > 10^{12}A$ that is completely out of the current experimental possibility (different value of parameters can be found in [52] [53] but the result is similar) so that the wave-packets do not overlap and the electrons can be considered as "distinguishable particles". In the first quantized scheme this fact implies that the total electrons wave function factorizes *i.e.* it can be written as the product of single wave functions. In chapter 5 the particle statistic will be treated in a more accurate way using the Wigner function in the second quantization formalism.

3.2 Quantum field Description

An alternative description to the N-particle Hamiltonian model (3.12) can be formulated in the second quantized formalism. In this formulation the N_e electrons are described by a matter-field operator $\hat{\Psi}(\theta, \bar{z})$ obeying the bosonic equal-time commutation relation and the normalization condition:

$$\left[\hat{\Psi}(\theta), \hat{\Psi}^\dagger(\theta')\right] = \delta(\theta - \theta'), \qquad \int_0^{2\pi} \hat{\Psi}^\dagger(\theta)\hat{\Psi}(\theta)d\theta = \hat{N}_e, \tag{3.26}$$

whereas the photons emitted (*i.e.* the single mode field) are described as in (3.6) by the creation and annihilation operators obeying the bosonic commutation relations (3.7)

The second quantized Hamiltonian can be obtained in terms of first quantized Hamiltonian (3.12):

$$\mathbf{H} = \int_0^{2\pi} \hat{\Psi}^\dagger(\theta)\hat{H}(\hat{\theta}, -i\partial_\theta, \hat{a}, \hat{a}^\dagger)\hat{\Psi}(\theta)d\theta. \tag{3.27}$$

and the Heisenberg equation for the fields are:

$$i\frac{\partial\hat{\Psi}}{\partial\bar{z}} = -\frac{1}{2\bar{\rho}}\frac{\partial^2\hat{\Psi}}{\partial\theta^2} + i\sqrt{\frac{\bar{\rho}}{N_e}}\left[\hat{a}^\dagger e^{-i\hat{\theta}} - \hat{a}e^{i\hat{\theta}}\right]\hat{\Psi} \tag{3.28}$$

$$\frac{d\hat{a}}{d\bar{z}} = \sqrt{\frac{\bar{\rho}}{N_e}}\int_0^{2\pi} d\theta\hat{\Psi}(\theta)^\dagger e^{-i\hat{\theta}}\hat{\Psi}(\theta) + i\delta\hat{a} \tag{3.29}$$

This set of equation can be also obtained using the path integral method [24] in the mean field approximation *i.e.*, assuming the minimal action principle (see Appendix **??**).

Let us now expand the matter-wave field in the momentum basis,

$$\hat{\Psi}(\theta) = \sum_{n=-\infty}^{\infty} \hat{c}_n u_n(\theta), \qquad \left[\hat{c}_n, \hat{c}_{n'}^\dagger\right] = \delta_{n,n'} \tag{3.30}$$

where $u_n(\theta) = (1/\sqrt{2\pi})e^{im\theta}$ are the eigenfunctions of $\hat{p}$ with eigenvalue n and $\hat{c}_n$ are the annihilation operator for the state with eigenvalue n. The evolution equations (3.28) and (3.29) become:

$$\frac{\partial\hat{c}_n}{\partial\bar{z}} = -i\frac{n^2}{2\bar{\rho}}\hat{c}_n + \sqrt{\frac{\bar{\rho}}{N_e}}\left[\hat{a}^\dagger\hat{c}_{n+1} - \hat{a}\hat{c}_{n-1}\right] \tag{3.31}$$

$$\frac{d\hat{a}}{d\bar{z}} = \sqrt{\frac{\bar{\rho}}{N_e}}\sum_{n=-\infty}^{\infty} \hat{c}_{n-1}^\dagger\hat{c}_n + i\delta\hat{a} \tag{3.32}$$

The bunching operator appearing as a driven term of the evolution equation for the photons (3.29)

$$\hat{B} = \frac{1}{\langle \hat{N}_e \rangle} \sum_{n=-\infty}^{\infty} \hat{c}_{n-1}^{\dagger} \hat{c}_n \tag{3.33}$$

is the quantum expression of the classical bunching parameter which can be view as a coherent superposition of different momentum states.

The Eqs.(3.31)-(3.32) has been investigated for the first time in the semi classical regime (steady state) [**?**] in which a and c_n are treated as a classical function. A fully quantum treatment of the steady state linear regime of Eqs. (3.28) and (3.29) has been given in [29] where the photons statistic are also treated; the initial condition assume the equilibrium state with no photons ($\langle \hat{a} \rangle_0 = 0$), all the electrons in the state with $n = 0$ ($\langle \hat{c}_0^{\dagger} \hat{c} \rangle_0 = N_e$). Then considering $\hat{c}_{\pm 1}$ and $\hat{a}$ as a fluctuation operator, we obtain the same quantum linear equation (3.21), in which $\hat{B} = \hat{c}_1 + \hat{c}_{-1}^{\dagger}$ and $\hat{P} = \hat{c}_1 - \hat{c}_{-1}^{\dagger}$ are respectively the quantum linear bunching and momentum bunching operator.

3.2.1 Quantum propagation model

A fully quantum propagation theory of FEL (in which both the electrons and the emitted field are quantized) is desirable but is out of the aim of this thesis. The propagation effects would need of a multi mode quantized photon field (the single mode approximation leads to a quantum steady state theory as in ref. [24] [29]. An alternative approach is the multiple scaling method which has been previously used in the classical FEL theory [10]. This method is similar to the "course-graining" approximation used in statistical mechanics, where the microscopic degree of freedom was mediated introducing a cut-of. We will introduce the multiple-scaling approach in the next section, at the moment, we want to stress the relation between the collective operator approach developed in the previous section and the above Quantum Field Description (see Eqs. (3.31)-(3.32)). It has been shown, using the path integral approach [24], that for a sufficiently large number of electrons the matter-wave field (3.30) and the photon field can be approximate by a classical field with the following scaling law:

$$\hat{\Psi} \to \sqrt{N_e}\Psi, \qquad \hat{a} \to \sqrt{N_e \bar{\rho}} A_r \tag{3.34}$$

In fact for $N_e \to \infty$ the quantum fluctuation can be neglected since they go as $1/\sqrt{N_e}$, and Eqs.(3.31)-(3.32) are satisfied also by the (3.34). This means that the FEL theory can be formulated essentially as a "mean field" theory that can be handled in a semi classical framework, where electron motion is quantized while radiation field is treated classically. As we have anticipated before, using this approximation we loose information about photons statistic and the quantum fluctuations, nevertheless, we keep intact quantum description of the electron-photon interaction. In fact, it has been shown [40] that the mean field approximation in the path integral formalism (*i.e.* taking "the classical" trajectory between all those possible ones in the quantum propagator $\langle i|f\rangle \simeq \exp\{(i/\hbar)S(i,f)\}$ where i and f are respectively the initial and the final generic quantum state) corresponds to the first quantum correction $\mathcal{O}(\hbar)$.

Using approximation (3.34) and introducing the time dependence in the radiation field $A_r(\bar{z}) \to A_r(\bar{z},\theta)$ (where $\theta = (k_r + k_w)z - v_r t$ with $v_r = ck_r/(k_r + k_w)$), from the (3.28) and (3.29) we obtain:

$$i\frac{\partial\Psi(\bar{z},\theta)}{\partial\bar{z}} = -\frac{1}{2\bar{\rho}}\frac{\partial^2\Psi(\bar{z},\theta)}{\partial\theta^2} - i\bar{\rho}\left[A_r(\bar{z},\theta)e^{-i\theta} - \text{h.c.}\right]\Psi(\bar{z},\theta) \tag{3.35}$$

$$\frac{\partial A_r(\bar{z},\theta)}{\partial\bar{z}} + \frac{1}{2\rho}\frac{\partial A_r(\bar{z},\theta)}{\partial\theta} = |\Psi(\bar{z},\theta)|^2\, e^{-i\theta} + i\delta A_r(\bar{z},\theta) \tag{3.36}$$

The first equation (3.35) is equivalent to the single particle Schrödinger equations for the matter-wave field interacting with a classical e.m. field, which can be obtain by the following single particle Hamiltonian (see 3.12 and 3.34):

$$\hat{H} = \sum_{j=1}^{N_e}\hat{H}_j, \qquad \hat{H}_j = \frac{\hat{p}_j^2}{2\bar{\rho}} - i\bar{\rho}\left[A_r(\bar{z},z_1)e^{i\hat{\theta}_j} - \text{h.c.}\right] \tag{3.37}$$

assuming a non interacting particle ensemble *i.e.* assuming that the Schrödinger electron wave function associated to the Hamiltonian (3.12) factorize *i.e.* $\psi(\theta_1,\theta_2,\ldots,\theta_n) = \psi(\theta_1)\psi(\theta_2)\ldots\psi(\theta_n)$. This fact implies that the dynamic of the system are ruled merely by the single Schrödinger evolution equation $i\partial\psi(\theta_j)/\partial\bar{z} = H_j\psi(\theta_j)$. Finally, we have shown that the mean field approximation, using the path integral method, is equivalent in the second quantized scheme [24] to the non interacting particle approximation in the Schrödinger picture (first quantized scheme) and both the descriptions can be view as a semi classical approximation.

3.2.2 Multiple Scaling Approach

In this section we introduce the multiple scaling approach which allows to take into account the existence of two different spatial scale lengths:

- The variation of the electrons distribution on the scale of the radiation wavelength λ_r describing the bunching on the variable θ
- The variation of the field envelope on the much longer scale of the cooperation length $l_c = \lambda_r/4\pi\rho$, described by $\bar{z_1} = 2\rho\theta = (z - \langle v_\parallel \rangle t)/l_c\langle\beta_\parallel\rangle$, *i.e.*, the coordinate along the bunch, in unit of cooperation length (note that some times $\beta \simeq 1$ ultra relativistic approximation).

Therefore we introduce two different time variables, θ and $\bar{z_1}$, in matter and radiation fields $A_r(\bar{z}, \theta, \bar{z_1})$ and $\Psi(\bar{z}, \theta, \bar{z_1})$ then the derivative respect to θ becomes $\partial/\partial\theta \rightarrow \partial/\partial\theta + 2\rho\partial/\partial\bar{z_1}$. As shown in the Appendix (A) expanding Ψ and A_r in terms of power of 2ρ, it is a good approximation taking the zero order terms of the series. In fact usually the value of ρ is about 10^{-4}. The multiple scaling method permit us to modified the equations (3.35)-(3.36) including the propagation dependence [28, 30, 31]:

$$i\frac{\partial\Psi(\bar{z},\theta,\bar{z_1})}{\partial\bar{z}} = -\frac{1}{2\bar{\rho}}\frac{\partial^2\Psi(\bar{z},\theta,\bar{z_1})}{\partial\theta^2} + i\bar{\rho}\left[A_r^*(\bar{z},\bar{z_1})e^{-i\theta} - \text{h.c.}\right]\Psi(\bar{z},\theta,\bar{z_1}) \quad (3.38)$$

$$\frac{\partial A_r(\bar{z},\bar{z_1})}{\partial\bar{z}} + \frac{\partial A_r(\bar{z},\bar{z_1})}{\partial\bar{z_1}} = \frac{1}{2\pi}\int_0^{2\pi} d\theta|\Psi(\bar{z},\theta,\bar{z_1})|^2\ e^{-i\theta} + i\delta A_r(\bar{z},\bar{z_1}) \quad (3.39)$$

The above set of equations describe the light propagation in the quantum FEL model ,*i.e.*, yields the spatio-temporal evolution of the radiation field amplitude $A_r(\bar{z}, \bar{z_1})$ and the matter wave field $\Psi(\bar{z}, \theta, \bar{z_1})$. Notice that the wave function Ψ depends only parametrically on $\bar{z_1}$ as a consequence of the spatial dependence of the field amplitude $A_r(\bar{z}, \bar{z_1})$. Moreover we assume that Ψ is a periodic function of θ; this hypothesis is reasonable if the bunch length is much greater than the radiation wavelength and gives rise to a description of the electron beam in terms of the cooperation length l_c instead of wavelength λ_r ($l_c \simeq \rho^{-1}\lambda_r$). Eqs. (3.38) and (3.39) describe the pulsed regime of FELs for a particle sample that initially is unbunched on the scale of the radiation wavelength λ_r , *i.e.*, such that $\Psi(\bar{z} = 0, \theta, \bar{z_1})$

is independent of θ. It can be shown that eq.(3.38) implies:

$$\frac{\partial}{\partial \bar{z}} \int_0^{2\pi} d\theta \; |\Psi(\bar{z}, \theta, \bar{z_1})|^2 = 0. \tag{3.40}$$

Hence the dimensionless density profile

$$I_0(\bar{z_1}) = \int_0^{2\pi} d\theta \; |\Psi|^2 \tag{3.41}$$

is independent on $\bar{z}$. This means that the spatial distributions of the particle does not change appreciably on the slow scale $\bar{z_1}$ during the interaction with the radiation. The classical propagation Eqs. (2.51)-(2.53) does not contain any explicit parameter while Eqs. (3.38)-(3.39) depend on $\bar{\rho}$. Note that $\bar{\rho}|A_r|^2 = |a|^2/N_e$ is the ratio between the photon and electron density. We will shown in the next section that Eqs. (3.35)-(3.36) admit a classical limit for $\bar{\rho} \to 0$: this limit can be done in a natural way by using a Wigner formalism instead of the usual Schrödinger like equation.

3.2.3 Momentum expansion

Eqs. (3.38)-(3.39) are conveniently solved in the momentum representation, in fact the "θ-periodic" electron wave function can be written as a Fourier series of momentum eigenstates $e^{in\theta}$:

$$\Psi(\bar{z}, \theta, \bar{z_1}) = \frac{1}{\sqrt{2\pi}} \sum_{n=-\infty}^{+\infty} c_n(\bar{z}, \bar{z_1}) e^{in\theta}. \tag{3.42}$$

where $|c_n(\bar{z}, \bar{z_1})|^2$ is the local probability to have an electron with momentum $p = n(\hbar k)$ at $\bar{z}$ and $\bar{z_1}$. So inserting Eq. (3.42) into Eqs.(3.38)-(3.39) we obtain

$$\frac{\partial c_n}{\partial \bar{z}} = -iE_n c_n - \bar{\rho}\left[A_r c_{n-1} - A_r^* c_{n+1}\right] \tag{3.43}$$

$$\frac{\partial A_r}{\partial \bar{z}} + \frac{\partial A_r}{\partial \bar{z_1}} = \sum_{n=-\infty}^{+\infty} c_n c_{n-1}^* + i\delta A_r \tag{3.44}$$

where $E_n = n^2/(2\bar{\rho}) + n\delta$, and $B = \sum_{n=-\infty}^{+\infty} c_n c_{n-1}^*$ is the bunching factor. Eqs. (3.43)-(3.44) are the discrete QFEL model. They are our working 1D equations and their fully statistical numerical analysis will be discussed afterwards in the next chapter. As in the classical case, a first approach to this set of Eqs. can be done using the linear approximation.

Linear Analysis

We now perform a stability analysis of Eqs. (3.38)-(3.39) when the electrons initially occupy an arbitrary momentum eigenstate with momentum $n(\hbar k)$. Moreover we assume that the system is in an equilibrium state with no field, $A_r = 0$, and all the electrons in the state n , with $c_n = 1$ and $c_m = 0$ for all $m \neq n$. Looking for solutions of the linearized equations proportional to $e^{i(\lambda\bar{z}+\bar{\omega}z_1)}$ (where $\bar{\omega} = (l_c/c)(\omega' - \omega_r) = (\omega' - \omega_r)/(2\rho\omega_r)$ is the frequency shift of the radiation field with respect to the resonant frequency ω_r), one obtains the quantum dispersion relation

$$(\lambda - \Delta_n)\left(\lambda^2 - \frac{1}{4\bar{\rho}^2}\right) + 1 = 0, \tag{3.45}$$

$$\Delta_n = \delta + \frac{n}{\bar{\rho}} - \bar{\omega}. \tag{3.46}$$

Note that the dispersion relation in Eq. (3.45) reduces to that of Eq.(3.22) when $n = 0$ and $\bar{\omega} = 0$. The behavior of the imaginary part of λ as a function of Δ_n is the same as that shown in fig. 3.1, with Δ_n instead of δ. We recall that, when $\bar{\rho} < 1$, the resonance moves from $\Delta_n = 0$ to $\Delta_n = 1/(2\bar{\rho})$, with a width of $4\sqrt{\bar{\rho}}$ in units of Δ_n. This corresponds, in the momentum space, to a shift of $\hbar k/2$ with a width $4\bar{\rho}^{3/2}(\hbar k)$. Let us explain in more exhaustive way the above relations: first of all we note that assuming $\gamma_0 \simeq \gamma_r \simeq \gamma$ then $\bar{\omega} - \delta$ can be written as follows:

$$\bar{\omega} - \delta = \frac{\omega' - \omega_r}{2\rho\omega_r} - \frac{\gamma_r - \gamma_0}{\rho\gamma_0} \simeq \frac{\gamma^2 - \gamma_r^2}{2\rho\gamma_r^2} - \frac{\gamma_r - \gamma_0}{\rho\gamma_0} \simeq \frac{\gamma - \gamma_r}{\rho\gamma_r} - \frac{\gamma_r - \gamma_0}{\rho\gamma_r} \simeq \frac{\gamma - \gamma_0}{\rho\gamma_r}.$$

in terms of the momentum spread $\Delta(p) = mc(\gamma - \gamma_0)$ we obtain $\bar{\omega} - \delta = \Delta(p)/(\bar{\rho}\hbar k_r)$ then the detuning parameter (3.46) becomes:

$$\Delta_n = \frac{1}{\bar{\rho}}\left(n - \frac{\Delta(p)}{\hbar k_r}\right) \tag{3.47}$$

The resonant condition then becomes

$$\Delta_n = \frac{1}{2\bar{\rho}} \rightarrow \Delta(p) = (2n-1)\frac{\hbar k_r}{2} \tag{3.48}$$

The above relation shows explicitly that the electron momentum recoil is in unit of the emitted photon momentum. Moreover from eq (3.47) it follows that the separation between two different resonant emission is

$$\Delta_n - \Delta_{n-1} = 1/\bar{\rho} \tag{3.49}$$

Let us now consider a fixed value of $\bar{\rho}$ and plot $\mathrm{Im}(\lambda)$ for $\delta = 0$ as a function of frequency shift $\bar{\omega}$, as shown in fig. 3.2. It can be seen that the regions of the spectrum corresponding to gain ($\mathrm{Im}(\lambda) > 0$) appear as a series of discrete lines corresponding to different values of n. Each of these lines is centred on $\bar{\omega} = (2n-1)/(2\bar{\rho})$, equally separated by a distance $1/\bar{\rho}$, and has a width of $4\sqrt{\bar{\rho}}$. The transition to the classical limit of a broad, continuous gain spectrum can be seen from fig. 3.2 to occur when the line separation becomes smaller than the line width, i.e. $4\bar{\rho}^{3/2} > 1$ or $\bar{\rho} > (1/2)^{4/3} \approx 0.4$.

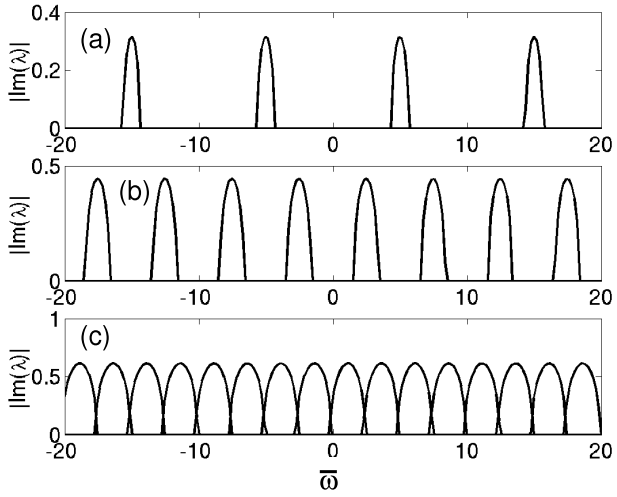

Figure 3.2: Imaginary part of the unstable root of the cubic equation (2.81) vs. $\bar{\omega} = (\omega' - \omega)/(2\rho\omega)$ for $\delta = 0$, (a) $\bar{\rho} = 0.1$, (b) $\bar{\rho} = 0.2$, and (c) $\bar{\rho} = 0.4$. Each line is centered around $\bar{\omega} = (2n-1)/(2\bar{\rho})$ and has a width $4\sqrt{\bar{\rho}}$. For $\bar{\rho} > 0.4$ the lines overlap and the spectrum becomes continuous.

The physical reason for these discrete frequencies is that in the quantum regime the electron recoils by $\hbar k$, so that electrons undergo a transition from an energy $E_n \propto p^2 \propto n^2$, to the state with energy $E_{n-1} \propto (n-1)^2$. Hence, the transition frequency varies as $1 - 2n$, as shown above. As discussed in [**?**], for $\bar{\rho} \gg 1$ the electrons have almost the same probability of transition from the momentum state n to the momentum states $n \pm 1$ (i.e. $|c_{n+1}|^2 \approx |c_{n-1}|^2$), absorbing or emitting a photon. On the contrary, in the case $\bar{\rho} < 1$, $|c_{n+1}|^2 \ll |c_{n-1}|^2$, i.e. the particles can only emit a photon with transition $n \to n-1$, behaving approximately as a two-level system [30] described by the Maxwell-Bloch equations [5].

3.2.4 The Energy spread

A complete description of the FEL dynamics must be include the inhomogeneous effects due to the broadening of the resonance, caused by for instance a spread of initial electron energy γ_0. The significance of the inclusion of the inhomogeneous effects is that it allows us obtain an upper limit for the initial energy spread in the electron beam driving a FEL in the quantum regime. A complete analysis of the inhomogeneous effect has been given in [32], whereas here we show only the basic method. Eqs. (3.35)-(3.36) have been derived assuming a mono energetic electron beam, where all electrons entered the FEL undulator with the same momentum. More precisely, the parameter $\delta = (\gamma_0 - \gamma_r)/\rho\gamma_r$ describes the detuning of the initial electron energy γ_0 from the resonant γ_r defined by the central frequency $\omega_r = k_r c$ of the emitted radiation. We wish to generalize the models used until now to include the more physically realistic situation of an initial distribution for the electrons' energy; so we take a normalized distribution centered around the resonant detuning δ_r, such that

$$\int_{-\infty}^{+\infty} G(\delta)\, d\delta = 1, \qquad \int_{-\infty}^{+\infty} G(\delta)\, \delta\, d\delta = \delta_r \tag{3.50}$$

In order to take into account the energy spread distribution (3.50) we modify the Eqs. 3.43 and 3.44 including the δ-dependence in the coefficient $c_n(\bar{z}, \bar{z_1}) \rightarrow c_n(\bar{z}, \bar{z_1}, \delta)$, which can be interpreted quantum mechanically as the probability amplitude to find an electron with a detuning δ and a momentum $p = n(\hbar k)$. The evolution equation of the c_n (3.35) and the evolution equation of the radiation field (3.36) change as follows:

$$\frac{\partial c_n}{\partial \bar{z}} = -iE_n c_n - \bar{\rho}\left[A_r c_{n-1} - A_r^* c_{n+1}\right] \tag{3.51}$$

$$\frac{\partial A_r}{\partial \bar{z}} + \frac{\partial A_r}{\partial \bar{z_1}} = \sum_{n=-\infty}^{+\infty} \int_{-\infty}^{\infty} d\delta G(\delta) c_n c_{n-1}^* \tag{3.52}$$

The field evolution equation is different from the ideal "cold" case (3.36) because its driven term, the bunching factor, has been weighted over the distribution $G(\delta)$. This implies a loss of gain that is proportional to the width of the distribution, whereas if the width of the distribution tend to zero *i.e.* $G(\delta) \rightarrow \delta(\delta - \delta_r)$ Eqs.(3.39) tends to Eqs.(3.36).

3.3 Wigner approach and classical limit

Up to now, the quantum 1D-model for FELs is based on a Schrödinger equation for the matter-wave function Ψ (eq. 3.35), describing the particles, and on the Maxwell equation for the radiation field A_r (eq. 3.36), coupled in a self-consistent way. It is well-known that the Schrödinger equation can be transformed into an equation for the Wigner quasi-probability distribution function. In general, there are several reasons in order to describe the particles with a Wigner function W instead of a matter-wave function Ψ:

- The equation for W shows explicitly the classical limit for $\bar{\rho} \gg 1$;
- The Wigner function may describe also mixed states, whereas a wave-function Ψ always assumes a pure state, i.e. a perfectly coherent particle sample; this assumption does not correspond to the real situation for FELs
- For the same reasons of the previous point, a Wigner distribution can be more easily extended to a 3D geometry, in which the particles have a transverse distribution in position and velocity space. In fact a realistic electron beam has a transverse dimension and an angular divergence much larger than the quantum limit implied by the Heisenberg Uncertainty Principle.

For these reasons, it is important to obtain an alternative quantum description of the FELs in terms of a Wigner function for the particles. In the second chapter we have obtained a Maxwell-Vlasov equation (see eq.(2.109)) where the classical distribution function $f(\theta, \bar{z}, \bar{p})$ is periodic on θ in $(0, 2\pi)$. In the classical picture the choice of θ-domain has no consequence on the momentum variable, but in the quantum description they are intrinsically related, since if θ is a periodic variable in $(0, 2\pi]$, then necessarily the conjugated momentum variable p is discrete. This problem was solved by J.P. Bizarro introducing a "Discrete Wigner function" for rotational angular variable θ-p [41, 42, 44].

$$W_m(\theta, \bar{z}) = \frac{1}{\pi} \int_{-\pi/2}^{+\pi/2} d\theta' \, e^{-2im\theta'} \, \Psi^* \left(\theta - \theta', \bar{z}\right) \Psi \left(\theta + \theta', \bar{z}\right). \tag{3.53}$$

The momentum is now represented by the discrete label m. This definition keeps all the required useful properties of the Wigner function as a quasi-probability distribution, i.e. tracing it over one variable gives the probability distribution for the

other:

$$\int_{-\pi}^{+\pi} W_m(\theta, \bar{z})\, d\theta = |c_m(\bar{z})|^2 \tag{3.54}$$

$$\sum_{m=-\infty}^{+\infty} W_m(\theta, \bar{z}) = |\Psi(\theta, \bar{z})|^2 \tag{3.55}$$

This implies the normalization of the discrete Wigner function

$$\sum_{m=-\infty}^{+\infty} \int_{-\pi}^{+\pi} W_m(\theta, \bar{z})\, d\theta = 1. \tag{3.56}$$

Inserting in (3.53) the Fourier expansion (3.42) we obtain

$$W_m(\theta, \bar{z}) = \frac{1}{2\pi} \sum_{m', m''} c^*_{m'}(t) c_{m''}(t) e^{-i(m'-m'')\theta} \mathrm{sinc}\left[(2m - m' - m'')\,\frac{\pi}{2}\right]. \tag{3.57}$$

Following ref. [41] [44], we write

$$W_m(\theta, \bar{z}) = w_m(\bar{z}) + \sum_{m'=-\infty}^{+\infty} \mathrm{sinc}\left[(m - m' - 1/2)\,\pi\right]\, w_{m'+1/2}(\theta, \bar{z}). \tag{3.58}$$

where

$$w_m(\theta, \bar{z}) = \frac{1}{2\pi} \sum_{m'=-\infty}^{+\infty} c^*_{m+m'}(\bar{z}) c_{m-m'}(\bar{z}) e^{-i2m'\theta} \tag{3.59}$$

$$w_{m+1/2}(\theta, \bar{z}) = \frac{1}{2\pi} \sum_{m'=-\infty}^{+\infty} c^*_{m+m'+1}(\bar{z}) c_{m-m'}(\bar{z}) e^{-i(2m'+1)\theta}. \tag{3.60}$$

The introduction of two new functions $w_m(\theta)$ and $w_{m+1/2}(\theta)$ is necessary in order to distinguish the two contributions of evenness and oddness in the Wigner function (3.57), and it is necessary in order to obtain a dynamical equation for the Wigner function.

These integer and half-integer small Wigner functions are orthogonal to each other:

$$\int_{-\pi}^{+\pi} d\theta\, w_m(\theta, \bar{z}) w_{m+\frac{1}{2}}(\theta, \bar{z}) = 0 \tag{3.61}$$

for all m, n, and contain all the information needed to determine $W_m(\theta, \bar{z})$. The probabilities for the momentum m and the phase θ can be derived directly from the

$w_m(\theta)$ and $w_{m+1/2}(\theta)$ too:

$$|c_m(\bar{z})|^2 = \int_{-\pi}^{+\pi} d\theta\, w_m(\theta, \bar{z}) \tag{3.62}$$

$$|\Psi(\theta, \bar{z})|^2 = \sum_{m=-\infty}^{+\infty} \{w_m(\theta, \bar{z}) + w_{m+1/2}(\theta, \bar{z})\} \tag{3.63}$$

The importance of the integer and half-integer small Wigner functions is that, while for the $W_m(\theta, \bar{z})$ it is not possible to find a closed evolution equation, it can be done for $w_s(\theta, \bar{z})$ where $s = m$ (eq. 3.59) or $s = m + 1/2$ (eq. 3.60) (with $m \in Z$) is half integer number. Deriving Eqs.(3.59)-(3.60) with respect to $\bar{z}$ and inserting Eqs (3.51) for the amplitudes $c_n(\bar{z})$ we obtain, after some algebra,

$$\frac{\partial w_s(\theta, \bar{z})}{\partial \bar{z}} + \frac{s}{\bar{\rho}} \frac{\partial w_s(\theta, \bar{z})}{\partial \theta} - \bar{\rho} \left(A_r e^{i\theta} + A_r^* e^{-i\theta}\right) \left\{w_{s+1/2}(\theta, \bar{z}) - w_{s-1/2}(\theta, \bar{z})\right\} = 0 \tag{3.64}$$

where $s = m$ or $s = m + 1/2$. The finite difference term in the potential represents the momentum exchange between the electrons and the emitted photons; in fact, treating $s/\bar{\rho}$ as a continuous variable and using the eq.(3.3) and the definitions of $\bar{\rho}$ (2.112) we obtain:

$$\frac{s}{\bar{\rho}} + \frac{1}{2\bar{\rho}} \rightarrow \frac{1}{mc\gamma\rho} \left(mc(\gamma - \gamma_0) + \frac{\hbar k_r}{2}\right) \tag{3.65}$$

which shows that the momentum recoil is in unit of discret packet equal to the photon momentum $\hbar k_r$.

The bunching of the electron beam can be written in this new formalism too:

$$\langle e^{-i\theta} \rangle = \sum_{n=-\infty}^{\infty} c_n c_{n-1}^* = \sum_{m=-\infty}^{+\infty} \int_{-\pi}^{+\pi} d\theta e^{-i\theta} w_{m+1/2}(\theta, \bar{z}) \tag{3.66}$$

so that Eq.(3.64) can be closed by coupling it to the equation for the radiation field

$$\frac{\mathrm{d}A_r}{\mathrm{d}\bar{z}} = \sum_{m=-\infty}^{+\infty} \int_{-\pi}^{+\pi} \mathrm{d}\theta e^{-i\theta} w_{m+1/2}(\theta, \bar{z}) + i\delta A_r \tag{3.67}$$

Eqs. (3.64) and (3.67), in the case of a pure state, are equivalent to Eqs. (3.43) and (3.44).

Classical limit

The most important requirement that each Quantum theory must be satisfy is the existence of the "Classical limit" *i.e.* should exist one parameter which, in general, represent the characteristic scale of the theory. When the scale length of the physical phenomenon is of the order of the Plank constant $\hbar$ then the theory must take into account the quantum effect whereas when the scale length is much greater than $\hbar$ the quantum effects are mediated and disappear, so the classical description can be used. The parameter which rules the transition between the classical and the quantum description in our Quantum FEL theory is the QFEL parameter $\bar{\rho}$ (see eq. 2.112). When $\bar{\rho}$ is less then unity the momentum spread of the electron is of the order of the photon momentum (each electron emit one photon) and the quantum effect becomes relevant, on the contrary when $\bar{\rho}$ is much greater than unity the momentum spread of the electron is much larger then the photon momentum (each electron emits many photons), and we are in a classical framework. The classical limit $\bar{\rho} \to \infty$ can be done in a natural way using the Wigner formalism as follows: Note that for $\bar{\rho} \gg 1$ the discrete momentum variable s can be converted in a continuous variable normalizing it to $\bar{\rho}\ \bar{p} = s/\bar{\rho}$, as a consequence, the discrete Wigner function becomes a continuous function of $\bar{p}$, $w_s(\theta) \to W(\bar{p}, \theta)$. Now we take in to account the potential term of the evolution equation (3.64) and omitting the time and spatial dependence we perform the classical limit $\bar{\rho} \to \infty$:

$$\bar{\rho}\left\{w_{s+1/2} - w_{s-1/2}\right\} \to \underbrace{\left\{\frac{W(\bar{p}+\frac{1}{2\bar{\rho}}) - W(\bar{p}-\frac{1}{2\bar{\rho}})}{1/\bar{\rho}}\right\} \to \frac{\partial f(\bar{p})}{\partial \bar{p}}}_{\bar{\rho}\to\infty} \tag{3.68}$$

Hence for $\bar{\rho} \gg 1$ the discrete Wigner evolution equation (3.64) reduced to the corresponding Vlasov equation for the classical distribution $f(\theta, \bar{p}, \bar{z})$ whit $\bar{p} \in (-\infty, +\infty)$ and $\theta \in (0, 2\pi]$.

$$\frac{\partial f}{\partial \bar{z}} + \bar{p}\frac{\partial f}{\partial \theta} - \left[\left(g^* A_r e^{i\theta} + c.c.\right)\right]\frac{\partial f}{\partial \bar{p}} = 0 \tag{3.69}$$

$$\frac{\partial A_r}{\partial \bar{z}} + \frac{\partial A_r}{\partial \bar{z}_1} = \int_{-\pi}^{+\pi} d\theta \int_R d\bar{p}\ e^{-i\theta} f - i\delta A_r \tag{3.70}$$

These equations agree with equations (2.109) in the one dimensional limit *i.e.* from Eqs. (5.16) imposing $X = 0,\ b = 0,\ g(\bar{x}) = 1$.

The Wigner picture generalize the Schrödinger picture *i.e.* Eqs. (3.64 and (3.67) contains as particular case (pure state) Eqs.(3.43) and (3.44)); therefore it will can extended to a more realistic three dimensional model. The equivalence of the two different pictures can be shows numerically as follows: Since $w_s(\theta,\bar{z})$ is periodic in θ, it can be expanded in a Fourier series:

$$w_s(\theta,\bar{z}) = \frac{1}{2\pi}\sum_{k=-\infty}^{+\infty} w_s^k(\bar{z})\exp(ik\theta). \tag{3.71}$$

Using (3.71), Eqs.(3.64) and (3.67) become:

$$\frac{\partial w_s^k}{\partial \bar{z}} + ik\frac{s}{\bar{\rho}}w_s^k - \bar{\rho}\left[A_r\left(w_{s+1/2}^{k-1} - w_{s-1/2}^{k-1}\right) + A_r^*\left(w_{s+1/2}^{k+1} - w_{s-1/2}^{k+1}\right)\right] = 0 \tag{3.72}$$

$$\frac{\mathrm{d}A_r}{\mathrm{d}\bar{z}} = \sum_{m=-\infty}^{+\infty} w_{m+1/2}^1 + i\delta A_r \tag{3.73}$$

The Fourier components $w_s^k(\bar{z})$ are related to the Fourier components $c_m(\bar{z})$ of the wave function $\Psi(\theta,\bar{z})$,

$$w_m^{2k} = c_{m+k}^* c_{m-k} \tag{3.74}$$

$$w_{m+1/2}^{2k+1} = c_{m+k+1}^* c_{m-k}. \tag{3.75}$$

In particular, $w_m^0 = |c_m|^2$ are the momentum probabilities and $w_{m+1/2}^1 = c_{m+1}^* c_m$ are the m-th bunching components, describing the overlapping between the m and $m+1$ states.

A numerical analysis has shown full agreement between the solutions of Eqs. (3.72)-(3.73) and Eqs.(3.43)-(3.44). As example Fig.3.3 shows the intensity $\bar{\rho}|A_r|^2$,the bunching $|b| = |\sum_m w_{m+1/2}^1|$, w_0^0, w_{-1}^0 and $|w_{-1/2}^1|$ vs. $\tilde{z} = \sqrt{\bar{\rho}}\bar{z}$ for $\bar{\rho} = 0.1$ and $\delta = 5$ (quantum regime). The initial conditions are $w_0^0(0) = |c_0|^2 = 1-\epsilon^2$, $w_{-1}^0(0) = |c_{-1}|^2 = \epsilon^2$, such that $|c_0|^2 + |c_{-1}|^2 = 1$ and $w_{-1/2}^1(0) = c_0^* c_{-1}\epsilon\sqrt{1-\epsilon^2}$, where $\epsilon = 10^{-2}$. In this regime only two momentum states, $m = 0$ and $m = -1$ are significantly populated. The crosses in fig.3.3 represent the intensity $\bar{\rho}|A_r|^2$ and the bunching $|b| = |\sum_m c_m c_{m-1}^*|$, as calculated from the solution of Eqs.(3.43)-(3.44). Fig.3.4 shows $|A_r|^2$ and b vs. $\bar{z}$ for $\bar{\rho} = 5$ and $\delta = 0$ (classical regime). In both the quantum and classical regime the two solutions overlap perfectly.

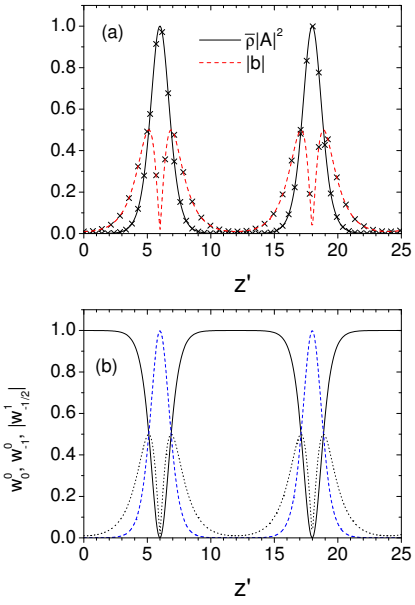

Figure 3.3: Quantum regime, for $\bar{\rho} = 0.1$ and $\delta = 5$. (a): Intensity $\bar{\rho}|A_r|^2$ (continuous line) and bunching $|b|$ (dashed line) vs. $\tilde{z} = \sqrt{\bar{\rho}}\bar{z}$. The crosses represent the solution of Eqs.(3.43)-(3.44). (b): w_0^0 (continuous line), w_{-1}^0 (dashed line) and $|w_{-1/2}^1|$ (dotted line) vs. $\tilde{z}$.

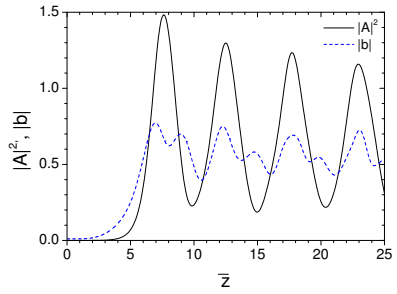

Figure 3.4: Classical regime, for $\bar{\rho} = 5$, $\delta = 0$. Intensity $|A_r|^2$ (continuous line) and bunc hing $|b|$ (dashed line) vs. $\bar{z}$.

Chapter 4

Numerical Analysis of the 1D QFEL SASE regimes

In this chapter we solve numerically the set of 1D QFEL equations (3.43) and (3.44) derived in the previous chapter.

$$\frac{\partial c_n}{\partial \bar{z}} = -iE_n c_n - \bar{\rho}\left[A_r c_{n-1} - A_r^* c_{n+1}\right] \tag{4.1}$$

$$\frac{\partial A_r}{\partial \bar{z}} + \frac{\partial A_r}{\partial \bar{z_1}} = \sum_{n=-\infty}^{+\infty} c_n c_{n-1}^* + i\delta A_r \tag{4.2}$$

where $E_n = n^2/(2\bar{\rho}) + n\delta$, and $b = \sum_{n=-\infty}^{+\infty} c_n c_{n-1}^*$ is the bunching factor. Note that in the 1D approximation these equations are equivalent to Eqs.(3.72) and (3.73) if the Wigner function is defined in terms of a pure state (see section (3.3)).

We will show that the discrete gain spectrum of the quantum regime shown in Fig.(3.2), can give rise to a phenomenon of "Quantum purification" in which the random spiking behaviour, proper of the classical regime, almost disappears and strong narrowing of the spectrum occurs. Moreover we will show that the spectral line-width of single spike is $\Delta\omega/\omega \simeq \lambda_r/l_b$, similarly to the spectrum line-width of a wave train long l_b with wavelength λ_r.

The simulation assumes that all electrons are initially in the momentum state $n = 0$ *i.e.* the electrons are treated as bosons and the energy spread effects are neglected. The initial conditions for all the simulations are:

$$A_r(z_1, \bar{z} = 0) = 0,$$

$$c_{-1}(\bar{z}_1, \bar{z} = 0) = b_0 e^{i\phi(\bar{z}_1)}$$
$$c_0(\bar{z}_1, \bar{z} = 0) = \sqrt{1 - b_0^2} \tag{4.3}$$

where $b_0 = 0.01$ and $\phi(\bar{z}_1)$ is a randomly fluctuating phase with values in the range $[0, 2\pi)$.

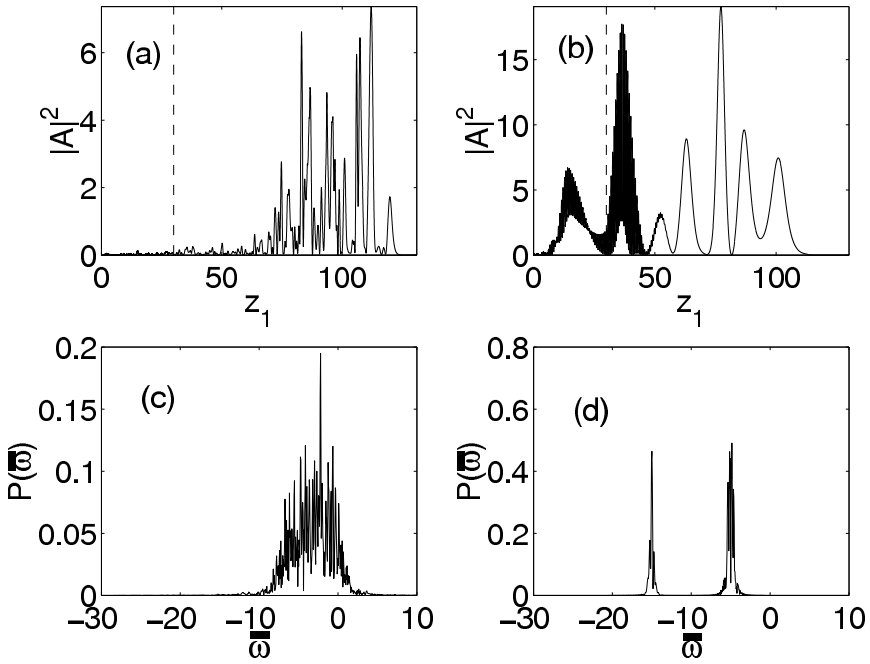

Figure 4.1: Numerical solutions of Eq. (3.43)-(3.44), for $l_b = 30l_c$ and $\delta = 0$, in the classical regime ($\bar{\rho} = 5$ and $\bar{z} = 30$) (a, c) and in the quantum regime ($\bar{\rho} = 0.1$ and $\bar{z} = 150$) (b, d): Graphs (a) and (b) show the scaled intensity and Graphs (c) and (d) show the corresponding scaled power spectra as a function of scaled frequency $\bar{\omega} = (\omega' - \omega_r)/2\rho\omega_r$, where ω_r is the resonance frequency. The dotted line in (a) and (b) mark the front edge of the electron pulse. The frequency shift in (d) is in agreement with that predicted from Fig. 3.2(a).

Fig. 4.1(a) and (b) show the field intensity as a function of $\bar{z}_1$ at $\bar{z} = 30$ for the classical regime and $\bar{z} = 150$ for the quantum regime, respectively. Fig 4.1(c) and (d) show the corresponding classical and quantum power spectra of the radiated field versus $\bar{\omega} = (\omega' - \omega_r)/2\rho\omega_r$, where ω_r is the resonant frequency. It can be seen that there is a dramatic difference between the classical evolution (Figs 4.1(a,c)) and the quantum evolution (Figs 4.1(b,d)). The temporal structure in the classical limit (Fig.4.1(a)) is almost chaotic, with a broad spectrum. In contrast, the

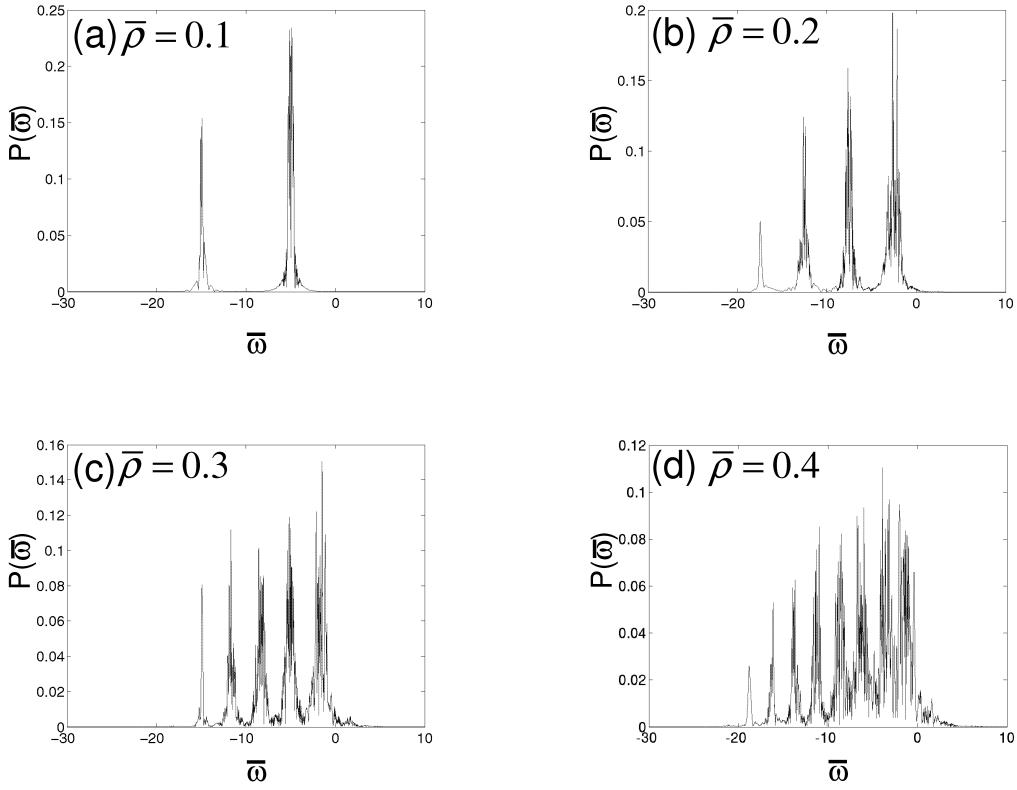

Figure 4.2: The transition from quantum SASE to classical SASE: Scaled power spectra, $P(\bar{\omega})$, as a function of scaled frequency $\bar{\omega} = (\omega' - \omega_r)/2\rho\omega_r$ for $\bar{z} = 150$, calculated from a numerical solution of Eqs. (3.43)-(3.44) for $\delta = 0$ when (a) $\bar{\rho} = 0.1$, (b) $\bar{\rho} = 0.2$, (c) $\bar{\rho} = 0.3$, and (d) $\bar{\rho} = 0.4$.

temporal behaviour in the quantum limit (Fig.4.1(b)) shows a purification of the initially noisy evolution, and the corresponding spectrum is composed by narrow lines, the positions of which are in agreement with those predicted by linear theory (see Fig.3.2(a)). Note that the line separation $1/\bar{\rho}$ corresponds in real units to the relativistic recoil frequency. In fact, in the simple case when $\delta = 0$ and using the relations (3.46), the resonant shift between two different emission can be written as

$$\Delta_n - \Delta_{n-1} = \bar{\omega}' - \bar{\omega}'' = \frac{\omega' - \omega_r}{2\rho\omega_r} - \frac{\omega'' - \omega_r}{2\rho\omega_r} = \frac{\omega_{rec}}{2\rho\omega_r} \tag{4.4}$$

where $\omega_{rec} = \omega' - \omega''$. Finally using Eq.(3.49) and the definition of $\bar{\rho}$ we obtain [29]

$$\omega_{rec} = 2\hbar k_r^2/m\gamma_r. \tag{4.5}$$

Note that the recoil frequency in atomics physics is associated to the relativistic energy recoil $E_{rec} = p_{rec}^2/2m\gamma_r$ for an electron interacting whit photons whose energy is $\hbar\omega_r$, through the relation $\omega_{rec} = E_{rec}/\hbar$; where the momentum recoil in the moving electron frame is $p_{rec} = 2\hbar k_r$.

The left hand side of Fig. 4.1(b) is the rapid beat between the two frequencies of Fig. 4.1(d). For small values of $\bar{z}$ only the frequency with $\bar{\omega} = -1/(2\bar{\rho})$ appears. Increasing $\bar{z}$ additional lines down shifted by $1/\bar{\rho}$ also appear.

The transition from the quantum regime of SASE to the classical regime is demonstrated in fig. 4.2, which shows the scaled power spectra, $P(\bar{\omega})$, for different values of $\bar{\rho}$ for $\bar{z} = 150$. It can be seen that there is a transition from discrete, narrow lines to a quasi-continuous spectrum when $\bar{\rho} \geq 0.4$, in agreement with the predictions of the linear analysis described in the previous section.

The reason for "Quantum Purification" of the SASE spectrum is as follows [39]: The maximum induced energy spread in an FEL is $\Delta(\gamma)/\gamma \simeq \rho$ (see Eq.2.89), this relation can be written also in terms of momentum spread $\Delta(p) = mc(\gamma - \gamma_0)$ and the QFEL parameter $\bar{\rho}$ (Eq.5.17) as

$$\frac{\Delta(p)}{\hbar k_r} \simeq \bar{\rho} \tag{4.6}$$

The QFEL parameter can be interpreted as the ratio between the classical momentum spread and the photon recoil , so that quantum effects become important when $\bar{\rho} \lesssim 1$, since in this case the discreteness of momentum exchange is relevant. This allows to explain in a simply way the origin of the broad and spiky classical spectrum and the reduction to a single line in the quantum regime. The radiation emission is due to the transition between adjacent recoil momentum states ($p^{(n)} = n\hbar k_r$), which are equally spaced by the photon momentum . The emitted frequencies in the transitions $n \rightarrow n-1$ are also equally spaced, since they are proportional to the difference between the corresponding kinetics energies. In the classical regime ($\bar{\rho} \gg 1$) many momentum states becomes occupied (see Eq. (4.6)), and the multiple transitions between the different momentum states lead to a multi-frequency spectrum with equally spaced lines and an envelope width equal to $\Delta\omega/\omega \simeq 2\Delta\gamma/\gamma \simeq 2\rho$. The several transitions occur randomly under the gain curve and this leads to the multiple-line chaotic spectrum observed in the classical SASE. Note also that, since the radiation is emitted in a time l_b/c , each line has a Fourier transformed line-

width ($\Delta\omega/\omega = \lambda_r/l_b$). Hence, assuming there are always enough random bunches to negate presence of long space with zero intensity between the spikes one can estimate that the average number of spikes N_s in a bunch of length l_b in the classical regime are given approximatively by the ratio between the envelope spectral width and the single spike spectral line-width [17], *i.e.*

$$N_s \sim \frac{2\rho}{\lambda_r/l_b} = \frac{l_b}{2\pi l_c}. \tag{4.7}$$

Conversely, in the quantum regime $\bar{\rho} \lesssim 1$, the momentum spread $\Delta(p)$ cannot be larger than the photon recoil $\hbar k_r$ and a single transition occurs, whose line-width is

$$\left(\frac{\Delta\omega}{\omega}\right)_{QFEL} \simeq \frac{\lambda_r}{l_b} \tag{4.8}$$

Hence, the ratio between the quantum and the classical line-width is given by Eq. (4.7). For instance, for a beam with $Q = 1$ nC and l_b=1 ps in the Angstrom region the QFEL line-width (see Eq.(4.8)) is of the order of 10^{-7} , whereas the line-width of the envelope of the classical SASE spectrum is of the order of 10^{-3}. Hence QFEL naturally produces transform limited radiation which would be useful for ultra-high resolution studies of processes.

4.1 Statistical proprieties of QFEL Radiation

The Self Amplified Superradiant Emission (SASE) mode for FEL is made up of three basic ingredients [17, 30, 31]:

- High-gain regime *i.e.* collective instability
- Propagation or 'slippage' effects
- Start-up from noise

This imply that the process of amplification in the SASE FEL starting from shot-noise in the electron beam have essentially a stochastic nature. Therefore a rigorous analysis of the FELs process must be done in terms of probabilistic statement. A complete study of the statistical proprieties of the SASE in the classical frame-work has been done by Saldin et al. in [18, 19]. Here we present a fully analysis of

the SASE FEL radiation spectral proprieties in both quantum and classical regime comparing the different results.

We have run on a parallel computer the equations (4.1)-(4.2). Each run yields a statistical ensemble of N_j shots, whose statistics is then investigated. In particular, we calculate:

1. The average value and the standard deviation of the integrated energy in the quantum regime $\bar{\rho} = 0.2$ for different value of the bunch length (Fig. (4.4))

2. The average value and the standard deviation of the istantaneous power in the quantum regime $\bar{\rho} = 0.2$ (Fig. (4.5))

3. The average and single shot spectrum value in the quantum regime $\bar{\rho} = 0.2$ for different position in the magnetic wiggler (Fig.(4.7))

4. The standard deviation of the average spectrum in the quantum regime $\bar{\rho} = 0.2$ for different value of the bunch length (Fig. (4.8)) and for different value of $\bar{\rho}$ (Fig. (4.9))

5. The standard deviation of the average spectrum in the classical and in the quantum regime (Fig. (4.10)) (normalized to the saturation length)

6. The line-width of the single spectral spike (Fig. (4.11))

As in the previous simulation we assume that all electrons are initially in the momentum state $n = 0$ with the initial conditions (4.3). Moreover, the initial bunching amplitude $|b_0|$ is randomly generated with a negative exponential distribution for $|b_0|^2$ [20, 18] (see fig.4.3).

The 1D quantum model depends only by the QFEL parameter $\bar{\rho}$. Then we introduce a convenient quantum scaling, *i.e.* we rescale all variables and parameters in terms of $\bar{\rho}$:

$$\tilde{z} = \sqrt{\bar{\rho}}\bar{z}, \quad \tilde{z_1} = \sqrt{\bar{\rho}}\bar{z_1}, \quad \tilde{\omega} = \bar{\omega}/\sqrt{\bar{\rho}} = \tilde{l_c}(\omega - \omega_r)/c, \quad \tilde{A} = \sqrt{\bar{\rho}}A_r. \quad (4.9)$$

The new scaled amplitude is such that $|\tilde{A}|^2 = \bar{\rho}|A_r|^2 = \langle N_{phot}/N_e \rangle$ is the average number of photons emitted per electron, and

$$\tilde{l_g} = \frac{l_g}{\sqrt{\bar{\rho}}} \quad \text{and} \quad \tilde{l_c} = \frac{l_g}{\sqrt{\bar{\rho}}} \quad (4.10)$$

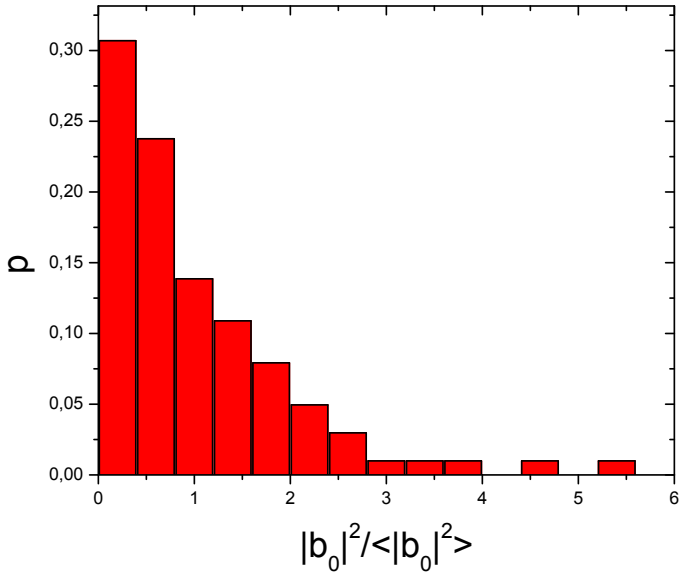

Figure 4.3: Initial distribution of $|b_0|^2$ generated in the code.

are respectively the quantum gain length (3.23) and the quantum cooperation length. Using the quantum scaling low in Eq. (4.9) our working equations (4.1)-(4.2) become:

$$\frac{\partial c_n}{\partial \tilde{z}} = -i\tilde{E}_n c_n - \left[\tilde{A}c_{n-1} - \tilde{A}^* c_{n+1}\right] \tag{4.11}$$

$$\frac{\partial \tilde{A}}{\partial \tilde{z}} + \frac{\partial \tilde{A}}{\partial \tilde{z_1}} = \sum_{n=-\infty}^{+\infty} c_n c_{n-1}^* + i\tilde{\delta}\tilde{A} \tag{4.12}$$

where $\tilde{E}_n = n^2/2\bar{\rho}^{3/2} + n\tilde{\delta}$ with $\tilde{\delta} = \delta/\sqrt{\bar{\rho}}$.

4.2 Average Energy of SASE radiation

The average energy E vs. $\tilde{z}$ is defined as

$$E(\tilde{z}) = \frac{1}{\tilde{l}_b}\int_0^{\tilde{l}_b+\tilde{z}} d\tilde{z_1}|\tilde{A}(\tilde{z},\tilde{z_1})|^2. \tag{4.13}$$

As we have been shown before in the quantum regime the radiation spectrum is composed by a single narrow line, centered around $\tilde{\omega} = -1/(2\bar{\rho}^{3/2})$, which corresponds to a frequency $\omega \approx \omega_s - \omega_{rec}$ down shifted with respect to the classical resonant frequency ω_s by the relativistic recoil frequency, $\omega_{rec} = 2\hbar k_s^2/m\gamma_0$ (see eq.(4.5)).

The spectrum in the exponential regime, up to saturation, is well approximated by a Gaussian curve. In fact, from the linear theory (see section 3.2.3) [27, 29, 32, 33].

$$|\tilde{A}(\tilde{\omega},\tilde{z})|^2 \approx \frac{1}{4}\langle|b_0(\tilde{\omega})|^2\rangle e^{\sqrt{4-(\tilde{\omega}-\tilde{\omega}_0)^2}\tilde{z}} \approx \frac{1}{4}\langle|b_0(\tilde{\omega})|^2\rangle e^{2\tilde{z}} e^{-(\tilde{\omega}-\tilde{\omega}_0)^2/2\sigma^2}. \tag{4.14}$$

where $\sigma = \sqrt{2/\tilde{z}}$. An approximated solution for equation (4.13) can be obtained as follows: the initial bunching amplitude is given by

$$|b_0(\bar{z_1})|^2 = \frac{1}{N_e^2}\sum_{i,j}\exp[i(\phi(\bar{z_1})_i^0 - \phi(\bar{z_1})_j^0)] = \frac{1}{N_e} + \frac{1}{N_e^2}\sum_{i\neq j}\exp[i(\phi(\bar{z_1})_i^0 - \phi(\bar{z_1})_j^0)], \tag{4.15}$$

starting from noise the initial phases $\phi^0(\bar{z_1})$ is random variable, so that the last sum with $i \neq j$ vanishes and the initial bunching amplitude average over a λ_r distance can be approximated by $\langle|b_0|\rangle \simeq 1/\sqrt{N_{\lambda_r}}$, where $N_{\lambda_r} = I/(ec)\lambda_r$ is the number of electrons within a longitudinal distance λ_r, I and e are respectively the current of the e-beam and the charge of the single electron. Since $b_0(\tilde{\omega})$ is the Fourier transform of $b_0(\tilde{z_1})$, then using Parsifal theorem $\Delta\tilde{\omega}\langle|\tilde{b}_0(\tilde{\omega})|^2\rangle \sim \tilde{l_b}/N_{\lambda_r}$. Moreover taking $\Delta\tilde{\omega} \sim 1/(2\rho\sqrt{\bar{\rho}})$, from (4.14) we obtain, in the limit of very long beam,

$$E(\tilde{z}) \approx \frac{2\pi}{\tilde{l_b}}\int_{-\infty}^{+\infty} d\tilde{\omega}|\tilde{A}(\tilde{\omega},\tilde{z})|^2 \approx \frac{\pi\rho\sqrt{\pi\bar{\rho}}}{N_\lambda\sqrt{\tilde{z}}}e^{2\tilde{z}} \approx \frac{\sqrt{\pi}}{2N_c\sqrt{\tilde{z}}}e^{2\tilde{z}}, \tag{4.16}$$

where $N_c = N_{\lambda_r}(\lambda_r/\tilde{l_c})$ is the number of electrons in the cooperation length $\tilde{l_c}$.

Fig.4.4a shows E vs. $\tilde{z}$ for $\bar{\rho} = 0.2$ and three different beam lengths: $\tilde{l_b} = 22.36$ (black continuous line), $\tilde{l_b} = 17.89$ (blued dashed line) and $\tilde{l_b} = 13.42$ (red dotted line). The values are the average of a sample of 303 shots. The saturation is reached after approximately nine quantum gain length (*i.e.* $\tilde{z} = 9$). The maximum of E is approximately 0.7, so that on average the number of emitted photons is the 70% of the total number of electrons in the beam. We note that E is independent on the beam length $\tilde{l_b}$ for a sufficiently long electron beam. Fig.4.4a shows also the fit of E in the linear regime made by the function $(\alpha/\sqrt{\tilde{z}})\exp(\beta\tilde{z})$, as it results from the analytical expression (4.16). The fit yields $\alpha = 3\times10^{-7}$ and $\beta = 1.9$, in rather good agreement with the expected value from the approximated equation (4.16), $\alpha = 5\times10^{-7}$ and $\beta = 2$.

Fig. 4.4b shows the relative fluctuation σ_E/E vs. $\tilde{z}$ for the three different beam lengths. It is seen that the fluctuations reach their maximum at the end of the linear regime. The first local minimum corresponds to the saturation point ($\tilde{z} = 9$). Notice that the fluctuations decrease when the electron bunch length increases.

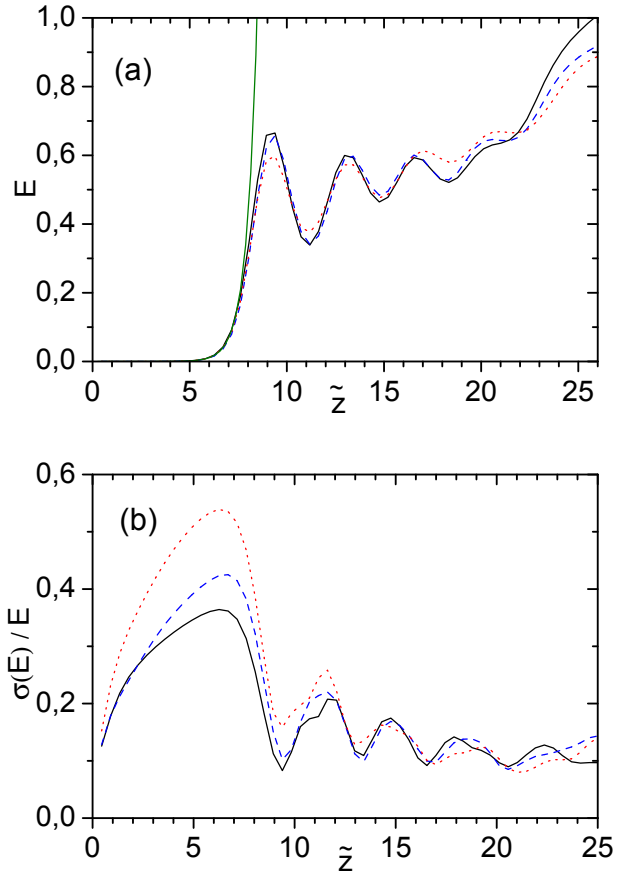

Figure 4.4: (a): Average energy E vs. $\tilde{z}$ for $\bar{\rho} = 0.2$, $\tilde{l_b} = 22.36$ (black continuous line), $\tilde{l_b} = 17.89$ (blued dashed line) and $\tilde{l_b} = 13.42$ (red dotted line).The green line shows the approximated solution (4.16); (b): Relative fluctuation σ_E/E vs. $\tilde{z}$ for the three different beam lengths of (a).

Fig.4.5 shows the instantaneous power $P = |\tilde{A}|^2$, averaged over the statistical sample, and their fluctuations σ_P/P vs. $\tilde{z}$ in the middle of the electron beam ($\tilde{z_1} = \tilde{l_b}/2$). In the linear regime of SASE mode operation the value of the deviation is close to unity, and its minimum at saturation.

In fig.4.6 we show the histograms of the probability density distributions, $p(P)$, of the instantaneous output power and $p(E)$, of the average energy, at different dimensionless wiggler length $\tilde{z}$. We observe that in the linear regime $p(P)$ is still a negative exponential distribution (see the case $\tilde{z} = 5$ in fig.4.6), whereas the energy distribution $p(E)$ follows a Gamma distribution $p(x) = (M^M/\Gamma(M))x^{M-1}\exp(-Mx)$,

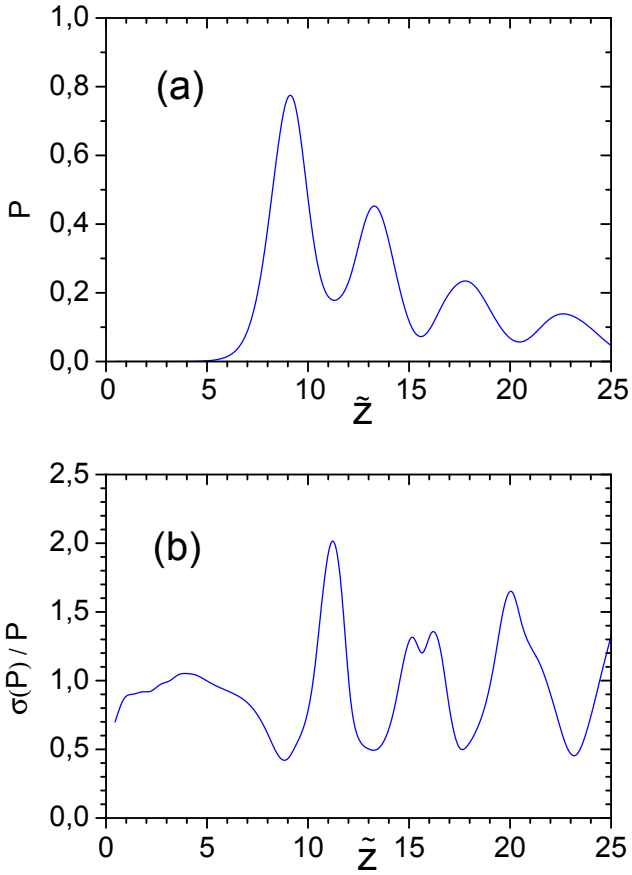

Figure 4.5: Instantaneous power $P = |\tilde{A}|^2$ (a) averaged over 303 shots and their fluctuations σ_P/P (b) vs. $\tilde{z}$ at $\tilde{z}_1 = \tilde{l}_b/2$, for $\bar{\rho} = 0.2$ and $\tilde{l}_b = 22.36$.

where $x = E/\langle E\rangle$, $M = \sigma_x^{-2} \approx 8.37$ and $\sigma_x = \sigma_E/\langle E\rangle = 0.346$.

After saturation, the energy distribution can be approximated by a Gaussian distribution. Note also that whereas in the linear regime the energy fluctuations $\sigma(E)/E$ is inversely proportional to $\sqrt{\tilde{l}_b}$ and grows with $\tilde{z}$, after saturation it is almost stationary and independent on $\tilde{l}_b$ (see fig.4.4b).

Finally, we have investigated the dependence of M on the beam length $\tilde{l}_b$ and on the wiggler length $\tilde{z}$. A numerical fit shows that $M \approx C(\tilde{l}_b/\tilde{z})$ with $C \approx 1.5 \pm 0.2$. Whereas the linear dependence on the beam length is the same as in the classical case, the dependence on $\tilde{z}$ is rather unexpected, since the frequency bandwidth is $\sigma = \sqrt{2/\tilde{z}}$, so that $M \propto \tilde{l}_b\sigma^2$, instead of the more usual relation $M \propto \tilde{l}_b\sigma$ obtained in the classical regime.

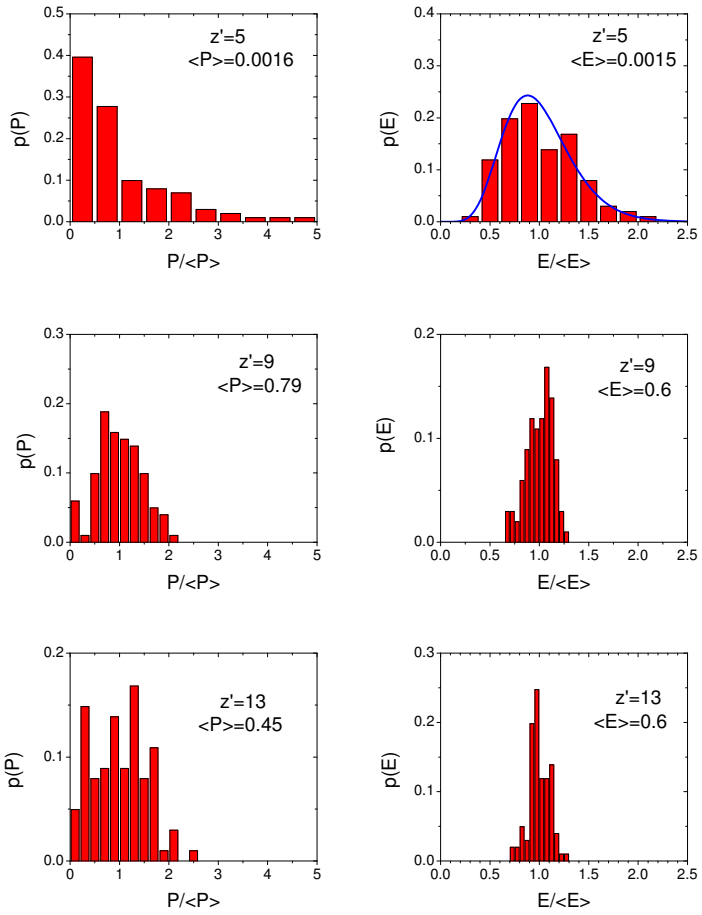

Figure 4.6: Histograms of the probability density distributions, $p(P)$, of the instantaneous output power and $p(E)$, of the average power, at $\tilde{z} = 5, 9, 13$. Calculations have been performed over 303 independent statistical events.

4.3 Spectral proprieties of SASE radiation

The single-shot radiation spectrum is mainly composed by a single narrow line, as it can be see in fig.4.7, showing the spectrum vs. $\tilde{\omega}$ at different $\tilde{z}$ for $\tilde{l}_b = 22\tilde{l}_c$, and $\bar{\rho} = 0.2$. The figure shows two typical single-shot spectra and the spectrum averaged over 303 shots. We observe that initially (e.g. for $\tilde{z} = 1$) the spectrum is broad and contains many spikes . However, during the exponential regime the spectrum cleans up and the single shot produces a single main spectral line. Note also that the spectral line of the single-shot spectrum is much narrower than the average spectral line.

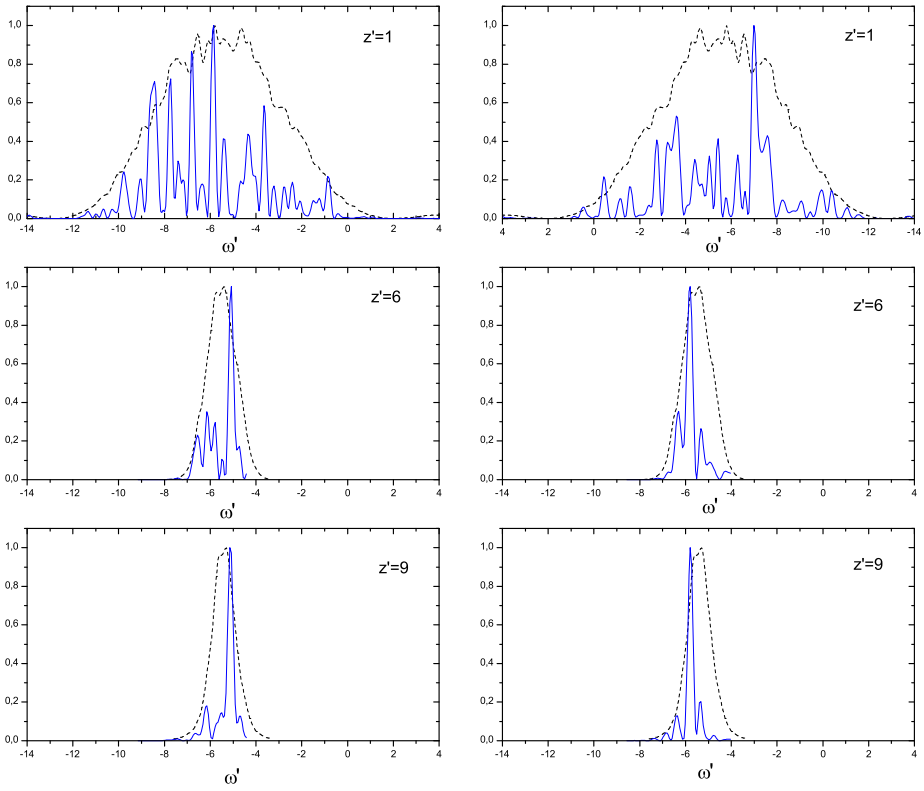

Figure 4.7: Average spectrum and single-shot spectrum for $l_b = 22\tilde{l_c}$ at different $\tilde{z}$, $\bar{\rho} = 0.2$

The average spectral width σ vs. $\tilde{z}$ is plotted in fig.4.8 for different beam lengths $\tilde{l_b}$. It can be seen that σ is independent on l_b and it reaches a minimum (~ 0.5) at saturation (i.e. at $\tilde{z} = 9$). The dashed line is the approximated solution $\sqrt{2/\tilde{z}}$ obtained in the linear regime (see eq.(4.14)). After saturation, the spectral width increases and the shape acquires some structure.

Fig.4.9 compares the average spectral width $\sigma_{\bar{\omega}} = \sqrt{\bar{\rho}}\tilde{\sigma}$ vs. z/z_{sat} obtained in the quantum regime ($\bar{\rho} = 0.2$) with the one obtained in the classical regime ($\bar{\rho}$ =2). The width in the quantum regime is a factor $\sqrt{\bar{\rho}}$ smaller than the classical one,

The scaling as $\sqrt{\bar{\rho}}$, in the quantum regime $\bar{\rho} \leq 1$ is demonstrated by fig.(4.10), where $\sigma' = \sigma_\omega/\sqrt{\bar{\rho}}$ is plotted for three different case $\bar{\rho} = 0.1$, 0.2 and 0.3 with

$l_b = 22\tilde{l_c}$.

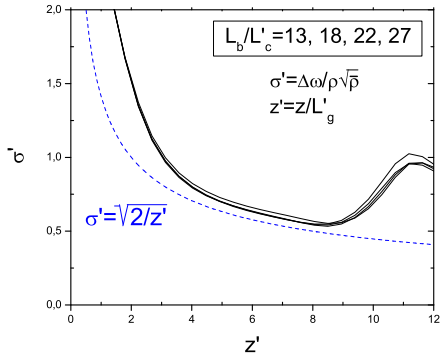

Figure 4.8: Average spectral width for different bunch lenght, $\bar{\rho} = 0.2$

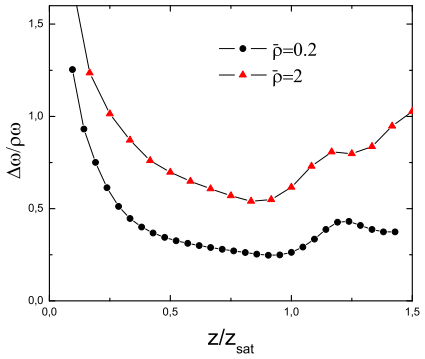

Figure 4.9: Average spectral width for different $\bar{\rho} = 0.1\ , 0.2\ , 0.3\ ,\ l_b = 22\tilde{l_c}$

Finally we have studied the evolution of the single shot spike width σ_ω^{spikes}: fig.4.11 shows σ_ω^{spikes} vs. $1/\tilde{l_b}$ for different value of $\tilde{l_b}$ where $\tilde{l_b} = l_b/\tilde{l_c}$. This simulation confirms our prediction of Eq.(4.8); in fact the data are well interpolate by the linear relation $\sigma_\omega^{spikes} \simeq 2\pi/\tilde{l_b}$ which, back to dimensionless variables, can be written as $\Delta\omega/\omega = \lambda_r/l_b$ [17, 35, 31].

Note that in this analysis the energy spread effects have been neglected, so this scaling low is not bounded below. In fact should there exist an intrinsic limit to the

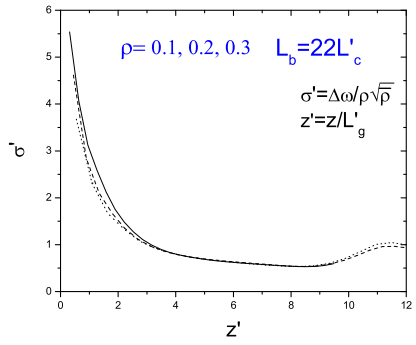

Figure 4.10: quantum average spectral width ($\bar{\rho} = 0.2$) and classical average spectral width ($\bar{\rho} = 2$), $l_b = 30\tilde{l_c}$

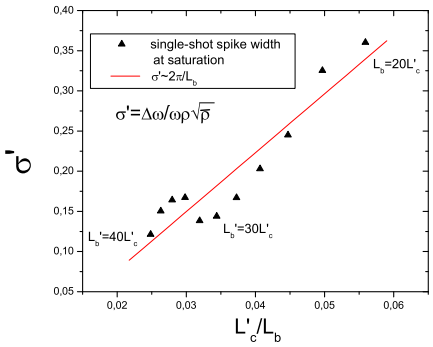

Figure 4.11: spectral width of the spike at $z_{sat} =$ for $\bar{\rho} = 0.2$ vs. $l_b/\tilde{l_c}$.

narrowing of the single spike due to the longitudinal energy fluctuations *i.e.* when the e-beam is characterized by a longitudinal temperature different from zero.

Chapter 5

Quantum 3D Free Electron Laser Model

The one-dimensional analysis of the quantum FEL suggests that an experiment in the X-ray region, confirming the existence of the "quantum purification" phenomenon (see chapter (3) and (4) and [30, 31, 47]), could be envisaged in a near future. Therefore, the extension of the 1D quantum model to a "more realistic" 3D scheme is more than ever necessary. In the classical framework, the extension from 1D to 3D is rather straightforward, as shown by the different classical models present in the literature [56, 57, 51, 52]. Several SASE-FEL experiments based on these theories are actually in progress [53, 54, 55] and some numerical friendly codes were been developed for the 3D simulations, as for instance `GENESIS` [50]. In this experiment the device is composed by magnetic wiggler, for instance in the LCLS-project at SLAC the magnetic wiggler is long about 10^2 m while, as we have shown in Section (2.3.3), a future QFEL experiment needs a laser wiggler instead of the static magnetic wiggler and the beam requirement are much stronger that in the classical case. In particular the energy spread and the emittance requirements of the electron beam are under the actual experimental possibility, but we trust in the next future technology evolution. The experimental requirement for an X-ray future experiment will be treated exhaustively in the next chapter.

The extension from 1D to a 3D theory in a quantum framework is not so straightforward as in the classical case. This fact is principally linked to the different nature of the electron-radiation interaction along the longitudinal and transverse directions.

In fact, whereas along the longitudinal axis the photon recoil effect is dominant and needs a quantum description, on the contrary in the transverse dynamics the quantum effects appear less relevant. For these reasons, a model describing either the quantum behaviour along the longitudinal and the approximately classical behaviour along the transverse coordinates, is demanded.

As we have shown in chapter 3 and following [24, 29], in the 1D quantum model the electrons are treated as "non interacting" bosons, *i.e.* the electron-electron interaction is neglected and the electrons of the beam communicate each other via the radiation field. In particular the e-beam is described by a Schrödinger mean-field operator obeying the bosonic equal-time commutation relation. The extension of the 1D model into a 3D geometry does not leads to a correct model, because the 3D Schrödinger equation describes a pure state (*i.e.* $\Delta x \Delta p_x \sim \hbar$) with a transverse normalized emittance $\epsilon_n = \gamma \epsilon_r$ equal to the Compton wavelength $\epsilon_n \simeq \lambda\!\!\!^{-}_c$ and a transverse momentum distribution with a width near to the Heisenberg's Uncertainty Principle (HUP) limit *i.e.* $\Delta x'_{pure} \sim \lambda\!\!\!^{-}_c/(\sigma\gamma_r)$. However we are interested to describing only electron beams in which the transverse momentum distribution is thermal, *i.e.* with a width $\Delta x'_{therm} \sim \epsilon_n/(\sigma\gamma_r)$ much larger than the quantum limit. Therefore our system should be described by a mixed state with $\Delta x \Delta p_x \gg \hbar$ which can be conveniently represented by a Wigner distribution function. The Wigner distribution function was introduced in section 3.3 in terms of the pure state $\Psi(\theta)$ (see Eq.(3.53)). However it can be defined also in terms of the density operator ϱ that describes more general mixed state [44] (for a pure state $\varrho = |\psi\rangle\langle\psi|$). Up to now we have used the first quantization formalism, but we shall see in the following that the Wigner function can be also defined in the second quantization formalism, in which the multi particles nature of the FEL process can be treated in a more natural way. In this chapter we develop a 3D Quantum FEL theory starting from a new point of view following the quantum statistical approach developed in [45]; obviously our intent is to obtain a set of coupled equations which describes the evolution of a 3D electron beam interacting with a e.m./ laser wiggler field. This set of equations must be admit three fundamental limits:

1. transverse classical limit *i.e.* there should exist a parameter ruling the transition from the quantum to the classical behaviour for the transverse motion only;

2. 1D limit *i.e.* the 3D equations should reduce to Eqs.(3.64)-(3.67) when transverse effects are neglected;

3. full classical limit *i.e.* the 3D Maxwell-Wigner equations should reduce to the 3D classical Maxwell-Vlasov equations.

The chapter is organized as follows: in section 5.1 we introduce the Wigner distribution function in terms of the second quantization formalism, then we discuss some reasonable simplification which lead to the One Particle Wigner Distributions (1PW) definition. In section 5.2 we obtain the three dimensional FEL Hamiltonian in second quantization scheme. In section 5.3 we derive the evolution equation for the 1PW using the Von Neumann evolution equation and the 3D Hamiltonian obtained in section 5.2. In section 5.4 we obtain the 3D evolution equation for the slowly varying amplitude of the radiation field A_r using the multiple scaling method. Finally in section 5.5 we perform the Classical Transverse limit in order to obtain the required set of equations which describe the 3D QFEL dynamics.

5.1 3D Wigner Distribution

In spite of the common Hamiltonian structure there are considerable differences between the classical and the quantum formalism. In the classical case the observables are describe by functions while in the quantum case these functions becomes operators acting on the abstract Hilbert space. It is well known that due to the "Weyl correspondence rule" there exists a representation of the quantum mechanics that is much closer to the classical mechanics. Here we review only the basic concepts which are necessary for our attempts. We start by noting that an arbitrary operator $\hat{O}$, in the second quantization formalism, can be written in terms of the Schrödinger operator as follows:

$$\begin{aligned} \mathbf{O} = O_0 \;&+\; \int \mathrm{d}\mathbf{x}_1 \; \mathbf{\Psi}^\dagger(\mathbf{x}_1)\, \hat{O}_1 \; \mathbf{\Psi}(\mathbf{x}_1) + \dots \\ &+\; (s!)^{-1} \int \mathrm{d}\mathbf{x}_1 \dots \mathrm{d}\mathbf{x}_s \; \mathbf{\Psi}^\dagger(\mathbf{x}_1) \dots \mathbf{\Psi}^\dagger(\mathbf{x}_s) \hat{O}_s \mathbf{\Psi}(\mathbf{x}_1) \dots \mathbf{\Psi}(\mathbf{x}_s) \\ &+\; \dots \end{aligned} \tag{5.1}$$

Here the Schrödinger operator can represent both fermions or bosons, depending on the choice of the commutation rules; for example, the Schrödinger operator defined

by the Eqs.(3.26), is a boson operator. Here we define general commutation rules valid for both cases:

$$\begin{aligned}\left[\mathbf{\Psi}(\mathbf{x}),\mathbf{\Psi}^{\dagger}(\mathbf{x}')\right]_{\theta} &= \delta(\mathbf{x}-\mathbf{x}')\\ \left[\mathbf{\Psi}^{\dagger}(\mathbf{x}),\mathbf{\Psi}^{\dagger}(\mathbf{x}')\right]_{\theta} &= \left[\mathbf{\Psi}(\mathbf{x}),\mathbf{\Psi}(\mathbf{x}')\right]_{\theta} = 0\end{aligned} \tag{5.2}$$

where $\theta = \pm$ with $[a,b]_{-} = ab - ba$ for bosons and $[a,b]_{+} = ab + ba$ for fermions.

The average value of the (5.1) operator is expressed in terms of the density matrix ϱ as

$$\begin{aligned}\langle\mathbf{O}\rangle &= \mathrm{Tr}\varrho\mathbf{O}\\ &= \sum_{s}(s!)^{-1}\int \mathrm{d}\mathbf{x}_1\ldots\mathrm{d}\mathbf{x}_s\ \mathrm{Tr}\left\{\varrho\mathbf{\Psi}^{\dagger}(\mathbf{x}_1)\ldots\mathbf{\Psi}^{\dagger}(\mathbf{x}_s)\hat{O}_s\mathbf{\Psi}(\mathbf{x}_1)\ldots\mathbf{\Psi}(\mathbf{x}_s)\right\}\end{aligned} \tag{5.3}$$

Note that it is always possible to move the time dependence from the operator to the density matrix *i.e.* if the operator is time dependent then

$$\mathrm{Tr}\varrho\mathbf{O}(t) = \mathrm{Tr}\varrho(t)\mathbf{O} \tag{5.4}$$

(see ref.[45] for the demonstration).

Now using the "Weyl correspondence rule" we write the first quantized operator in term of classical variables

$$\hat{O} = \int \mathrm{d}\mathbf{k}_1\mathrm{d}\mathbf{j}_1\ldots\mathrm{d}\mathbf{k}_s\mathrm{d}\mathbf{j}_s\beta(\mathbf{k}_1\mathbf{j}_1,\ldots,\mathbf{k}_s\mathbf{j}_s)\exp\left(-i\sum_{n=1}^{s}\mathbf{k}_n\cdot\hat{\mathbf{q}}_{\mathbf{n}}+\mathbf{j}_n\cdot\hat{\mathbf{p}}_{\mathbf{n}}\right) \tag{5.5}$$

where $\mathbf{q}_{\perp n}$, $\mathbf{p}_{\perp n}$ are position and momentum canonical conjugate variables and $\beta(\mathbf{k}_1\mathbf{j}_1,\ldots,\mathbf{k}_s\mathbf{j}_s)$ is a function such that $\beta(-\ldots) = \beta^{*}(+\ldots)$ in order to ensure the hermitian character of the operator $\hat{O}$.

The above representation permits us, making same algebra [45] [46], to obtain the representation of the average value of a general quantum observable:

$$\langle\mathbf{O}\rangle = \sum_{s=1}^{\infty}(s!)^{-1}\int \mathrm{d}\mathbf{q}_1\mathrm{d}\mathbf{p}_1\ldots\mathrm{d}\mathbf{q}_s\mathrm{d}\mathbf{p}_s\ O_s(\mathbf{q}_1\mathbf{p}_1,\ldots,\mathbf{q}_s\mathbf{p}_s)\ W_s(\mathbf{q}_1\mathbf{p}_1,\ldots,\mathbf{q}_s\mathbf{p}_s) \tag{5.6}$$

where we have defined the *s-particle Wigner function* $W_s(\mathbf{q}_1\mathbf{p}_1,\ldots,\mathbf{q}_s\mathbf{p}_s)$ as follows:

$$\begin{aligned}W_s(\mathbf{q}_1\mathbf{p}_1,\ldots,\mathbf{q}_s\mathbf{p}_s) = (8\pi^3)^{-s}\int \mathrm{d}\mathbf{j}_1\ldots\mathrm{d}\mathbf{j}_s\exp\left(-i\sum_{n=1}^{s}\mathbf{j}_n\cdot\mathbf{p}_n\right)\\ \times\mathrm{Tr}\left\{\varrho\mathbf{\Psi}^{\dagger}(\mathbf{q}_1-\frac{1}{2}\hbar\mathbf{j}_1)\ldots\Psi^{\dagger}(\mathbf{q}_s-\frac{1}{2}\hbar\mathbf{j}_s)\Psi(\mathbf{q}_1+\frac{1}{2}\hbar\mathbf{j}_1)\ldots\Psi(\mathbf{q}_s+\frac{1}{2}\hbar\mathbf{j}_s)\right\}\end{aligned} \tag{5.7}$$

with normalization:

$$\int \mathrm{d}\mathbf{q}_1\mathrm{d}\mathbf{p}_1 \ldots \mathrm{d}\mathbf{q}_s\mathrm{d}\mathbf{p}_s W_s(\mathbf{q}_1\mathbf{p}_1, \ldots, \mathbf{q}_s\mathbf{p}_s) = \frac{N!}{(N-s)!} \tag{5.8}$$

The (5.6) representations is the quantum analog to the average value of a general observable in classical statistical mechanics. However this is only an analogy, in fact it is well known that the phase space (q, p) of a system can not have the same meaning in the classical and in the quantum mechanics. In the latter case we can not represent a pure state of the system by a point in phase space because of the Heisenberg's principle. In spite of this fact, the statistical representation of a many-body system is possible in term of a distribution vector,

$$\mathbf{W} = \{W_s(\mathbf{q}_1\mathbf{p}_1, \ldots, \mathbf{q}_s\mathbf{p}_s); s = 1, \ldots, \} \tag{5.9}$$

whose component are s-particle Wigner functions. In terms of these functions, and in terms of the sets of observable $O_s(\mathbf{q}_1\mathbf{p}_1, \ldots, \mathbf{q}_s\mathbf{p}_s)$ the "formulation" of quantum mechanics is identical to the classical one.

As shown before, since the time dependence can be included within the statistic operator, the evolution equation for the reduced Wigner function is related to the basic Von Neumann equation for the density matrix:

$$i\hbar\frac{\partial}{\partial t}\varrho(t) = [H, \varrho(t)]_- \tag{5.10}$$

Let us note that the Von Neumann equation is independent of the representation chosen for the operator. The Von Neumann equation shows that the evolution equation depends by the Hamiltonian of the system, so usually (for almost all physical systems) the Hamiltonian is made up by the sum of one-particle and two-particle operators which in general are respectively the kinetic term and the interaction potential term. This means that instead of all s-component in the Wigner distribution vector we could considerate the first two terms only (s=1,2). This shows that in classifying the operators as in Eq.(5.1) we bring out a feature of a great simplicity, which is very helpful, especially in dealing with a system of many particles. The s-representation of the operator in Eq.(5.1) can be interpreted as the sum of s terms $\mathbf{O} = \mathbf{O}_0 + \mathbf{O}_1 + \mathbf{O}_2 + \ldots$ each of them represents: for $s = 1$ a system of N non

interacting particles, for $s = 2$ a system of N interacting particles where the interaction is limited only between two neighbours ..., an so on. Since the FEL dynamics is described by a single particle Hamiltonian (see Eq.(3.12)), we consider only the first term ($s = 1$) of the Wigner vector (5.9), which corresponds to the One Particle Wigner Distribution (1PW) (for simplicity $W_1 = W$).

$$W(\mathbf{q},\mathbf{p}) = (8\pi^3)^{-1} \int \mathrm{d}\mathbf{j}\, \exp\left(-i\mathbf{j}\cdot\mathbf{p}\right) \mathrm{Tr}\left\{ \varrho\ \mathbf{\Psi}^{\dagger}(\mathbf{q} - \frac{1}{2}\hbar\mathbf{j})\mathbf{\Psi}(\mathbf{q} + \frac{1}{2}\hbar\mathbf{j}) \right\} \quad (5.11)$$

with normalization:

$$\int \mathrm{d}\mathbf{q}\ \mathrm{d}\mathbf{p}\ W(\mathbf{q},\mathbf{p}) = N. \quad (5.12)$$

Then, the average value of a general quantum observable can be written as:

$$\langle \mathbf{O} \rangle = \int \mathrm{d}\mathbf{q}\ \mathrm{d}\mathbf{p}\ O_s(\mathbf{q},\mathbf{p})\ W(\mathbf{q},\mathbf{p}) \quad (5.13)$$

Note that an extension of the model in which the two particle Wigner function is also included can be of interest principally for two reasons: 1) In this work the 3D space charge effects have been neglected. However, if these effects are considered, a two-particle operator is needed, (this operator represents the Columbian potential between electrons) in the 3D QFEL Hamiltonian, 2) as we shall see in section 5.3 and in appendix C the 1PW formalism is independent on the statistic of the particles *i.e.* different choice of the commutation rules ($\theta = +$ for fermions or $\theta = -$ for bosons) bring to the same evolution equation for the 1PW. The first difference between fermions and bosons appears in the two-particle ($s = 2$) Wigner function.

5.2 Quantum 3D Hamiltonian

In this section we obtain the second quantized FEL Hamiltonian. Let start from the Classical 3D Hamiltonian obtained in chapter (2.108); we drop, for simplicity, the charge term (see section. (2.1.2)).

$$\bar{H} = \frac{\bar{p}^2}{2} + \frac{b}{2}\bar{\mathbf{p}}_{\perp}^2 + \bar{p}\left[\frac{\xi}{2\rho}(1 - |g|^2) - \frac{bX}{4}\bar{\mathbf{p}}_{\perp}^2\right] + \frac{\xi}{\rho X}|g|^2 + i\left(g^* A_r e^{i\theta} - c.c.\right), \quad (5.14)$$

where $\bar{\mathbf{x}}_\perp = (\bar{x}, \bar{y})$ and $\bar{\mathbf{p}}_\perp = (\bar{p}_x, \bar{p}_y y)$. The variables are defined in the "Classical 3D Universal Scaling" (see Eq.(2.104)):

$$\begin{cases} \theta = (k_r + k_l)\, z - c\,(k_r - k_l)\, t, \\ \\ \bar{z} = \dfrac{z}{l_g}, \quad \bar{z_1} = \dfrac{\bar{z} - \bar{v}_e \bar{t}}{l_c \bar{\beta}_e} \\ \\ \bar{p} = \dfrac{\gamma - \gamma_r}{\rho \gamma_r}, \quad \delta = \dfrac{\gamma_0 - \gamma_r}{\rho \gamma_r} \\ \\ \bar{\mathbf{x}}_\perp = \mathbf{x}_\perp / \sigma, \quad \bar{\mathbf{p}}_\perp = \dfrac{\sigma}{\epsilon_r} \beta_\perp \\ \\ A_r = \dfrac{\omega}{\omega_p \sqrt{\rho \gamma}} a_r. \end{cases} \tag{5.15}$$

and σ is the rms electron 'radius' at the beam waist, ϵ_r is the rms beam emittance and ω_p is the plasma frequency. Note that $g = g(\mathbf{x}_\perp, \bar{z})$ in Eqs. (**??**) and (5.19) represents the transverse laser wiggler profile whose analytic form will be specified in the next chapter. The three dimensional parameters are defined as follows:

$$X = 2k\epsilon_r, \qquad b = \frac{l_g}{\beta^*} = \frac{l_g \epsilon_r}{\sigma^2} \qquad \xi = \frac{a_0^2}{1 + a_0^2}. \tag{5.16}$$

The physical meaning of each single term of the Hamiltonian will be discussed in detail in the next chapter.

At the beginning of this chapter we have prefigured that should there exist one parameter which rules the transition between the quantum and classical regime on the longitudinal direction and one parameter which rules the transition from quantum and classical regime on the transverse direction. At this point we write explicitly the form of this two important parameters.

- QFEL parameter (see Eq.(2.112)).

$$\bar{\rho} = \rho \frac{mc\gamma_r}{\hbar k_r} \tag{5.17}$$

- Transverse parameter:

$$\alpha = \frac{\hbar}{mc\gamma_r\epsilon_r} \tag{5.18}$$

The meaning of $\bar{\rho}$ is well known, while it is possible to note that the transverse parameter α can be obtained by the ratio between the width of a thermal and cold momentum distributions as we have defined at the beginning of the chapter, *i.e.* $\alpha = \Delta x_{pure}/\Delta x'_{therm} = \lambda\!\!\!^{-}_c/\epsilon_n$. The transverse parameter α plays a fundamental rule for the transition between the quantum and classical transverse dynamics. In fact when $\alpha \sim 1$ the transverse emittance is of the order of the Compton wavelength *i.e.* we are describing a 3D ultracold e-beam. On the contrary when $\alpha \ll 1$ the transverse emittance ϵ_n is much larger than the Compton wavelength *i.e.* we have a thermal transverse momentum distribution.

First quantized Hamiltonian

In order to quantize the system, let introduce the new longitudinal and transverse momenta scaled in terms of the parameters defined in Eqs. (5.17) and (5.18) such that:

$$\begin{cases} p = \dfrac{mc(\gamma - \gamma_0)}{\hbar k} \;\rightarrow\; p = \bar{p}\bar{\rho} - \delta \\ \\ \mathbf{p}_\perp = \left(\dfrac{mc\gamma_r\sigma}{\hbar}\right)\beta_\perp \;\rightarrow\; \mathbf{p}_\perp = (\alpha^{-1})\bar{\mathbf{p}}_\perp \end{cases} \tag{5.19}$$

These new variables are even canonical conjugate and satisfy the Poisson brackets rules (PBR):

$$\{\theta, p\} = 1 \quad \text{and} \quad \{x, p_x\} = 1, \;\; \{y, p_y\} = 1 \tag{5.20}$$

In order to quantize the Hamiltonian we adopt the canonical quantization rules, such that the dynamical variables become operators in Hilbert space,

$$\mathbf{x}_\perp \rightarrow \hat{\mathbf{x}}_\perp, \quad \mathbf{p}_\perp \rightarrow \hat{\mathbf{p}}_\perp = -i\nabla_{\mathbf{x}_\perp}, \qquad \theta \rightarrow \hat{\theta}, \quad p \rightarrow \hat{p} = -i\partial_\theta. \tag{5.21}$$

and the Poisson bracket (5.20) becomes Quantum Commutation Rules (QCR)

$$\{x, p_x\} = 1 \rightarrow [\hat{x}, \hat{p}_x]_- = i, \;\; \{y, p_y\} = 1 \rightarrow [\hat{y}, \hat{p}_y]_- = i \quad \text{and} \quad \{\theta, p\} = 1 \rightarrow [\hat{\theta}, \hat{p}]_- = i \tag{5.22}$$

The first quantized Hamiltonian $\bar{H}(\hat{\theta}, \hat{p},\ \hat{\mathbf{x}}_\perp, \hat{\mathbf{p}}_\perp; \bar{z} \mid \bar{z_1})$ can be written as follows:

$$\bar{H} = \bar{K} + \bar{D} + \bar{U}_1 + \bar{U}_2 \tag{5.23}$$

where

$$\begin{cases} \bar{K} = \dfrac{1}{2\bar{\rho}}\hat{p}^2 + \dfrac{\alpha b}{2}\hat{\mathbf{p}}_\perp^2 \\ \\ \bar{D} = \hat{p}\left[\delta + \dfrac{\xi}{2\rho}(1 - |g(\hat{\mathbf{x}}_\perp, \bar{z})|^2) - \dfrac{bX}{4}\alpha^2\hat{\mathbf{p}}_\perp^2\right] \\ \\ \bar{U}_1 = -i\bar{\rho}\left(g^*(\hat{\mathbf{x}}_\perp, \bar{z})A_r(\hat{\mathbf{x}}_\perp, \bar{z}, \bar{z_1})e^{i\hat{\theta}} - h.c.\right) \\ \\ \bar{U}_2 = \dfrac{\xi}{\alpha\rho X}|g(\hat{\mathbf{x}}_\perp, \bar{z})|^2 \end{cases} \tag{5.24}$$

are respectively the Kinetic operator $\bar{K}$, the Detuning operator $\bar{D}$ and the potential operators $\bar{U}_1\ \ \bar{U}_2$.

Note that $\bar{z_1}$-dependence is parametric, so we will omit it in the following. Moreover note that from Eq. (5.19) the new longitudinal and transverse momenta are proportional to $\hbar^{-1}$ (in fact $\hbar$ does not appear in the commutation rules (5.22)) moreover the new Hamiltonian (5.34) is also proportional to $\hbar^{-1}$ then the Von Neumann evolution equation (5.10) becomes:

$$i\frac{\partial}{\partial\bar{z}}\varrho(\bar{z}) = \left[\bar{H}, \varrho(\bar{z})\right]_- \tag{5.25}$$

Second quantized Hamiltonian

In order to define a second quantized Hamiltonian let introduce the Schrödinger operator which creates (or annihilate) one particle in the $(\theta, \mathbf{x}_\perp)$ position.

$$\mathbf{\Psi}(\theta, \bar{\mathbf{x}}_\perp) = \frac{1}{\sqrt{(2\pi)^3}}\sum_{m\in Z}\int_{R^2} \mathrm{d}\mathbf{k}_\perp^2\ \mathbf{c}_m(\mathbf{k}_\perp)\ e^{im\theta}\ e^{i\mathbf{k}_\perp\cdot\bar{\mathbf{x}}_\perp} \tag{5.26}$$

where the θ-periodicity of Ψ has been used. The commutation rules for the Schrödinger field operator (5.26) are:

$$\left[\mathbf{\Psi}^\dagger(\theta, \bar{\mathbf{x}}_\perp), \mathbf{\Psi}(\theta', \bar{\mathbf{x}}_\perp)\right]_\theta = \delta(\bar{\mathbf{x}}_\perp - \bar{\mathbf{x}}'_\perp)\delta(\theta - \theta'). \tag{5.27}$$

and the normalization condition is:

$$\int_0^{2\pi} \mathrm{d}\theta \int_{R^2} \mathrm{d}^2\mathbf{x}\ \mathbf{\Psi}^\dagger(\theta, \bar{\mathbf{x}}_\perp)\mathbf{\Psi}(\theta, \bar{\mathbf{x}}_\perp) = \mathbf{N}_e \tag{5.28}$$

The creation and annihilation operators acts on a the generic state of the multi particle Fock space

$$|n_m(\mathbf{k}_\perp)\rangle = \prod_{m\in Z} |n_m(\mathbf{k}_\perp)\rangle \tag{5.29}$$

where $n_m(\mathbf{k}_\perp)$ represents the number of electrons within the quantum state with discrete longitudinal momentum m and continuous transverse momentum $\mathbf{k}_\perp$. The action of the creator and annihilator operators on a Fock state (5.29) is different for bosons or fermions since it depends on the choice of the quantum commutation rules:

$$\begin{aligned}
\Big[\mathbf{c}_n(\mathbf{k}_\perp), \mathbf{c}^\dagger_{n'}(\mathbf{k}'_\perp)\Big]_\theta &= \delta(\mathbf{k}_\perp - \mathbf{k}'_\perp)\ \delta_{n,n'} \\
\Big[\mathbf{c}_n(\mathbf{k}_\perp), \mathbf{c}_{n'}(\mathbf{k}'_\perp)\Big]_\theta &= 0 \\
\Big[\mathbf{c}^\dagger_n(\mathbf{k}_\perp), \mathbf{c}^\dagger_{n'}(\mathbf{k}'_\perp)\Big]_\theta &= 0
\end{aligned} \tag{5.30}$$

where $\theta = \pm 1$ and $[a, b]_\pm = ab \pm ba$. For an ensemble of N bosonic particles the initial state can be assumed with all electrons in the same longitudinal $\bar{m}$ and transverse $\bar{\mathbf{k}}_\perp$ momentum state:

$$|n_{\bar{m}}(\bar{\mathbf{k}}_\perp)\rangle = |0_0, 0_1, \ldots, N_e, 0_{\bar{m}+1} \ldots, 0_\infty\rangle \quad \text{BOSONS} \tag{5.31}$$

Conversely if we treat an ensemble of N fermionic particles in the initial state, they can not stay all in the same quantum state because of the Pauli Principle, so we assume that all the particles have the same longitudinal momentum $\bar{m}$ but a different transverse momentum $\mathbf{k}_\perp$, in order to have a different quantum state for each particle (we neglect spin).

$$|n_{\bar{m}}(\mathbf{k}_\perp)\rangle = |0_0(\mathbf{k}_\perp), 0_1(\mathbf{k}_\perp), \ldots, n_{\bar{m}}(\mathbf{k}_\perp), 0_{\bar{m}+1}(\mathbf{k}_\perp) \ldots, 0_\infty(\mathbf{k}_\perp)\rangle \text{ FERMIONS} \tag{5.32}$$

We shall see, in the following, how the initial conditions is describes by the 1PW. Note that we have neglected the energy spread effects, since in each of the above

mentioned initial state (Eqs.5.31-5.32) all the particles are in the same longitudinal momentum state $\bar{m}$. Now, the second quantized Hamiltonian can be obtained in terms of the first quantized Hamiltonian (5.34):

$$\mathbf{H} = \int_0^{2\pi} \mathrm{d}\theta \int_{R^2} \mathrm{d}^2\mathbf{x}\ \mathbf{\Psi}^\dagger(\theta, \bar{\mathbf{x}}_\perp)\ \bar{H}(\hat{\theta}, \hat{p},\ \hat{\mathbf{x}}_\perp, \hat{\mathbf{p}}_\perp; \bar{z} \mid \bar{z_1})\ \mathbf{\Psi}(\theta, \bar{\mathbf{x}}_\perp) \tag{5.33}$$

With a standard calculation which is reported in the Appendix C we obtain the expression of the second quantized Hamiltonian in terms of the creation and annihilation operators,

$$\mathbf{H} = \mathbf{K} + \mathbf{D} + \mathbf{U}_1 + \mathbf{U}_2 \tag{5.34}$$

where

$$\begin{cases} \mathbf{K} = \sum_m \int_{R^2} \mathrm{d}^2\mathbf{k}_\perp \left[\frac{1}{2\bar{\rho}} m^2 + \frac{\alpha b}{2}\mathbf{k}_\perp^2\right] \mathbf{c}_m^\dagger(\mathbf{k}_\perp)\mathbf{c}_m(\mathbf{k}_\perp), \\ \mathbf{D} = \sum_m \int_{R^2} \mathrm{d}^2\mathbf{k}_\perp \left[\left(\delta + \frac{\xi}{2\rho}\right) m - \frac{bX}{4}\alpha^2 m \mathbf{k}_\perp^2\right] \mathbf{c}_m^\dagger(\mathbf{k}_\perp)\mathbf{c}_m(\mathbf{k}_\perp) + \\ \quad - \frac{\xi}{2\rho}\sum_m m \int_{R^2} \frac{\mathrm{d}^2\mathbf{q}_\perp}{2\pi} g_f(\mathbf{q}_\perp, \bar{z}) \int_{R^2} \mathrm{d}^2\mathbf{k}_\perp\ \ \mathbf{c}_m^\dagger(\mathbf{k}_\perp)\mathbf{c}_m(\mathbf{k}_\perp + \mathbf{q}_\perp), \\ \mathbf{U}_1 = -i\bar{\rho}\sum_m \int_{R^2} \mathrm{d}^2\mathbf{k}_\perp \int_{R^2} \frac{\mathrm{d}^2\mathbf{q}_\perp}{2\pi} \left\{ G_f(\mathbf{q}_\perp, \bar{z}, \bar{z_1})\ c_m^\dagger(\mathbf{k}_\perp)\mathbf{c}_m(\mathbf{k}_\perp + \mathbf{q}_\perp) + \right. \\ \qquad\qquad \left. G_f^*(\mathbf{q}_\perp, \bar{z}, \bar{z_1})\ c_m^\dagger(\mathbf{k}_\perp)\mathbf{c}_m(\mathbf{k}_\perp - \mathbf{q}_\perp) \right\}, \\ \mathbf{U}_2 = \frac{\xi}{\rho\alpha X}\sum_m \int_{R^2} \frac{\mathrm{d}^2\mathbf{q}_\perp}{2\pi} g_f(\mathbf{q}_\perp, \bar{z}) \int_{R^2} \mathrm{d}^2\mathbf{k}_\perp\ \ \mathbf{c}_m^\dagger(\mathbf{k}_\perp)\mathbf{c}_m(\mathbf{k}_\perp + \mathbf{q}_\perp). \end{cases} \tag{5.35}$$

The functions $g_f(\mathbf{q}_\perp, \bar{z})$ and $G_f(\mathbf{q}_\perp, \bar{z}, \bar{z_1})$ are respectively the Fourier transform of the real function $|g(\bar{\mathbf{x}}_\perp, \bar{z})|^2 = (2\pi)^{-1}\int_R \mathrm{d}^2\mathbf{q}_\perp\ e^{-i\mathbf{x}_\perp\cdot\mathbf{q}_\perp} g_f(\mathbf{q}_\perp, \bar{z})$ and of the Complex function $g(\bar{\mathbf{x}}_\perp, \bar{z})A_r(\mathbf{x}_\perp, \bar{z}, \bar{z_1}) = (2\pi)^{-1}\int_R \mathrm{d}^2\mathbf{q}_\perp\ e^{-i\mathbf{x}_\perp\cdot\mathbf{q}_\perp} G_f(\mathbf{q}_\perp, \bar{z}, \bar{z_1})$.

5.3 3D Wigner evolution equation

We start from the definitions of the 1PW in the second quantized scheme (5.11). It is possible write the 1PW in terms of angular variables on the longitudinal direction

and continuous canonical variables in transverse direction. As we have shown in section 3.3, if θ is periodic then p must be discrete (*i.e.* θ and p are rotational variables) and consequently we have to use the discrete Wigner function introduced in chapter 3 [41]. After this consideration the 1PW (5.11) can be written as follows:

$$\begin{aligned} W_n(\theta, \bar{\mathbf{x}}_\perp, \mathbf{p}_\perp, \bar{z}, \bar{z_1}) &= \frac{1}{\pi^3} \int_{-\frac{\pi}{2}}^{+\frac{\pi}{2}} d\theta' \int \mathrm{d}^2\bar{\mathbf{x}}_\perp \, e^{-i2(\bar{\mathbf{x}}'_\perp \cdot \mathbf{p}_\perp + \theta' n)} \times \\ &\quad \mathrm{Tr}\left\{ \varrho(\bar{z}, \bar{z_1}) \, \mathbf{\Psi}^\dagger(\theta - \theta', \bar{\mathbf{x}}_\perp - \bar{\mathbf{x}}'_\perp) \Psi(\theta + \theta', \bar{\mathbf{x}}_\perp + \bar{\mathbf{x}}'_\perp) \right\} \end{aligned} \tag{5.36}$$

A long but straightforward calculation (see Appendix C) leads to a Wigner representation in terms of the creator and annihilator operators:

$$\begin{aligned} W_n(\theta, \bar{\mathbf{x}}_\perp, \mathbf{p}_\perp, \bar{z}, \bar{z_1}) &= \sum_{\mu=0,1} \sum_m \mathrm{sinc}[(n - m - \mu/2)\pi] w_{m+\mu/2}(\theta, \bar{\mathbf{x}}_\perp, \mathbf{p}_\perp, \bar{z}, \bar{z_1}) \\ w_{m+\mu/2}(\theta, \bar{\mathbf{x}}_\perp, \mathbf{p}_\perp, \bar{z}, \bar{z_1}) &= \frac{1}{2\pi^3} \sum_{m'} e^{-i2\theta(m'+\mu/2)} \int_{R^2} \mathrm{d}^2\mathbf{k}_\perp e^{-i2\bar{\mathbf{x}}_\perp \cdot \mathbf{k}_\perp} \times \\ &\quad \mathrm{Tr}\left\{ \varrho(\bar{z}, \bar{z_1}) \, \mathbf{c}^\dagger_{m+m'+\mu}(\mathbf{p}_\perp + \mathbf{k}_\perp) c_{m-m'}(\mathbf{p}_\perp - \mathbf{k}_\perp) \right\} \end{aligned} \tag{5.37}$$

Note that this definition is similar to the 1D Wigner function which has been introduced in section (3.3), in particular the half integer character of the index which leads to a definition of two different Wigner functions $w_{m+\mu/2}$. All the difference from the definition of the continuous Wigner function are in the longitudinal variables (θ, p) which have been studied in detail in section (3.3).

Tracing the Wigner function over one variable, we obtain the probability distribution for the other variables. In particular, the momentum and the position distributions are respectively:

$$\begin{aligned} P_m(\bar{z}, \bar{z_1}, \mathbf{p}_\perp) &= \int_{-\pi}^{+\pi} \mathrm{d}\theta \int_{R^2} \mathrm{d}^2\bar{\mathbf{x}}_\perp \, w_m(\theta, \bar{\mathbf{x}}_\perp, \mathbf{p}_\perp, \bar{z}, \bar{z_1}) \\ &\quad \mathrm{Tr}\left\{ \varrho(\bar{z}, \bar{z_1}) \, \mathbf{c}^\dagger_m(\mathbf{p}_\perp) c_m(\mathbf{p}_\perp) \right\} \end{aligned} \tag{5.38}$$

$$Q(\theta, \bar{\mathbf{x}}_\perp, \bar{z}, \bar{z_1}) = \sum_m \int_{R^2} \mathrm{d}^2\mathbf{p}_\perp \, \left\{ w_m(\theta, \bar{\mathbf{x}}_\perp, \mathbf{p}_\perp, \bar{z}, \bar{z_1}) + w_{m+1/2}(\theta, \bar{\mathbf{x}}_\perp, \mathbf{p}_\perp, \bar{z}, \bar{z_1}) \right\} \tag{5.39}$$

Note that the half-integer functions $w_{m+1/2}$ do not contribute to the integral in P_m [41] because of $\int_{-\pi}^{+\pi} \mathrm{d}\theta \; w_{m+1/2} = 0$. As a consequence we can defined the current density (normalized to unity at the peak) in term of the integer Wigner function

only

$$J(\bar{\mathbf{x}}_\perp, \bar{z}, \bar{z_1}) = \sum_m \int_{-\pi}^{+\pi} \mathrm{d}\theta \int_{R^2} \mathrm{d}^2\mathbf{p}_\perp \; w_m(\theta, \bar{\mathbf{x}}_\perp, \mathbf{p}_\perp, \bar{z}, \bar{z_1}) \tag{5.40}$$

$$I_0(\bar{z_1}) = \int_{R^2} \mathrm{d}^2\bar{\mathbf{x}}_\perp \; J(\bar{\mathbf{x}}_\perp, \bar{z}, \bar{z_1}) \tag{5.41}$$

Note that as in the 1D theory (see section 3.2.2), in 3D geometry the dimensionless longitudinal beam profile (5.41) does not depend on $\bar{z}$ (*i.e.* is stationary). This means that, thank to the multiple scaling approach (see the next section (5.4), and the Appendix (A)), the spatial distribution of the particles does not change appreciably on the slow scale $\bar{z_1}$ during the interaction with the radiation.

The evolution equation of the 1PW can be obtained in term of the integer and half integer Wigner function $w_{m+\mu/2}$

$$\frac{\partial}{\partial\bar{z}} W_n(\theta, \bar{\mathbf{x}}_\perp, \mathbf{p}_\perp; \bar{z}) = \sum_{\mu=0,1} \sum_m \mathrm{sinc}[(n-m-\mu/2)\pi] \frac{\partial}{\partial\bar{z}} w_{m+\mu/2}(\theta, \bar{\mathbf{x}}_\perp, \mathbf{p}_\perp; \bar{z}). \tag{5.42}$$

Then using the Von Neumann evolution equation (5.25) we obtain:

$$\begin{aligned} \frac{\partial}{\partial\bar{z}} w_{m+\mu/2}(\theta, \bar{\mathbf{x}}_\perp, \mathbf{p}_\perp; \bar{z}) &= \frac{i}{\pi^3} \sum_{m'} e^{-i2\theta(m'+\mu/2)} \int_{R^2} \mathrm{d}^2\mathbf{k}_\perp e^{-i2\bar{\mathbf{x}}_\perp\cdot\mathbf{k}_\perp} \times \\ &\quad \mathrm{Tr}\, \left\{ \varrho(\bar{z}) \left[\mathbf{H},\ \mathbf{c}^\dagger_{m+m'+\mu}(\mathbf{p}_\perp + \mathbf{k}_\perp) c_{m-m'}(\mathbf{p}_\perp - \mathbf{k}_\perp) \right] \right\} \end{aligned} \tag{5.43}$$

where we have used the cyclical of the trace

$$\mathrm{Tr}\, \{[\mathbf{H}, \varrho(\bar{z})]\ \mathbf{X}\} = \mathrm{Tr}\, \{\varrho(\bar{z})\, [\mathbf{H}, \mathbf{X}]\}\,. \tag{5.44}$$

in order to extract the time dependence from the commutator. Note that, in the 1PW evolution equation, the commutators between the Hamiltonian and the creator and annihilator operators give the same result both for bosons and fermions, since they are independent with respect to the QCR choice. Appendix (C) reports in detail the demonstration which leads, after a long calculation, to the fully evolution equation of the 1PW $w_s(\theta, \bar{\mathbf{x}}_\perp, \mathbf{p}_\perp; \bar{z}, \bar{z_1})$ in the following integro-differential form (spatial ($\mathbf{x}_\perp$ and θ) and temporal ($\bar{z}$ and $\bar{z_1}$) dependence are omitted for simplicity):

$$\left\{\frac{\partial}{\partial\bar{z}}+\left[\frac{s}{\bar{\rho}}+\left(\delta+\frac{\xi}{2\rho}\right)-\frac{bX}{4}\alpha^2\mathbf{p}_\perp^2\right]\frac{\partial}{\partial\theta}+\alpha b\left[1-\frac{s\alpha X}{2}\right]\mathbf{p}_\perp\nabla_{\bar{\mathbf{x}}_\perp}+\frac{bX}{8}\alpha^2\frac{\partial}{\partial\theta}\nabla^2_{\bar{\mathbf{x}}_\perp}\right\}w_s(\mathbf{p}_\perp)$$
$$-i\frac{\xi}{\rho\alpha X}\left[1-\frac{s\alpha X}{2}\right]\int_{R^2}\frac{\mathrm{d}^2\mathbf{q}_\perp}{2\pi}g_f(\mathbf{k}_\perp,\bar{z})e^{-i\bar{\mathbf{x}}_\perp\cdot\mathbf{q}_\perp}\left\{w_s\left(\mathbf{p}_\perp-\frac{\mathbf{q}_\perp}{2}\right)-w_s\left(\mathbf{p}_\perp+\frac{\mathbf{q}_\perp}{2}\right)\right\}$$
$$-\frac{\xi}{4\rho}\int_{R^2}\frac{\mathrm{d}^2\mathbf{q}_\perp}{2\pi}g_f(\mathbf{k}_\perp,\bar{z})e^{-i\bar{\mathbf{x}}_\perp\cdot\mathbf{q}_\perp}\left\{\frac{\partial}{\partial\theta}\left[w_s\left(\mathbf{p}_\perp-\frac{\mathbf{q}_\perp}{2}\right)+w_s\left(\mathbf{p}_\perp+\frac{\mathbf{q}_\perp}{2}\right)\right]\right\}$$
$$-\bar{\rho}\int_{R^2}\frac{\mathrm{d}^2\mathbf{q}_\perp}{2\pi}\left\{e^{i\theta}G_f(\mathbf{k}_\perp,\bar{z},\bar{z_1})e^{-i\bar{\mathbf{x}}_\perp\cdot\mathbf{q}_\perp}-e^{-i\theta}G_f^*(\mathbf{k}_\perp,\bar{z},\bar{z_1})e^{i\bar{\mathbf{x}}_\perp\cdot\mathbf{q}_\perp}\right\}\times$$
$$\left\{w_{s-1/2}\left(\mathbf{p}_\perp-\frac{\mathbf{q}_\perp}{2}\right)-w_{s+1/2}\left(\mathbf{p}_\perp+\frac{\mathbf{q}_\perp}{2}\right)\right\}. \tag{5.45}$$

where $s=m+\mu/2$ is integer ($\mu=0$) or half integer ($\mu=1$), with $m\in Z$. The above integro-differential evolution equation describes a three dimensional electron beam interacting with a laser wiggler field and with a self radiation e.m. field . Its numerical solution is unworkable, however we shall see in the following that, performing the classical limit on the transverse variable, we obtain a basic evolution equation which will be our working equation.

5.4 3D Field evolution equation

The evolution equation for the three dimensional e.m. field A_r in terms of the classical Vlasov distribution has been obtained in section (2.1.2) using the SVEA approximation and the multiple scaling method:

$$\left(\frac{\partial}{\partial\bar{z}}+\frac{\partial}{\partial\bar{z_1}}-ia\nabla^2_{\bar{\mathbf{x}}_\perp}\right)A_r(\bar{\mathbf{x}}_\perp,\bar{z},\bar{z_1})=g(\bar{\mathbf{x}}_\perp,\bar{z})\;B(\bar{\mathbf{x}}_\perp,\bar{z},\bar{z_1})+i\delta A_r(\bar{\mathbf{x}}_\perp,\bar{z},\bar{z_1})$$
$$B(\bar{\mathbf{x}}_\perp,\bar{z},\bar{z_1})=\int_{-\pi}^{+\pi}\mathrm{d}\theta\;e^{-i\theta}\;n(\theta,\bar{\mathbf{x}}_\perp,\bar{z},\bar{z_1}).$$
$$n(\theta,\bar{\mathbf{x}}_\perp,\bar{z},\bar{z_1})\int_R\mathrm{d}p\int_{R^2}\mathrm{d}^2\mathbf{p}_\perp\int_{-\pi}^{+\pi}\mathrm{d}\theta\;e^{-i\theta}\;f(\theta,p,\bar{\mathbf{x}}_\perp,\mathbf{p}_\perp,\bar{z},\bar{z_1}). \tag{5.46}$$

where B is the bunching operator, n is the density of the particle in the spatial position $(\theta,\mathbf{x}_\perp)$ at $(\bar{z},\bar{z_1})$, f is the classical distribution function, g is the laser wiggler profile and $a=l_g/Z_r$ is the radiation diffraction parameter (see section (3.2.2)). Using the quantum analogous $Q(\theta,\bar{\mathbf{x}}_\perp,\bar{z},\bar{z_1})$ (see Eq.5.39) of the classical density $n(\theta,\bar{\mathbf{x}}_\perp,\bar{z},\bar{z_1})$, the quantum bunching operator can be written as:

$$\mathbf{B}(\bar{\mathbf{x}}_\perp,\bar{z},\bar{z_1}) \;=\; \int_{-\pi}^{+\pi}\mathrm{d}\theta\;e^{-i\theta}Q(\theta,\bar{\mathbf{x}}_\perp,\bar{z},\bar{z_1})$$

$$= \int_{-\pi}^{+\pi} \mathrm{d}\theta \; e^{-i\theta} \sum_m \int_{R^2} \mathrm{d}^2\mathbf{p}_\perp \; w_{m+1/2}(\theta, \bar{\mathbf{x}}_\perp, \mathbf{p}_\perp, \bar{z}, \bar{z_1}). \quad (5.47)$$

Let us shown that, similarly to 1D Quantum field description (3.33), the 3D bunching operator (5.47), defined in a second quantization Wigner formalism, involves a coherent superposition of different longitudinal momentum state. In fact using the explicit definition of the 1PW (see Eq.5.38) in the momentum space, we obtain:

$$\begin{aligned}
\mathbf{B}(\bar{\mathbf{x}}_\perp, \bar{z}, \bar{z_1}) &= \sum_m \int_{R^2} \mathrm{d}^2\mathbf{p}_\perp \sum_{m'} \int_{-\pi}^{+\pi} \frac{\mathrm{d}\theta}{2\pi} \; e^{-i2\theta(m'+1)} \int_{R^2} \frac{\mathrm{d}^2\mathbf{k}_\perp}{\pi^2} e^{-i2\bar{\mathbf{x}}_\perp \cdot \mathbf{k}_\perp} \times \\
&\quad \mathrm{Tr} \; \left\{ \varrho(\bar{z}) \; \mathbf{c}^\dagger_{m+m'+1}(\bar{z_1}, \mathbf{p}_\perp + \mathbf{k}_\perp) c_{m-m'}(\bar{z_1}, \mathbf{p}_\perp - \mathbf{k}_\perp) \right\} \\
&= \sum_m \int_{R^2} \mathrm{d}^2\mathbf{p}_\perp \int_{R^2} \frac{\mathrm{d}^2\mathbf{k}_\perp}{\pi^2} e^{-i2\bar{\mathbf{x}}_\perp \cdot \mathbf{k}_\perp} \times \\
&\quad \mathrm{Tr} \; \left\{ \varrho \; \mathbf{c}^\dagger_m(\bar{z}, \bar{z_1}, \mathbf{p}_\perp + \mathbf{k}_\perp) \mathbf{c}_{m-1}(\bar{z}, \bar{z_1}, \mathbf{p}_\perp - \mathbf{k}_\perp) \right\} \quad (5.48)
\end{aligned}$$

where in the final step we moved the z-dependence from the statistic operator ϱ to creator and annihilator operators using Eq.(5.4). Note that neglecting the transverse dependence ($\perp \rightarrow 0$) in the non realistic limit of zero temperature ($T \rightarrow 0$) the bunching factor (5.48) becomes

$$B(\bar{\mathbf{x}}_\perp, \bar{z}, \bar{z_1}) \underbrace{\rightarrow}_{\perp \rightarrow 0} \sum_m \mathrm{Tr} \; \left\{ \varrho \; \mathbf{c}^\dagger_m(\bar{z}, \bar{z_1}) \mathbf{c}_{m-1}(\bar{z}, \bar{z_1}) \right\} \underbrace{\rightarrow}_{T \rightarrow 0} \sum_m \langle \mathbf{c}^\dagger_m(\bar{z}, \bar{z_1}) \mathbf{c}_{m-1}(\bar{z}, \bar{z_1}) \rangle \quad (5.49)$$

where we have used $\lim_{T\rightarrow 0} \varrho = lim_{T\rightarrow 0} e^{-\beta \mathbf{H}} = \mathbf{I}$ whit $\beta = 1/(k_b T)$ (k_b is the Bolzman constant).

The evolution equation of the emitted field, in terms of the 1PW is:

$$\begin{aligned}
&\left(\frac{\partial}{\partial \bar{z}} + \frac{\partial}{\partial \bar{z_1}} - ia \nabla^2_{\bar{\mathbf{x}}_\perp} \right) A_r = g(\bar{\mathbf{x}}_\perp, \bar{z}) \mathbf{B}(\bar{\mathbf{x}}_\perp, \bar{z}, \bar{z_1}) \\
&= g(\bar{\mathbf{x}}_\perp, \bar{z}) \int_{-\pi}^{+\pi} \mathrm{d}\theta \; e^{-i\theta} \sum_m \int_{R^2} \mathrm{d}^2\mathbf{p}_\perp \; w_{m+1/2}(\theta, \bar{\mathbf{x}}_\perp, \mathbf{p}_\perp, \bar{z}, \bar{z_1}) + i\delta A_r
\end{aligned} \quad (5.50)$$

5.5 3D Wigner Model for QFEL

The integro-differential evolution equation (5.45) describes an electron beam with a transverse normalized emittance till to the "ultra cold" limit of the Compton wavelength $\epsilon_n \geq \lambda\!\!\!^{-}_c$. However, as we have anticipate in section (5.2), we are interested in describing an electron beam in which the transverse momentum distribution is thermal, with a width $\Delta x'_{therm} \sim \epsilon_n/(\sigma\gamma_r)$ much larger than the quantum limit $\lambda\!\!\!^{-}_c/(\sigma\gamma_r)$. As anticipated in section (5.2), the parameter controlling this limiting process is α (see Eq.(5.18)). We start expanding the integral in Eq.(5.45) within the following formula's (see Appendix (D)):

$$\begin{aligned}
&\int_{R^2} \frac{\mathrm{d}^2\mathbf{q}_\perp}{2\pi} f(\mathbf{q}_\perp) e^{-i\bar{\mathbf{x}}_\perp\cdot\mathbf{q}_\perp} \left[w_s\left(\mathbf{p}_\perp - \frac{\mathbf{q}_\perp}{2}\right) \pm w_s\left(\mathbf{p}_\perp + \frac{\mathbf{q}_\perp}{2}\right)\right] \\
&= \sum_{n=0}^{+\infty} [(-1)^n] \begin{cases} \left[\dfrac{1}{2^{2n-1}(2n)!}\right] \nabla^{2n}_{\mathbf{p}_\perp} w_s(\mathbf{p}_\perp)\, \nabla^{2n}_{\bar{\mathbf{x}}_\perp} f(\bar{\mathbf{x}}_\perp) & (+) \\ \left[\dfrac{i}{2^{2n}(2n+1)!}\right] \nabla^{2n+1}_{\mathbf{p}_\perp} w_s(\mathbf{p}_\perp)\, \nabla^{2n+1}_{\bar{\mathbf{x}}_\perp} f(\bar{\mathbf{x}}_\perp) & (-) \end{cases}
\end{aligned} \tag{5.51}$$

The Eqs. (5.51) can be converted into α-power expansion (see Eq.(5.18)), introducing the "classical" momentum variable (see Eq.(5.19)).

$$\bar{\mathbf{p}}_\perp = \alpha\mathbf{p}_\perp = \frac{\sigma}{\epsilon_r}\eta_\perp \quad \rightarrow \quad \sum_{n=0}^{+\infty} \partial^n_{\mathbf{p}_\perp} w_s(\mathbf{p}_\perp) = \sum_{n=0}^{+\infty} \alpha^n \partial^n_{\bar{\mathbf{p}}_\perp} w_s(\bar{\mathbf{p}}_\perp) \tag{5.52}$$

where $\eta_\perp = d\mathbf{x}_\perp/dz$.

Finally, using Eqs. (5.52) and (5.51), the 1PW evolution equation (5.45) can be written in the following form:

$$\frac{\partial}{\partial\bar{z}} w_{m+\mu/2}(\theta, \bar{\mathbf{x}}_\perp, \bar{\mathbf{p}}_\perp; \bar{z}) = \sum_{n=0}^{+\infty} \alpha^n \Omega^{(n)}_{m+\mu/2}(\theta, \bar{\mathbf{x}}_\perp, \bar{\mathbf{p}}_\perp; \bar{z}) \tag{5.53}$$

The explicit form of $\Omega^{(n)}_{m+\mu/2}$ is reported in Appendix (C), here we stress that typical values of the beam normalized beam emittance are $\epsilon_n \simeq 10^{-7}$m rad, and $\lambda\!\!\!^{-}_c \simeq 10^{-13}$m, so that the typical values for α is 10^{-6} which is very small , especially if we consider that deriving the 3D Hamiltonian we have neglected terms proportional to

ρ whose typical value is $10^{-4}-10^{-5}$. So we are allowed to retain only the zero-order term in α-power expansion (5.53) *i.e.* $\Omega^{(0)}$. The zero-order evolution equation of the 1PW coupled to the evolution equation of the self radiation e.m. field form our QFEL model, which describes an ultra relativistic e-beam interacting with with a laser wiggler field and with the radiation field.

$$\begin{aligned}\frac{\partial w_s}{\partial \bar{z}} &+ b\ \bar{\mathbf{p}}_\perp \cdot \nabla_{\bar{\mathbf{x}}_\perp} w_s - \left\{ \frac{s}{\bar{\rho}} + \frac{\xi}{2\rho}(1-|g|^2) - \frac{bX}{4}\bar{\mathbf{p}}_\perp^2 \right\} \frac{\partial w_s}{\partial \theta} \qquad (5.54)\\ &- \bar{\rho}\left(g^* A_r e^{i\theta} - g A_r^* e^{-i\theta}\right)\left[w_{s+1/2} - w_{s-1/2}\right] - \frac{\xi}{\rho X}\nabla_{\bar{\mathbf{x}}_\perp}|g|^2 \cdot \nabla_{\bar{\mathbf{p}}_\perp} w_s = 0,\\ \frac{\partial A_r}{\partial \bar{z}} + \frac{\partial A_r}{\partial \bar{z}_1} &- ia\nabla^2_{\bar{\mathbf{x}}_\perp} A_r = g\sum_m \int_{R^2} \mathrm{d}^2\bar{\mathbf{p}}_\perp \int_{-\pi}^{+\pi} \mathrm{d}\theta e^{-i\theta} w_{m+1/2} + i\delta A_r. \qquad (5.55)\end{aligned}$$

where $b = l_g/\beta^*$ and $a = l_g/Z_r$ are respectively the diffraction parameter for the electron beam and for the radiation field; while $X = b/a$ is the ratio between the diffraction lengths which controls the geometric condition between electron beam and radiation beam (see chapter 6). A complete investigation of each term of the Eqs. (5.54) and (5.55) will be done in the next chapter, whereas we limit our dissertation to the initial condition and the classical limit.

We assume that at $z = 0$ all the electrons have the same longitudinal momentum $m_0 = 0$ (no energy spread), while the transverse continuous momentum $\mathbf{k}_\perp$ are continuously distributed in $(-\infty, \infty)$, such that the Pauli principles is satisfied *i.e.* the total momentum vector $\mathbf{K}_{tot} \propto \mathbf{k}_\parallel + \mathbf{k}_\perp$ is different for each electron within the beam. The initial distribution is given imposing $m = m' = \mu = 0$ in Eq. (5.38), so we have:

$$w_0(\bar{\mathbf{x}}_\perp, \mathbf{p}_\perp) = \frac{1}{\pi^2}\int_{R^2} \mathrm{d}^2\mathbf{k}_\perp e^{-i2\bar{\mathbf{x}}_\perp\cdot\mathbf{k}_\perp} \mathrm{Tr}\left\{ \varrho\ \mathbf{c}_0^\dagger(\bar{\mathbf{p}}_\perp + \mathbf{k}_\perp) c_0(\bar{\mathbf{p}}_\perp - \mathbf{k}_\perp)\right\}. \qquad (5.56)$$

Note that assuming $\mathbf{k}_\perp = 0$ and $\varrho = \mathbf{I}$ we obtain $w_0(\bar{\mathbf{x}}_\perp, \mathbf{p}_\perp) = \langle |c_0^\dagger(\bar{\mathbf{p}}_\perp)|^2\rangle$ which can be assume as a Gaussian distribution in the phase space $(\bar{\mathbf{x}}_\perp, \bar{\mathbf{p}}_\perp)$ (see Eq (6.41)). It is important to note that Eq.(5.54) reduces to a Vlasov equation in the classical limit $\bar{\rho} \gg 1$. In fact, for $\bar{\rho} \to \infty$ the new longitudinal momentum, $\bar{p} = s/\bar{\rho}$, can be treated as a continuous variable and $w_s(\theta, \bar{\mathbf{x}}_\perp, \bar{\mathbf{p}}_\perp, \bar{z}, \bar{z}_1) \to \bar{\rho} f(\theta, \bar{p}, \bar{\mathbf{x}}_\perp, \bar{\mathbf{p}}_\perp, \bar{z}, \bar{z}_1)$ then we get:

$$\left[w_{s+\frac{1}{2}} - w_{s-\frac{1}{2}}\right] \to \bar{\rho}\left[f\left(\bar{p} + \frac{1}{2\bar{\rho}}\right) - f\left(\bar{p} - \frac{1}{2\bar{\rho}}\right)\right] \to \frac{\partial}{\partial \bar{p}} f\left(\bar{p}\right) \qquad (5.57)$$

where f is a classical electron distribution function. In this limit, Eqs. (5.54) and (5.55) reduce to the classical Vlasov-Maxwell Eqs.(2.109) obtained in the second chapter. The quantum evolution for w_s, Eq.(5.54), contains the quantization of the longitudinal momentum in units of $\hbar k$ (as the 1D model) and describes the transverse dynamics by the same classical terms appearing in the Vlasov Eq.(2.109).

Chapter 6

Toward QFEL experiment

In the previous chapter we got a complete set of evolution equations which describe the 3D FEL dynamics in the quantum regime; this set of equations differ from that of the 1D model (see Eqs.(3.64)-(3.67) in section (3.3)) by the same 3D terms of the classical Maxwell-Vlasov (see Eqs. 2.109 in section 2.1.2). In this chapter we discuss the meaning of the 3D extra terms and the requirements that the e-beam and the wiggler field should be satisfied in order to preserve the high gain saturation in FEL process. All the 3D effects can be controlled by two parameters only, $\tilde{a}$ and $\tilde{b}$, or by its combination (for example $X = b/a$) and by the laser wiggler parameters. As in the 1D model (chapter 3 and 4) we assume the quantum scaling *i.e.* all variables and parameters are rescaled in terms of the QFEL-parameter $\bar{\rho}$.

$$\tilde{z} = \bar{z}\sqrt{\bar{\rho}} = \frac{z}{\tilde{l}_g}, \quad \tilde{z}_1 = \bar{z}_1\sqrt{\bar{\rho}} = \frac{z_1}{\tilde{l}_c}, \quad \tilde{a} = \frac{a}{\sqrt{\bar{\rho}}} = \frac{\tilde{l}_g}{Z_r}, \quad \tilde{b} = \frac{b}{\sqrt{\bar{\rho}}} = \frac{\tilde{l}_g}{\beta^*}. \tag{6.1}$$

where from Eqs.(4.10)

$$\tilde{l_g} = \frac{l_g}{\sqrt{\bar{\rho}}} = \frac{\lambda_l}{8\pi\rho\sqrt{\bar{\rho}}} \quad \text{and} \quad \tilde{l_c} = \frac{l_g}{\sqrt{\bar{\rho}}} = \frac{\lambda_r}{4\pi\rho\sqrt{\bar{\rho}}} \tag{6.2}$$

are the quantum gain and cooperation lengths. Note that in Eq. (6.2) the magneto static wiggler wavelength was replaced by the laser wiggler wavelength using the substitution $\lambda_w \to \lambda_l/2$. Finally we scale the detuning and the wiggler parameters, and the radiation field

$$\tilde{\delta} = \frac{\delta}{\sqrt{\bar{\rho}}} = \frac{\gamma - \gamma_0}{\rho\gamma_r\sqrt{\bar{\rho}}}, \qquad \tilde{\xi} = \xi/\sqrt{\bar{\rho}} = \frac{a_0^2}{(1+a_0^2)\sqrt{\bar{\rho}}}, \qquad \tilde{A} = \sqrt{\bar{\rho}}A_r = \sqrt{\bar{\rho}}\frac{a_0 a_r}{2\rho^2(1+a_0^2)} \tag{6.3}$$

where a_0 is the laser wiggler amplitude and $a_r = (e/mc^2)E(\mathbf{x}_\perp, \bar{z})/k_r$ (see section 2.1) .

The new scaled field amplitude is such that $|\tilde{A}|^2 = \bar{\rho}|A_r|^2 = \langle N_{phot}/N_e \rangle$ is the average number of photons emitted per electron.

From Eqs. (5.54) and (5.54) using the quantum scaling we obtain

$$\frac{\partial w_s}{\partial \tilde{z}} + \tilde{b}\ \bar{\mathbf{p}}_\perp \cdot \nabla_{\bar{\mathbf{x}}_\perp} w_s + \left\{ \frac{s}{\bar{\rho}^{3/2}} + \frac{\tilde{\xi}}{2\rho}(1-|g|^2) - \frac{\tilde{b}^2}{4\tilde{a}}\bar{\mathbf{p}}_\perp^2 \right\} \frac{\partial w_s}{\partial \theta} \tag{6.4}$$
$$- \left(g^* \tilde{A} e^{i\theta} - g\tilde{A}^* e^{-i\theta} \right) \left[w_{s+1/2} - w_{s-1/2} \right] - \frac{\tilde{\xi}}{\rho}\frac{\tilde{a}}{\tilde{b}} \nabla_{\bar{\mathbf{x}}_\perp} |g|^2 \cdot \nabla_{\bar{\mathbf{p}}_\perp} w_s = 0.$$

$$\left(\frac{\partial}{\partial \tilde{z}} + \frac{\partial}{\partial \tilde{z}_1} - i\tilde{a}\nabla^2_{\bar{\mathbf{x}}_\perp} \right) \tilde{A} = g \sum_m \int_{R^2} \mathrm{d}^2 \bar{\mathbf{p}}_\perp \int_{-\pi}^{+\pi} \mathrm{d}\theta e^{-i\theta} w_{m+1/2} + i\tilde{\delta}\tilde{A}. \tag{6.5}$$

Let us discuss the meaning of each single 3D extra term of Eqs.(6.4) and (6.5).

- For the second term in the curl parenthesis in Eq.(6.4) the following correspondence to unscaled variables holds

$$\tilde{b}\,\bar{\mathbf{p}}_\perp \cdot \nabla_{\bar{\mathbf{x}}_\perp} \rightarrow \bar{\eta}_\perp \cdot \nabla_{\mathbf{x}_\perp}. \tag{6.6}$$

  where $\bar{\eta}_\perp = \tilde{l}_g \eta_\perp = d\mathbf{x}_\perp/d\bar{z}$. This term describes the transverse drift of the beam, responsible of the beam section increasing from the waist position $\bar{z}_0$ as $\sigma(\tilde{z}) = \sigma\sqrt{1 + [(\tilde{z} - \tilde{z}_0)/\sqrt{\bar{\rho}}\beta^*]^2}$ in the free space and for a Gaussian beam.

- The second and third terms in the curl parenthesis in Eq.(6.4) account for the change of the FEL resonance induced by the beam emittance and by the laser wiggler profile.

$$\frac{\tilde{b}^2}{4\tilde{a}}\bar{\mathbf{p}}_\perp^2 \sim \frac{1}{2\rho\sqrt{\bar{\rho}}}\ \frac{\epsilon_n^2}{\sigma^2(1+a_0^2)}, \tag{6.7}$$

$$\frac{\tilde{\xi}}{2\rho}(1-|g|^2) \sim \frac{1}{2\rho\sqrt{\bar{\rho}}}\frac{\Delta a_0^2}{1+a_0^2} \tag{6.8}$$

  where in the first relation the maximum divergence angle $|\eta_\perp| \sim \epsilon_n/\gamma_r\sigma$ has been assumed

- For the last term in Eq.(6.4) the following correspondence to unscaled variables holds

$$-\frac{\tilde{\xi}}{\rho}\frac{\tilde{a}}{\tilde{b}}\ \nabla_{\bar{\mathbf{x}}_\perp}|g|^2\ \cdot \nabla_{\bar{\mathbf{p}}_\perp} \rightarrow \mathbf{x}''_\perp \cdot \nabla_{\mathbf{x}'_\perp}, \tag{6.9}$$

where $\mathbf{x}''_\perp = -(a_0^2/2\gamma_r^2)(\nabla_{\mathbf{x}_\perp}|g|^2)$ is the ponderomotive force due to the laser transverse gradient.

6.1 Beam requirementss and Scaling laws for QFEL

In order to operate a FEL in the high-gain quantum regime, the energy spread must be less than the QFEL line width, *i.e.* $\Delta\gamma/\gamma < \rho\sqrt{\bar{\rho}}$ (see sections 3.1.1 and 3.2.3). As we have shown in chapter 2 (see Eq. (2.101)) emittance is an other cause of inhomogeneous broadening of the radiation line width, due to the beam divergence. In fact, since the resonant wavelength depends on the divergence angle $\eta_\perp$ according to Eq.(2.99)

$$\lambda_r = \frac{\lambda_l(1 + a_0^2 + \gamma^2\eta_\perp^2)}{4\gamma^2}, \qquad \text{with} \quad 0 \le \eta_\perp \le \frac{\epsilon_n}{\gamma\sigma}, \tag{6.10}$$

the inhomogeneous broadening due to emittance is

$$\frac{\Delta\lambda}{\lambda_r} \approx \frac{2\Delta\gamma}{\gamma} \approx \frac{\epsilon_n^2}{\sigma^2(1 + a_0^2)} \le 2\rho\sqrt{\bar{\rho}}. \tag{6.11}$$

This inequality can be written, using the definitions of $\tilde{l}_g$ and Z_r, as

$$\epsilon_n \le \frac{\gamma\lambda_r}{2\pi}\sqrt{\frac{Z_r}{\tilde{l}_g}} \tag{6.12}$$

or, in terms of our 3D parameters $\tilde{a}$ and $\tilde{b}$, as

$$\frac{\tilde{b}}{2\sqrt{\tilde{a}}} < 1. \tag{6.13}$$

This condition arises naturally in our model, since the term (6.7) in Eq.(6.4) accounts for the change of the FEL resonance induced by emittance.

Another important constraint on the beam emittance arise when a $\mathtt{TEM}_{00}$ Gaussian laser wiggler is used instead of magnetic wiggler. In this case

$$g(\bar{\mathbf{x}}_\perp, \tilde{z}) = \frac{1}{[1 - i\tilde{d}(\tilde{z} - \tilde{z}_0)]}\exp\left\{\frac{-|\bar{\mathbf{x}}_\perp|^2}{4\sigma_l^2[1 - i\tilde{d}(\tilde{z} - \tilde{z}_0)]}\right\}, \tag{6.14}$$

where $\sigma_l = R/\sigma = a_2$, $\tilde{d} = \tilde{l}_g/Z_l$, $Z_l = 4\pi R^2/\lambda_l$, and R is the minimum rms laser radius ($R = w_0/2$) at the beam waist position $\tilde{z}_0$. In fig.6.1 is shown the evolution in 2D geometry of the Gaussian laser profile assuming $\tilde{d} = 0.2$, $Z_l = 6.5$mm and

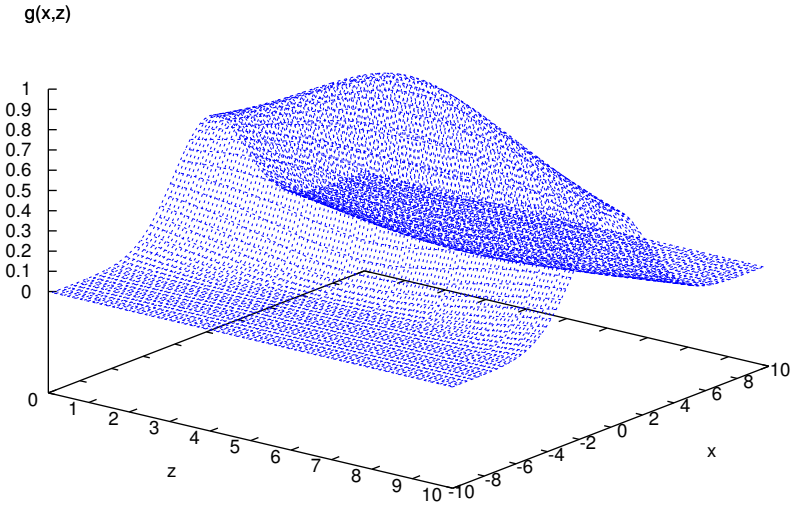

Figure 6.1: Evolution of transverse Gaussian laser beam in 2D geometry for $\tilde{d} = 0.2$, $Z_l = 6.5$mm and $\sigma_l = 2$

$\sigma_l = 2$. Imposing that the electron beam does not diverge appreciably during the interaction with the laser wiggler, *i.e.* in a laser Rayleigh range Z_l, then it should be

$$\beta^* \geq Z_l. \tag{6.15}$$

From the definitions of β^* and Z_l it follows:

$$\epsilon_n \leq \frac{\gamma \lambda_l}{4\pi} \left(\frac{\sigma}{R}\right)^2. \tag{6.16}$$

This condition can be quite restrictive if $\sigma << R$. In terms our dimensionless parameters, Eq.(6.15) is written as $\tilde{b} \leq \tilde{d}$. In addition we must impose from Eq. (6.8) the following condition

$$1 - |g|^2 \lesssim 2\rho/\tilde{\xi} \tag{6.17}$$

in order to preserve the resonant relation; this means that we need a "very flat" laser profile; for example using $\bar{\rho} = 0.2$, $\rho = 10^{-4}$ and $\tilde{\xi} \sim 10^{-2}$ (see ref. [39]) we have $1 - |g|^2 \lesssim 10^{-2}$. An alternative to $\texttt{TEM}_{00}$ could be the Super-Gaussian (SG)

[64],

$$g_\mu(\mathbf{r},0) = \exp[-(\mathbf{r}/w_0)^\mu] \qquad (\mu \geq 2) \qquad \mathbf{r} = \sqrt{x^2+y^2} \tag{6.18}$$

which becomes more and more box shaped for increasing μ. However, the evaluation of the free-space propagation of the field with the SG profile cannot be performed in a closed form for $\mu > 2$, and it must be calculated numerically. A particular flattened laser beam profile, which have a simple propagation law, was proposed by F. Gory [61, 62], the Flattened Gaussian Beam (FGB) and by A.A.Tovard the Multiple Gaussian Beam (MGB) [63]. Such lasers can be produced by suitable transparency films [61, 62] or by overlapping different Gaussian beams [63]. In both cases, it is possible to realize a laser which remains almost transversally flat within few Rayleigh ranges Z_l from the beam waist. The free-space propagation for FGB and MGB laser profile are obtained in Appendix E. Here we show the analytic expression for the FGB:

$$g_m(\bar{x},\tilde{z}) = \frac{A_m}{\sqrt{1-i\tilde{d}(\tilde{z}-\tilde{z}_0)}} \sum_{m=-M}^{M} \exp\left\{\frac{-(\bar{x}-2m\sigma_l)^2}{4\sigma_l^2[1-i\tilde{d}(\tilde{z}-\tilde{z}_0)]}\right\}, \tag{6.19}$$

where $A_m = 1/\sum_{m=-M}^{M}\exp\{-m^2\}$, $\sigma_l = R/\sigma = a_2$, $\tilde{d} = \tilde{l}_g/Z_l$, $Z_l = 4\pi R^2/\lambda_l$, and R is the minimum rms laser radius ($R = w_0/2$) at the beam waist position $\tilde{z}_0$. The FGB becomes more and more box shaped for increasing the number (M) of the overlapped Gaussian beam. The number which control the slope of the FGB profile is $m = 2M+1$ where M is the number of Gaussian beam, so the $\mathtt{TEM}_{00}$ Gaussian beam (see fig. (6.1)) correspond to $m = 0$. Figure 6.2 shows the evolution of FGB using $\tilde{d} = 0.2$, $Z_l = 6.5$mm and $\sigma_l = 2$, for two different case (a) overlapping $M = 3$ Gaussian beam ($m = 1$) and (b) overlapping $M = 5$ Gaussian beam ($m = 2$).

As anticipated previously the Eqs. (6.4) and (6.5) depend only by few parameters; on the contrary the experimental parameters are several. We fix few parameters obtaining the formulae of the others in terms of the fundamental too. Let start from the definition of the QFEL parameter (see Eq. (5.17)) in terms of the wavelengths and the fundamental FEL resonant relation :

$$\bar{\rho} = \rho\gamma\frac{\lambda_r}{\lambda_c}, \qquad \gamma = \sqrt{\frac{\lambda_l(1+a_0^2)}{4\lambda_r}} \tag{6.20}$$

where $\lambda_c = h/mc \simeq 0.024$ Å is the Compton wavelength. Therefore we fix the independent parameters:

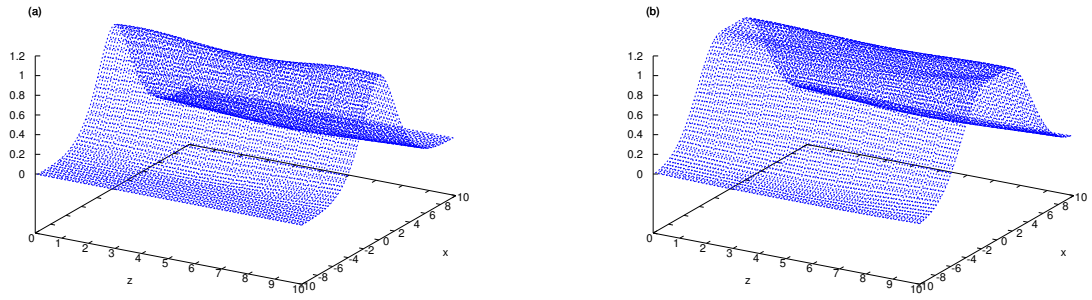

Figure 6.2: Evolution of FGB $g_m(\tilde{z},\ \bar{x})$ in 2D geometry with $\tilde{d} = 0.2$, $Z_l = 6.5$mm and $\sigma_l = 2$ for (a) $m = 1$ and (b) $m = 2$.

1. QFEL-parameter: $\bar{\rho}$
2. radiation wavelength: λ_r
3. laser wiggler wavelength: λ_r
4. wiggler parameter: a_0
5. number of amplitude gain lengths for interaction length: $a_1 = L_{int}/\tilde{l}_g$
6. the ratio between the laser wiggler and the rms beam radius at the focal point: $a_2 = R/\sigma$
7. normalized beam emittance: ϵ_n

where the interaction length can be defined as $L_{int} = c\tau_{int} \simeq Z_l$, $Z_l = 4\pi R^2/\lambda_l = 4\pi(\sigma a_2)^2/\lambda_l$ is the laser Rayleigh range, $\tau_{int} = \tau_l/2$ and τ_l is the laser pulse duration.

Using Eqs. (6.20) the QFEL parameters is related to the classical FEL parameter ρ by

$$\rho = \bar{\rho}\frac{\lambda_c}{\gamma\lambda_r} = \bar{\rho}\frac{2\lambda_c}{\sqrt{\lambda_r\lambda_l(1+a_0^2)}} \tag{6.21}$$

The FEL parameter (2.89) can be also written as [39, 9]

$$\rho = \frac{1}{2\gamma}\left(\frac{I}{I_A}\right)^{1/3}\left(\frac{u_e\lambda_l a_0}{4\pi\sigma}\right) \tag{6.22}$$

where $I_A \simeq 17$kA is the Alfven current. Assuming as current density the peak current I divided by the effective surface $2\pi\sigma^2$ for a transversally Gaussian or $\pi\sigma^2$ for a flat top shape of the current, the parameter u_e is 1 or $\sqrt{2}$ respectively. From Eqs. (6.20) and (6.22) with same algebra we obtain

$$I(A) = 3 \cdot 10^2 \frac{\bar{\rho}^3 \sigma^2}{u_e^2 \lambda_r^3 \lambda_l^2 a_0^2}. \tag{6.23}$$

where the units are λ_r(Å), $\lambda_l(\mu\text{m})$, $R(\mu\text{m})$ and $\sigma(\mu\text{m})$. For a given σ the electron current is proportional to $\bar{\rho}^3$, so that, going from the quantum to the classical regime, if $\bar{\rho}^3$ increases for instance by a factor 10, the current increases by a factor 10^3. This is one of the reasons why the use of a laser wiggler may be much more convenient in the quantum regime that in the classical one (see section 2.3.3). The relation between a_0 and the laser power P is, in agreement with [8]

$$P(TW) = \left(\frac{R a_0}{2.4 u_l \lambda_l} \right)^2 \tag{6.24}$$

where u_l is the laser wiggler analogue to u_e.

Now using the Eqs. (6.20), (6.21), (6.22), (6.23), (6.24) and (6.2), we obtain a useful formulae for the main experimental parameters, expressed as a function of the independent parameters $\bar{\rho}$, λ_r(Å), $\lambda_l(\mu\text{m})$, ϵ_n(mm-mrad), a_0, a_1, a_2:

$$\gamma \simeq 50 \sqrt{\frac{\lambda_l}{\lambda_r}(1 + a_0^2)}, \tag{6.25}$$

$$\rho \simeq 4.8 \cdot 10^{-4} \frac{\bar{\rho}}{\sqrt{\lambda_r \lambda_l (1 + a_0^2)}}, \tag{6.26}$$

$$l_g(\text{mm}) \simeq 8.3 \cdot 10^{-2} \sqrt{\frac{\lambda_r \lambda_l^3 (1 + a_0^2)}{\bar{\rho}^3}}, \tag{6.27}$$

$$\sigma(\text{mm}) \simeq 1.8 \frac{\sqrt{a_1}}{a_2} \left[\frac{\lambda_r \lambda_l^5 (1 + a_0^2)}{\bar{\rho}^3} \right]^{1/4}, \tag{6.28}$$

$$P(\text{TW}) \simeq 0.57 \frac{a_1 a_0^2}{u_l^2} \sqrt{\frac{\lambda_r \lambda_l (1 + a_0^2)}{\bar{\rho}^3}}, \tag{6.29}$$

$$\tau(\text{ps}) \simeq 0.27 \, a_1 \sqrt{\frac{\lambda_r \lambda_l^3 (1 + a_0^2)}{\bar{\rho}^3}} \tag{6.30}$$

$$I(\text{A}) \simeq 989 \frac{a_1}{a_0^2 a_2^2 u_e^2} \sqrt{\frac{\lambda_l}{\lambda_r^5}(1 + a_0^2) \bar{\rho}^3} \tag{6.31}$$

Since the dimensionless parameters in Eqs. (6.4)-(6.5) becomes:

$$\tilde{b} \simeq 0.5 \ \frac{a_2^2}{a_1\sqrt{1+a_0^2}}\sqrt{\frac{\lambda_r}{\lambda_l^2}}\epsilon_n, \tag{6.32}$$

$$\tilde{a} \simeq 2\cdot 10^{-4} \ \frac{a_2^2}{a_1}\frac{\lambda_r}{\lambda_l} \tag{6.33}$$

$$\frac{\tilde{b}^2}{4\tilde{a}} \simeq 320 \ \frac{a_2^2\epsilon_n^2}{a_1(1+a_0^2)}\frac{1}{\lambda_l} \tag{6.34}$$

$$\frac{\tilde{\xi}}{2\rho} \simeq 10^3 \ a_0^2\sqrt{\frac{\lambda_r\lambda_l}{(1+a_0^2)\bar{\rho}^3}} \tag{6.35}$$

$$\tilde{d} \simeq 2 \ \frac{1}{a_1} \tag{6.36}$$

6.2 Numerical analysis

In order to solve the set of coupled Eqs. (6.4)-(6.5) we expand the θ-periodic Wigner function in to a Fourier series.

$$w_s(\theta, \bar{\mathbf{x}}_\perp, \bar{\mathbf{p}}_\perp, \tilde{z}, \tilde{z_1}) = \frac{1}{2\pi}\sum_{k\in Z} w_s^k(\bar{\mathbf{x}}_\perp, \bar{\mathbf{p}}_\perp, \tilde{z}, \tilde{z_1})e^{ik\theta} \tag{6.37}$$

This leads to obtain our working equations:

$$\begin{aligned}
\frac{\partial {w_s}^k}{\partial\tilde{z}} &+ ik\left\{\frac{s}{\bar{\rho}^{3/2}} + \frac{\tilde{\xi}}{2\rho}(1-|g|^2) - \frac{\tilde{b}^2}{4\tilde{a}}\bar{\mathbf{p}}_\perp^2\right\} w_s^k \\
&- \left(g^*\tilde{A}w_{s+1/2}^{k-1} - g^*\tilde{A}w_{s-1/2}^{k-1} + g\tilde{A}^*w_{s+1/2}^{k+1} - g\tilde{A}^*w_{s-1/2}^{k+1}\right) \\
&+ \left[\tilde{b}\bar{\mathbf{p}}_\perp\cdot\nabla_{\bar{\mathbf{x}}_\perp} - \frac{\tilde{\xi}}{\rho}\frac{\tilde{a}}{\tilde{b}}\left(\nabla_{\bar{\mathbf{x}}_\perp}|g|^2\right)\cdot\nabla_{\bar{\mathbf{p}}_\perp}\right] w_s^k = 0,
\end{aligned} \tag{6.38}$$

$$\left(\frac{\partial}{\partial\tilde{z}} + \frac{\partial}{\partial\tilde{z_1}} - i\tilde{a}\nabla_{\bar{\mathbf{x}}_\perp}^2\right)\tilde{A} = g\sum_{m\in Z}\int_{R^2} \mathrm{d}^2\bar{\mathbf{p}}_\perp w_{m+1/2}^1(\bar{\mathbf{x}}_\perp, \bar{\mathbf{p}}_\perp, \tilde{z}, \tilde{z_1}) + i\tilde{\delta}\tilde{A} \tag{6.39}$$

From the definition of the 1PW in Eq. (5.38) follows

$$\begin{aligned}
w_m^{2k} &= \frac{1}{\pi^2}\int_{R^2} \mathrm{d}^2\mathbf{k}_\perp e^{-i2\bar{\mathbf{x}}_\perp\cdot\mathbf{k}_\perp} \times \mathrm{Tr}\ \left\{\varrho\ \mathbf{c}_{m+k}^\dagger(\mathbf{p}_\perp+\mathbf{k}_\perp)c_{m-k}(\mathbf{p}_\perp-\mathbf{k}_\perp)\right\} \\
w_{m+1/2}^{2k+1} &= \frac{1}{\pi^2}\int_{R^2} \mathrm{d}^2\mathbf{k}_\perp e^{-i2\bar{\mathbf{x}}_\perp\cdot\mathbf{k}_\perp} \times \mathrm{Tr}\ \left\{\varrho\ \mathbf{c}_{m+k+1}^\dagger(\mathbf{p}_\perp+\mathbf{k}_\perp)c_{m-k}(\mathbf{p}_\perp-\mathbf{k}_\perp)\right\}
\end{aligned} \tag{6.40}$$

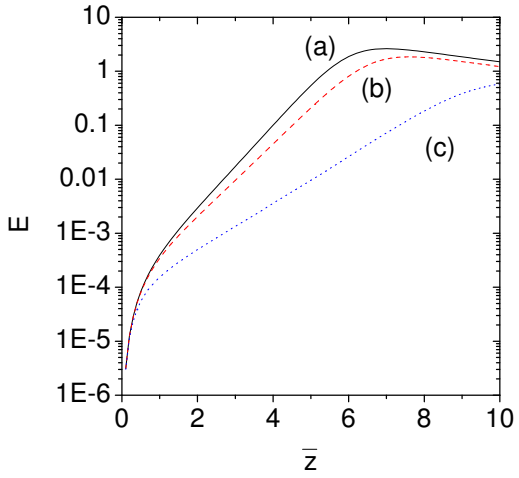

Figure 6.3: Total radiated energy, $E(\tilde{z}) = \int d^2\bar{\mathbf{x}}_t |\tilde{A}|^2$, vs. $\tilde{z}$ for $\bar{\rho} = 0.2$, $\tilde{a} = 1.6 \times 10^{-4}$, $g = 1$ and (a) $\tilde{b} = 0$, (b) $\tilde{b} = \sqrt{a}$, (c) $b = 2\sqrt{a}$. The electron beam focuses at $\bar{z}_0 = 5$.

In particular for $\mathbf{k}_\perp = 0$ and $\varrho = I$, $w_m^0(\bar{\mathbf{p}}_\perp) = \langle |\mathbf{c}_m(\mathbf{p}_\perp)|^2 \rangle$ is the 3D momentum probability distribution and $w_{m+1/2}^1(\bar{\mathbf{p}}_\perp) = \langle \mathbf{c}_{m+1}^\dagger(\mathbf{p}_\perp)\mathbf{c}_m(\mathbf{p}_\perp) \rangle$ is the 3D m-th bunching component distribution.

A numerical parallel code `QFEL3D` has been developed for solving the coupled Eqs.(6.38) and (6.39) based on finite-difference integration of the motion equations on a Cartesian three-dimensional spatial grid [49]. The electron motion is described by a 7D Wigner function (*i.e.* $w_s(\theta, \bar{x}, \bar{y}, \bar{p}_x, \bar{p}_y | \tilde{z}, \tilde{z}_1)$ and the energy spread variable $\tilde{\delta}$), which is continuous in the transverse phase-space and discrete in the longitudinal phase-space variables. From a numerical point of view a 7D space simulation imply an enormous time-cost, then the use of parallel computing is necessary. For this reason here we present two different simulations: the first is done integrating the set of evolution equations (6.38)-(6.39) in 3D geometry and assuming a uniform laser wiggler ($g = 1$), while the latter is done integrating Eqs.(6.38)-(6.39) in 2D geometry assuming the two level approximation (see section 6.2.1) and using the FGB introduced previously (see Eq. 6.19). We did not considerate in both simulations the propagation effects, which have been investigated extensively in chapter 4, and the electrons' energy spread $\tilde{\delta}$, which however can be taken into account introducing an inhomogeneous broadening (see section (3.2.4)) [32]. Both simulations are done

in the quantum regime *i.e.* $\bar{\rho} = 0.2$ assuming as initial condition an electron beam described by a thermal state of energy $mc^2\gamma_0$ and transverse phase space distribution

$$w(\bar{\mathbf{x}}_\perp, \bar{\mathbf{p}}_\perp, \tilde{z} = 0) = w_0^0(\bar{\mathbf{x}}_\perp, \bar{\mathbf{p}}_\perp) \propto \exp\{-|\bar{\mathbf{x}}_\perp + b\tilde{z}_0\bar{\mathbf{p}}_\perp|^2/2 - |\bar{\mathbf{p}}_\perp|^2/2\} \qquad (6.41)$$

with the waist position at $\tilde{z} = \tilde{z}_0$ (see Eqs. (5.56) and (6.40)).

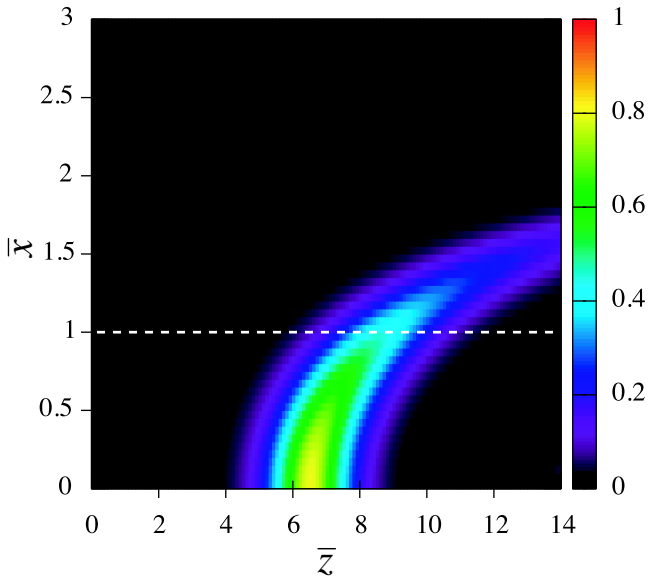

Figure 6.4: (Color) Radiation intensity $|\tilde{A}|^2$ as a function of transverse coordinate $\bar{\mathbf{x}}_\perp$ and of wiggler position $\tilde{z}$. Parameters same as for curve (b) in Fig. 6.3. The dashed line corresponds to the electron beam rms radius σ. As a reference, the 1D model intensity would saturate to unity.

Let us show preliminary results by the first 3D simulation: assuming $g = 1$, the system depends on the diffraction and emittance parameters only, *i.e.* $\tilde{a}$ and $\tilde{b}$. The interaction is taken over 10 gain lengths ($\bar{z}_{max} = a_2 = c\tau_{int}/\tilde{l}_g = 10$), with the beam waist in the middle, $\bar{z}_0 = 5$. A set of possible experimental parameters corresponding to this simulation is listed in Table 6.1.

We have considered three different values of the beam emittance in order to investigate its effect on the gain: (a) $\epsilon_n = 0$, i.e. $b = 0$; (b) $\epsilon_n = 0.05$, i.e. $b = \sqrt{a} = 0.013$; (c) $\epsilon_n = 0.1$, i.e. $b = 0.025 = 2\sqrt{a}$ (where the emittance is in mm-mrad). Figure 6.3 shows the total FEL radiation energy, $E(\bar{z}) = \int d^2\bar{\mathbf{x}}_\perp |\tilde{A}|^2$, vs. $\tilde{z}$ for the cases (a)-(c) in table 6.1 . Figure 6.4 shows a color map of the intensity in the plane

$(\bar{x}, \bar{z})$ for the (b) case in table 6.1. It can be seen that intensity saturates to a lower level in the beam halo with respect to the beam axis, and that the gain changes along the transverse direction. Notice that the total emitted energy and the on-axis peak intensity can reach a significant fraction of the 1D model for the proposed parameters (b) in table 6.1.

6.2.1 Two level system

The full 3D simulation of our working equations (6.38)-(6.39) shown that the most important effects which inhibit the gain process comes from the resonant term (Eqs. 6.8), moreover a simulation of the complete evolution equations (5.54)-(5.55) which taken into account also the propagation effects due to the $\tilde{z_1}$ derivative require a very long computation time. A preliminary study can be done assuming some approximation; in fact the 1D and 3D simulation have shown that when $\bar{\rho} \lesssim 1$ only the two state $n = 0, -1$ are involve, others level occurs only for very long interaction length [49]. This consideration permit us to approximate our working equation, considering the $n = 0, -1$ level only.

From Eqs. (6.40) for a two level system follows that $P_0(\bar{\mathbf{x}}_\perp) = \int_{R^2} \mathrm{d}^2\bar{\mathbf{p}}_\perp w_0^0(\bar{\mathbf{x}}_\perp, \bar{\mathbf{p}}_\perp)$ and $P_{-1}(\bar{\mathbf{x}}_\perp) = \int_{R^2} \mathrm{d}^2\bar{\mathbf{p}}_\perp w_{-1}^0(\bar{\mathbf{x}}_\perp, \bar{\mathbf{p}}_\perp)$ are the 3D probabilities distributions for $m = 0$ and $m = -1$ momentum levels, while $\mathcal{B}(\bar{\mathbf{x}}_\perp) = \int_{R^2} \mathrm{d}^2\bar{\mathbf{p}}_\perp w_{-1/2}^1(\bar{\mathbf{x}}_\perp, \bar{\mathbf{p}}_\perp)$ represents the 3D bunching factor (or polarization).

We define the two level variables as follows:

$$\begin{cases} \mathcal{D} = w_0^0 - w_{-1}^0 & \text{Population difference} \\ \mathcal{B} = w_{-1/2}^1 & \text{Polarizzation} \end{cases} \tag{6.42}$$

In terms of this new variables our working equations (6.38) and (6.39) become:

$$\begin{aligned} &\left\{ \frac{\partial}{\partial\tilde{z}} + \tilde{b}\bar{\mathbf{p}}_\perp\nabla_{\bar{\mathbf{x}}_\perp} - \frac{\tilde{\xi}}{2\rho}\frac{\tilde{a}}{\tilde{b}}\nabla_{\bar{\mathbf{x}}_\perp}|g|^2\cdot\nabla_{\bar{\mathbf{p}}_\perp} \right\}\mathcal{D} = -2\left(\tilde{A}\mathcal{B}^* + c.c.\right) \\ &\left\{ \frac{\partial}{\partial\tilde{z}} + \tilde{b}\bar{\mathbf{p}}_\perp\nabla_{\bar{\mathbf{x}}_\perp} - \frac{\tilde{\xi}}{2\rho}\frac{\tilde{a}}{\tilde{b}}\nabla_{\bar{\mathbf{x}}_\perp}|g|^2\cdot\nabla_{\bar{\mathbf{p}}_\perp} + i\left(\frac{\tilde{\xi}}{2\rho}(1-|g|^2) - \frac{\tilde{b}^2}{4\tilde{a}}|\bar{\mathbf{p}}_\perp|^2\right)\right\}\mathcal{B} = \tilde{A}\mathcal{D} \\ &\left\{ \frac{\partial}{\partial\tilde{z}} + \frac{\partial}{\partial\tilde{z_1}} - i\tilde{a}\nabla^2_{\bar{\mathbf{x}}_\perp} \right\}\tilde{A} = g\int_{R^2} d^2\bar{\mathbf{p}}_\perp\mathcal{B} + i\tilde{\delta}\tilde{A} \end{aligned} \tag{6.43}$$

For these simulations we assume all electrons in the same longitudinal quantum state $m = 0$ and with a continuously distributed transverse momentum (see Eq.

6.41). The interaction is taken over 7 gain lengths ($\bar{z}_{max} = a_2 = c\tau_{int}/\tilde{l}_g = 7$), with the beam waist $\bar{z}_0 = 5$. Note that, during the time evolution the total probability $P_0(\bar{\mathbf{x}}_\perp) + P_{-1}(\bar{\mathbf{x}}_\perp) = w_0^0(\bar{\mathbf{x}}_\perp)$ is conserved (see fig. (6.8)). For simplicity we neglect the defocusing term 6.9 in Eqs. (6.43). In fact deriving with respect to $\bar{x}$ Eq.(6.14), the coefficient in Eq. (6.7) becomes $(\tilde{\xi}/(\rho a_2^2))(\tilde{a}/\tilde{b})$ whose numerical value is typically 10^{-2}. In figure 6.5 we show the field intensity as a function of $\tilde{z}$ (A_1) and the 2D gain as a function of the inhomogeneous term $\tilde{b}^2/4\tilde{a}$ (A_2) obtained assuming a uniform laser wiggler profile ($g = 1$). Note that the gain is Halved for $\tilde{b}^2/4\tilde{a} \sim 2$ *i.e.* $\tilde{b}/2\sqrt{\tilde{a}} \sim 1.4$ confirming the validity of the inhomogeneous condition in Eq.6.13.

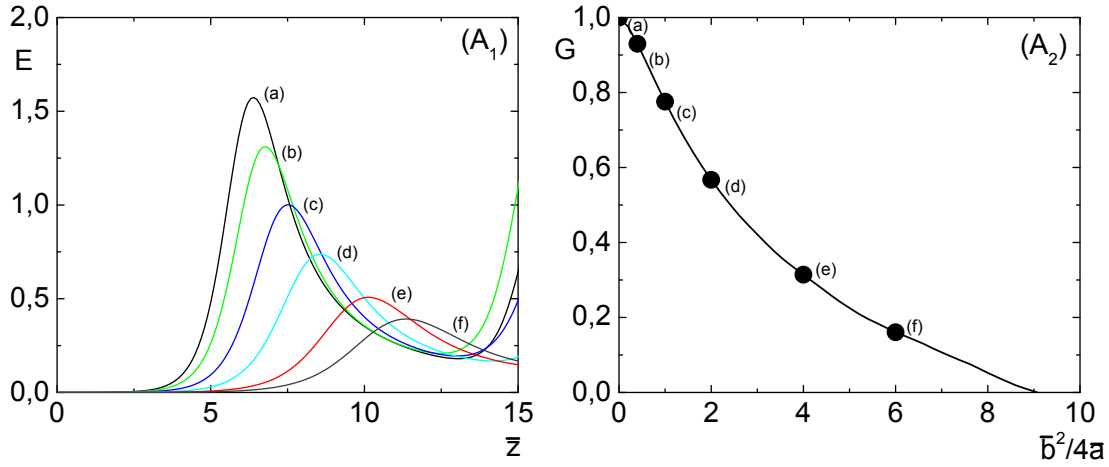

Figure 6.5: Fig.(a): Radiation intensity $E(\tilde{z}) = \int_R \mathrm{d}\bar{x}|\tilde{A}(\tilde{z},\bar{x})|^2$ as a function of $\tilde{z}$ for different values of the inhomogeneous term $\tilde{b}^2/4\tilde{a}$. Fig.(b): Gain $G(\tilde{b}^2/4\tilde{a}) = \int_R \mathrm{d}\bar{x}G(\bar{x},\tilde{b}^2/4\tilde{a})$ as a function of the inhomogeneous term $\tilde{b}^2/4\tilde{a}$ calculated at $\tilde{z} = 6$

The introduction of the transverse laser profile cause two different effects on the FEL process: the first is due to the decrease of the gain caused by the presence of the transverse laser profile in the driving term of the field evolution equation (6.43), this imply that the transverse gain distribution $G(\bar{x},\tilde{z})$ is proportional to that of the laser profile, *i.e.* the number of wiggler photons which interact with the electrons is lower in the beam halo with respect to the beam axis (see figure 6.2). Since the total 3D gain ($G(\tilde{z}) = \int_R \mathrm{d}\bar{x}G(\bar{x},\tilde{z})$) using the laser profile is smaller with respect to the uniform case $g = 1$, moreover the reduction degree of the gain is proportional to the slope of the laser profile. The latter effect induced by the laser profile, which is the most critical, cause a decrease of gain till to the complete inhibition of the high

gain process; this is due to the change from the fundamental resonance induced by the term $\tilde{\xi}/2\rho(1-|g(\bar{x},\tilde{z})|^2)$ in the second equation of (6.43). Figure (6.9) shows the field intensity $E(\tilde{z}) = \int_R \mathrm{d}\bar{x}|\tilde{A}(\bar{x},\tilde{z})|^2$ as a function of $\tilde{z}$ (figures A,C,E) and the 2D gain G as a function of $\tilde{\xi}/2\rho$ (figures B,D,F) for different choice of FGB profile ($m = 0$ A B, $m = 1$ C D, $m = 2$ E F). Note that, as was shown in figures (6.9 B,D,F), increasing the flatness (*i.e.* increasing m) the decrease of the gain is reduced.

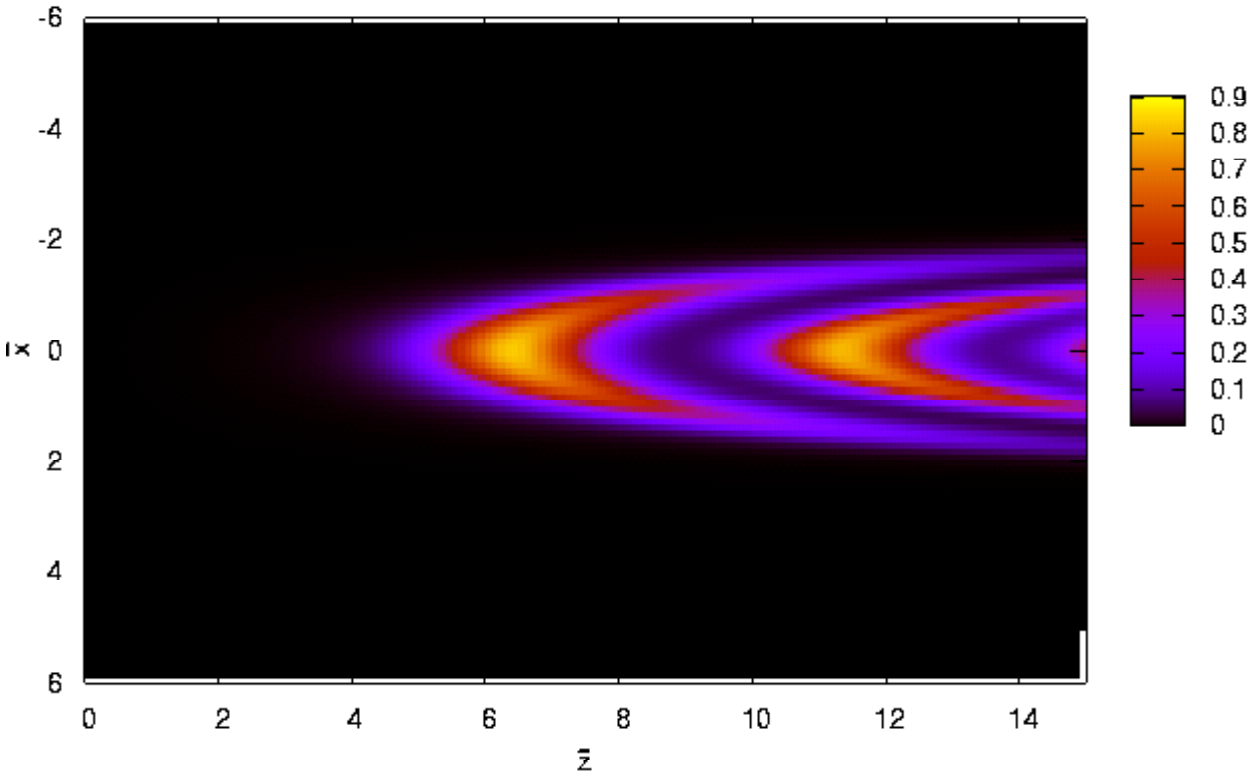

Figure 6.6: Radiation intensity $|\tilde{A}|^2$ as a function of transverse coordinate $\bar{x}$ and of the number of interaction lengths $\tilde{z}$ for the parameters listed in table 6.2. As a reference, the 1D model intensity would saturate to unity.

From the discussion about the beam and laser wiggler requirements in section 6.1 and using the numerical result showed in figure 6.5 for the emittance requirements and in figure 6.9 for the laser wiggler profile requirements we deduce that in order to obtain the high gain regime the value of emittance must be equal or less than 1mm-mrad, moreover FGB profile with $m \geq 1$ is necessary in order to have a sufficient

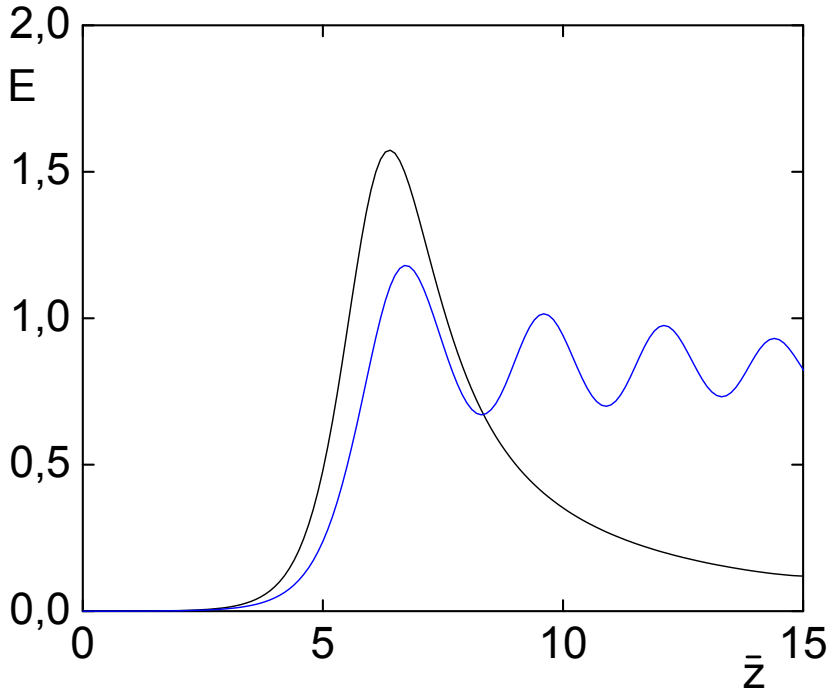

Figure 6.7: Radiation intensity $|\tilde{A}|^2$ as a function of the number of interaction lengths $\tilde{z}$: (dark line) ideal case, (blu line) parameters same as table 6.2.

fraction of the on-axis peak intensity compared to that of the 1D model. A set of possible experimental parameters corresponding to this simulation is listed in Table 6.2. As shown in table 6.2, if the emittance and the laser wiggler profile are both included the requirements become more stringent.

Figure 6.6 shows the radiation intensity $|\tilde{A}|^2$ as a function of transverse coordinate $\bar{x}$ and of the number of gain lengths $\tilde{z}$ obtained using the value of experimental parameter listed in table 6.2; while in figure 6.7 the radiation intensity as a function of the number of gain lengths $\tilde{z}$ (from table 6.2) is compared with the optimum 2D ideal case ($\tilde{\xi}/2\rho = \tilde{a} = \tilde{b} = 0$). Note that the diffraction effect caused a lower descend for the emitted field in the beam halo with respect to that on the beam axis. This give an additional contribute to the transverse integration after saturation time. The probability distributions $P_0(\bar{x}, \tilde{z})$ and $P_{-1}(\bar{x}, \tilde{z})$ for the $m = 0$ and $m = -1$ momentum state are showed in fig. 6.8.

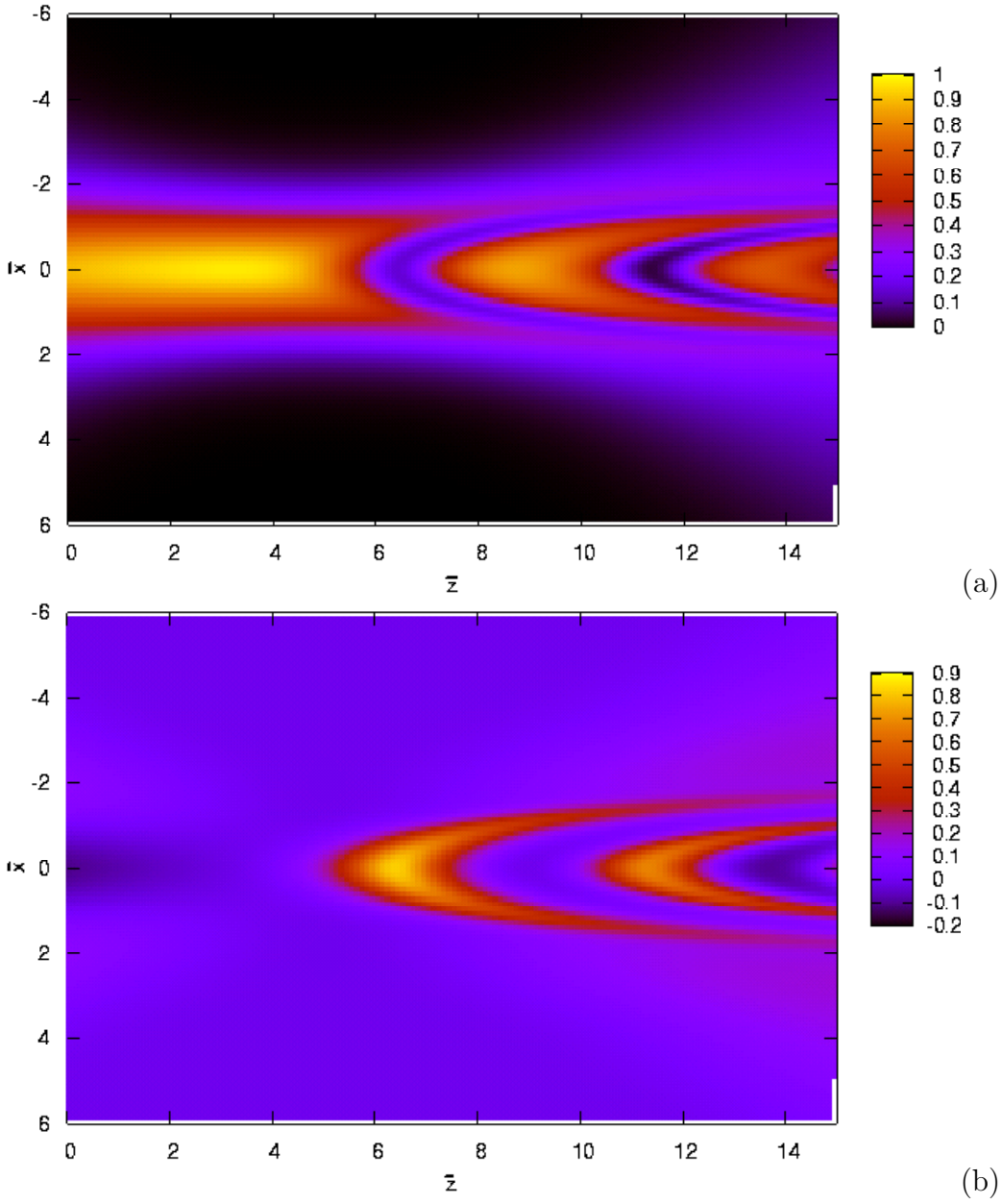

Figure 6.8: Probability distribution for $m = 0$ momentum state $P_0(\bar{x})$ (Fig. (a)) and for $m = -1$ momentum state $P_0(\bar{x})$ (Fig. (b)), as a function of transverse coordinate $\bar{x}$ and of wiggler position $\tilde{z}$.

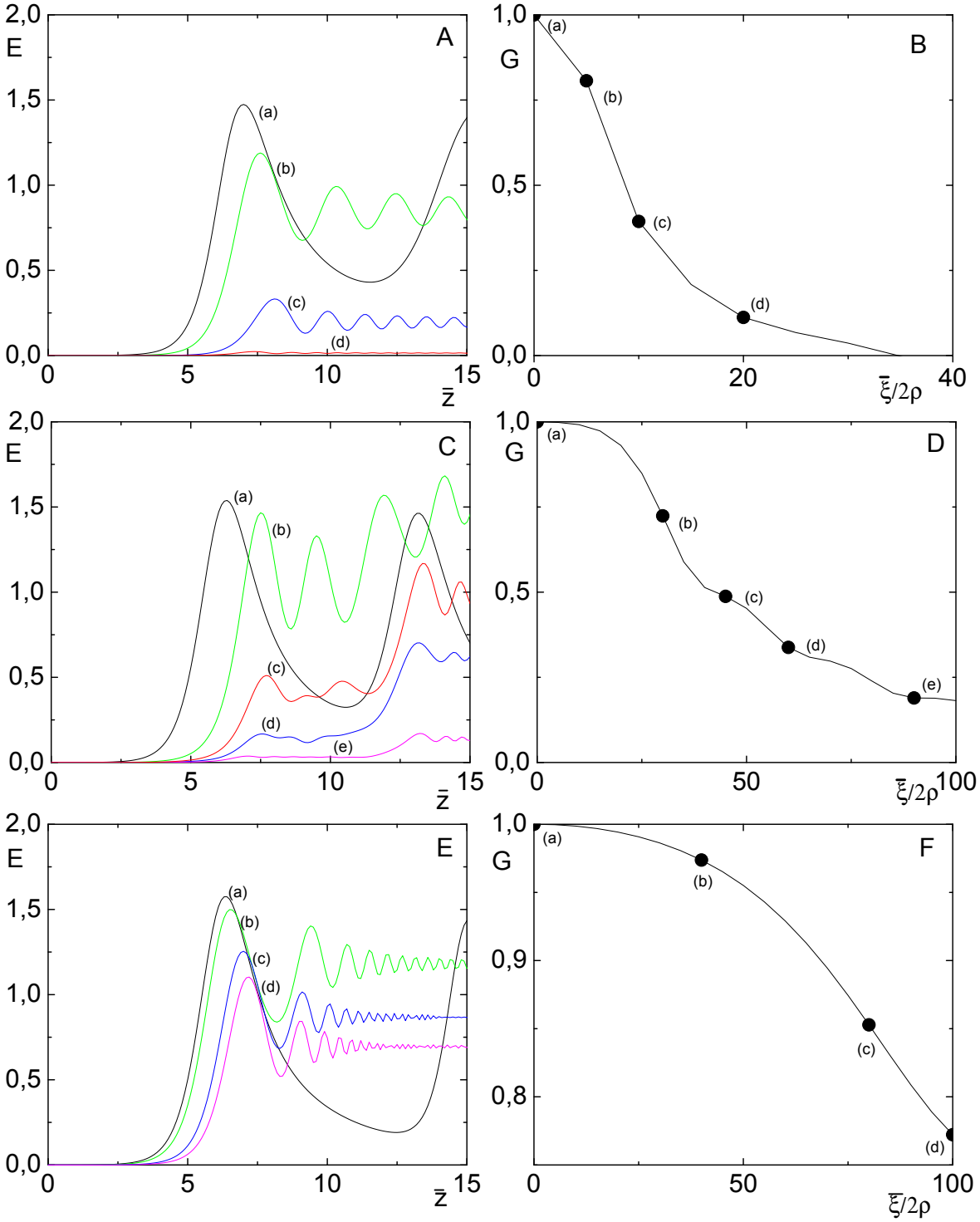

Figure 6.9: field intensity $E(\tilde{z}) = \int_R \mathrm{d}\bar{x}|\tilde{A}(\bar{x},\tilde{z})|^2$ vs. $\tilde{z}$ for different values of $\tilde{\xi}/2\rho$ and Gain $G(\tilde{\xi}/2\rho) = \int_R \mathrm{d}\bar{x}G(\bar{x},\tilde{\xi}/2\rho)$ vs. $\tilde{\xi}/2\rho$ for $m = 0$ (A,B), $m = 1$ (C,D), $m = 2$ (E,F)

Independent parameters	**symbol**	**value**
QFEL-parameter	$\bar{\rho}$	0.2
radiation wavelength	λ_r(Å)	2
laser wiggler wavelength	$\lambda_l(\mu\text{m})$	1
laser wiggler parameter	a_0	0.15
Interaction length in unit of $\tilde{l}_g$	a_1	10
ratio between laser and e-beam radius	a_2	2
FEL parameter	ρ	$6 \cdot 10^{-5}$
gain length	$\tilde{l}_g$(mm)	1.3
laser wiggler parameters	**symbol**	**value**
laser Rayleigh range	Z_l(mm)	6.5
laser radius	$R(\mu\text{m})$	22.8
laser power	P(TW)	2
laser duration	τ_l(ps)	88
length and time interaction	l_{int}(mm), τ_{int}(ps)	13.2, 44
e-beam parameters	**symbol**	**value**
e-beam energy	γ	36
e-beam radius	$\sigma(\mu\text{m})$	11.4
bunch length	$l_b(\mu\text{m})$	347
peak current	I(A)	863

numerical parameters	**symbol**	**(a)**	**(b)**	**(c)**
normalized emittance	ϵ_n(mm-mrad)	0	0.05	0.1
e-beam diffraction	$\tilde{b}$	0	0.013	0.025
field diffraction	$\tilde{a}$	0	$1.6 \cdot 10^{-4}$	$1.6 \cdot 10^{-4}$
resonant shift emittance	$\tilde{b}/2\sqrt{\tilde{a}}$	0	0.5	1

Table 6.1: Set of possible experimental parameters using uniform laser wiggler $g = 1$

Independent parameters	**symbol**	**value**
QFEL-parameter	$\bar{\rho}$	0.2
radiation wavelength	λ_r(Å)	2.5
laser wiggler wavelength	$\lambda_l(\mu\text{m})$	1
normalized emittance	ϵ_n(mm-mrad)	0.05
laser wiggler parameter	a_0	0.05
Interaction length in unit of $\tilde{l}_g$	a_1	7
ratio between laser and e-beam radius	a_2	2
FEL parameter	ρ	$6.6 \cdot 10^{-5}$
gain length	$\tilde{l}_g$(mm)	1.47
laser wiggler parameters	**symbol**	**value**
laser Rayleigh range	Z_l(mm)	5.0
laser radius	$R(\mu\text{m})$	20
laser power	P(TW)	0.17
laser duration	τ_l(ps)	67
length and time interaction	l_{int}(mm), τ_{int}(ps)	20.1, 33.4
e-beam parameters	**symbol**	**value**
e-beam energy	γ	31.7
e-beam radius	$\sigma(\mu\text{m})$	10
bunch length	$l_b(\mu\text{m})$	97.3
peak current	I(A)	3083
numerical parameters	**symbol**	**(value)**
e-beam diffraction	$\tilde{b}$	$2.3 \cdot 10^{-2}$
field diffraction	$\tilde{a}$	$2.9 \cdot 10^{-4}$
resonant shift emittance	$\tilde{b}/2\sqrt{\tilde{a}}$	0.68
resonant shift laser	$\tilde{\xi}/2\rho$	46
laser diffraction	$\tilde{d}$	0.29

Table 6.2: Set of possible experimental parameters using the FGB laser wiggler with $m = 6$

Conclusions

In this thesis we have presented the 3D time dependent quantum model for a FEL with a laser wiggler based on a fluid description, in which the electrons of the beam are described by a Wigner distribution function which is continuous in the transverse phase-space and discrete in the longitudinal phase-space variables [41]. This model extend the 1D Schrödinger-Maxwell model discussed in chapter 3, where the electron beam is described by a wave function $\Psi(\theta, \bar{z})$. The 3D Wigner function has been obtained in terms of the creation and annihilation operator in the finite temperature second quantization formalism as formulate by Balescu [45] and it has a broader validity than the Schrödinger equation, since it can also describe a statistical mixture of states, which cannot be represented by a wave function but rather by a density operator. The evolution equation for the Wigner function has been obtained starting from the Liouville-Von Neumann evolution equation for the density operator and using the 3D Hamiltonian in a second quantization scheme obtained in section (5.2), while the evolution equation for the radiation e.m. field has been obtained, starting from the paraxial Maxwell equations, in the slowly varying envelope approximation (section 2.1.2). The propagation (or "slippage") effects have been considered using the multiple scaling method *i.e* considering the existence of two different spatial length scales: the variation of the electrons distribution on the radiation wavelength scale describing the bunching on the variable θ and the variation of the field envelope on the much longer scale of the cooperation length l_c (typically $l_c \sim 10^4 \lambda_r$).

From the dynamical point of view our model treats both fermions and bosons similarly, so that the "Preparata hypothesis" [24] *i.e* the electrons in FEL can be treated as bosons (see also section 3.1.2) [37, 36], is no longer necessary. The resulting model describes the 3D spatial and temporal evolution of electron and radiation beams, including diffraction, propagation, laser wiggler, emittance and quantum re-

coil effects. It reduces to the 3D Maxwell-Vlasov model in the classical limit $\bar{\rho} \gg 1$ and can be solved numerically. Using quantum universal scaling (Eq. (5.19)) the 3D extra terms in our model depend only on two parameters , which are related to the diffraction (or Rayleigh range) of the radiation and electron beam, and on the laser wiggler parameters which are related to the particular transverse profile of the laser.

We have performed two different numerical analyses:

• In chapter 4 we numerically solved the 1D quantum model in the SASE operation mode performing a complete statistical analysis of SASE FEL spectral proprieties, confirming the existence of the phenomenon of "Quantum purification" predicted in [30]. In this new quantum regime the spectrum of the emitted radiation is mainly composed of a single narrow line whose line width is proportional to the ratio between the radiation wavelength and the bunch length; on the contrary, in the classical regime the spectrum is composed of many such random spikes, whose number is proportional to the ratio between bunch and cooperation lengths.

• In chapter 6 we have presented a study concerning the effective possibility for a future experiment confirmation of this quantum regime. We have discussed the experimental requirements for a Quantum X-ray FEL with a laser wiggler, obtaining useful quantum scaling laws for the main experimental parameters (Eqs. (6.31)). In particular, we have studied the decrease of gain caused by the inhomogeneous broadening of the radiation line width, due to beam divergence and transverse laser profile. Since same important constrain (see Eqs. (6.12), (6.16) and (6.17)), which must be satisfied in order to preserve the quantum high gain process, are derived.

Preliminary 3D numerical simulations confirm that the most critical 3D effects arise from the change of FEL resonance due to emittance of the beam (6.12) and transverse laser profile (6.17). The inhomogeneous broadening due to the emittance has been investigated in details for the quantum regime *i.e.* in the two level approximation and a useful numerical fit relation describing the gain as a function of the inhomogeneous term has been obtained. It shows how FEL action is suppressed for beam emittance values which violate the inhomogeneous condition of Eq. (6.13).

The transverse laser profile effects have been also numerical investigated in the quantum regime. In particular we have shown that a flattened laser beam profile [61, 62] is preferible to the usual $\mathtt{TEM}_{00}$ Gaussian beam in order to preserve the high

gain regime. We have shown numerically that the decrease of the gain caused by the laser profile is strongly reduced using a flattened laser profile. Finally we performed a numerical analysis in the quantum regime taking into account both the emittance and the laser profile effects, obtaining a set of possible experimental parameters for a future QFEL experiment (table 6.2).

On the basis of the numerical analysis and the examples of experimental parameters considered above, we conclude that, although beams with emittance below the required inhomogeneous limit, Eq. (6.12), are presently far from being produced, the big advantages of QFEL motivate a large effort for its realization. In fact the quantum regime of a FEL with a laser wiggler can be a convenient X-ray source, since the emitted radiation has the important property of high temporal coherence with no spiking, whereas in the classical regime many random spikes are observed. This is the fundamental difference between the quantum and the classical regimes. Furthermore, the full line width of the spectrum in the classical regime can be three or four orders of magnitude larger than the single spectral line width obtained in the quantum regime.

Appendix A

Multiple Scaling method

We start from the Eqs.(3.35) and (3.36) in chapter 3.

$$i\frac{\partial\Psi(\bar{z},\theta)}{\partial\bar{z}} = -\frac{1}{2\bar{\rho}}\frac{\partial\Psi(\bar{z},\theta)}{\partial\theta^2} - i\bar{\rho}\left[A_r(\bar{z},\theta)e^{-i\theta} - \text{h.c.}\right]\Psi(\bar{z},\theta) \tag{A.1}$$

$$\frac{\partial A_r(\bar{z},\theta)}{\partial\bar{z}} + \frac{1}{2\rho}\frac{\partial A_r(\bar{z},\theta)}{\partial\theta} = |\Psi(\bar{z},\theta)|^2\ e^{-i\theta} + i\delta A_r(\bar{z},\theta) \tag{A.2}$$

We introduce the new variable $z_1 = \epsilon\theta$ with $\epsilon = 2\rho$, since $\epsilon \simeq 10^-4$ then we can treated θ and z_1 as independent variables. The matter wave field and the radiation field become respectivelly $A_r(\bar{z},\theta) \to A_r(\bar{z},z_1\theta)$ and $\Psi(\bar{z},\theta) \to \Psi(\bar{z},z_1,\theta)$.

Using the following chain rule

$$\frac{\partial}{\partial\theta} = \frac{\partial}{\partial\theta} + \epsilon\frac{\partial}{\partial z_1} \tag{A.3}$$

Eqs.(A.1) and (A.2) become:

$$i\frac{\partial\Psi}{\partial\bar{z}} = -\frac{1}{2\bar{\rho}}\left(\frac{\partial^2}{\partial\theta^2} + 2\epsilon\frac{\partial^2}{\partial\theta\partial z_1} + \epsilon^2\frac{\partial^2}{\partial z_1^2}\right)\Psi - i\bar{\rho}\left[A_r e^{-i\theta} - A_r^* e^{i\theta}\right]\Psi, \tag{A.4}$$

$$\left(\epsilon\frac{\partial}{\partial\bar{z}} + \frac{\partial}{\partial\theta} + \epsilon\frac{\partial}{\partial\theta}\right)A_r = \epsilon|\Psi|^2\ e^{-i\theta} + i\epsilon\delta A_r \tag{A.5}$$

Now we expand the matter wave field and the radiation field in power of ϵ

$$\Psi = \Psi^{(0)} + \epsilon\Psi^{(1)} + \ldots \tag{A.6}$$

$$A_r = A_r^{(0)} + \epsilon A_r^{(1)} + \ldots \tag{A.7}$$

Introducing the series expansions of Eq.(A.2) in to Eqs.(A.4) and (A.5) we obtain equations relating the coefficients of the various power of ϵ. We are only interested

to the zeroth and the first-order (*i.e.* $\epsilon \to 0$). For the matter wave field $\Psi(\theta, \bar{z}, z_1)$ the zeroth order is

$$i\frac{\partial \Psi^{(0)}}{\partial \bar{z}} = -\frac{1}{2\bar{\rho}}\frac{\partial^2 \Psi^{(0)}}{\partial \theta^2} - i\bar{\rho}\left[A_r^{(0)}e^{-i\theta} - A_r^{(0)} * e^{i\theta}\right]\Psi^{(0)}, \tag{A.8}$$

Which corresponds to Eq.(3.38), whereas for the radiation field $A_r(\theta, \bar{z}, z_1)$ the zeroth and the first-order are respectively,

$$\frac{\partial A_r^{(0)}}{\partial \theta} = 0, \tag{A.9}$$

$$\frac{\partial A_r^{(1)}}{\partial \theta} = |\Psi^{(0)}|^2 e^{-i\theta} + i\delta A_r^{(0)} - \frac{\partial A_r^{(0)}}{\partial \bar{z}} - \frac{\partial A_r^{(0)}}{\partial z_1}. \tag{A.10}$$

hence $A_r^{(0)} = A_r^{(0)}(\bar{z}, z_1)$ is a slowly varying function of z_1 and does not depend on θ.

integrating both sides of Eq.(A.10) over θ between 0 and 2π and assuming that $A^{(1)}$ is a periodic function of θ, we obtain

$$\left(\frac{\partial}{\partial \bar{z}} + \frac{\partial}{\partial \bar{z}}\right) A_r^{(0)} = \frac{1}{2\pi}\int_0^{2\pi} |\Psi^{(0)}|^2 e^{-i\theta} + i\delta A_r^{(0)}. \tag{A.11}$$

which corresponds to Eq.(3.39).

Appendix B

Quantum 3D Hamiltonian

Let start from the Classical 3D Hamiltonian obtained in section (2.3.2)

$$H = \frac{\bar{p}^2}{2} + \frac{b}{2}\bar{\mathbf{p}}_\perp^2 + \bar{p}\left[\frac{\xi}{2\rho}(1-|g|^2) - \frac{bX}{4}\bar{\mathbf{p}}_\perp^2\right] + \frac{\xi}{\rho X}|g|^2 - i\left(g^* A_r e^{i\theta} - c.c.\right) \quad \text{(B.1)}$$

with the relative associated equations of motion (we drop, for simplicity, the charge term (see section. (2.1.2))

$$\begin{cases} \dfrac{d\bar{\mathbf{x}}_\perp}{d\bar{z}} = \nabla_{\bar{\mathbf{p}}_\perp} H = b\ \bar{\mathbf{p}}_\perp \\ \dfrac{d\bar{\mathbf{p}}_\perp}{d\bar{z}} = -\nabla_{\bar{\mathbf{x}}_\perp} H = -\dfrac{\xi}{\rho X}\nabla_{\mathbf{x}_\perp}|g|^2 \\ \dfrac{d\theta}{d\bar{z}} = -\partial_{\bar{p}} H = \bar{p} + \left[\dfrac{\xi}{2\rho}(1-|g|^2) - \dfrac{bX}{4}\bar{\mathbf{p}}_\perp^2\right] \\ \dfrac{d\bar{p}}{d\bar{z}} = -\partial_\theta H = -\left(g^* A_r e^{i\theta} + c.c.\right) \end{cases} \quad \text{(B.2)}$$

where $\bar{\mathbf{x}}_\perp = (\bar{x}, \bar{y})$ and $\bar{\mathbf{p}}_\perp = (\bar{p}_x, \bar{p}_y y)$. The variables are defined in the "Classical 3D Universal Scaling" (see Eq.(2.104)):

$$\begin{cases} \theta = (k_r + k_l)\, z - c\,(k_r - k_l)\, t, \\ \\ \bar{z} = z/l_g, \quad \bar{z_1} = (\bar{z} - \bar{v}_e \bar{t})/l_c \bar{\beta}_e \\ \\ \bar{p} = \dfrac{\gamma - \gamma_r}{\rho \gamma_r}, \quad \delta = (\gamma_0 - \gamma_r)/\rho\gamma_r \\ \\ \bar{\mathbf{x}}_\perp = \mathbf{x}_\perp/\sigma, \quad \bar{p}_\perp = \dfrac{\sigma}{\epsilon_r}\beta_\perp \\ \\ A_r = \dfrac{\omega}{\omega_p \sqrt{\rho\gamma}} a_r. \end{cases} \tag{B.3}$$

and σ is the rms electron 'radius' at the beam waist, ϵ_r is the rms beam emittance and $\omega_p = \sqrt{e^2 n_0/(\epsilon_0 m_e)}$ is the plasma frequency. Note that $g = g(\mathbf{x}_\perp, \bar{z})$ in Eqs. (B.1) and (B.3) represents the transverse laser wiggler profile, whose analytic form will be specified in the Appendix E. The three dimensional parameter are defined as follows:

$$X = 2k\epsilon_r, \qquad b = \frac{l_g}{\beta^*} = \frac{l_g \epsilon_r}{\sigma^2} \qquad \xi = \frac{a_0^2}{1 + a_0^2}. \tag{B.4}$$

The QFEL parameter and the transverse parameter are respectively:

$$\bar{\rho} = \rho \frac{mc\gamma_r}{\hbar k_r}, \quad \alpha = \frac{\hbar}{mc\gamma_r \epsilon_r} \tag{B.5}$$

In order to quantize the system let introduce the new longitudinal and transverse momenta scaled in terms of the parameters defined in Eq. (B.5) such that:

$$\begin{cases} p = \dfrac{mc(\gamma - \gamma_0)}{\hbar k} \;\rightarrow\; p = \bar{p}\bar{\rho} - \delta \\ \\ \mathbf{p}_\perp = \left(\dfrac{mc\gamma_r \sigma}{\hbar}\right) \beta_\perp \;\rightarrow\; \mathbf{p}_\perp = (\alpha^{-1})\bar{\mathbf{p}}_\perp \end{cases} \tag{B.6}$$

These new variables are even canonical conjugate and satisfy the Poisson brackets rules:

$$\{\theta, p\} = 1 \quad \text{and} \quad \{x, p_x\} = 1, \;\; \{y, p_y\} = 1 \tag{B.7}$$

In order to quantize the Hamiltonian we adopt the canonical quantization rules, such that the dynamical variables become operators in Hilbert space,

$$\mathbf{x}_\perp \to \hat{\mathbf{x}}_\perp, \quad \mathbf{p}_\perp \to \hat{\mathbf{p}}_\perp = -i\nabla_{\mathbf{x}_\perp}, \qquad \theta \to \hat{\theta}, \quad p \to \hat{p} = -i\partial_\theta. \tag{B.8}$$

and the Poisson brackets (B.7) become Quantum Commutation Rules (QCR)

$$\{x, p_x\} = 1 \to [\hat{x}, \hat{p}_x]_- = i, \;\; \{y, p_y\} = 1 \to [\hat{y}, \hat{p}_y]_- = i \quad \text{and} \quad \{\theta, p\} = 1 \to [\hat{\theta}, \hat{p}]_- = i \tag{B.9}$$

The first quantized Hamiltonian $\bar{H}(\hat{\theta}, \hat{p},\ \hat{\mathbf{x}}_\perp, \hat{\mathbf{p}}_\perp; \bar{z} \mid \bar{z_1})$ can be written as follows:

$$\bar{H} = \bar{H}_1 + \bar{H}_2 + \bar{H}_3 \tag{B.10}$$

whit

$$\begin{cases} \bar{H}_1 = \dfrac{1}{2\bar{\rho}}\hat{\mathbf{p}}_\perp^2 + \dfrac{\alpha b}{2}\hat{\mathbf{p}}_\perp^2 + \left(\delta + \dfrac{\xi}{2\rho}\right)\hat{p} - \dfrac{bX}{4}\alpha^2\hat{\mathbf{p}}_\perp^2 \\ \\ \bar{H}_2 = +\dfrac{\xi}{\alpha\rho X}|g(\hat{\mathbf{x}}_\perp, \bar{z})|^2 - \dfrac{\xi}{2\rho}|g(\hat{\mathbf{x}}_\perp, \bar{z})|^2\hat{p} \\ \\ \bar{H}_3 = -i\bar{\rho}\left(g^*(\hat{\mathbf{x}}_\perp, \bar{z})A_r(\hat{\mathbf{x}}_\perp, \bar{z}, \bar{z_1})e^{i\hat{\theta}} - g(\bar{\mathbf{x}}_\perp, \bar{z})A_r^*(\hat{\mathbf{x}}_\perp, \bar{z}, \bar{z_1})e^{-i\hat{\theta}}\right) \end{cases} \tag{B.11}$$

Note that the dependence on $\bar{z_1}$ is parametric only. The Hamiltonian in second quantization formalism can be obtained introducing the Schrödinger operator which creates (or annihilates) one particle in the $(\theta, \mathbf{x}_\perp)$ position.

$$\mathbf{\Psi}(\theta, \bar{\mathbf{x}}_\perp) = (2\pi)^{-3/2}\sum_{m\in Z}\int_{R^2} \mathrm{d}^2\mathbf{k}_\perp\ \mathbf{c}_m(\mathbf{k}_\perp)\ e^{im\theta}\ e^{i\mathbf{k}_\perp\cdot\bar{\mathbf{x}}_\perp} \tag{B.12}$$

Here we assume that the FEL system is periodic in the longitudinal direction (*i.e* θ), as the FEL is usually considerate. The commutation rules for the Schrödinger field operator (B.12) are:

$$\left[\mathbf{\Psi}^\dagger(\theta, \bar{\mathbf{x}}_\perp), \mathbf{\Psi}(\theta', \bar{\mathbf{x}}_\perp)\right]_\theta = \delta(\bar{\mathbf{x}}_\perp - \bar{\mathbf{x}}'_\perp)\delta(\theta - \theta'). \tag{B.13}$$

and the normalization condition is:

$$\int_0^{2\pi}\mathrm{d}\theta\int_{R^2}\mathrm{d}^2\mathbf{x}\ \mathbf{\Psi}^\dagger(\theta, \bar{\mathbf{x}}_\perp)\mathbf{\Psi}(\theta, \bar{\mathbf{x}}_\perp) = \mathbf{N}_e \tag{B.14}$$

The creation and annihilation operators acts on a the generic state of the multi particle Fock space

$$|n_m(\mathbf{k}_\perp)\rangle \equiv \prod_{m\in Z} |n_m(\mathbf{k}_\perp)\rangle \tag{B.15}$$

where $n_m(\mathbf{k}_\perp)$ represents the number of electrons within the quantum state with discrete longitudinal momentum m and continuous transverse momentum $\mathbf{k}_\perp$. The action of the creator and annihilator operators on a Fock state (5.29) is different for bosons or fermions since it depends on the choice of the Quantum Commutation Rules (QCR):

$$\begin{aligned}
\Big[\mathbf{c}_n(\mathbf{k}_\perp), \mathbf{c}^\dagger_{n'}(\mathbf{k}'_\perp)\Big]_\theta &= \delta(\mathbf{k}_\perp - \mathbf{k}'_\perp)\ \delta_{n,n'} \\
\Big[\mathbf{c}_n(\mathbf{k}_\perp), \mathbf{c}_{n'}(\mathbf{k}'_\perp)\Big]_\theta &= 0 \\
\Big[\mathbf{c}^\dagger_n(\mathbf{k}_\perp), \mathbf{c}^\dagger_{n'}(\mathbf{k}'_\perp)\Big]_\theta &= 0
\end{aligned} \tag{B.16}$$

where $\theta = \pm 1$ and $[a,b]_\pm = ab \pm ba$. The D-dimensional Dirac Delta and the 1-dimensional Kronecker Delta are defined respectively as follows:

$$\delta^D(\mathbf{x}-\mathbf{x}') = \frac{1}{(2\pi)^D}\int_{R^D} \mathrm{d}^D\mathbf{y}\ e^{i\mathbf{y}(\mathbf{x}-\mathbf{x}')}, \quad \delta_{m,m'} = \frac{1}{(2\pi)}\int_0^{2\pi} \mathrm{d}\theta e^{i\theta(m-m')}. \tag{B.17}$$

The second quantized Hamiltonian $\mathbf{H}$ can be obtained in terms of the first quantized Hamiltonian (B.10):

$$\mathbf{H} = \mathbf{H_1} + \mathbf{H_2} + \mathbf{H_3}, \tag{B.18}$$

where

$$\mathbf{H_i} = \int_0^{2\pi} \mathrm{d}\theta \int_{R^2} \mathrm{d}^2\bar{\mathbf{x}}_\perp\ \mathbf{\Psi}^\dagger(\theta, \bar{\mathbf{x}}_\perp)\ \bar{H}_i\ \mathbf{\Psi}(\theta, \bar{\mathbf{x}}_\perp), \quad i = 1,2,3 \tag{B.19}$$

Here we introduce some convenient definitions:

- The functions $g_f(\mathbf{q}_\perp, \bar{z})$ and $G_f(\mathbf{q}_\perp, \bar{z}, \bar{z_1})$ are respectively the 2D Fourier transform of the real function

  $$|g(\bar{\mathbf{x}}_\perp, \bar{z})|^2 = (2\pi)^{-1}\int_R \mathrm{d}^2\mathbf{q}_\perp\ e^{-i\mathbf{x}_\perp\cdot\mathbf{q}_\perp} g_f(\mathbf{q}_\perp, \bar{z}) \tag{B.20}$$

  and of the Complex function

  $$F(\mathbf{x}_\perp, \bar{z}, \bar{z_1}) = g(\bar{\mathbf{x}}_\perp, \bar{z}) A_r(\mathbf{x}_\perp, \bar{z}, \bar{z_1}) = (2\pi)^{-1}\int_R \mathrm{d}^2\mathbf{q}_\perp\ e^{-i\mathbf{x}_\perp\cdot\mathbf{q}_\perp} G_f(\mathbf{q}_\perp, \bar{z}, \bar{z_1}). \tag{B.21}$$

- All the parameters are defined as follows:

$$a_1 = \frac{1}{2\bar{\rho}}, \quad a_2 = \frac{\alpha b}{2}, \quad a_3 = \frac{\xi}{2\rho}, \quad a_4 = \frac{bX}{4}\alpha^2, \quad a_5 = \frac{\xi}{\alpha\rho X} \tag{B.22}$$

The FEL Hamiltonian in term of the creation and annihilation operators can be calculated as follows: For the first term of Eq. (B.18) we have

$$\begin{aligned}
\mathbf{H}_1 &= (2\pi)^{-3} \sum_{m,m'} \int_0^{2\pi} \mathrm{d}\theta \int_{R^2} \mathrm{d}^2\bar{\mathbf{x}}_\perp \int_{R^2} \mathrm{d}^2\mathbf{k}_\perp \int_{R^2} \mathrm{d}^2\mathbf{k}'_\perp \; e^{-i(\theta m + \bar{\mathbf{x}}_\perp \cdot \mathbf{k}_\perp)} \times \\
&\quad \left(-a_1\partial_\theta^2 - a_2\nabla^2_{\bar{\mathbf{x}}_\perp} - i(a_3+\delta)\partial_\theta - ia_4\partial_\theta\nabla^2_{\bar{\mathbf{x}}_\perp}\right) e^{i(\theta m' + \bar{\mathbf{x}}_\perp \cdot \mathbf{k}'_\perp)} \; \mathbf{c}^\dagger_m(\mathbf{k}_\perp)\mathbf{c}_{m'}(\mathbf{k}'_\perp) \\
&= (2\pi)^{-3} \sum_{m,m'} \int_0^{2\pi} \mathrm{d}\theta \int_{R^2} \mathrm{d}^2\bar{\mathbf{x}}_\perp \int_{R^2} \mathrm{d}^2\mathbf{k}_\perp \int_{R^2} \mathrm{d}^2\mathbf{k}'_\perp e^{-i\theta(m-m')} e^{-i\bar{\mathbf{x}}_\perp \cdot (\mathbf{k}_\perp - \mathbf{k}'_\perp)} \\
&\quad \left(a_1 m'^2 + a_2\mathbf{k}'^2_\perp + (a_3+\delta)m' - a_4 m'\mathbf{k}'^2_\perp\right) \mathbf{c}^\dagger_m(\mathbf{k}_\perp)\mathbf{c}_{m'}(\mathbf{k}'_\perp) \\
&= \sum_{m,m'} \int_{R^2} \mathrm{d}^2\mathbf{k}_\perp \int_{R^2} \mathrm{d}^2\mathbf{k}'_\perp \delta_{m,m'}\delta(\mathbf{k}_\perp - \mathbf{k}'_\perp) \\
&\quad \left(a_1 m'^2 + a_2\mathbf{k}'^2_\perp + (a_3+\delta)m' - a_4 m'\mathbf{k}'^2_\perp\right) \mathbf{c}^\dagger_m(\mathbf{k}_\perp)\mathbf{c}_{m'}(\mathbf{k}'_\perp)
\end{aligned}$$

where we have used the Dirac and Kronecker Delta functions as defined in Eq.(B.17). Integrating on $\mathbf{k}'_\perp$ and summing on m' we obtain:

$$\begin{aligned}
\mathbf{H}_1 &= \sum_m \int_{R^2} \mathrm{d}^2\mathbf{k}_\perp \; h_1(m, \mathbf{k}_\perp, a_i)\mathbf{c}^\dagger_m(\mathbf{k}_\perp)\mathbf{c}_m(\mathbf{k}_\perp) \\
&\quad h_1(m, \mathbf{k}_\perp, a_i) = a_1 m^2 + a_2\mathbf{k}^2_\perp + (a_3+\delta)m - a_4 m\mathbf{k}^2_\perp
\end{aligned} \tag{B.23}$$

For the second term of Eq. (B.18) we have

$$\begin{aligned}
\mathbf{H}_2 &= (2\pi)^{-3} \sum_{m,m'} \int_0^{2\pi} \mathrm{d}\theta \int_{R^2} \mathrm{d}^2\bar{\mathbf{x}}_\perp \int_{R^2} \mathrm{d}^2\mathbf{k}_\perp \int_{R^2} \mathrm{d}^2\mathbf{k}'_\perp \; e^{-i(\theta m + \bar{\mathbf{x}}_\perp \cdot \mathbf{k}_\perp)} \times \\
&\quad \left[(a_5 + ia_3\partial_\theta)\int_{R^2} \frac{\mathrm{d}^2\mathbf{q}_\perp}{2\pi} g_f(\mathbf{q}_\perp, \bar{z}) e^{-i\bar{\mathbf{x}}_\perp \cdot \mathbf{q}_\perp}\right] e^{+i(\theta m' + bar\mathbf{x}_\perp \cdot \mathbf{k}'_\perp)} \mathbf{c}^\dagger_m(\mathbf{k}_\perp)\mathbf{c}_{m'}(\mathbf{k}'_\perp) \\
&= (2\pi)^{-3} \sum_{m,m'} \int_0^{2\pi} \mathrm{d}\theta \int_{R^2} \mathrm{d}^2\bar{\mathbf{x}}_\perp \int_{R^2} \mathrm{d}^2\mathbf{k}_\perp \int_{R^2} \mathrm{d}^2\mathbf{k}'_\perp \int_{R^2} \frac{\mathrm{d}^2\mathbf{q}_\perp}{2\pi} \; g_f(\mathbf{q}_\perp, \bar{z}) \times \\
&\quad e^{-i\theta(m-m')} e^{-i\bar{\mathbf{x}}_\perp \cdot (\mathbf{k}_\perp - \mathbf{k}'_\perp + \mathbf{q}_\perp)} \left(a_5 - a_3 m'\right) \mathbf{c}^\dagger_m(\mathbf{k}_\perp)\mathbf{c}_{m'}(\mathbf{k}'_\perp) \\
&= \sum_{m,m'} \int_{R^2} \mathrm{d}^2\mathbf{k}_\perp \int_{R^2} \mathrm{d}^2\mathbf{k}'_\perp \int_{R^2} \frac{\mathrm{d}^2\mathbf{q}_\perp}{2\pi} \; g_f(\mathbf{q}_\perp, \bar{z})\delta_{m,m'} \; \delta(\mathbf{k}_\perp - \mathbf{k}'_\perp) \left(a_5 - a_3 m'\right) \mathbf{c}^\dagger_m(\mathbf{k}_\perp)\mathbf{c}_{m'}(\mathbf{k}'_\perp)
\end{aligned}$$

Integrating on $\mathbf{k}'_\perp$ and summing on m' we obtain:

$$\begin{aligned}
\mathbf{H}_2 &= \sum_m \; h_2(m, a_i) \int \mathrm{d}^2\mathbf{k}_\perp \int_{R^2} \frac{\mathrm{d}^2\mathbf{q}_\perp}{2\pi} \; g_f(\mathbf{q}_\perp, \bar{z}) \; \mathbf{c}^\dagger_m(\mathbf{k}_\perp)\mathbf{c}_{m'}(\mathbf{k}'_\perp) \\
&\quad h_2(m, a_i) = a_5 - a_3 m
\end{aligned} \tag{B.24}$$

For the last term of Eq. (B.18) we have

$$\begin{aligned}
\mathbf{H}_3 &= (2\pi)^{-3}\sum_{m,m'}\int_0^{2\pi}\mathrm{d}\theta\int_{R^2}\mathrm{d}^2\bar{\mathbf{x}}_\perp\int_{R^2}\mathrm{d}^2\mathbf{k}_\perp\int_{R^2}\mathrm{d}^2\mathbf{k}'_\perp\; e^{-i(\theta m+\bar{\mathbf{x}}_\perp\cdot\mathbf{k}_\perp)}\times \\
&\quad\left[-i\bar{\rho}\int_{R^2}\frac{\mathrm{d}^2\mathbf{q}_\perp}{2\pi}\left\{G_f(\mathbf{q}_\perp,\bar{z},\bar{z_1})e^{-i\bar{\mathbf{x}}_\perp\cdot\mathbf{q}_\perp}e^{i\theta}-h.c.\right\}\right]\; e^{+i(\theta m'+\bar{\mathbf{x}}_\perp\cdot\mathbf{k}_\perp)}\mathbf{c}_m^\dagger(\mathbf{k}_\perp)\mathbf{c}_{m'}(\mathbf{k}'_\perp) \\
&= -i\bar{\rho}(2\pi)^{-3}\sum_{m,m'}\int_0^{2\pi}\mathrm{d}\theta\int_{R^2}\mathrm{d}^2\bar{\mathbf{x}}_\perp\int_{R^2}\mathrm{d}^2\mathbf{k}_\perp\int_{R^2}\mathrm{d}^2\mathbf{k}'_\perp\int_{R^2}\frac{\mathrm{d}^2\mathbf{q}_\perp}{2\pi}\;\mathbf{c}_m^\dagger(\mathbf{k}_\perp)\mathbf{c}_{m'}(\mathbf{k}'_\perp) \\
&\quad\left\{G_f(\mathbf{q}_\perp,\bar{z},\bar{z_1})e^{-i\theta(m-m'-1)}e^{-i\bar{\mathbf{x}}_\perp(\mathbf{k}_\perp-\mathbf{k}'_\perp+\mathbf{q}_\perp)}-G_f^*(\mathbf{q}_\perp,\bar{z},\bar{z_1})e^{-i\theta(m-m'+1)}e^{-i\bar{\mathbf{x}}_\perp(\mathbf{k}_\perp-\mathbf{k}'_\perp-\mathbf{q}_\perp)}\right\}
\end{aligned}$$

Similarly to Eqs.(B.23)-(B.24) we integrate on $\mathbf{k}'_\perp$ and sum on m' using the Dirac and Kronecker Delta functions obtaining:

$$\begin{aligned}
\mathbf{H}_3 &= -i\bar{\rho}\sum_m\int\mathrm{d}^2\mathbf{k}_\perp\int_{R^2}\frac{\mathrm{d}^2\mathbf{q}_\perp}{2\pi}\left\{G_f(\mathbf{q}_\perp,\bar{z},\bar{z_1})\mathbf{c}_m^\dagger(\mathbf{k}_\perp)\mathbf{c}_{m-1}(\mathbf{k}_\perp+\mathbf{q}_\perp)-\right. \\
&\qquad\left. G_f^*(\mathbf{q}_\perp,\bar{z},\bar{z_1})\mathbf{c}_m^\dagger(\mathbf{k}_\perp)\mathbf{c}_{m+1}(\mathbf{k}_\perp-\mathbf{q}_\perp)\right\} \quad \text{(B.25)}
\end{aligned}$$

Appendix C

3D Wigner evolution equation

We start from the One Particle Wigner Function (1PW) defined in terms of the creation and annihilation operators [45] as was been obtained in chapter 5 Eq.(5.37), considering angular variables in longitudinal direction and canonical variables in transverse directions [41]

$$W_n(\theta,\bar{\mathbf{x}}_\perp,\mathbf{p}_\perp,\bar{z},\bar{z_1}) = \frac{1}{\pi^3}\int_{-\frac{\pi}{2}}^{+\frac{\pi}{2}} d\theta' \int_{R^2} \mathrm{d}^2\bar{\mathbf{x}}'_\perp \; e^{-i2(\bar{\mathbf{x}}'_\perp\cdot\mathbf{p}_\perp+\theta' n)} \times \quad \text{(C.1)}$$
$$\mathrm{Tr}\left\{\varrho\; \mathbf{\Psi}^\dagger(\theta-\theta',\bar{\mathbf{x}}_\perp-\bar{\mathbf{x}}'_\perp)\Psi(\theta+\theta',\bar{\mathbf{x}}_\perp+\bar{\mathbf{x}}'_\perp)\right\}$$

where $\varrho=\varrho(\bar{z},\bar{z_1})$. Using the Fock space representations of the Schroedinger field operator of Eq. (B.12) the Eq.(C.2) becomes:

$$W_n(\theta,\bar{\mathbf{x}}_\perp,\mathbf{p}_\perp) = \frac{1}{(2\pi^2)^3}\sum_{m,m'}\int_{R^2}\mathrm{d}^2\bar{\mathbf{x}}_\perp\int_{R^2}\mathrm{d}^2\mathbf{k}_\perp\int_{R^2}\mathrm{d}^2\mathbf{k}'_\perp\; e^{-i\mathbf{x}'_\perp\cdot(2\mathbf{p}_\perp-\mathbf{k}_\perp-\mathbf{k}'_\perp)}\times \quad \text{(C.2)}$$
$$\int_{\frac{\pi}{2}}^{-\frac{\pi}{2}} d\theta'\; e^{-i\theta'(2n-m-m')}e^{i\mathbf{x}'_\perp\cdot(\mathbf{k}_\perp-\mathbf{k}'_\perp)}\; e^{i\theta(m-m')}\;\mathrm{Tr}\left\{\varrho\;\mathbf{c}^\dagger_m(\mathbf{k}_\perp)\mathbf{c}_m(\mathbf{k}'_\perp)\right\}.$$

Considering the following formula where $\mathrm{sinc}(x)=\sin(x)/x$

$$\frac{1}{\pi}\int_{\frac{\pi}{2}}^{-\frac{\pi}{2}} d\theta'\; e^{-i\theta'\xi}=\mathrm{sinc}\left(\xi\frac{\pi}{2}\right)=\begin{cases}1 & \text{if } \xi=0\\ 0 & \text{if } \xi=2k\\ \dfrac{(-1)^k}{2k+1}\dfrac{\pi}{2} & \text{if } \xi=2k+1\end{cases} \quad \text{(C.3)}$$

and Using the Dirac Delta function in Eq.(B.17) we obtain:

$$W_n(\theta,\bar{\mathbf{x}}_\perp,\mathbf{p}_\perp) = \frac{1}{2\pi^3}\sum_{m,m'}\int_{R^2}\mathrm{d}^2\mathbf{k}_\perp \mathrm{sinc}[(2n-m-m')\pi/2]\; e^{-i2\bar{\mathbf{x}}_\perp\cdot(\mathbf{p}_\perp-\mathbf{k}_\perp)}e^{-i\theta(m-m')}\times$$

$$\mathrm{Tr}\left\{\varrho\ \mathbf{c}_m^\dagger(\mathbf{k}_\perp)\mathbf{c}_{m'}(2\mathbf{p}_\perp-\mathbf{k}'_\perp)\right\} \tag{C.4}$$

Let consider two different cases $m+m'=2l,\quad m-m'=2l'$ and $m+m'=2l+1,\quad m-m'=2l'+1$ with $l,l'\in Z$, moreover we introduce a new momentum variable $\mathbf{k}'_\perp=\mathbf{k}_\perp-\mathbf{p}_\perp$. Therefore, using Eq.(C.3) and neglecting the prime the Eq. (C.4) can be written as:

$$\begin{aligned} W_n(\theta,\bar{\mathbf{x}}_\perp,\mathbf{p}_\perp) &= \frac{1}{2}\sum_{\mu=0,1}\sum_m \mathrm{sinc}[(n-m-\mu/2)\pi]w_{m+\mu/2}(\theta,\bar{\mathbf{x}}_\perp,\mathbf{p}_\perp) \\ w_{m+\mu/2}(\theta,\bar{\mathbf{x}}_\perp,\mathbf{p}_\perp) &= \frac{1}{\pi^3}\sum_{m'\in Z}\int_{R^2}\mathrm{d}^2\mathbf{k}_\perp\ e^{-i2\theta(m'+\mu/2)}e^{-i2\bar{\mathbf{x}}_\perp\cdot\mathbf{k}_\perp}\times \\ &\quad \mathrm{Tr}\left\{\varrho\ \mathbf{c}^\dagger_{m+m'+\mu}(\mathbf{p}_\perp+\mathbf{k}_\perp)\mathbf{c}_{m-m'}(\mathbf{p}_\perp-\mathbf{k}_\perp)\right\} \end{aligned} \tag{C.5}$$

The evolution equation of the discrete 1PW W_n is related to the evolution equations of the two discrete functions w_m and $w_{m+1/2}$ (1pw).

$$\partial_z W_n = \frac{1}{2}\sum_{\mu=0,1}\sum_m \mathrm{sinc}[(n-m-\mu/2)\pi]\partial_z w_{m+\mu/2} \tag{C.6}$$

Moreover the evolution equations for the 1pw are related to the evolution equation for the density operator ϱ which contain all the time dependence

$$\partial_{\bar{z}}\varrho = i\left[\varrho,\ \mathbf{H}\right]. \tag{C.7}$$

Therefore the evolution equations for the 1pw can be written as:

$$\begin{aligned} \frac{\partial}{\partial\bar{z}}w_{m+\mu/2}(\theta,\bar{\mathbf{x}}_\perp,\mathbf{p}_\perp;\bar{z}) &= \frac{i}{\pi^3}\sum_{m'}e^{-i2\theta(m'+\mu/2)}\int_{R^2}\mathrm{d}^2\mathbf{k}_\perp e^{-i2\bar{\mathbf{x}}_\perp\cdot\mathbf{k}_\perp}\times \\ &\quad \mathrm{Tr}\ \left\{\varrho(\bar{z})\left[\mathbf{H},\ \mathbf{c}^\dagger_{m+m'+\mu}(\mathbf{p}_\perp+\mathbf{k}_\perp)\mathbf{c}_{m-m'}(\mathbf{p}_\perp-\mathbf{k}_\perp)\right]\right\} \end{aligned} \tag{C.8}$$

where we have used the cyclical of the trace

$$\mathrm{Tr}\ \left\{[\mathbf{H},\varrho(\bar{z})]\ \mathbf{X}\right\} = \mathrm{Tr}\ \left\{\varrho(\bar{z})\left[\mathbf{H},\mathbf{X}\right]\right\}. \tag{C.9}$$

in order to extract the time dependence from the commutator. Using the Hamiltonian in (B.18) and the evolution equation for the density operator in (C.7) the Eq.(C.8) can be written as:

$$\partial_z w_{m+\mu/2} = \Sigma_1+\Sigma_2+\Sigma_3 \tag{C.10}$$

where

$$\Sigma_i = \frac{i}{\pi^3}\sum_{m'} e^{-i2\theta(m'+\mu/2)}\int_{R^2} \mathrm{d}^2\mathbf{k}_\perp e^{-i2\bar{\mathbf{x}}_\perp\cdot\mathbf{k}_\perp}\times \quad (C.11)$$
$$\mathrm{Tr}\left\{\varrho(\bar{z})\left[\mathbf{H}_i,\ \mathbf{c}^\dagger_{m+m'+\mu}(\mathbf{p}_\perp+\mathbf{k}_\perp)\mathbf{c}_{m-m'}(\mathbf{p}_\perp-\mathbf{k}_\perp)\right]\right\}$$

Before calculate the three contributions Σ_i for the evolution equation (C.10) we remark that in the 1PW formalism the commutator between the FEL Hamiltonian and the creator and annihilator operators appearing in Eq. (C.12) gives the same result using both fermions and bosons, since it is independent on the QCR choice (B.16). In fact, using the following formulae:

$$[ab,c]_- = a\,[b,c]_- - [c,a]_-\,b = a\,[b,c]_+ - [c,a]_+\,b \quad (C.12)$$

and defining $\mathbf{c}_i \equiv \mathbf{c}_{m_i}(\mathbf{k}_{\perp i})$ and $\Delta_{(i,j)} \equiv \delta_{m_i,m_j}\delta(\mathbf{k}_{\perp i},\mathbf{k}_{\perp j})$ with $m \in Z$ and $\mathbf{k}_\perp \in R^2$ we obtain:

$$\left[\mathbf{c}_1^\dagger\mathbf{c}_2,\mathbf{c}_3^\dagger\mathbf{c}_4\right] = \left\{\mathbf{c}_1^\dagger\left[\mathbf{c}_2,\mathbf{c}_3^\dagger\right]_\pm\mathbf{c}_4 - \mathbf{c}_3^\dagger\left[\mathbf{c}_4,\mathbf{c}_1^\dagger\right]_\pm\mathbf{c}_2\right\} = \left\{\mathbf{c}_1^\dagger\mathbf{c}_4\Delta_{(2,3)} - \mathbf{c}_3^\dagger\mathbf{c}_2\Delta_{(4,1)}\right\} \quad (C.13)$$

where in the last equality of Eq.(C.13) we have used the QCR (B.16). Note that the commutator from Hamiltonian and the creator and annihilator operators is (for the 1PW) always of the form $\left[\mathbf{c}_1^\dagger\mathbf{c}_2,\mathbf{c}_3^\dagger\mathbf{c}_4\right]$ which is manifestly invariant with respect to the QCR choice, as shown in Eq.(C.13). Here in after we assume a bosons QCR ($[\ldots]_- \to [\ldots]$).

Let calculate the first term of Eq.(C.10) using the explicit expression of the second quantized Hamiltonian in Eq. (B.23)

$$\begin{aligned}
\Sigma_1 &= \frac{i}{\pi^3}\sum_{m'}\int_{R^2}\mathrm{d}^2\mathbf{k}_\perp\ e^{-i2\theta(m'+\mu/2)}e^{-i2\bar{\mathbf{x}}_\perp\cdot\mathbf{k}_\perp}\ \mathrm{Tr}\left\{\varrho\left[\mathbf{H}_1,\mathbf{c}^\dagger_{m+m'+\mu}(\mathbf{p}_\perp+\mathbf{k}_\perp)\mathbf{c}_{m-m'}(\mathbf{p}_\perp-\mathbf{k}_\perp)\right]\right\}\\
&= -\frac{i}{\pi^3}\sum_{m',m''}\int_{R^2}\mathrm{d}^2\mathbf{k}_\perp\int_{R^2}\mathrm{d}^2\mathbf{k}'_\perp\ e^{-i2\theta(m'+\mu/2)}e^{-i2\bar{\mathbf{x}}_\perp\cdot\mathbf{k}_\perp}h_1(m'',\mathbf{k}'_\perp,a_i)\times\\
&\quad \mathrm{Tr}\left\{\varrho\left[\mathbf{c}^\dagger_{m''}(\mathbf{k}'_\perp)\mathbf{c}_{m''}(\mathbf{k}'_\perp),\mathbf{c}^\dagger_{m+m'+\mu}(\mathbf{p}_\perp+\mathbf{k}_\perp)\mathbf{c}_{m-m'}(\mathbf{p}_\perp-\mathbf{k}_\perp)\right]\right\}\\
&= \frac{i}{\pi^3}\sum_{m',m''}\int_{R^2}\mathrm{d}^2\mathbf{k}_\perp\int_{R^2}\mathrm{d}^2\mathbf{k}'_\perp\ e^{-i2\theta(m'+\mu/2)}e^{-i2\bar{\mathbf{x}}_\perp\cdot\mathbf{k}_\perp}h_1(m'',\mathbf{k}'_\perp,a_i)\times\\
&\quad \mathrm{Tr}\left\{\varrho\left\{\mathbf{c}^\dagger_{m''}(\mathbf{k}'_\perp)\left[\mathbf{c}_{m''}(\mathbf{k}'_\perp),\mathbf{c}^\dagger_{m+m'+\mu}(\mathbf{p}_\perp+\mathbf{k}_\perp)\right]\mathbf{c}_{m-m'}(\mathbf{p}_\perp-\mathbf{k}_\perp)+\right.\right.\\
&\quad \left.\left.\mathbf{c}^\dagger_{m+m'+\mu}(\mathbf{p}_\perp+\mathbf{k}_\perp)\left[\mathbf{c}^\dagger_{m''}(\mathbf{k}'_\perp),\mathbf{c}_{m-m'}(\mathbf{p}_\perp-\mathbf{k}_\perp)\right]\mathbf{c}_{m''}(\mathbf{k}'_\perp)\right\}\right\}
\end{aligned}$$

$$
\begin{aligned}
&= \frac{i}{\pi^3}\sum_{m',m''}\int_{R^2}\mathrm{d}^2\mathbf{k}_\perp\int_{R^2}\mathrm{d}^2\mathbf{k}_\perp{}'\; e^{-i2\theta(m'+\mu/2)}e^{-i2\bar{\mathbf{x}}_\perp\cdot\mathbf{k}_\perp}h_1(m'',\mathbf{k}'_\perp,a_i)\times\\
&\quad \mathrm{Tr}\left\{\varrho\left\{\mathbf{c}^\dagger_{m''}(\mathbf{k}'_\perp)\mathbf{c}_{m-m'}(\mathbf{p}_\perp-\mathbf{k}_\perp)\delta_{(m'',m+m'+\mu)}\delta(\mathbf{k}'_\perp,\mathbf{p}_\perp+\mathbf{k}_\perp)\;-\right.\right.\\
&\quad \left.\left.\mathbf{c}^\dagger_{m+m'+\mu}(\mathbf{p}_\perp+\mathbf{k}_\perp)\mathbf{c}_{m''}(\mathbf{k}'_\perp)\delta_{(m'',m-m')}\delta(\mathbf{k}'_\perp,\mathbf{p}_\perp-\mathbf{k}_\perp)\right\}\right\}
\end{aligned}
$$

where we have used the QCR in Eq.(B.16) and the Dirac and Kronecker Delta functions as defined in Eq.(B.17). Integrating on $\mathbf{k}'_\perp$ and summing on m'' we obtain:

$$
\begin{aligned}
\Sigma_1 &= \frac{i}{\pi^3}\sum_{m'}\int_{R^2}\mathrm{d}^2\mathbf{k}_\perp\; e^{-i2\theta(m'+\mu/2)}e^{-i2\bar{\mathbf{x}}_\perp\cdot\mathbf{k}_\perp}\times\\
&\quad \{h_1(m+m'+\mu,\mathbf{p}_\perp+\mathbf{k}_\perp,a_i)-h_1(m-m',\mathbf{p}_\perp-\mathbf{k}_\perp,a_i)\}\\
&\quad \mathrm{Tr}\left\{\varrho\;\mathbf{c}^\dagger_{m+m'+\mu}(\mathbf{p}_\perp+\mathbf{k}_\perp)\mathbf{c}_{m-m'}(\mathbf{p}_\perp-\mathbf{k}_\perp)\right\}. \qquad \text{(C.14)}
\end{aligned}
$$

Let calculate the second term of Eq.(C.10) using the explicit expression of the second quantized Hamiltonian in Eq. (B.24)

$$
\begin{aligned}
\Sigma_2 &= \frac{i}{\pi^3}\sum_{m'}\int_{R^2}\mathrm{d}^2\mathbf{k}_\perp\; e^{-i2\theta(m'+\mu/2)}e^{-i2\bar{\mathbf{x}}_\perp\cdot\mathbf{k}_\perp}\left\{\mathrm{Tr}\;\varrho\left[\mathbf{H}_2,\mathbf{c}^\dagger_{m+m'+\mu}(\mathbf{p}_\perp+\mathbf{k}_\perp)\mathbf{c}_{m-m'}(\mathbf{p}_\perp-\mathbf{k}_\perp)\right]\right\}\\
&= \frac{i}{\pi^3}\sum_{m',m''}\int_{R^2}\mathrm{d}^2\mathbf{k}_\perp\int_{R^2}\mathrm{d}^2\mathbf{k}_\perp{}'\; e^{-i2\theta(m'+\mu/2)}e^{-i2\bar{\mathbf{x}}_\perp\cdot\mathbf{k}_\perp}\int_{R^2}\frac{\mathrm{d}^2\mathbf{q}_\perp}{2\pi}g_f(\bar{z},\mathbf{q}_\perp)h_2(m'',a_i)\times\\
&\quad \mathrm{Tr}\left\{\varrho\;\left[\mathbf{c}^\dagger_{m''}(\mathbf{k}'_\perp)\mathbf{c}_{m''}(\mathbf{k}'_\perp+\mathbf{q}_\perp),\mathbf{c}^\dagger_{m+m'+\mu}(\mathbf{p}_\perp+\mathbf{k}_\perp)\mathbf{c}_{m-m'}(\mathbf{p}_\perp-\mathbf{k}_\perp)\right]\right\}\\
&= \frac{i}{\pi^3}\sum_{m',m''}\int_{R^2}\mathrm{d}^2\mathbf{k}_\perp\int_{R^2}\mathrm{d}^2\mathbf{k}_\perp{}'\; e^{-i2\theta(m'+\mu/2)}e^{-i2\bar{\mathbf{x}}_\perp\cdot\mathbf{k}_\perp}\int_{R^2}\frac{\mathrm{d}^2\mathbf{q}_\perp}{2\pi}g_f(\bar{z},\mathbf{q}_\perp)h_2(m'',a_i)\times\\
&\quad \mathrm{Tr}\left\{\varrho\;\left\{\mathbf{c}^\dagger_{m''}(\mathbf{k}'_\perp)\left[\mathbf{c}_{m''}(\mathbf{k}'_\perp+\mathbf{q}_\perp),\mathbf{c}^\dagger_{m+m'+\mu}(\mathbf{p}_\perp+\mathbf{k}_\perp)\right]\mathbf{c}_{m-m'}(\mathbf{p}_\perp-\mathbf{k}_\perp)\;+\right.\right.\\
&\quad \left.\left.\mathbf{c}^\dagger_{m+m'+\mu}(\mathbf{p}_\perp+\mathbf{k}_\perp)\left[\mathbf{c}^\dagger_{m''}(\mathbf{k}'_\perp),\mathbf{c}_{m-m'}(\mathbf{p}_\perp-\mathbf{k}_\perp)\right]\mathbf{c}_{m''}(\mathbf{k}'_\perp+\mathbf{q}_\perp)\right\}\right\}\\
&= \frac{i}{\pi^3}\sum_{m',m''}\int_{R^2}\mathrm{d}^2\mathbf{k}_\perp\int_{R^2}\mathrm{d}^2\mathbf{k}_\perp{}'\; e^{-i2\theta(m'+\mu/2)}e^{-i2\bar{\mathbf{x}}_\perp\cdot\mathbf{k}_\perp}\;\int_{R^2}\frac{\mathrm{d}^2\mathbf{q}_\perp}{2\pi}g_f(\bar{z},\mathbf{q}_\perp)h_2(m'',a_i)\\
&\quad \mathrm{Tr}\left\{\varrho\;\left\{\mathbf{c}^\dagger_{m''}(\mathbf{k}'_\perp)\mathbf{c}_{m-m'}(\mathbf{p}_\perp-\mathbf{k}_\perp)\delta_{(m'',m+m'+\mu)}\delta(\mathbf{k}'_\perp+\mathbf{q}_\perp,\mathbf{p}_\perp+\mathbf{k}_\perp)\;-\right.\right.\\
&\quad \left.\left.\mathbf{c}^\dagger_{m+m'+\mu}(\mathbf{p}_\perp+\mathbf{k}_\perp)\mathbf{c}_{m''}(\mathbf{k}'_\perp+\mathbf{q}_\perp)\delta_{(m'',m-m')}\delta(\mathbf{k}'_\perp,\mathbf{p}_\perp-\mathbf{k}_\perp)\right\}\right\}
\end{aligned}
$$

where, again, we have used the QCR in Eq.(B.16) and the Dirac and Kronecker Delta functions as defined in Eq.(B.17). Integrating on $\mathbf{k}'_\perp$ and summing on m'' we

obtain:

$$\begin{aligned}\Sigma_2 &= \frac{i}{\pi^3}\sum_{m'}\int_{R^2}\mathrm{d}^2\mathbf{k}_\perp\, e^{-i2\theta(m'+\mu/2)}e^{-i2\bar{\mathbf{x}}_\perp\cdot\mathbf{k}_\perp}\\ &\quad \mathrm{Tr}\Big\{\varrho h_2(m+m'+\mu,a_i)\mathbf{c}^\dagger_{m+m'+\mu}(\mathbf{p}_\perp+\mathbf{k}_\perp-\mathbf{q}_\perp)\mathbf{c}_{m-m'}(\mathbf{p}_\perp-\mathbf{k}_\perp)-\\ &\quad h_2(m-m',a_i)\mathbf{c}^\dagger_{m+m'+\mu}(\mathbf{p}_\perp+\mathbf{k}_\perp)\mathbf{c}_{m-m'}(\mathbf{p}_\perp-\mathbf{k}_\perp+\mathbf{q}_\perp)\Big\} \qquad \text{(C.15)}\end{aligned}$$

Let calculate the third term of Eq.(C.10) using the explicit expression of the second quantized Hamiltonian in Eq. (B.25)

$$\begin{aligned}\Sigma_3 &= \frac{i}{\pi^3}\sum_{m'}\int_{R^2}\mathrm{d}^2\mathbf{k}_\perp\, e^{-i2\theta(m'+\mu/2)}e^{-i2\bar{\mathbf{x}}_\perp\cdot\mathbf{k}_\perp}\,\mathrm{Tr}\Big\{\varrho\Big[\mathbf{H}_3,\mathbf{c}^\dagger_{m+m'+\mu}(\mathbf{p}_\perp+\mathbf{k}_\perp)\mathbf{c}_{m-m'}(\mathbf{p}_\perp-\mathbf{k}_\perp)\Big]\Big\}\\
&= \frac{\bar\rho}{\pi^3}\sum_{m',m''}\int_{R^2}\mathrm{d}^2\mathbf{k}_\perp\int_{R^2}\mathrm{d}^2\mathbf{k}_\perp{}'\, e^{-i2\theta(m'+\mu/2)}e^{-i2\bar{\mathbf{x}}_\perp\cdot\mathbf{k}_\perp}\,\mathrm{Tr}\Big\{\varrho\times\\
&\quad \int_{R^2}\frac{\mathrm{d}^2\mathbf{q}_\perp}{2\pi}G_f(\bar z,\bar z_1,\mathbf{q}_\perp)\Big[\mathbf{c}^\dagger_{m''}(\mathbf{k}'_\perp)\mathbf{c}_{m''-1}(\mathbf{k}'_\perp+\mathbf{q}_\perp),\mathbf{c}^\dagger_{m+m'+\mu}(\mathbf{p}_\perp+\mathbf{k}_\perp)\mathbf{c}_{m-m'}(\mathbf{p}_\perp-\mathbf{k}_\perp)\Big]-\\
&\quad \int_{R^2}\frac{\mathrm{d}^2\mathbf{q}_\perp}{2\pi}G^*_f(\bar z,\bar z_1,\mathbf{q}_\perp)\Big[\mathbf{c}^\dagger_{m''}(\mathbf{k}'_\perp)\mathbf{c}_{m''+1}(\mathbf{k}'_\perp-\mathbf{q}_\perp),\mathbf{c}^\dagger_{m+m'+\mu}(\mathbf{p}_\perp+\mathbf{k}_\perp)\mathbf{c}_{m-m'}(\mathbf{p}_\perp-\mathbf{k}_\perp)\Big]\Big\}\\
&= \frac{\bar\rho}{\pi^3}\sum_{m',m''}\int_{R^2}\mathrm{d}^2\mathbf{k}_\perp\int_{R^2}\mathrm{d}^2\mathbf{k}_\perp{}'\, e^{-i2\theta(m'+\mu/2)}e^{-i2\bar{\mathbf{x}}_\perp\cdot\mathbf{k}_\perp}\,\mathrm{Tr}\Big\{\varrho\times\\
&\quad \int_{R^2}\frac{\mathrm{d}^2\mathbf{q}_\perp}{2\pi}G_f(\bar z,\bar z_1,\mathbf{q}_\perp)\times\\
&\quad \Big\{\mathbf{c}^\dagger_{m''}(\mathbf{k}'_\perp)\Big[\mathbf{c}_{m''-1}(\mathbf{k}'_\perp+\mathbf{q}_\perp),\mathbf{c}^\dagger_{m+m'+\mu}(\mathbf{p}_\perp+\mathbf{k}_\perp)\Big]\mathbf{c}_{m-m'}(\mathbf{p}_\perp-\mathbf{k}_\perp)+\\
&\quad \mathbf{c}^\dagger_{m+m'+\mu}(\mathbf{p}_\perp+\mathbf{k}_\perp)\Big[\mathbf{c}^\dagger_{m''}(\mathbf{k}'_\perp),\mathbf{c}_{m-m'}(\mathbf{p}_\perp-\mathbf{k}_\perp)\Big]\mathbf{c}_{m''-1}(\mathbf{k}'_\perp+\mathbf{q}_\perp)\Big\}-\\
&\quad \int_{R^2}\frac{\mathrm{d}^2\mathbf{q}_\perp}{2\pi}G^*_f(\bar z,\bar z_1,\mathbf{q}_\perp)\times\\
&\quad \Big\{\mathbf{c}^\dagger_{m''}(\mathbf{k}'_\perp)\Big[\mathbf{c}_{m''+1}(\mathbf{k}'_\perp-\mathbf{q}_\perp),\mathbf{c}^\dagger_{m+m'+\mu}(\mathbf{p}_\perp+\mathbf{k}_\perp)\Big]\mathbf{c}_{m-m'}(\mathbf{p}_\perp-\mathbf{k}_\perp)+\\
&\quad \mathbf{c}^\dagger_{m+m'+\mu}(\mathbf{p}_\perp+\mathbf{k}_\perp)\Big[\mathbf{c}^\dagger_{m''}(\mathbf{k}'_\perp),\mathbf{c}_{m-m'}(\mathbf{p}_\perp-\mathbf{k}_\perp)\Big]\mathbf{c}_{m''+1}(\mathbf{k}'_\perp-\mathbf{q}_\perp)\Big\}\Big\}\\
&= \frac{\bar\rho}{\pi^3}\sum_{m',m''}\int_{R^2}\mathrm{d}^2\mathbf{k}_\perp\int_{R^2}\mathrm{d}^2\mathbf{k}_\perp{}'\, e^{-i2\theta(m'+\mu/2)}e^{-i2\bar{\mathbf{x}}_\perp\cdot\mathbf{k}_\perp}\,\mathrm{Tr}\Big\{\varrho\times\\
&\quad \Big\{\int_{R^2}\frac{\mathrm{d}^2\mathbf{q}_\perp}{2\pi}G_f(\bar z,\bar z_1,\mathbf{q}_\perp)\times\\
&\quad \Big\{\mathbf{c}^\dagger_{m''}(\mathbf{k}'_\perp)\mathbf{c}_{m-m'}(\mathbf{p}_\perp-\mathbf{k}_\perp)\,\delta_{(m''-1,m+m'+\mu)}\,\delta(\mathbf{k}'_\perp+\mathbf{q}_\perp,\mathbf{p}_\perp+\mathbf{k}_\perp)-\\
&\quad \mathbf{c}^\dagger_{m+m'+\mu}(\mathbf{p}_\perp+\mathbf{k}_\perp)\mathbf{c}_{m''-1}(\mathbf{k}'_\perp+\mathbf{q}_\perp)\,\delta(m'',m-m')\,\delta(\mathbf{k}'_\perp,\mathbf{p}_\perp-\mathbf{k}_\perp)\Big\}-\end{aligned}$$

$$\int_{R^2}\frac{\mathrm{d}^2\mathbf{q}_\perp}{2\pi}G_f^*(\bar{z},\bar{z_1},\mathbf{q}_\perp)\times$$
$$\Big\{\mathbf{c}^\dagger_{m''}(\mathbf{k}'_\perp)\mathbf{c}_{m-m'}(\mathbf{p}_\perp-\mathbf{k}_\perp)\;\delta_{(m''+1,m+m'+\mu)})\;\delta(\mathbf{k}'_\perp-\mathbf{q}_\perp,\mathbf{p}_\perp+\mathbf{k}_\perp)-$$
$$\mathbf{c}^\dagger_{m+m'+\mu}(\mathbf{p}_\perp+\mathbf{k}_\perp)\mathbf{c}_{m''+1}(\mathbf{k}'_\perp-\mathbf{q}_\perp)\;\delta_{(m'',m-m')}\;\delta(\mathbf{k}'_\perp,\mathbf{p}_\perp-\mathbf{k}_\perp)\Big\}\Big\}$$

Integrating on $\mathbf{k}'_\perp$ and summing on m'' we obtain:

$$\begin{aligned}\Sigma_3 &= \frac{\bar{\rho}}{\pi^3}\sum_{m'}\int_{R^2}\mathrm{d}^2\mathbf{k}_\perp\;e^{-i2\theta(m'+\mu/2)}e^{-i2\bar{\mathbf{x}}_\perp\cdot\mathbf{k}_\perp}\;\mathrm{Tr}\Big\{\varrho\times\\
&\int_{R^2}\frac{\mathrm{d}^2\mathbf{q}_\perp}{2\pi}G_f(\bar{z},\bar{z_1},\mathbf{q}_\perp)\times\Big\{\mathbf{c}^\dagger_{m+m'+\mu+1}(\mathbf{p}_\perp+\mathbf{k}_\perp-\mathbf{q}_\perp)\mathbf{c}_{m-m'}(\mathbf{p}_\perp-\mathbf{k}_\perp)-\\
&\qquad\mathbf{c}^\dagger_{m+m'+\mu}(\mathbf{p}_\perp+\mathbf{k}_\perp)\mathbf{c}_{m-m'-1}(\mathbf{p}_\perp-\mathbf{k}_\perp+\mathbf{q}_\perp)\Big\}-\\
&\int_{R^2}\frac{\mathrm{d}^2\mathbf{q}_\perp}{2\pi}G_f^*(\bar{z},\bar{z_1},\mathbf{q}_\perp)\times\Big\{\mathbf{c}^\dagger_{m+m'+\mu-1}(\mathbf{p}_\perp+\mathbf{k}_\perp+\mathbf{q}_\perp)\mathbf{c}_{m-m'}(\mathbf{p}_\perp-\mathbf{k}_\perp)-\\
&\qquad\mathbf{c}^\dagger_{m+m'+\mu}(\mathbf{p}_\perp+\mathbf{k}_\perp)\mathbf{c}_{m-m'+1}(\mathbf{p}_\perp-\mathbf{k}_\perp-\mathbf{q}_\perp)\Big\}\Big\}. \quad \text{(C.16)}\end{aligned}$$

Now we calculate the three terms in Eqs.(C.14),(C.15) and (C.16) in terms of the 1pw in order to obtain a close Wigner evolution equation. Before start we remark same relations which will useful for the following. Using the explicit definition of the 1pw in Eq.(5.38) we obtain:

$$\begin{aligned}\partial_\theta w_{m+\mu/2}(\theta,\mathbf{x}_\perp,\mathbf{p}_\perp) &= \frac{1}{2\pi^3}\sum_{m'}(-i2(m'+\mu/2))\,e^{-i2\theta(m'+\mu/2)}\int_{R^2}\mathrm{d}^2\mathbf{k}_\perp e^{-i2\bar{\mathbf{x}}_\perp\cdot\mathbf{k}_\perp}\times\\
&\mathrm{Tr}\;\Big\{\varrho(\bar{z},\bar{z_1})\;\mathbf{c}^\dagger_{m+m'+\mu}(\mathbf{p}_\perp+\mathbf{k}_\perp)c_{m-m'}(\mathbf{p}_\perp-\mathbf{k}_\perp)\Big\} \quad \text{(C.17)}\end{aligned}$$

then we associate the term $-i2(m'+\mu/2)$ to $\partial_\theta w$. Similarly to Eq.(C.17) we obtain the following rules:

$$-i2(m'+\mu/2)\to\partial_\theta w,\;\;-i2\mathbf{k}_\perp\to\partial_{\bar{\mathbf{x}}_\perp}w,\;\;-4(m'+\mu/2)^2\to\partial^2_\theta w,\;\;-4\mathbf{k}^2_\perp\to\partial^2_{\bar{\mathbf{x}}_\perp}w. \quad \text{(C.18)}$$

Moreover we omit the explicit time and spatial dependences that is not useful for the demonstration; in particular $w_{m+\mu/2}(\theta,\bar{\mathbf{x}}_\perp,\mathbf{p}_\perp,\bar{z},\bar{z_1})\to w_{m+\mu/2}(\mathbf{p}_\perp)$, $g_f(\bar{z},\mathbf{q}_\perp)\to g_f(\mathbf{q}_\perp)$ and $G_f(\bar{z},\bar{z_1},\mathbf{q}_\perp)\to G_f(\mathbf{q}_\perp)$.

DIM Σ_1:

Let start from the term Σ_1 in Eq.(C.14):

$$\Sigma_1 = \frac{1}{\pi^3}\sum_{m'}\int_{R^2}\mathrm{d}^2\mathbf{k}_\perp\;e^{-i2\theta(m'+\mu/2)}e^{-i2\bar{\mathbf{x}}_\perp\cdot\mathbf{k}_\perp}$$

$$i\left\{h_1(m+m'+\mu,\mathbf{p}_\perp+\mathbf{k}_\perp,a_i)-h_1(m-m',\mathbf{p}_\perp-\mathbf{k}_\perp,a_i)\right\}$$
$$\mathrm{Tr}\left\{\varrho\,\mathbf{c}^\dagger_{m+m'+\mu}(\mathbf{p}_\perp+\mathbf{k}_\perp)\mathbf{c}_{m-m'}(\mathbf{p}_\perp-\mathbf{k}_\perp)\right\} \tag{C.19}$$

where $ih_1(m,\mathbf{k}_\perp,a_i)=i\left(a_1m^2+a_2\mathbf{k}_\perp^2+a_3m-a_4m\mathbf{k}_\perp^2\right)$

$$\begin{aligned}
& i\{h_1(m+m'+\mu,\mathbf{p}_\perp+\mathbf{k}_\perp,a_i)-h_1(m-m',\mathbf{p}_\perp-\mathbf{k}_\perp,a_i)\}= \\
+\;& ia_1[(m+m'+\mu)^2-(m-m')^2] \\
+\;& ia_2[(\mathbf{p}_\perp+\mathbf{k}_\perp)^2-(\mathbf{p}_\perp-\mathbf{k}_\perp)^2] \\
+\;& i(a_3+\delta)[(m+m'+\mu)-(m-m')] \\
-\;& ia_4[(m+m'+\mu)(\mathbf{p}_\perp+\mathbf{k}_\perp)^2-(m-m')(\mathbf{p}_\perp-\mathbf{k}_\perp)^2]
\end{aligned} \tag{C.20}$$

Now using the relations in Eq.(C.18), for each single term of Eq.(C.20), we obtain:

- $ia_1[(m+m'+\mu)^2-(m-m')^2]\rightarrow 4ia_1(m+\mu/2)(m'+\mu/2)\rightarrow -2a_1(m+\mu/2)\partial_\theta$
- $ia_2[(\mathbf{p}_\perp+\mathbf{k}_\perp)^2-(\mathbf{p}_\perp-\mathbf{k}_\perp)^2]\rightarrow 4ia_2\mathbf{p}_\perp\mathbf{k}_\perp\rightarrow -2a_2\mathbf{p}_\perp\partial_{\bar{\mathbf{x}}_\perp}$
- $i(a_3+\delta)[(m+m'+\mu)-(m-m')]\rightarrow 2ia_3(m'+\mu/2)\rightarrow -a_3\partial_\theta$
- $-ia_4[(m+m'+\mu)(\mathbf{p}_\perp+\mathbf{k}_\perp)^2-(m-m')(\mathbf{p}_\perp-\mathbf{k}_\perp)^2]=$
  $-ia_4\left\{m[(\mathbf{p}_\perp+\mathbf{k}_\perp)^2-(\mathbf{p}_\perp-\mathbf{k}_\perp)^2]+m'[(\mathbf{p}_\perp+\mathbf{k}_\perp)^2+(\mathbf{p}_\perp-\mathbf{k}_\perp)^2]+\mu[(\mathbf{p}_\perp+\mathbf{k}_\perp)^2]\right\}=$
  $-ia_4\left\{4\mathbf{p}_\perp\mathbf{k}_\perp m+2m'(\mathbf{p}_\perp^2+\mathbf{k}_\perp^2)+\mu(\mathbf{p}_\perp^2+\mathbf{k}_\perp^2)+2\mu\mathbf{p}_\perp\mathbf{k}_\perp\right\}=$
  $-ia_4\left\{4\mathbf{p}_\perp\mathbf{k}_\perp(m+\mu/2)+2\mathbf{p}_\perp^2(m'+\mu/2)+2\mathbf{k}_\perp^2(m'+\mu/2)\right\}=$
  $+a_4\left\{2\mathbf{p}_\perp(m+\mu/2)\partial_{\bar{\mathbf{x}}_\perp}+\mathbf{p}_\perp^2\partial_\theta-\frac{1}{4}\partial_\theta\partial^2_{\bar{\mathbf{x}}_\perp}\right\}$

Using the explicit definition of the parameters $a_1\ldots a_4$ in Eq.(B.22) we can write the evolution equation of the 1pw Σ_1 relative to the first $\mathbf{H}_1$ Hamiltonian:

$$\begin{aligned}
\Sigma_1 \;=\; & -\left\{\left\{\frac{(m+\mu/2)}{\bar\rho}+\left(\delta+\frac{\xi}{2\rho}\right)-\frac{bX}{4}\alpha^2\mathbf{p}_\perp^2\right\}\partial_\theta\right. \\
& \left.-\alpha b\mathbf{p}_\perp\left\{1-\alpha X(m+\mu/2)\right\}\partial_{\bar{\mathbf{x}}_\perp}+\frac{bX}{16}\alpha^2\partial_\theta\partial^2_{\bar{\mathbf{x}}_\perp}\right\}w_{m+\mu/2}(\mathbf{p}_\perp)
\end{aligned} \tag{C.21}$$

DIM Σ_2:

Let start from the term Σ_2 in Eq.(C.15):

$$\Sigma_2 \;=\; \frac{1}{\pi^3}\sum_{m'}\int_{R^2}\mathrm{d}^2\mathbf{k}_\perp\int_{R^2}\frac{\mathrm{d}^2\mathbf{q}_\perp}{2\pi}g_f(\mathbf{q}_\perp)\,e^{-i2\theta(m'+\mu/2)}e^{-i2\bar{\mathbf{x}}_\perp\cdot\mathbf{k}_\perp}\,\mathrm{Tr}\Big\{\varrho\times$$

$$i\Big\{h_2(m+m'+\mu,a_i)\mathbf{c}^\dagger_{m+m'+\mu}(\mathbf{p}_\perp+\mathbf{k}_\perp-\mathbf{q}_\perp)\mathbf{c}_{m-m'}(\mathbf{p}_\perp-\mathbf{k}_\perp)- \\ h_2(m-m',a_i)\mathbf{c}^\dagger_{m+m'+\mu}(\mathbf{p}_\perp+\mathbf{k}_\perp)\mathbf{c}_{m-m'}(\mathbf{p}_\perp-\mathbf{k}_\perp+\mathbf{q}_\perp)\Big\}\Big\} \quad \text{(C.22)}$$

where $ih_2(m,a_i)=ia_5-ia_3m$

Introducing the new variable $\mathbf{k}'_\perp=\mathbf{k}_\perp-\mathbf{q}_\perp/2$ we obtain the following relations:

$$\mathbf{p}_\perp+\mathbf{k}_\perp-\mathbf{q}_\perp\to\mathbf{p}^-_\perp+\mathbf{k}'_\perp\ ,\ \mathbf{p}_\perp-\mathbf{k}_\perp\to\mathbf{p}^-_\perp-\mathbf{k}'_\perp \\ \mathbf{p}_\perp+\mathbf{k}_\perp\to\mathbf{p}^+_\perp+\mathbf{k}'_\perp\ ,\ \mathbf{p}_\perp-\mathbf{k}_\perp+\mathbf{q}_\perp\to\mathbf{p}^+_\perp-\mathbf{k}'_\perp \\ e^{-i2\bar{\mathbf{x}}_\perp\cdot\mathbf{k}_\perp}\to e^{-i2\bar{\mathbf{x}}_\perp\cdot\mathbf{k}'_\perp}\cdot e^{-i\bar{\mathbf{x}}_\perp\cdot\mathbf{q}_\perp}. \quad \text{(C.23)}$$

where we have defined $\mathbf{p}^\pm_\perp=\mathbf{p}_\perp\pm\mathbf{q}_\perp/2$. Since, neglecting the prime in $\mathbf{k}'_\perp$, we have:

$$\begin{aligned}\Sigma_2 &= \frac{1}{\pi^3}\sum_{m'}\int_{R^2}\mathrm{d}^2\mathbf{k}_\perp\int_{R^2}\frac{\mathrm{d}^2\mathbf{q}_\perp}{2\pi}\,g_f(\mathbf{q}_\perp)\,e^{-i\bar{\mathbf{x}}_\perp\cdot\mathbf{q}_\perp}\,e^{-i2\theta(m'+\mu/2)}e^{-i2\bar{\mathbf{x}}_\perp\cdot\mathbf{k}_\perp}\,\mathrm{Tr}\Big\{\varrho\times \\ &\quad i\Big\{[a_5-a_3(m+m'+\mu)]\mathbf{c}^\dagger_{m+m'+\mu}(\mathbf{p}^-_\perp+\mathbf{k}_\perp)\mathbf{c}_{m-m'}(\mathbf{p}^-_\perp-\mathbf{k}_\perp)- \\ &\quad [a_5+a_3(m-m')]\mathbf{c}^\dagger_{m+m'+\mu}(\mathbf{p}^+_\perp+\mathbf{k}_\perp)\mathbf{c}_{m-m'}(\mathbf{p}^+_\perp-\mathbf{k}_\perp)\Big\}\Big\} \\ &= \frac{1}{\pi^3}\sum_{m'}\int_{R^2}\mathrm{d}^2\mathbf{k}_\perp\int_{R^2}\frac{\mathrm{d}^2\mathbf{q}_\perp}{2\pi}g_f(\mathbf{q}_\perp)e^{-i\bar{\mathbf{x}}_\perp\cdot\mathbf{q}_\perp}\,e^{-i2\theta(m'+\mu/2)}e^{-i2\bar{\mathbf{x}}_\perp\cdot\mathbf{k}_\perp}\,\mathrm{Tr}\Big\{\varrho\times \\ &\quad \Big\{[ia_5-ia_3(m+\mu/2)-ia_3(m'+\mu/2)]\mathbf{c}^\dagger_{m+m'+\mu}(\mathbf{p}^-_\perp+\mathbf{k}_\perp)\mathbf{c}_{m-m'}(\mathbf{p}^-_\perp-\mathbf{k}_\perp)- \\ &\quad [ia_5-ia_3(m+\mu/2)+ia_3(m'+\mu/2)]\mathbf{c}^\dagger_{m+m'+\mu}(\mathbf{p}^+_\perp+\mathbf{k}_\perp)\mathbf{c}_{m-m'}(\mathbf{p}^+_\perp-\mathbf{k}_\perp)\Big\}\Big\} \quad \text{(C.24)}\end{aligned}$$

Since using the relations in Eq.(C.18) and the explicit definitions of the parameters a_5 and a_3 in Eq.(B.22) the evolution equation for the 1pw Σ_2 relative to the Hamiltonian $\mathbf{H}_2$ in Eq.(B.24) can be written as follows

$$\begin{aligned}\Sigma_2 &= i\frac{\xi}{\rho\alpha X}[1-\alpha X(m+\mu/2)]\int_{R^2}\frac{\mathrm{d}^2\mathbf{q}_\perp}{2\pi}g_f(\mathbf{q}_\perp)\,e^{-i\bar{\mathbf{x}}_\perp\cdot\mathbf{q}_\perp}\left\{w_{m+\mu/2}(\mathbf{p}^-_\perp)-w_{m+\mu/2}(\mathbf{p}^+_\perp)\right\} \\ &\quad +\frac{\xi}{4\rho}\int_{R^2}\frac{\mathrm{d}^2\mathbf{q}_\perp}{2\pi}g_f(\mathbf{q}_\perp)\,e^{-i\bar{\mathbf{x}}_\perp\cdot\mathbf{q}_\perp}\left\{\partial_\theta\left[w_{m+\mu/2}(\mathbf{p}^-_\perp)+w_{m+\mu/2}(\mathbf{p}^+_\perp)\right]\right\} \quad \text{(C.25)}\end{aligned}$$

where $\mathbf{p}^\pm_\perp=\mathbf{p}_\perp\pm\mathbf{q}_\perp/2$.

DIM Σ_3

We start from Eq.(C.16) which can be written as follows

$$\Sigma_3 = \Sigma_{3,1}-\Sigma_{3,2}-\Sigma_{3,3}+\Sigma_{3,4} \quad \text{(C.26)}$$

where

$$\begin{aligned}
\Sigma_{3,1} &= \frac{\bar{\rho}}{\pi^3}\sum_{m'}\int_{R^2} \mathrm{d}^2\mathbf{k}_\perp\, e^{-i2\theta(m'+\mu/2)}e^{-i2\bar{\mathbf{x}}_\perp\cdot\mathbf{k}_\perp}\times \\
&\quad \mathrm{Tr}\Big\{\varrho\int_{R^2}\frac{\mathrm{d}^2\mathbf{q}_\perp}{2\pi}G_f(\mathbf{q}_\perp)\,\mathbf{c}^\dagger_{m+m'+\mu+1}(\mathbf{p}_\perp+\mathbf{k}_\perp-\mathbf{q}_\perp)\mathbf{c}_{m-m'}(\mathbf{p}_\perp-\mathbf{k}_\perp)\Big\} \\
\Sigma_{3,2} &= \frac{\bar{\rho}}{\pi^3}\sum_{m'}\int_{R^2} \mathrm{d}^2\mathbf{k}_\perp\, e^{-i2\theta(m'+\mu/2)}e^{-i2\bar{\mathbf{x}}_\perp\cdot\mathbf{k}_\perp}\times \\
&\quad \mathrm{Tr}\Big\{\varrho\int_{R^2}\frac{\mathrm{d}^2\mathbf{q}_\perp}{2\pi}G_f(\mathbf{q}_\perp)\,\mathbf{c}^\dagger_{m+m'+\mu}(\mathbf{p}_\perp+\mathbf{k}_\perp)\mathbf{c}_{m-m'-1}(\mathbf{p}_\perp-\mathbf{k}_\perp+\mathbf{q}_\perp)\Big\} \\
\Sigma_{3,3} &= \frac{\bar{\rho}}{\pi^3}\sum_{m'}\int_{R^2} \mathrm{d}^2\mathbf{k}_\perp\, e^{-i2\theta(m'+\mu/2)}e^{-i2\bar{\mathbf{x}}_\perp\cdot\mathbf{k}_\perp}\times \\
&\quad \mathrm{Tr}\Big\{\varrho\int_{R^2}\frac{\mathrm{d}^2\mathbf{q}_\perp}{2\pi}G^*_f(\mathbf{q}_\perp)\,\mathbf{c}^\dagger_{m+m'+\mu-1}(\mathbf{p}_\perp+\mathbf{k}_\perp+\mathbf{q}_\perp)\mathbf{c}_{m-m'}(\mathbf{p}_\perp-\mathbf{k}_\perp)\Big\} \\
\Sigma_{3,4} &= \frac{\bar{\rho}}{\pi^3}\sum_{m'}\int_{R^2} \mathrm{d}^2\mathbf{k}_\perp\, e^{-i2\theta(m'+\mu/2)}e^{-i2\bar{\mathbf{x}}_\perp\cdot\mathbf{k}_\perp}\times \\
&\quad \mathrm{Tr}\Big\{\varrho\int_{R^2}\frac{\mathrm{d}^2\mathbf{q}_\perp}{2\pi}G^*_f(\mathbf{q}_\perp)\,\mathbf{c}^\dagger_{m+m'+\mu}(\mathbf{p}_\perp+\mathbf{k}_\perp)\mathbf{c}_{m-m'+1}(\mathbf{p}_\perp-\mathbf{k}_\perp-\mathbf{q}_\perp)\Big\}
\end{aligned}$$

For each of the four above mentioned terms we have:

- $\Sigma_{3,1}$:

  Introducing the new variable $\mathbf{k}'_\perp = \mathbf{k}_\perp - \mathbf{q}_\perp/2$ we obtain the following relations:

$$\begin{aligned}
&\mathbf{p}_\perp+\mathbf{k}_\perp-\mathbf{q}_\perp \to \mathbf{p}^-_\perp+\mathbf{k}'_\perp \quad , \quad \mathbf{p}_\perp-\mathbf{k}_\perp \to \mathbf{p}^-_\perp-\mathbf{k}'_\perp, \\
&e^{-i2\bar{\mathbf{x}}_\perp\cdot\mathbf{k}_\perp} \to e^{-i2\bar{\mathbf{x}}_\perp\cdot\mathbf{k}'_\perp}\cdot e^{-i\bar{\mathbf{x}}_\perp\cdot\mathbf{q}_\perp}, \\
&e^{-i2\theta(m'+\mu/2)} \to e^{-i2\theta(m'+\mu^+/2)}\cdot e^{i\theta}.
\end{aligned}$$

  where we have defined $\mathbf{p}^\pm_\perp = \mathbf{p}_\perp \pm \mathbf{q}_\perp/2$ and $\mu^\pm = \mu \pm 1$. Since, neglecting the prime in $\mathbf{k}'_\perp$, we have:

$$\begin{aligned}
\Sigma_{3,1} &= \bar{\rho}\frac{e^{i\theta}}{\pi^3}\sum_{m'}\int_{R^2} \mathrm{d}^2\mathbf{k}_\perp\, e^{-i2\theta(m'+\mu^+/2)}e^{-i2x\mathbf{k}_\perp}\times \\
&\quad \mathrm{Tr}\Big\{\varrho\int_{R^2}\frac{\mathrm{d}^2\mathbf{q}_\perp}{2\pi}G_f(\mathbf{q}_\perp)e^{-i\bar{\mathbf{x}}_\perp\cdot\mathbf{q}_\perp}\,\mathbf{c}^\dagger_{m+m'+\mu^+}(\mathbf{p}^-_\perp+\mathbf{k}_\perp)\mathbf{c}_{m-m'}(\mathbf{p}^-_\perp-\mathbf{k}_\perp)\Big\} \\
&= \bar{\rho}e^{i\theta}\int_{R^2}\frac{\mathrm{d}^2\mathbf{q}_\perp}{2\pi}G_f(\mathbf{q}_\perp)e^{-i\bar{\mathbf{x}}_\perp\cdot\mathbf{q}_\perp}w_{m+\mu^+/2}(\mathbf{p}^-_\perp) \qquad \text{(C.27)}
\end{aligned}$$

- $\Sigma_{3,2}$:

  Introducing the new variables $\mathbf{k}'_\perp = \mathbf{k}_\perp - \mathbf{q}_\perp/2$ and $m'' = m' + 1$ we obtain the following relations:

$$\begin{aligned}
&\mathbf{p}_\perp + \mathbf{k}_\perp \to \mathbf{p}^+_\perp + \mathbf{k}'_\perp \quad , \quad \mathbf{p}_\perp - \mathbf{k}_\perp + \mathbf{q}_\perp \to \mathbf{p}^+_\perp - \mathbf{k}'_\perp \\
&m + m' + \mu \to m + m'' + \mu^- \ , \ m - m' - 1 \to m - m'' \\
&e^{-i2\bar{\mathbf{x}}_\perp \cdot \mathbf{k}_\perp} \longrightarrow e^{-i2\bar{\mathbf{x}}_\perp \cdot \mathbf{k}'_\perp} \cdot e^{-i\bar{\mathbf{x}}_\perp \cdot \mathbf{q}_\perp} \\
&e^{-i2\theta(m'+\mu/2)} \longrightarrow e^{-i2\theta(m''+\mu^-/2)} \cdot e^{i\theta}
\end{aligned}$$

  Since, neglecting the prime in $\mathbf{k}'_\perp$ and in m'', we have:

$$\begin{aligned}
\Sigma_{3,2} &= \bar{\rho}\frac{e^{i\theta}}{\pi^3}\sum_{m'}\int_{R^2} \mathrm{d}^2\mathbf{k}_\perp \, e^{-i2\theta(m'+\mu^-/2)} e^{-i2x\mathbf{k}_\perp} \times \\
&\quad \mathrm{Tr}\Big\{\varrho \int_{R^2} \frac{\mathrm{d}^2\mathbf{q}_\perp}{2\pi} G_f(\mathbf{q}_\perp) e^{-i\bar{\mathbf{x}}_\perp \cdot \mathbf{q}_\perp} \, \mathbf{c}^\dagger_{m+m'+\mu^-}(\mathbf{p}^+_\perp + \mathbf{k}_\perp)\mathbf{c}_{m-m'}(\mathbf{p}^+_\perp - \mathbf{k}_\perp)\Big\} \\
&= \bar{\rho}e^{i\theta}\int_{R^2} \frac{\mathrm{d}^2\mathbf{q}_\perp}{2\pi} G_f(\mathbf{q}_\perp) e^{-i\bar{\mathbf{x}}_\perp \cdot \mathbf{q}_\perp} w_{m+\mu^-/2}(\mathbf{p}^+_\perp) \qquad \text{(C.28)}
\end{aligned}$$

- $\Sigma_{3,3}$:

  Introducing the new variables $\mathbf{k}'_\perp = \mathbf{k}_\perp + \mathbf{q}_\perp/2$ we obtain the following relations:

$$\begin{aligned}
&\mathbf{p}_\perp + \mathbf{k}_\perp + \mathbf{q}_\perp \to \mathbf{p}^+_\perp + \mathbf{k}'_\perp \quad , \quad \mathbf{p}_\perp - \mathbf{k}_\perp \to \mathbf{p}^+_\perp - \mathbf{k}'_\perp, \\
&e^{-i2\bar{\mathbf{x}}_\perp \cdot \mathbf{k}_\perp} \longrightarrow e^{-i2\bar{\mathbf{x}}_\perp \cdot \mathbf{k}'_\perp} \cdot e^{i\bar{\mathbf{x}}_\perp \cdot \mathbf{q}_\perp} \\
&e^{-i2\theta(m'+\mu/2)} \longrightarrow e^{-i2\theta(m'+\mu^-/2)} \cdot e^{-i\theta}
\end{aligned}$$

  Since, neglecting the prime in $\mathbf{k}'_\perp$, we have:

$$\begin{aligned}
\Sigma_{3,3} &= \bar{\rho}\frac{e^{-i\theta}}{\pi^3}\sum_{m'}\int_{R^2} \mathrm{d}^2\mathbf{k}_\perp{}' \, e^{-i2\theta(m'+\mu^-/2)} e^{-i2x\mathbf{k}_\perp} \times \\
&\quad \mathrm{Tr}\Big\{\varrho \int_{R^2} \frac{\mathrm{d}^2\mathbf{q}_\perp}{2\pi} G^*_f(\mathbf{q}_\perp) e^{i\bar{\mathbf{x}}_\perp \cdot \mathbf{q}_\perp} \, \mathbf{c}^\dagger_{m+m'+\mu^-}(\mathbf{p}^+_\perp + \mathbf{k}_\perp)\mathbf{c}_{m-m'}(\mathbf{p}^+_\perp - \mathbf{k}_\perp)\Big\} \\
&= \bar{\rho}e^{-i\theta}\int_{R^2} \frac{\mathrm{d}^2\mathbf{q}_\perp}{2\pi} G^*_f(\mathbf{q}_\perp) e^{i\bar{\mathbf{x}}_\perp \cdot \mathbf{q}_\perp} w_{m+\mu^-/2}(\mathbf{p}^+_\perp) \qquad \text{(C.29)}
\end{aligned}$$

- $\Sigma_{3,4}$:

  Introducing the new variables $\mathbf{k}'_\perp = \mathbf{k}_\perp + \mathbf{q}_\perp/2$ and $m'' = m' - 1$ we obtain the following relations:

$$\begin{aligned}
&\mathbf{p}_\perp + \mathbf{k}_\perp \to \mathbf{p}_\perp^- + \mathbf{k}'_\perp \quad , \quad \mathbf{p}_\perp - \mathbf{k}_\perp - \mathbf{q}_\perp \to \mathbf{p}_\perp^- - \mathbf{k}'_\perp \\
&m + m' + \mu \to m + m'' + \mu^+ \quad , \quad m - m' - 1 \to m - m'' \\
&e^{-i2\bar{\mathbf{x}}_\perp \cdot \mathbf{k}_\perp} \to e^{-i2\bar{\mathbf{x}}_\perp \cdot \mathbf{k}'_\perp} \cdot e^{i\bar{\mathbf{x}}_\perp \cdot \mathbf{q}_\perp} \\
&e^{-i2\theta(m'+\mu/2)} \to e^{-i2\theta(m''+\mu^+/2)} \cdot e^{-i\theta}
\end{aligned}$$

  Since, neglecting the prime in $\mathbf{k}'_\perp$ and in m'', we have:

$$\begin{aligned}
\Sigma_{3,4} \;&= \bar{\rho}\;\; \frac{e^{-i\theta}}{\pi^3} \sum_{m'} \int_{R^2} \mathrm{d}^2\mathbf{k}_\perp \; e^{-i2\theta(m'+\mu^+/2)} e^{-i2x\mathbf{k}_\perp} \times \\
&\qquad \mathrm{Tr}\Big\{ \varrho \int_{R^2} \frac{\mathrm{d}^2\mathbf{q}_\perp}{2\pi} G_f^*(\mathbf{q}_\perp) e^{i\bar{\mathbf{x}}_\perp \cdot \mathbf{q}_\perp} \; \mathbf{c}^\dagger_{m+m'+\mu^+}(\mathbf{p}_\perp^- + \mathbf{k}_\perp) \mathbf{c}_{m-m'}(\mathbf{p}_\perp^- - \mathbf{k}_\perp) \Big\} \\
&= \quad \bar{\rho} e^{-i\theta} \int_{R^2} \frac{\mathrm{d}^2\mathbf{q}_\perp}{2\pi} G_f^*(\mathbf{q}_\perp) e^{i\bar{\mathbf{x}}_\perp \cdot \mathbf{q}_\perp} w_{m+\mu^+/2}(\mathbf{p}_\perp^-) \qquad \text{(C.30)}
\end{aligned}$$

  finally, using Eqs. (C.27),(C.28),(C.29) and (C.30) the Eq. (C.26) becomes:

$$\Sigma_3 \;=\; \bar{\rho} \int_{R^2} \frac{\mathrm{d}^2\mathbf{q}_\perp}{2\pi} \left\{ e^{i\theta} G_f(\mathbf{q}_\perp) e^{-i\bar{\mathbf{x}}_\perp \cdot \mathbf{q}_\perp} + e^{-i\theta} G_f^*(\mathbf{q}_\perp) e^{i\bar{\mathbf{x}}_\perp \cdot \mathbf{q}_\perp} \right\} \left\{ w_{m+\mu^+/2}(\mathbf{p}_\perp^-) - w_{m+\mu^-/2}(\mathbf{p}_\perp^+) \right\} \qquad \text{(C.31)}$$

  Then we can can write the Full 1PW integro-differential evolution equation,

$$\begin{aligned}
&\partial_z w_s(\mathbf{p}_\perp) = \\
&-\left\{ \frac{(m+\mu/2)}{\bar{\rho}} + \left(\delta + \frac{\xi}{2\rho} \right) - \frac{bX}{4} \alpha^2 \mathbf{p}_\perp^2 \right\} \partial_\theta w_s(\mathbf{p}_\perp) \\
&-\alpha b \mathbf{p}_\perp \left\{ 1 - \alpha X(m+\mu/2) \right\} \nabla_{\bar{\mathbf{x}}_\perp} w_s(\mathbf{p}_\perp) + \frac{bX}{16} \alpha^2 \partial_\theta \nabla^2_{\bar{\mathbf{x}}_\perp} w_s(\mathbf{p}_\perp) \\
&+i \frac{\xi}{\rho \alpha X} [1 - \alpha X(m+\mu/2)] \int_{R^2} \frac{\mathrm{d}^2\mathbf{q}_\perp}{2\pi} g_f(\mathbf{q}_\perp) e^{-i\bar{\mathbf{x}}_\perp \cdot \mathbf{q}_\perp} \left\{ w_s(\mathbf{p}_\perp^-) - w_s(\mathbf{p}_\perp^+) \right\} \\
&+\frac{\xi}{4\rho} \int_{R^2} \frac{\mathrm{d}^2\mathbf{q}_\perp}{2\pi} g_f(\mathbf{q}_\perp) e^{-i\bar{\mathbf{x}}_\perp \cdot \mathbf{q}_\perp} \left\{ \partial_\theta \left[w_s(\mathbf{p}_\perp^-) + w_s(\mathbf{p}_\perp^+) \right] \right\} \\
&+\bar{\rho} \int_{R^2} \frac{\mathrm{d}^2\mathbf{q}_\perp}{2\pi} \left\{ G_f(\mathbf{q}_\perp) e^{-i\bar{\mathbf{x}}_\perp \cdot \mathbf{q}_\perp} e^{i\theta} + G_f^*(\mathbf{q}_\perp) e^{i\bar{\mathbf{x}}_\perp \cdot \mathbf{q}_\perp} e^{-i\theta} \right\} \left\{ w_{s^+}(\mathbf{p}_\perp^-) - w_{s^-}(\mathbf{p}_\perp^+) \right\}
\end{aligned} \qquad \text{(C.32)}$$

where $\mathbf{p}_\perp^\pm = \mathbf{p}_\perp \pm \mathbf{q}_\perp/2$, $s = m + \mu/2$ and $s^\pm = s \pm 1/2$.

Classical transverse limit

The integro-differential evolution equation (C.32) describes an electron beam with a transverse normalized emittance till to the "ultra cold" limit of the Compton wavelength $\epsilon_n \geq \lambda\!\!\!^{-}_c$. The numerical solution of the Eq. (C.32) is unworkable, however, as we have anticipate in section (5.2), we are interested in describing an electron beam in which the transverse momentum distribution is thermal, with a width $\Delta x'_{therm} \sim \epsilon_n/(\sigma\gamma_r)$ much larger than the quantum limit $\lambda\!\!\!^{-}_c/(\sigma\gamma_r)$. This fact permit us to simplify our model.

We start expanding the integral in Eq.(5.45) within the following formula's (see Appendix (D)):

$$\begin{aligned}
&\int_{R^2} \frac{\mathrm{d}^2\mathbf{q}_\perp}{2\pi} f(\mathbf{q}_\perp) e^{-i\bar{\mathbf{x}}_\perp\cdot\mathbf{q}_\perp} \left[w_s\left(\mathbf{p}_\perp + \frac{\mathbf{q}_\perp}{2}\right) \pm w_s\left(\mathbf{p}_\perp - \frac{\mathbf{q}_\perp}{2}\right)\right] \\
&= \sum_{n=0}^{+\infty} [(-1)^n] \begin{cases} \left[\dfrac{1}{2^{2n-1}(2n)!}\right] \nabla^{2n}_{\mathbf{p}_\perp} w_s\left(\mathbf{p}_\perp\right) \nabla^{2n}_{\bar{\mathbf{x}}_\perp} f(\bar{\mathbf{x}}_\perp) & (+) \\ \left[\dfrac{i}{2^{2n}(2n+1)!}\right] \nabla^{2n+1}_{\mathbf{p}_\perp} w_s\left(\mathbf{p}_\perp\right) \nabla^{2n+1}_{\bar{\mathbf{x}}_\perp} f(\bar{\mathbf{x}}_\perp) & (-) \end{cases}
\end{aligned}$$

then the Eq.(C.32) becomes:

$$\begin{aligned}
&\partial_z w_s(\mathbf{p}_\perp) = \\
&-\left\{\frac{s}{\bar{\rho}} + \left(\delta + \frac{\xi}{2\rho}\right) - \frac{bX}{4}\alpha^2\mathbf{p}_\perp^2\right\} \partial_\theta w_s(\mathbf{p}_\perp) \\
&-\alpha b\mathbf{p}_\perp \left\{1 - \alpha X\ s\right\} \nabla_{\bar{\mathbf{x}}_\perp} w_s(\mathbf{p}_\perp) + \frac{bX}{16}\alpha^2 \partial_\theta \nabla^2_{\bar{\mathbf{x}}_\perp} w_s(\mathbf{p}_\perp) \\
&+\frac{\xi}{\rho\alpha X}[1 + \alpha X(m + \mu/2)] \sum_{n=0}^{\infty} \frac{(-1)^n}{(2n+1)!2^{2n}} \nabla^{2n+1}_{\mathbf{p}_\perp} w_s(\mathbf{p}_\perp) \nabla^{2n+1}_{\bar{\mathbf{x}}_\perp} |g(\bar{\mathbf{x}}_\perp)|^2 \\
&+\frac{\xi}{4\rho} \sum_{n=0}^{\infty} \frac{(-1)^n}{(2n)!2^{2n-1}} \nabla^{2n}_{\mathbf{p}_\perp} \partial_\theta w_s(\mathbf{p}_\perp) \nabla^{2n}_{\bar{\mathbf{x}}_\perp} |g(\bar{\mathbf{x}}_\perp)|^2 \\
&-\bar{\rho} \sum_{n=0}^{\infty} \frac{i^n}{n!2^n} \nabla^n_{\mathbf{p}_\perp} \left\{w_{s^-}(\bar{\mathbf{p}}_\perp) - (-1)^n w_{s^+}(\bar{\mathbf{p}}_\perp)\right\} \nabla^n_{\bar{\mathbf{x}}_\perp} \left\{F(\bar{\mathbf{x}}_\perp) e^{i\theta} + F^*(\bar{\mathbf{x}}_\perp) e^{-i\theta}\right\}
\end{aligned} \tag{C.33}$$

Now we introduce the "classical" momentum variable (see Eq.(5.19))

$$\bar{\mathbf{p}}_\perp = \alpha \mathbf{p}_\perp = \frac{\sigma}{\epsilon_r}\eta_\perp \tag{C.34}$$

where the parameter $\alpha = \lambda\!\!\!^{-}_c/\epsilon_n$ (see Eq.(5.18)) represent the ratio between the longitudinal and transverse emittance. Since Eqs. (C.33) can be converted into α-power expansion

$$\begin{aligned}
&\partial_z w_s(\bar{\mathbf{p}}_\perp) = \\
&-\left\{\frac{s}{\bar{\rho}} + \left(\delta + \frac{\xi}{2\rho}\right) - \frac{bX}{4}\bar{\mathbf{p}}_\perp^2\right\}\partial_\theta w_s(\bar{\mathbf{p}}_\perp) \\
&-b\bar{\mathbf{p}}_\perp\left\{1 - \alpha X\ s\right\}\nabla_{\bar{\mathbf{x}}_\perp} w_s(\bar{\mathbf{p}}_\perp) + \frac{bX}{16}\alpha^2\partial_\theta\nabla^2_{\bar{\mathbf{x}}_\perp} w_s(\bar{\mathbf{p}}_\perp) \\
&+\frac{\xi}{\rho\alpha X}[1 + \alpha X(m + \mu/2)]\sum_{n=0}^{\infty}\frac{(-1)^n\alpha^{2n+1}}{(2n+1)!2^{2n}}\nabla^{2n+1}_{\bar{\mathbf{p}}_\perp} w_s(\bar{\mathbf{p}}_\perp)\nabla^{2n+1}_{\bar{\mathbf{x}}_\perp}|g(\bar{\mathbf{x}}_\perp)|^2 \\
&+\frac{\xi}{4\rho}\sum_{n=0}^{\infty}\frac{(-1)^n\alpha^{2n}}{(2n)!2^{2n-1}}\nabla^{2n}_{\bar{\mathbf{p}}_\perp}\partial_\theta w_s(\bar{\mathbf{p}}_\perp)\nabla^{2n}_{\bar{\mathbf{x}}_\perp}|g(\bar{\mathbf{x}}_\perp)|^2 \\
&-\bar{\rho}\sum_{n=0}^{\infty}\frac{i^n\alpha^n}{n!2^n}\nabla^n_{\bar{\mathbf{p}}_\perp}\left\{w_{s^-}(\bar{\mathbf{p}}_\perp) - (-1)^n w_{s^+}(\bar{\mathbf{p}}_\perp)\right\}\nabla^n_{\bar{\mathbf{x}}_\perp}\left\{F(\bar{\mathbf{x}}_\perp)e^{i\theta} + F^*(\bar{\mathbf{x}}_\perp)e^{-i\theta}\right\}
\end{aligned} \tag{C.35}$$

The Eq.(C.35) can be written in a more compact way:

$$\partial_z w_s(\bar{\mathbf{p}}_\perp) = \Omega^{(0)} + \alpha\Omega^{(1)} + \alpha^2\Omega^{(2)} + \ldots = \sum_{n=0}^{\infty}\alpha^n\Omega^{(n)} \tag{C.36}$$

where $\Omega_n = \Omega_n(\theta, \bar{\mathbf{x}}_\perp, \bar{\mathbf{p}}_\perp, s)$ and in particular the zero Ω_0, the first Ω_1 and the second order Ω_2 terms of the series expansion are defined as follows ($\delta = 0$ for simplicity):

$$\begin{aligned}
\Omega^{(0)} &= \left\{-\left[\frac{s}{\bar{\rho}} + \frac{\xi}{2\rho}\left(1 - |g(\mathbf{x}_\perp)|^2\right) - \frac{bX}{4}\bar{\mathbf{p}}_\perp^2\right]\partial_\theta - b\bar{\mathbf{p}}_\perp\nabla_{\bar{\mathbf{x}}_\perp} + \frac{\xi}{\rho X}\partial_{\bar{\mathbf{x}}_\perp}|g(\mathbf{x}_\perp)|^2\nabla_{\bar{\mathbf{p}}_\perp}\right\} w_s(\mathbf{p}_\perp) \\
&\quad +\bar{\rho}\left\{w_{s^+}(\bar{\mathbf{p}}_\perp) - w_{s^-}(\bar{\mathbf{p}}_\perp)\right\}\left\{F(\bar{\mathbf{x}}_\perp)e^{i\theta} + F^*(\bar{\mathbf{x}}_\perp)e^{-i\theta}\right\}
\end{aligned} \tag{C.37}$$

$$\begin{aligned}
\Omega^{(1)} &= \left\{+bXs\bar{\mathbf{p}}_\perp\nabla_{\bar{\mathbf{x}}_\perp} + \frac{\xi}{\rho}s\partial_{\bar{\mathbf{x}}_\perp}|g(\mathbf{x}_\perp)|^2\nabla_{\bar{\mathbf{p}}_\perp}\right\} w_s(\bar{\mathbf{p}}_\perp) \\
&\quad -i\frac{\bar{\rho}}{2}\nabla_{\bar{\mathbf{p}}_\perp}\left\{w_{s^+}(\bar{\mathbf{p}}_\perp) + w_{s^-}(\bar{\mathbf{p}}_\perp)\right\}\nabla_{\bar{\mathbf{x}}_\perp}\left\{F(\bar{\mathbf{x}}_\perp)e^{i\theta} + F^*(\bar{\mathbf{x}}_\perp)e^{-i\theta}\right\}
\end{aligned} \tag{C.38}$$

$$\begin{aligned}
\Omega^{(2)} &= \left\{\frac{bX}{16}\alpha^2\partial_\theta\nabla^2_{\bar{\mathbf{x}}_\perp} + \frac{\xi}{16\rho}\nabla^2_{\bar{\mathbf{p}}_\perp}\partial_\theta\nabla^2_{\bar{\mathbf{x}}_\perp}|g(\mathbf{x}_\perp)|^2 - \frac{\xi}{24\rho X}\nabla^3_{\bar{\mathbf{x}}_\perp}|g(\mathbf{x}_\perp)|^2\nabla^3_{\bar{\mathbf{p}}_\perp}\right\} w_s(\bar{\mathbf{p}}_\perp) \\
&\quad +\frac{\bar{\rho}}{8}\nabla^2_{\bar{\mathbf{p}}_\perp}\left\{w_{s^-}(\bar{\mathbf{p}}_\perp) - w_{s^+}(\bar{\mathbf{p}}_\perp)\right\}\nabla^2_{\bar{\mathbf{x}}_\perp}\left\{F(\bar{\mathbf{x}}_\perp)e^{i\theta} + F^*(\bar{\mathbf{x}}_\perp)e^{-i\theta}\right\}
\end{aligned} \tag{C.39}$$

Appendix D

Van Kampen Method

Consider the following expression where w and f are complex functions and $\mathbf{p}$, $\mathbf{q}$ and $\mathbf{x}$ are m-dimensional vectors:

$$\int_{R^m} \frac{\mathrm{d}^m\mathbf{q}}{2\pi}\tilde{f}(\mathbf{q})e^{-i\mathbf{x}\cdot\mathbf{q}}w\left(\mathbf{p}\pm\frac{\mathbf{q}}{2}\right) = \sum_{n=0}\frac{\nabla^n_{\mathbf{p}}w(\mathbf{p})}{n!}\int_{R^m}\frac{\mathrm{d}^m\mathbf{q}}{2\pi}\tilde{f}(\mathbf{q})e^{-i\mathbf{x}\cdot\mathbf{q}}\left(\pm\frac{\mathbf{q}}{2}\right)^n$$
$$= \sum_{n=0}\frac{\nabla^n_{\mathbf{p}}w(\mathbf{p})}{n!}\left(\pm\frac{i}{2}\nabla_{\mathbf{x}}\right)^n = \sum_{n=0}\frac{i^n(\pm)^n}{n!2^n}\nabla^n_{\mathbf{p}}w(\mathbf{p})\nabla_{\mathbf{x}}f(\mathbf{x}) \tag{D.1}$$

Moreover we have:

$$\int_{R^m}\frac{\mathrm{d}^m\mathbf{q}}{2\pi}\tilde{f}(\mathbf{q})e^{-i\mathbf{x}\cdot\mathbf{q}}\left\{w\left(\mathbf{p}_\perp+\frac{\mathbf{q}}{2}\right)\pm w\left(\mathbf{p}-\frac{\mathbf{q}}{2}\right)\right\}$$
$$= \sum_{n=0}\frac{\nabla^n_{\mathbf{p}}w(\mathbf{p})}{n!}\int_{R^m}\frac{\mathrm{d}^m\mathbf{q}}{2\pi}\tilde{f}(\mathbf{q})e^{-i\mathbf{x}\cdot\mathbf{q}}\left\{\left(+\frac{\mathbf{q}}{2}\right)^n\pm\left(-\frac{\mathbf{q}}{2}\right)^n\right\}$$
$$= \sum_{n=0}\frac{\nabla^n_{\mathbf{p}}w(\mathbf{p})}{n!}\left\{\left(+\frac{i}{2}\nabla_{\mathbf{x}}\right)^n\pm\left(-\frac{i}{2}\nabla_{\mathbf{x}}\right)^n\right\}f(\mathbf{x}) \tag{D.2}$$

where $\tilde{f}(\mathbf{q}_\perp)$ is the m-dimensional Fourier transform of $f(\mathbf{x}_\perp)$. The term in the curl parenthesis of Eq.(D.2) can be written as follows:

$$\frac{\left\{\left(+\frac{i}{2}\nabla_{\mathbf{x}}\right)^n+\left(-\frac{i}{2}\nabla_{\mathbf{x}}\right)^n\right\}}{n!} = \frac{i^n}{n!2^n}\nabla^n_{\mathbf{x}}\left\{1+(-1)^n\right\} = \frac{(i)^{2n}}{2^{2n-1}}\nabla^{2n}_{\mathbf{x}} = \frac{(-1)^n}{(2n)!2^{2n-1}}\nabla^{2n}_{\mathbf{x}}.$$
$$\frac{\left\{\left(+\frac{i}{2}\nabla_{\mathbf{x}}\right)^n-\left(-\frac{i}{2}\nabla_{\mathbf{x}}\right)^n\right\}}{n!} = \frac{i^n}{n!2^n}\nabla^n_{\mathbf{x}}\left\{1-(-1)^n\right\} = \frac{i^{2n+1}}{(2n+1)!2^{2n}}\nabla^{2n+1}_{\mathbf{x}} = i\frac{(-1)^n}{(2n+1)!2^{2n}}\nabla^{2n+1}_{\mathbf{x}}.$$

using the above relations Eqs.(D.1) becomes

$$\int_{R^m}\frac{\mathrm{d}^m\mathbf{q}}{2\pi}\tilde{f}(\mathbf{q})e^{-i\mathbf{x}\cdot\mathbf{q}}\left\{w\left(\mathbf{p}+\frac{\mathbf{q}}{2}\right)\pm w\left(\mathbf{p}-\frac{\mathbf{q}}{2}\right)\right\} =$$

$$\begin{cases} \displaystyle\sum_{n=0}^{\infty} \frac{(-1)^n}{(2n)!\ 2^{2n-1}} \nabla_{\mathbf{p}}^{2n} w(\mathbf{p}) \nabla_{\mathbf{x}}^{2n}\ f(\mathbf{x}) & + \\ i \displaystyle\sum_{n=0}^{\infty} \frac{(-1)^n}{(2n+1)!\ 2^{2n}} \nabla_{\mathbf{p}}^{2n+1} w(\mathbf{p}) \nabla_{\mathbf{x}}^{2n+1}\ f(\mathbf{x}) & - \end{cases} \tag{D.4}$$

Appendix E

Flattened laser beams

It results that an FEL with a laser wiggler works better if the transverse profile of the laser beam is approximately uniform ('flat-top') near the plane of the beam waist, $z = z_0$, within a distance of few Rayleigh ranges $Z_L = \pi w_0^2/\lambda_L$ (where $w_0 = 2R$, see [39]). In the 3D Wigner model for QFEL developped in chapter 5 (see also ref. [46]) the laser wiggler profile is described by the complex function $g(\bar{r}, \bar{z})$, where $\bar{r} = r/\sigma$ and $\bar{z} = z/L_g$. In particular, for a $\mathtt{TEM}_{00}$ Gaussian mode it reads:

$$g(\bar{r}, \bar{z}) = \frac{1}{[1 - i(\bar{z} - \bar{z}_0)/\bar{Z}_L]} \exp\left\{ -\frac{\bar{r}^2}{4a_2^2[1 - i(\bar{z} - \bar{z}_0)/\bar{Z}_L]} \right\} \tag{E.1}$$

where $a_2 = R/\sigma$ and $\bar{Z}_L = Z_L/L_g$.

In this appendix we obtain the expression of $g(\bar{r}, \bar{z})$ for two cases of flattened laser beams reported in the literature:

1. The Flattened Gaussian Beams (FGB), proposed by F. Gori [61, 62].

2. The Multiple Gaussian Beam (MGB), proposed by A.Tovar. [63]

We mention also the popular Super-Gaussian (SG) profile [64],

$$g_\gamma(r, 0) = \exp[-(r/w_0)^\gamma] \qquad (\gamma \geq 2) \tag{E.2}$$

which becomes more and more box shaped for increasing γ. However, the evaluation of the free-space propagation of the field with the SG profile cannot be performed in a closed form for $\gamma > 2$, and it must be calculated numerically. On the other hand, the FGB and MGB profiles have a simple propagation law, which yield the

analytical expression for $g(\bar{r}, \bar{z})$ to be included in our numerical code `QFEL3D` [49]. In the following, we describe the FGB and NGB profiles and we study their propagation in free-space, away from the beam waist plane, assumed for simplicity at $z = 0$. We will use physical spatial variables: polar $(\mathbf{r}, z)$ for the FGB and Cartesian $(\mathbf{x}, z)$ for MGB.

FLATTENED GAUSSIAN BEAM (FGB) PROFILE

FGB at the waist position $z = 0$

Let's start from a circularly symmetric Gaussian function $g(r, 0) = \exp[-(r/w_0)^2]$. Its shape can be flattened through multiplication by some suitable correction function. The limiting correction case is done by the function $\exp[(r/w_0)^2]$, which once expanded yields:

$$1 = \exp[-(r/w_0)^2] \cdot \exp[(r/w_0)^2] = \exp[-(r/w_0)^2] \cdot \sum_{n=0}^{\infty} \frac{(r/w_0)^{2n}}{n!}. \tag{E.3}$$

Truncating the sum at $n = N$, we define

$$F_N(r) = \exp[-(r/w_0)^2] \cdot \sum_{n=0}^{N} \frac{(r/w_0)^{2n}}{n!} \qquad N = 0, 1 \ldots. \tag{E.4}$$

For $N = 0$, $F_N(r)$ reduces to the Gaussian function $\exp[-(r/w_0)^2]$ and $\lim_{N\to\infty} F_N(r) = 1$. Therefore we can expected $F_N(r)$ to be near to unity for a certain interval and then go smoothly to zero. $F_N(r)$ for different N is shown in Fig.E.1. In order to approach the step profile $\Theta(w_0 - r)$ (where $\Theta(x) = 1$ for $x > 0$ and 0 for $x < 0$), $F_N(r)$ can be re-scaled changing r into the new variable $\sqrt{N+1}r$. The Flattened Gaussian Beam (FGB) profile of order N at the beam waist $z = 0$ is defined as:

$$g_N(r, 0) = \exp[-(N+1)(r/w_0)^2] \sum_{n=0}^{N} \frac{[\sqrt{N+1}(r/w_0)]^n}{n!}. \tag{E.5}$$

In Fig.E.2 the FGB profile $g_N(r, 0)$ of Eq.(E.5) is compared with the SG profile of Eq.(E.2) vs. r/w_0 for different values of N and γ.

FGB propagation law

The main advantage of using FGB's instead of SG beams consists is that a FGB can be easy rewritten as a superposition of Laguerre-Gaussian beams, whoise prop-

Flattened-Gaussian-Profile

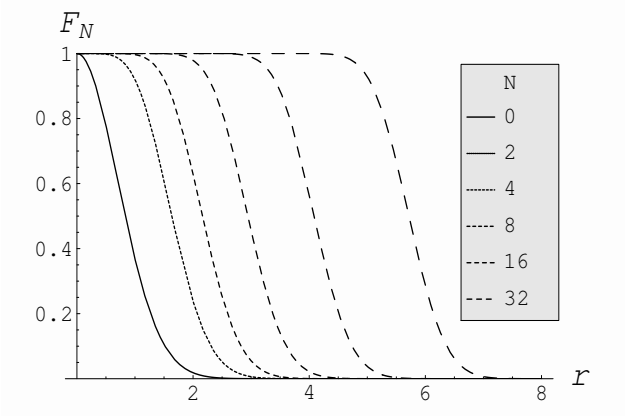

Figure E.1: $F_N(r)$ for different N and $w_0 = 1$

agation characteristics are also well known. In fact, Eq.(E.5) can be written as [61, 62]:

$$g_N(r,0) = \exp[-(N+1)(r/w_0)^2] \sum_{n=0}^{N} c_n^{(N)} L_n \left[\frac{2(N+1)r^2}{w_0^2}\right] \tag{E.6}$$

where L_n is the nth Laguerre polynomial and

$$c_n^{(N)} = (-1)^n \sum_{m=n}^{N} \frac{1}{2^m} \binom{n}{m}. \tag{E.7}$$

The paraxial propagation of a FGB is solved by using the well known propagation formula of Laguerre-Gaussian- beams, which yield

$$g_N(r,z) = \frac{1}{\sqrt{1+(z/Z_N)^2}} \exp\left\{ \left[\frac{i\pi}{\lambda_L R_N(z)} - \frac{1}{w_N^2(z)}\right] r^2 \right\} \sum_{n=0}^{N} c_n^{(N)} L_n \left[\frac{2r^2}{w_N^2(z)}\right] \exp[-i(2n+1)\Phi_N(z)] \tag{E.8}$$

where

$$w_N(z) = w_N(0)\sqrt{1+(z/Z_N)^2}, \tag{E.9}$$

$$\frac{1}{R_N(z)} = \frac{z}{z^2+Z_N^2}, \tag{E.10}$$

$$\Phi_N(z) = \arctan(z/Z_N) \tag{E.11}$$

and

$$Z_N = = \frac{\pi w_N(0)^2}{\lambda_L} \tag{E.12}$$

Super and Flattened Gaussian Profile

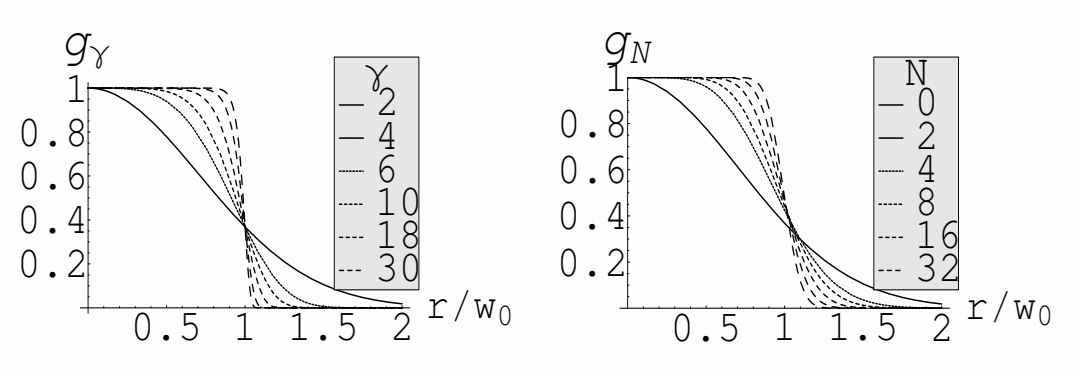

Figure E.2: FGB (right) and SG (left) profiles vs. r/w_0 for different values of γ and N

$$w_N(0) \;=\; \frac{w_0}{\sqrt{N+1}}. \tag{E.13}$$

Figures E.3 and E.4 show $|g_N(r,z)|$ vs. $r/w_N(0)$ and z/Z_N for several value of N.

MULTIPLE GAUSSIAN BEAMS (MGB)

MGB at the waist position $z = 0$

The Multiple Gaussian Beam (MGB) is composed of a sum of Gaussian function components, each with spot size w, but offset by w. The general formula for a MGB of order M, at the waist plane $z = 0$ and for the cartesian coordinate x, is [63]:

$$g_M(x, z=0) = \frac{\sum_{m=-M}^{M} \exp\left[-(x/w - m)^2\right]}{\sum_{m=-M}^{M} \exp(-m^2)}. \tag{E.14}$$

For $M = 0$ it reduces to the Gaussian function, whereas for $M = \infty$ it becomes the step function $\Theta(w - x)$. It is composed by $2M + 1$ Gaussian function components. The width of the MGB of order M is:

$$w_M = w\left\{M + \left[1 - \ln\left(\sum_{m=-M}^{M} \exp(-m^2)\right)\right]^{1/2}\right\} \tag{E.15}$$

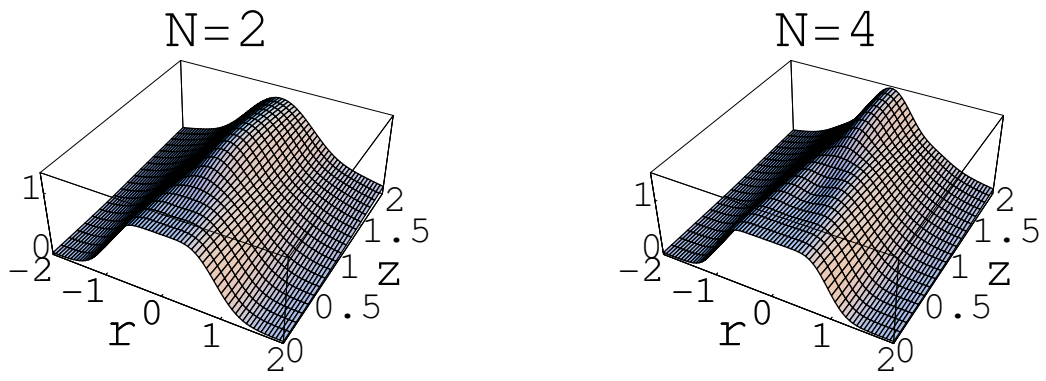

Figure E.3: Evolution of $|g_N(r,z)|$ for $N=2$ and $N=4$; r and z are in units of $w_N(0)$ and Z_N, respectively.

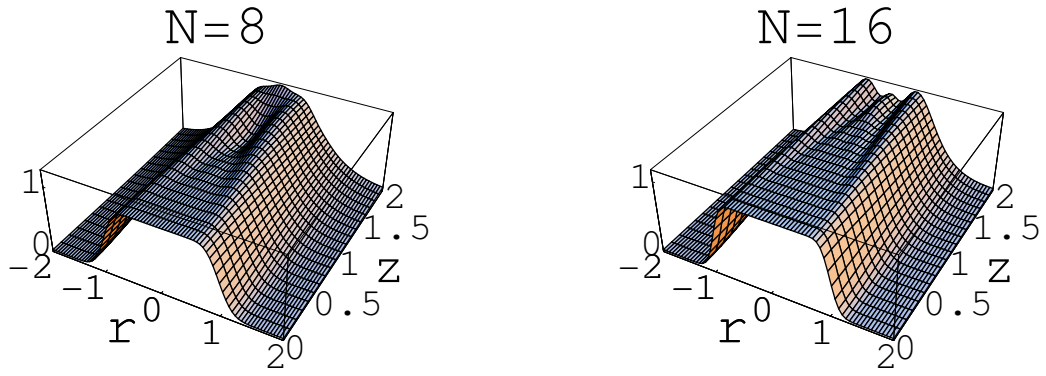

Figure E.4: Same as fig.E.3 but for $N=8$ and $N=16$.

MGB propagation law

The expression for the MGB outside the waist plane $z=0$ can be obtained analytically. The general treatment is reported in ref.[63]. In the free-space the formula is:

$$g_M(x,z) = \frac{A_M}{\sqrt{1+(z/Z_L)^2}} e^{i\Phi(z)} \sum_{m=-M}^{M} \exp\left\{\left[-\frac{1}{w^2(z)} + \frac{i\pi}{\lambda_L R(z)}\left(\frac{z}{Z_L}\right)\right](x-mw)^2\right\} \tag{E.16}$$

where $w(z) = w[1+(z/Z_L)]^{1/2}$, $1/R(z) = z/(z^2+Z_L^2)$, $\Phi(z) = \arctan(z/Z_L)$, $Z_L = \pi w^2/\lambda_L$ is the Rayleigh range and

$$A_M = \sum_{m=-M}^{M} \exp(-m^2) \tag{E.17}$$

Normalizzation

For a correct normalizzation of eq. (E.16) we have to normalize the radial coordinate with the effective widht $W_0(N)$ of the multi-Gaussian beam and the temporal coordinate z with the Rayleigh range.

$$r = r/W_0 \qquad z = z/z_r \tag{E.18}$$

With this normalizzation the Eqs.(E.11) becomes:

$$T_N(r,z) \;=\; C_0(N) \sum_{m=-N}^{N} e^{\left\{-\left[\frac{r-m}{(1+z^2)^{1/2}}\right]^2 [1+iz]\right\}} e^{\left[\frac{(i/2)ArcTan(z)}{(1+z^2)^{1/4}}\right]} \tag{E.19}$$

In figures E.5 and E.6 we shown the evolution in z of the FGB profile $\tilde{U}_N(r,z)$ for a different value of N.

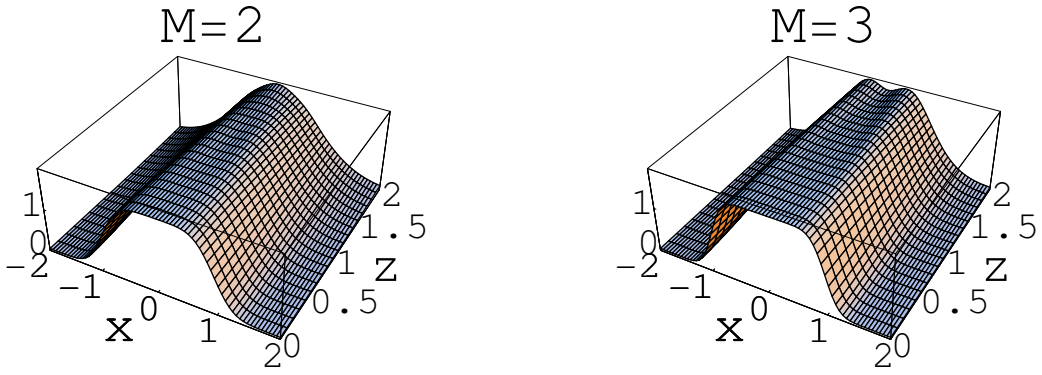

Figure E.5: Evolution of $T_N(r, z)$ for M=2 and M=3

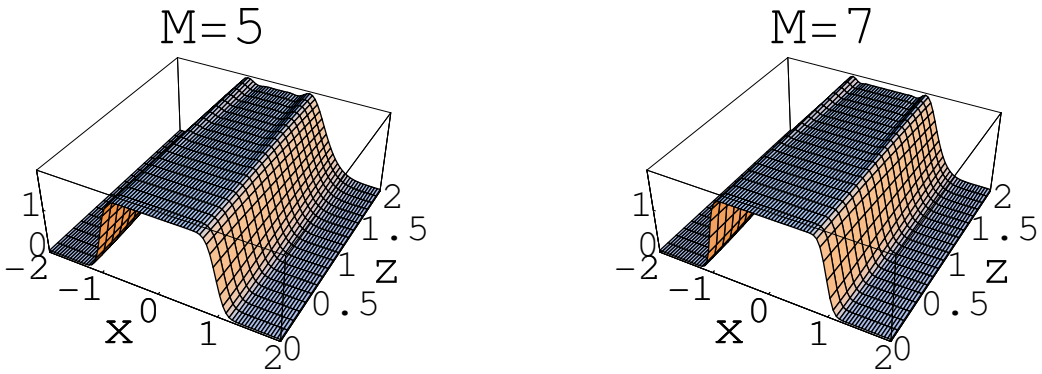

Figure E.6: Evolution of $T_N(r, z)$ for M=5 and M=7

Bibliography

Classical articles and text books

[1] J.D.Jackson: *Classical Electrodynamics* Willey, New York, 1975

[2] H.Goldstein: *Classical Mechanics* Addison-Wesley. Reading. MA).

[3] F.T.Arecchi and R.Bonifacio: IEEE J. *Quantum Electron* QE-1, 169, (1965)

[4] G.T.Moore and M.O.Scully, *Phys. Rev. A*, 21, 2000, (1980)

[5] E.T.Arecchi and R. Bonifacio, *IEEE J. Quantum Electron.* 1, 169 (1965)

[6] R. Bonifacio et al *Nuovo Cimento.* 9, 1990

[7] R. Bonifacio et al *Nuovo Cimento.* 11, 1992

[8] J.C.Gallardo, R.C.Fernow, R.Palmer, C. Pellegrini, *IEEE Journ. Quantum Electron. QE-17, 1436 (1981).* 24 (1988) 1557.

[9] M. Xie *Proceedings of the Particle Accelerator Conference*, Dallas, 1995, p.183.

[10] G.T.Moore and M.O.Scully *Phys. Rev. A*, 21, 6, (1980)

[11] R.Bonifacio, F.Casagrande and C. Pellegrini *Opt. Commun.*, 61, 55, (1986)

Classical SASE and Superradiance

[12] R.H.Dicke *Phys. Rev.* 93,99 (1954)

[13] R.Bonifacio (Editors) *Dissipative System in Quantum Optics*, (Springler, Berlin, 1982)

[14] R.Bonifacio, C. Pellegrini and L.M. Narducci. *Opt. Commun.*, 50, 373, (1984)

[15] R.Bonifacio, C. Marioli and N. Piovella *Opt. Commun.*, 68, 639, (1988)

[16] R.Bonifacio, B. Mcneil and P. Pierini and N. Piovella *Phys. Rev. A*, 40, 4467, (1989)

[17] R.Bonifacio, L. De Salvo, P. Pierini, N. Piovella and C. Pellegrini *Phys. Rev. A*, 73, 70 (1994)

[18] E.L.Saldin et al *Opt. Commun.*, 148 (1998) 383

[19] G. Geloni et al *physics/0506231* (June 2005)

[20] J.W. Goodman *Statistical Optics* Wiley Classical library Edition 2000

[21] K.J.Kim, *Phys. Rev. A*, 57 (1986) 1871

[22] J.M.Wang,L.H.Yu, *Nucl. Instrum.and Meth.* A 250 (1986) 396

[23] A.Gover, E.Dyunin, R. Aviv. *Proceedings of FEL 2006, Bessy,Berlin,Germany*

Quantum FEL

[24] G.Preparata, *Phys. Rev. A* 38 233 (1988)

[25] R.Bonifacio and F. Casagrande *Opt. Commun.*, 50, 251 (1984); *Nucl. Instrum.and Meth.* A 237 (1985) 168-179

[26] R.Bonifacio, C. Pellegrini and L. Narducci *Opt. Commun.*, 50,373, (1984)

[27] N. Piovella, M. Gatelli and R.Bonifacio, *Opt. Commun.*, 194, 167 (2001)

[28] R. Bonifacio, N. Piovella, G.R.M.Robb, M.M.Cola, *Opt. Commun.*, 252, 381-396 (2005)

[29] N. Piovella, M.M.Cola and R. Bonifacio, *Phys. Rev. A* 67 013817 (2003)

[30] R.Bonifacio, N.Piovella, G.R.M.Robb, *Nucl. Instr. and Meth.* A 543 (2005) 645-652

[31] R. Bonifacio, N. Piovella, G. R. M.Robb and Angelo Schiavi, *Phys. Rev. ST Accel. Beams* 9, 090701 (2006)

[32] N. Piovella and R. Bonifacio, *Nucl. Instrum.and Meth.* A 560, 240 (2006).

[33] L. Volpe and N. Piovella *Laser Physics* 17, (2007), 807

[34] C.B.Schroeder, C.Pellegrini and P. Chen, *Phys. Rev. E* 64, 056502 (2001)

[35] R. Bonifacio, M.M. Cola, N. Piovella, and G.R.M. Robb, Europhys. Lett. 69, 55 (2005) .

[36] K,J,Kim, *Proceeduing at Workshop on Single Pass High Gain FELs* ... Edit by R.Bonifacio, William A.Barletta Garda Lake Italy (1997)

[37] R.Bonifacio, *Proceeduing at Workshop on Single Pass High Gain FELs* ... Edit by R.Bonifacio, William A.Barletta Garda Lake Italy (1997)

[38] Julio Gea-Banacloche *Phys. Rev. A* 31, 3 (1985)

[39] R. Bonifacio, N. Piovella, M.M.Cola and L.Volpe *Nucl.Instrum.and Meth.* A 577, 240 (2007).

[40] M. Roncadelli e A. Defendi I cammini di Feynman, quaderni di fisica teorica, Universitã degli studi di Pavia Edizione web 2001

Wigner function

[41] J.P. Bizarro, *Phys. Rev.A* 49, 3255 (1984)

[42] P. Carruthers and M.M. Nieto, *Rev. of Mod. Phys.* 40 (1968) 411.

[43] R. Jackiw, *Journ. of Math Phys.* 9 (1968) 339.

[44] N. Piovella, M. M. Cola, L. Volpe, R. Gaiba, A. Schiavi, and R. Bonifacio *Optic. Commun.* 274 (2007) 347

[45] R. Balescu *Equilibrium and Nonequilibrium statistical mechanics*, A. Wiley New York (1974)

3D theory

[46] N.Piovella, M. M. Cola, L. Volpe, A. Schiavi and R. Bonifacio to be published on *Phys.Rev.Lett.* (2008)

[47] R. Bonifacio, N. Piovella, M.M. Cola, L. Volpe, A. Schiavi, and G.R.M. Robb, Proceedings of Fel Frontiers Conference, Elba island, (2007)

[48] M.M. Cola, L. Volpe, N. Piovella, A. Schiavi, and R.Bonifacio, Proceedings of Fel Frontiers Conference, Elba island, (2007).

[49] A. Schiavi, M.M. Cola, L. Volpe, N. Piovella, and R.Bonifacio, Proceedings of Fel Frontiers Conference, Elba island, (2007).

[50] Sven Reiche, *Numerical studies for a Single Pass High Gain Free-Electron Laser*, Doctorate thesis, http://pbpl.physics.ucla.edu/ reiche/.

[51] Y.H.Chin, K.J.Kim and M.Xie *Phys. Rev.A* 46, 10 (1992)

[52] R. Bacci, M.Ferrario, C.Maroli,V. Petrillo and L. Serafini *Phys. Rev. ST Accel. Beams* 9, 060704 (2006)

[53] The LCLS Design Study Group: LCLS Design Study Report, SLAC-R521, Stanford (1998) and http://www-ssrl.slac.stanford.edu/lcls/CDR.

[54] The European X-Ray Free Electron Laser: Technical Design Report, ISBN 978-3-935702-17-1, DESY 2006-097 (July 2007) and http://xfel.desy.de/tdr/tdr.

[55] T. Shintake, Status of the SCSS Test Accelerator and XFEL Project in Japan', EPAC'06, Edinburgh (2006) and http://www-xfel.spring8.or.jp.

[56] N.M. Kroll, P.L. Morton, and M.N. Rosenbluth, IEEE Journ. Quantum Electronics QE-17, 1436 (1981).

[57] T.M. Tran, and J.S. Wurtele, Physics Report 195, 1 (1990).

Laser wiggler

[58] J.Gea-Banacloche, G.T.Moore, R.R.shlicher, M.O.Scully and H. Walther, *IEEE J. of Quantum electron.,* Vol QE-23, pp 1558-1570(1987)

[59] P.Dobiasch, P. Meystre and M.O.Scully, *IEEE J. of Quantum electron.,* Vol QE-19, pp 1812 1820, (1983)

[60] J.Gea-Banacloche, G.T.Moore and M.O.Scully, *proc.* SPIE, vol. 453, pp 393-401 (1984)

[61] F. Gori, Opt. Commun. 107 (1994) 335.

[62] V. Bagini, R. Borghi, F. Gori, A.M. Pacileo, M. Santarsiero, D. Ambrosini, G, Schirripa Spagnolo, J. Opt. Soc. Am. A 13 (1996) 1385.

[63] A.A. Tovar, J. Opt. Soc. Am. A 18 (2001) 1897.

[64] S. De Silvestri, P. Laporta, V. Magni, and O. Svelto, IEEE J. Quantum Electron. QE-26 (1988) 1172.

Experiments

[65] Luis R. Elias, William M. Fairbank, John M. J. Madey, H. Alan Schwettman, and Todd I. Smith, *Phys. Rev. Lett*, 36, 717, (1976)

[66] D. A. G. Deacon , L. R. Elias, J. M. J. Madey, G. J. Ramian, H. A. Schwettman, and T. I. Smith, *Phys. Rev. Lett*, 38, 892, (1977)

[67] T.J.Orzechoski, et al., *Phys. Rev. Lett*, 54 (1985) 889

[68] J.Andruskow, et al, *Phys. Rev. Lett*, 85 (2000) 3825

[69] S.V.Milton, et al., *Science*, 292 (2001) 2037